Two-Phase Separated Flow Modelling Using Particle Tracking Technique

By

Vajira Priyantha Alawattage

A Doctoral Thesis

Submitted in partial fulfilment of the requirements for the award of
Doctor of Philosophy of De Montfort University

March 2005

De Montfort University
School of Engineering and Technology
Leicester UK
LE1 9BH

Abstract

A computational model capable of evaluating the mixing, evaporation and combustion characteristics of a liquid fuel spray injected into a high pressure co-flowing air stream was formulated based on a discrete separated flow approach. During the first part of the research project, a FORTRAN program providing the solution to equations necessary for particle tracking was completed. The model developed is capable of evaluating droplet trajectories, size and temperature histories by using gas phase properties (one-way coupling). This is also capable of calculating mass, momentum and energy source terms, which are required for gas phase calculations.

In the second phase of the research project, in order to model the mixing and evaporation characteristics of the spray combustion process using separated flow method based on deterministic trajectory approach, an in-house LHF code was modified to obtain the gas phase solution and the particle-tracking model was used to model the droplet phase. The solution result from this combined model (with two-way coupling) was then used with a combustion model in a 'mixed–is-burnt' type approach to obtain the combustion characteristics of the process.

Finally the predicted results from the separated flow model were compared with existing experimental data and it was observed that the results are reasonably agreeable. It was also shown that the model is capable of predicting the experimentally observed recirculation regions. In order to assess the applicability of the model over a wide range of operating conditions, a parametric study was carried out. The results from the studies were compared with the predictions of the in-house LHF type model and it was found that the separated flow model predictions were more realistic than the LHF predictions particularly in the radial direction.

Acknowledgements

The author would like to express his gratitude to De Montfort University for financial support through a bursary and to Prof. J. A. G. Knight for his help and other assistance provided during the project.

The author wishes to express his deep gratitude to his supervisors Prof. M.A.A Nazha and Dr. H.T.B. Rajakaruna for their supervision, guidance, suggestions and constructive criticism throughout this research project.

The author wishes to acknowledge the friendly help extended by his colleagues, Catalin Amza and Saman Chandrasiri. And also, the author would like to thank Andy Rylott for introducing him to SUN operating system

Finally the author expresses gratitude to his wife, Sriya, for her patience, understanding and support and enthusiastically sharing every experience to make success more enjoyable and disappointments more tolerable.

Contents

Nomenclature

A	Area
B	Spalding mass transfer number
C_D	Drag coefficient
C_A	Added mass term
C_H	Basset term (history term)
d	diameter
D_{10}	Arithmetic mean diameter
D_{32}	Sauter mean diameter
D_k	Particle diffusivity
f	Mixture fraction
f_B	Drift force
g	Body force term/ gravity term
G_b	Buoyancy production term
G_k	Mean production term
k	Turbulent kinetic energy
l	Mixing length; length scale
L	Enthalpy of evaporation
m	Mass
M	Mass fraction
$\dot{m}$	Mass flow rate
n_k	Number density
P	Pressure
$\dot{q}$	Heat transfer rate

S	Source term
Sc	Schmidt number
Sh	Sherwood number
T	Temperature
t	Time
u, U	Gas phase velocity
v	Droplet/particle velocity; Viscosity
V	Volume; droplet velocity
Y	Mass fraction

Greek Symbols

α	Volume fraction
θ	Spray angle
β	Thermal expancivity
σ	Prandtl/ Schmidt number
σ_k	effective Prandtl number for turbulent kinetic energy (constant)
σ_{kp}	Turbulent particle Schmidt number
ε	Turbulent kinetic energy dissipation rate
ε_{gas}	Gas/air momentum diffusivity
ε_p	Particle eddy diffusivity
ρ	Density
τ_A	Aerodynamic response time
τ_C	Time between drop collisions
Γ	Diffusivity

μ	Viscosity

Subscript

a,A	air
e	Effective
F	Fuel
g	Gas/air
k	k^{th} trajectory
m	mean; mixture
p, d	Particle/droplet
t	Turbulent
v	Vapour

Abbreviations

CFD	Computational Fluid Dynamics
DDM	Discrete Droplet Model
DSF	Deterministic Separated Flow
FEM	Finite Element Method
LHF	Locally Homogeneous Flow
PDF	Probability Density Function
PSIC	Particle-Source-In-Cell
SIMPLE	Semi-Implicit Method for Pressure Linked Equations
SSF	Stochastic Separated Flow
TDMA	Tri-Diagonal Matrix Algorithm

CHAPTER 1

Introduction

The chapter starts with a description of multi-phase flows and where these multi-phase flows occur in practical situations. Then this description continues describing why CFD techniques are used and the advantages of using these techniques over the traditional methods. This is then followed by objectives of this research project and outcomes.

1.0 Introduction

The study of multiphase flows[1] is a wide field of research of extremely high practical importance due to the proliferation of this type of flow in various natural and industrial applications [1, 2, 3, 4]. Natural systems include environmental particulate pollution problems associated with both the atmosphere and the hydrosphere. Typical applications to environmental problems involve predicting the effectiveness of natural flow phenomena for dispersing particulate pollutants to acceptable concentration levels. Many of these situations involve particulate releases from various local and area sources such as volcanoes, radioactive substance released from atomic bombs or nuclear power plants. In some cases the pollutants themselves can alter the environmental flows significantly, such as when dust concentrations affect the solar radiation reaching ground levels that changes the environmental temperature field [5, 6].

Technological applications of two-phase flow research involve a wide range of situations from interior dust and particle-pollutant control problems, to chemical systems involving particulate reactant mixing, to droplet sprays for combustion and drying purposes. The removal of particles and droplets from industrial effluents is a process of high practical importance because of introduction of strict pollutant control measures by authorities. At present various types of apparatus or systems are being used according to the particle or droplet sizes in order to separate those pollutant particles. These include settling chambers, cyclone separators and electrostatic precipitators which are designed and built using empirical formulas and years of experience. Even

---

[1] A gas flow containing liquid droplets or/and solid particles is called a two-phase flow or a multiphase flow

though these processes are used for years, it is still difficult to determine how modifying such a design affects its performance. Therefore development and implement of computational models or analysing methods may be used to improve the efficiency of current designs, predict the performance beyond the design limits and to use as a tool predict scale-up designs.

Spray is another type of two-phase flow process of great importance which has liquid droplets or solid particles as discrete or dispersed phase and gas as continuous phase. There are many applications of spray phenomena in power and propulsion devices and other industrial applications such as spray drying and sprinkler fire suppression systems etc. Above all, sprays with combustion are of greater importance due to the fact that the large portion of energy for propulsion, heating, and electrical power generation is derived from liquid fuels burning as atomised sprays. Today almost complete transport sector depends on the energy produced from fuel spray combustion. Other than this many industrial processes utilize spray combustion in furnaces, boilers, dryers and incinerators etc. Despite the fact that droplet formation by liquid atomization is already an extremely complex phenomena, the interactions of the droplets and their vapour with the turbulent gas mixture form an enormously complex fluid dynamic problem. Therefore the methods used for optimization or scale-up design of these processes are mainly done by empirical, based on experiments, semi empirical and model tests. Although these empirical methods are useful today and may be in future because of their simplicity, they have very narrow-range applicability beyond experimental or test conditions due to strong empirical nature.

Further more, examples of solid particle dispersion and mixing using turbulent flow can be found in a wide and varied number of technological applications. A typical listing of the general areas associated with these processes includes fluidised bed reactors, particle generation and reaction processes, solid transport, and separation processes.

Therefore it is clear that numerical models for turbulent fluid-particle flows can play a key role in addressing these technical problems. This is achieved by improving the understanding of the phenomenon and by aiding the design of engineering systems.

1.1 Advantages of Spray Combustion Modelling

Analysis of turbulent, two-phase, reacting flows finds useful applications in the design and development of power producing devices involving spray combustion [7]. The processes involved in the combustion of these sprays are varied and complex. These processes include, mixing of species, evaporation of liquid fuel and chemical reactions leading to explosion and formation of new species. Thus complete analysis is very difficult. Many predictive models cited in the literature make simplifying assumptions regarding the coupling between the dispersed phase and gas phases. The lack of adequate computational codes able to predict the collective behaviour of a two-phase flow, including particle interactions with the continuous phase, is a major drawback in the field.

Computational Fluid Dynamics (CFD) in general provides substantial savings to designers due to the relative low cost set up and analysis compared to an experimental facility [8]. These include:

- Substantial reduction of lead-time and cost of new designs.
- Ability to study systems when controlled experiments are difficult or impossible to perform, for example very large systems.
- Ability to perform detailed study of systems under hazardous conditions at and beyond its performance limits, for example fire and safety studies.
- Easy and economical to perform parametric studies, for example, to optimise system performance.

The ultimate aim of computational modelling of spray combustion is to develop codes capable of predicting the above phenomena in a qualitative and quantitative manner. Due to the tremendous complexity of the processes involved, the existing codes lag behind other computer aided engineering tools such as FEM codes written for stress analysis. In general, two spray modelling approaches are used namely, Locally Homogeneous Flow (LHF) method and Separated Flow (SF) method. SF approach takes into account the slip between the two-phases, which makes the problem more complex.

It is important to note that, when solving any flow problem, engineer or researcher must be aware that the underlying physical and chemical phenomena, is very complex. Therefore a clear understanding of the system is vital, because the results

generated by a computational model are as good as the accuracy and the applicability of physical and chemical theories or laws used in the model. On the other hand, almost every numerical algorithm has its own characteristic errors such as numerical diffusion, which can only be guessed on a basis of a thorough knowledge of the algorithms. Thus it is impossible to assess the validity of a model of such a complex problem or the accuracy of its results by any means other than by experimental data. Finally, it must be emphasised that computational fluid dynamics modelling is still not a direct substitution for experimentation, but a very powerful tool for solving problems.

1.2 Problem definition

When liquid fuel is sprayed into a combustion chamber, due to entrainment of surrounding gas, the spray forms a jet inside the chamber. In the case under consideration the jet has the following unique characteristics. The jet consists of evaporating and burning liquid fuel droplets suspended in a hot gas environment. The growth of the jet is confined by the chamber walls leading to a recirculating flow situation. There is slip between the droplets and the bulk gas, leading to momentum, mass and energy transfer between the two phases; for example, particles globally modify turbulence in the gas field. On the other hand turbulence in the gas phase modify particle motion. This situation becomes more complex with evaporating and burning droplets, and turn into a two-way coupling problem. The computer model that is to be developed at the end of this research will be capable of handling the above problem.

1.3 Objective

The overall aim of this research project was to develop a separated flow model for a reacting two-phase flow. This was achieved by modifying and extending the capabilities of an LHF type in-house developed two-phase spray combustion code [9] by including particle tracking routines [4, 6]. The outcome of modification of the LHF type code and the inclusion of the particle tracking routines is a separated flow type model. This main program is in fact a mixing program which produces fuel air mixture distribution of combustion chamber (The fuel air mixing temperature is arrived at by the method described in chapter 4). Therefore a separate program is used to model combustion which use air fuel equivalence ratio map obtained from the mixing program. These combustion data were particularly helpful when validating the model against experimental data because all the experimental data available to the author were obtained from combustion analysis.

1.3.1 Program of work

The overall aim of the project was achieved by realising the following specific objectives:

- Understanding the state of the art in spray combustion modelling by carrying out an extensive literature survey inclusive of Discrete Separated Flow models
- Understanding and become familiar with the in-house built LHF code
- Formulation and coding of a particle-tracking module

- Modification of the in-house built code and incorporation of the particle-tracking module into in-house code to transform it to a Separated Flow code
- Validation of the new code with in-house code and existing experimental results

1.4 Layout of the thesis

The literature survey has been carried out about multiphase flows in general and modelling of spray combustion in particular which is presented in ***Chapter 2***. This covers two-phase flows, droplet break up and particle tracking techniques. After understanding the relevant mathematical formulations available in the literature, the mathematical modelling of the two-phase separated flow model has been carried out. This includes description and formulation of gas (continuous) phase and formulation of droplet (discrete) phase using droplet trajectory module and this is presented in ***Chapter 3***. This trajectory module is able to calculate droplet life histories and source terms required for the continuous (gas) phase calculations. Calculation of droplet life histories is carried out based on gas-phase cell properties. This is followed by ***Chapter 4*** which describes how numerical formulation carried out, the problems encountered and how those were dealt with. The parametric study of the trajectory module alone and the separated flow model followed by experimental validation of the model are presented in ***Chapter 5***. Conclusions and recommendations are given in Chapter-6. Graphs and figures obtained during parametric study experimental validation are presented in ***appendices (A-H)*** and also nomenclature and references are presented in ***appendices I and J.***

CHAPTER 2

Literature Review:

Spray and its Modelling Methods

The literature on spray combustion modelling techniques is reviewed in this chapter. Spray characteristics, uses of spray combustion and related injector types used to achieve desired spray are reviewed in the first part of the chapter. This is followed by a review of the literature concerning different spray models based on Eulerian and Lagrangian approaches and their relative advantages and disadvantages. The discussion is focused on separated flow approaches, namely Two Fluid Method, Deterministic Separated Flow method and Stochastic Separated Flow method. And also, there are brief discussions about modelling turbulence and combustion.

2.0 Introduction

When dealing with numerical modelling of complex flow problems understanding the underlying physical and chemical phenomena is of paramount importance. This requires a great insight into thermo-chemistry, thermodynamics, fluid mechanics and numerical methods. Almost in every problem it is necessary to make certain assumptions and simplifications to reduce the complexity of the problem to a manageable level while preserving important features. Typical examples of the assumptions that may be made are, whether the problem can be treated as a two dimensional problem or whether it is necessary to address it as a three dimensional problem and whether the effects of pressure and density variations in the flow field can be neglected, or if the problem can be considered as steady state system [2, 8].

Another essential ingredient for modelling work is a good understanding of numerical solution algorithms. Generally, there are three mathematical concepts which are useful in determining the success of such an algorithm; convergence, consistency and stability. Convergence is a property of numerical methods, which approaches the exact solution, as the grid spacing or control volume size tends to zero. In practice, however, engineers or researchers need computational models that produce physically realistic results with good accuracy and with finite grid sizes. Consistent numerical schemes produce systems of algebraic equations, which can be demonstrated to be equivalent to the original governing equation, as grid spacing tends to zero. Stability is a property of numerical methods, which indicates the firmness of the method as the solution proceeds. From now on, this discussion will be

mainly focused on the modelling of two-phase flows. In this respect it is important to understand the definitions of a fluid particle flow in modelling context and also the primary terms of importance when defining a two phase flow [1, 2].

2.1 Fluid –Particle flows

Fluid particle flows are the flows wherein one phase is discrete or not continuous in the flow. These comprise gas-particle, gas droplet and liquid-particle flows. Another kind of discrete flow is bubbly flows in which the gas forms the discrete phase and the liquid is the continuous phase. In this study the main concern is about discrete phases which normally contain particles or droplets often called dispersed phase. When studying about these flows, it is important to define and understand some properties and parameters significant to dispersed phase.

2.1.1 Density and volume fraction

Since the particles phase is not a continuous phase when studying about these with continuous phase assumption, the density and volume of the particle phase are defined rather differently. Therefore it is important to understand the various density terms used in these equations; as a starting point in mathematically describing a two phase flow. Taking into account the dispersed phase elements in volume ΔV as shown in the fig.2.1.

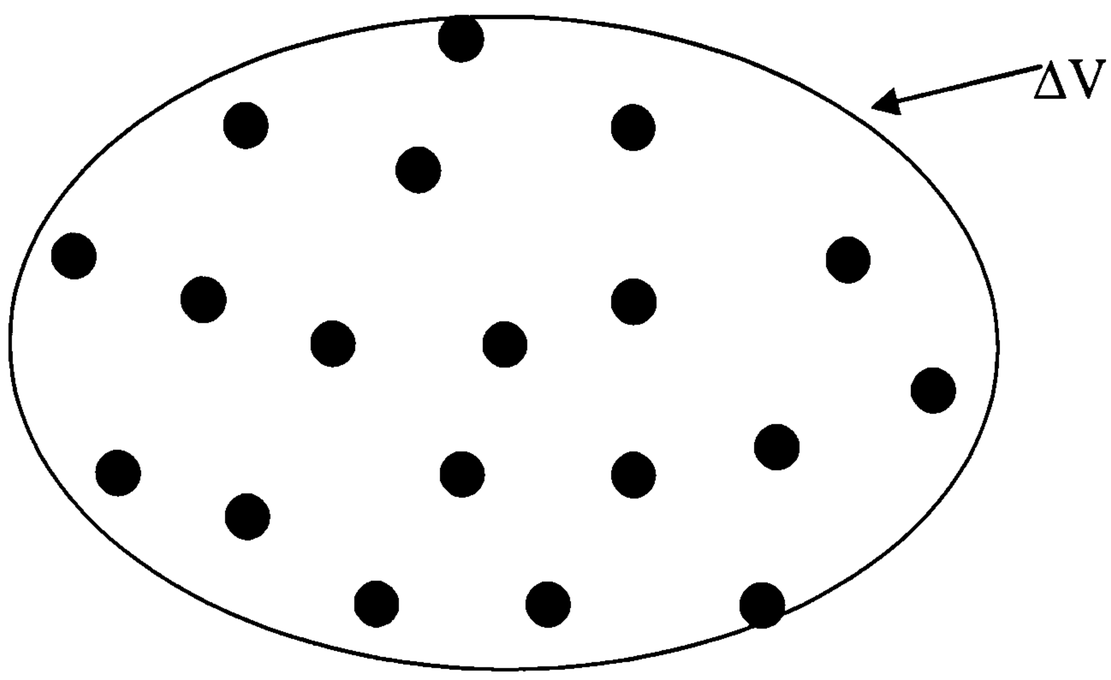

fig. 2.1

the volume fraction of the dispersed phase is defined as

$$\alpha_d = \frac{\Delta V_d}{\Delta V} \tag{2.1}$$

where ΔV_d is the sum of the volumes of the dispersed phase elements in ΔV. Similarly gas or continuous phase volume fraction is

$$\alpha_g = \frac{\Delta V_g}{\Delta V} \tag{2.2}$$

where ΔV_g is volume of the gas (air) in ΔV.

This gas phase volume fraction is also defined as *void fraction*. The sum of these volume fractions by definition is equal to unity [1].

$$\alpha_d + \alpha_g = 1 \tag{2.3}$$

The bulk density or the apparent density of the dispersed phase is the mass of the dispersed phase per unit volume of mixture

$$\overline{\rho}_d = nm_d \tag{2.4}$$

where m_d is the mass of one particle and n is the particle number density, which is defined as the number of particles per unit volume of the mixture.

Different densities defined for gas particle flow can be related as

$$\rho_m = \rho + \overline{\rho}_d = \rho + \sum \rho_k = \rho + (\sum n_k \pi d_k^3 / 6)\rho_d \qquad (2.5)$$

where

ρ_m	mixture density
$\overline{\rho}$	gas apparent density
$\overline{\rho}_d, \overline{\rho}_k$	particle apparent density
ρ_d	particle material density

It is possible to describe volume fraction of gas and particle phase using these density definitions.

$$\alpha_d = \frac{\overline{\rho}_d}{\rho_d} \qquad (2.6)$$

$$\alpha_g = 1 - \alpha_d = 1 - \frac{\overline{\rho}_d}{\rho_d} \qquad (2.7)$$

mixture density of the gas-particle flow can also be defined using gas and particle material density as

$$\rho_m = \alpha_g \rho_g + \alpha_d \rho_d \tag{2.8}$$

For dilute gas particle flows $\rho_d >> \overline{\rho}_d$, therefore gas material density is nearly equal to gas apparent density. It is also possible to show that a fuel spray with air fuel ratio of 1/15 has fuel volume fraction of less than 0.01% [2].

2.1.2 Gas-particle flow characteristic times

Flow regime can be identified using a number of characteristic times. These can be defined as [2];

Flow characteristic time (residence time) $\tau_f = L/v$ (2.9)

Particle relaxation (response) time $\tau_r = d_d^2 \rho_d / (18\mu)$ (2.10)

Particle relaxation time for mean motion $\tau_{r1} = \tau_r (1 + \mathrm{Re}_d^{2/3}/6)$ (2.11)

Particle-particle impaction time $\tau_{pp} = \dfrac{1}{c\pi n_d r_d^2 u_d'}$ (2.12)

Where

$$\mathrm{Re}_d = \frac{|v - u_d|}{d_d \nu}$$

and c is an empirical flow constant, L a length scale of the flow, u_d' is droplet fluctuating velocity.

Crowe et al [1] obtained particle impaction time slightly differently using particle collision frequency equation, which is given by

$$\tau_{pp} = \frac{1}{n\pi d^2 u_{rd}} \tag{2.13}$$

where u_{rd} is particle-particle relative velocity

The different flow regions of the gas particle flow can be identified according to the magnitude of the ratio of a certain characteristic time to the other [2]. Both Zhou et al [2] and Crowe et al argued that it is possible to define dilute and dense nature of a flow considering the following characteristic time ratios.

$\frac{\tau_{rl}}{\tau_{pp}} << 1$ Dilute suspension flow

$\frac{\tau_{rl}}{\tau_{pp}} >> 1$ Dense Suspension flow

The methods used to identify these will be discussed in detail later in this chapter.

2.1.3 Particle Dynamics

When analysing gas-particle flows, it is important to find out how particle dynamics influence the gas or bulk flow as well as how the gas flow effect particle dynamics. Very useful insight into particle flows can be made by studying dynamics of a single particle in a gaseous flow. This will be covered next in this literature review.

2.1.3.1 Particle momentum equation

The particle trajectory can be determined by solving its equation of motion. This equation can be deduced from Newton's Second Law of Motion if all the forces acting on a particle immersed in a turbulent flow are mathematically quantified. In order to do that it is important to identify all the forces acting on a particle in a turbulent flow. These forces can be categorised as [1, 2]:

1. Forces that act on a particle due to the motion of particle
2. Forces that act on a particle due to the motion of surrounding fluid.
3. Forces that act on a particle irrespective of the fact that the particle is in motion or immersed in a flowing fluid (body forces, e.g. gravity and electromagnetic forces).
4. Forces that act on a particle immersed in fluid irrespective of either particle or fluid motion (e.g. buoyancy forces).

Various formulations have been given, initially by Basset (1888) and Boussinesq (1903) and Oseen (1927) for a spherical particle moving through a fluid, then recently by Gatignol (1983). The particle motion equation accepted by researchers at present is the modified Riley [10, 11] equation and this can be written as follows:

$$\rho_p \frac{\pi d^3}{6}\frac{dV}{dt} = \frac{\pi d^2}{8}\rho_g C_D (U-v)|v-U| - \rho_g \frac{\pi d^3}{6} C_A \frac{d(v-U)}{dt} + \frac{\pi d^3}{6}(\rho_p - \rho_g)g$$

$$+\rho_g \frac{\pi d^3}{6}\frac{DU}{Dt} - \frac{\pi d^2}{4} C_H \sqrt{\frac{\rho_g \mu}{\pi}} \int_{-\infty}^{t} \frac{d(v-U)}{dt}(t-\tau)^{-1/2} d\tau \qquad (2.14)$$

where ρ_p and ρ_g are the particle and fluid (gas) densities, d is the particle diameter; v and U are the instantaneous velocity vectors of the particle and gas phase respectively. In the above equation, d/dt is the temporal derivative along the discrete particle trajectory and D/Dt is the temporal derivative along the fluid motion, g is the gravity vector and μ is the fluid viscosity. Coefficients C_d, C_A and C_H are correction factors applied to the drag term, added mass term and Basset term respectively to account for non-small particle Reynolds numbers and acceleration numbers. For dense particles in turbulent flows ($\rho_p >> \rho_g$), the particle motion equation can be simplified to drag and gravity force terms [5, 12].

2.2 Fluid –Particle flow modelling

Numerical models for fluid particle flows are based either on one-way or two-way coupling. In a model based on one-way coupling it is assumed that the presence of the particulate phase has a negligible effect on the carrier phase. The assumption of one-way coupling is typically valid for small particle-fluid mass concentration ratios [12]. Two-way coupled models include the effect of the particles on the carrier phase. For example, a two-phase turbulent flow model that includes the effect of the particles on the turbulent velocity fluctuations would be two-way coupled. When particle-particle collisions become frequent, which is the case for dense disperse flow, the turbulence of the carrier phase can be affected by the oscillatory motion resulting from the particle collisions. Elghobashi (1994) identifies this effect as four-way coupling [13].

The ideal numerical model for a fluid-particle flow would provide the properties of each particle in the flow field and the detailed properties of the carrier phase at any point in the fluid. Thus the motion of each particle, as well as the particle temperature and mass, would be obtained by integrating the particle equations using the local velocity, temperature, and density of the carrier flow and accounting for all particle-particle collisions. The model for the carrier phase would require the direct solution of the Navier-Stokes equations including the boundary conditions imposed by all the particles in the field. Such an exact model is still well beyond current computational capability. This has lead to the use of simplified models to carry out the numerical analysis.

2.2.1 Two Phase Modelling of Spray Combustion

Modelling of evaporating and burning sprays is a complex problem due to the diverse phenomena that must be considered, including: the hydrodynamic characteristics of injection and spray formation; the transport characteristics of individual droplets; the turbulent two-phase flow of a spray, and chemical phenomena in a turbulent environment leading to the formation of product species and pollutants [14,15].

Since the objective of this chapter is to examine the current status of spray combustion models, and models of this type cannot be effectively discussed without giving consideration to important elemental processes such as spray formation and transformation characteristics of droplets, these matters are considered next. Firstly overall combustion systems involving sprays are considered. Then methods of injection and spray characteristics are discussed.

2.3 Spray combustion systems

Fuel sprays are burnt in a variety of combustion systems and each present different problem to the development of a spray model due to variations involved in flow configuration and the number of independent variables required. Table -1 summarizes several cases, which are typical to a range of practical applications [16, 17].

In a pre-vaporizing system, the spray is injected into an air stream. It is assumed that the droplets are fully evaporated before reaching the flame. This is a typical configuration for afterburners and the carburettor of a spark ignition engine. This kind of combustion is known as premixed combustion and is currently being examined as a way of reducing NO_x in steady state combustion systems. For this type of flow one-dimensional models can provide useful results except near the injector. Generally, the two-phase portion of the flow is non-reacting.

In liquid-fuelled rocket engines, both fuel and oxidizer are injected from one end providing a more or less premixed combustion system. In many practical rocket engine designs, flow in the axial direction is dominant; therefore one-dimensional models could be used for performance predictions. In these models mixing effects are important in near injector region, and when only few injectors are used, more complex models must be considered.

Application	Configuration	Independent variables	Structure
Prevaporizing System Afterburners Lean combustors Carburettor Ramjets	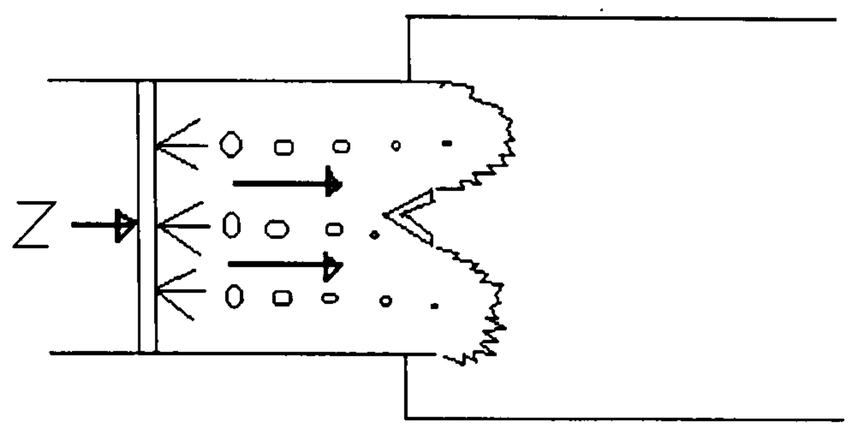	Z	Steady non-burning
Liquid rocket engines	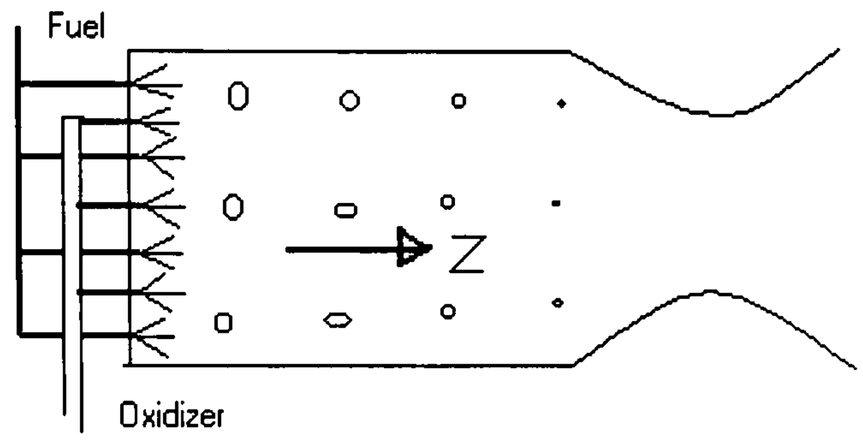	Z	Steady, more or less premixed
Gas turbine combustors	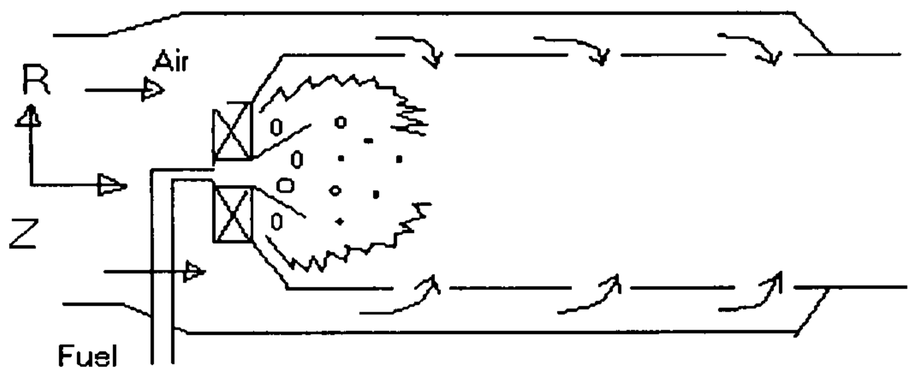	R, Z	Steady, diffusion flame
Industrial furnace	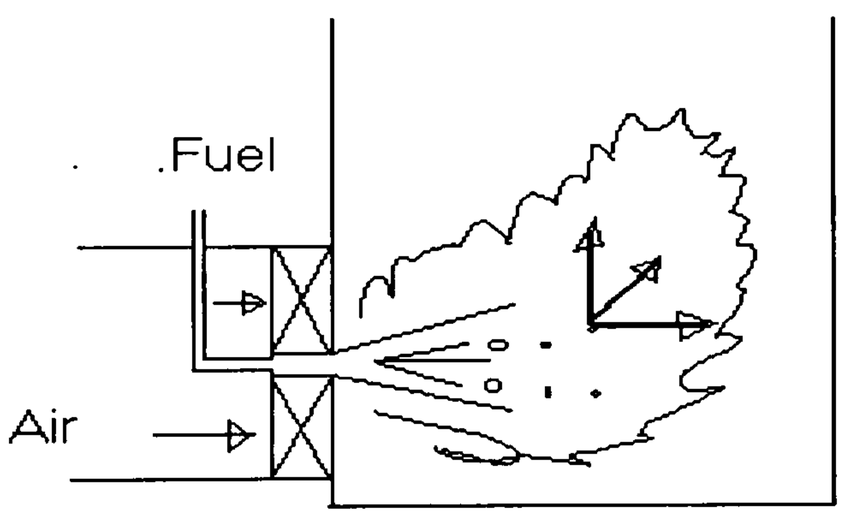	X, Y, Z	Steady, diffusion flame
Diesel engine	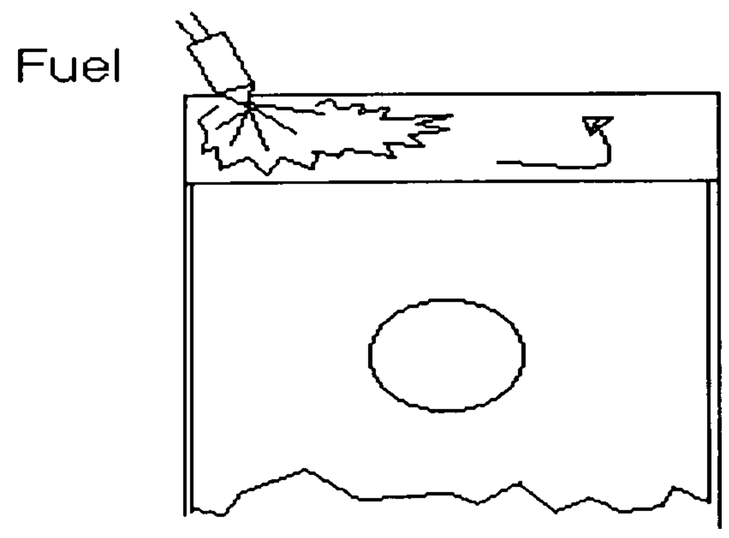	t, X, Y, Z	Transient diffusion flame ignition characteristics needed

Table –1

A gas turbine combustion system can be divided into three different zones, a primary zone where liquid is injected into a nearly stoichiometric flow of air yielding a two-phase flow; a secondary zone where combustion is completed; and a dilution zone where the combustion products are mixed with air to reduce the temperature of the flow to the levels acceptable for expansion through the turbine. The fuel and air are not extensively premixed before combustion, leading to a diffusion flame structure where mixing of fuel and oxygen strongly influences the rate of reaction. One-dimensional models are not effective for this type of configuration. Modelling is primarily done using 2D or 3D CFD codes. Industrial furnaces are similar to gas turbines, although unsymmetrical configurations are more common and buoyancy effects can be important due to the large size of the components and lower gas velocities. 2D or 3D CFD models are used according to the particular application.

Diesel engines represent the most difficult modelling problem. The process is primarily a diffusion flame, but it is transient and fuel impingement on surfaces may be important. The flow is three dimensional, and prediction of ignition characteristics is necessary since the combustion process is intermittent.

2.4 Injector types

As discussed earlier, designers of combustion systems can influence the combustion process to a great extent by varying the design of the injector. Injectors may be separated into two main categories: [16]

- Pressure atomisers, where only the liquid passes through the injector.

- Twin-fluid atomisers, where atomisation of the liquid is aided by a flow of high velocity gas through the injector passages.

Injector properties involve the distribution of droplet sizes, spray angle and whether the spray pattern completely fills the region covered by the spray; i.e. full cone, or has a region along the axis of the injector free of droplets; i.e. hollow cone. These properties may be altered by changing the injector geometry and the fuel flow rate. The motion and properties of the gas within the combustion chamber also influence the spray pattern [18, 19]. Table -2 shows some injector types used in combustion systems. From the injector types listed on the diagram the type most relevant to the applications considered in this project is the pressure atomiser. Typical configurations of this type are described briefly below.

The plain orifice pressure atomising nozzle illustrated in table -2 requires a large pressure drop to achieve good atomisation. It is most frequently used in diesel engines. The spray pattern is of a full cone type. To provide better droplet distribution

in irregular volumes in large engines, multiple orifices are used. An internal valve is used to prevent injection at low pressure ratios to ensure reasonably well-atomised spray throughout the intermittent atomisation process.

The Pintle injector is functionally the same as the plain orifice atomiser. The main difference is that the injector valve is extended through the orifice allowing larger spray angles to be achieved, which reduce the need for multiple orifices.

The swirl-type pressure atomising nozzle achieves good atomisation at lower pressure ratios by centrifugal force. As the liquid sheet leaves the surface, instabilities are developed forming ligaments, which subsequently break-up into droplets. The spill-type nozzle maintains adequate swirl at low discharge rates by recirculating a portion of the flow. Multiple nozzles, such as duplex type, maintain good atomisation over a wide range of flow rates by varying the number of active nozzles. The impinging jet injector achieves atomisation by impacting two or more liquid streams near the injector face. This arrangement is widely used in liquid rocket engines. The resulting spray has a flattened fan like pattern unless more than two streams are used.

Type	Configuration	Structure	Application
Pressure atomising injectors			
Plain orifice	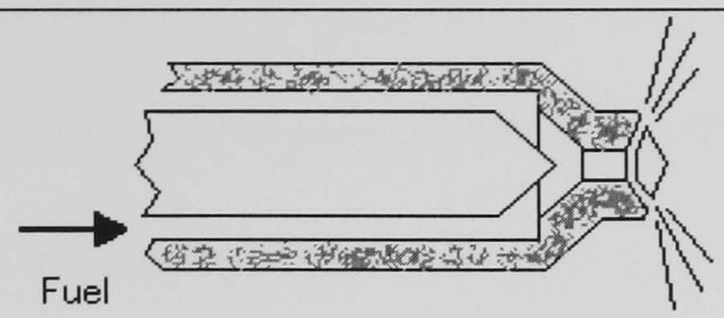	Hollow cone	Diesel engines
Pintle nozzle	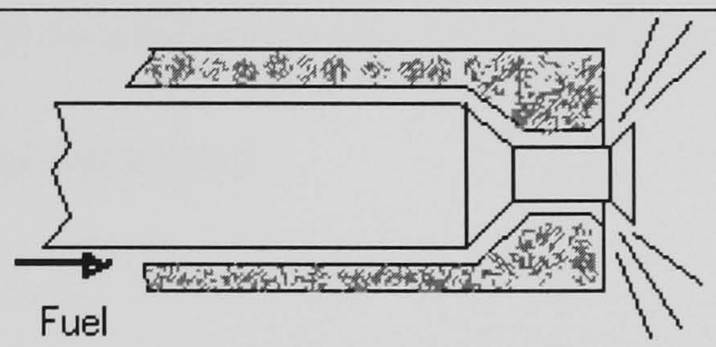	Full cone or multiple cones	Diesel engines Gas turbines
Swirl nozzle (spill type) return	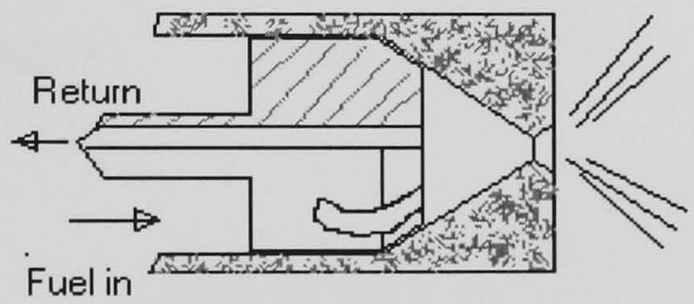	Hollow cone	Furnaces Gas turbines
Impinging jet	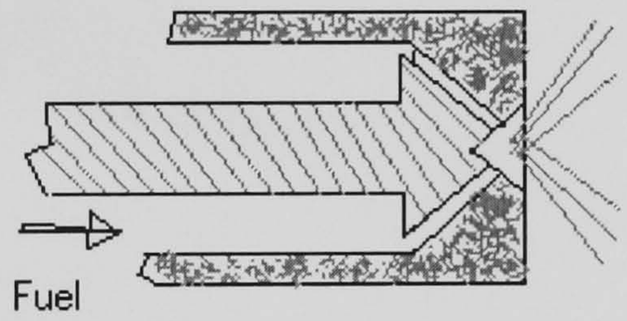	Fan spray	Rocket engines
Twin fluid injectors			
Internal mixing	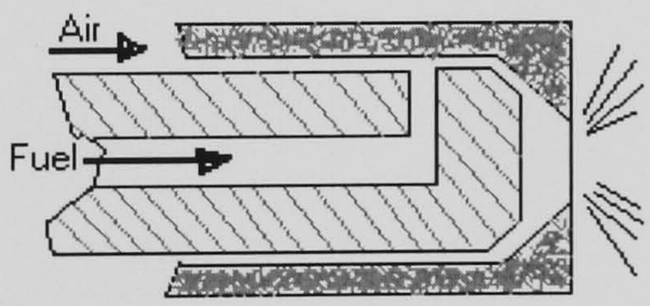	Full or hollow cone	Furnaces Gas turbines
External mixing	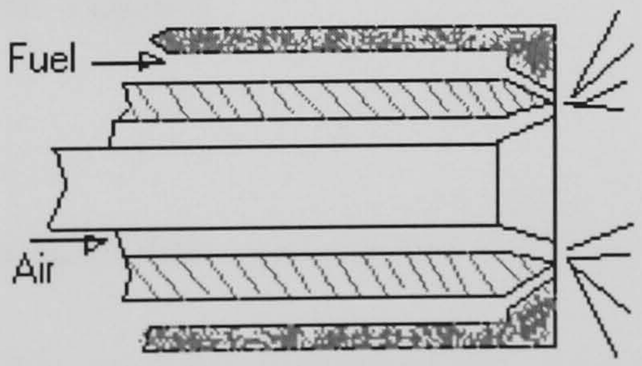	Hollow cone	Furnaces Gas turbines

Table. 2

2.5 Structure of the Spray

Spray modelling requires comprehensive understanding of the structure of the spray and how different sections of the spray interact with the gas phase. Within a fuel spray three different regions can be identified, namely dense, dilute and fully mixed region, as shown in fig.2.2. In this report mainly discussed how the spray combustion can be modelled treating it as a dilute flow [20, 21], which is true for the larger potion of the fuel spray.

Fig. 2.2

2.5.1 Dense flow region

This is near the exit of the injector and it is a typical example for dense dispersed flow. This region involves the transition between an all-liquid flow in a passage, which marks exit of the injector, and the dilute dispersion of droplets that marks the start of the dilute spray region. Thus, large liquid volume fractions are a

basic feature of this region. In dense sprays, liquid phase mostly contains irregularly shaped liquid elements, rather than spherical ones. Other important phenomena in dense sprays are collisions of liquid elements, effects of liquid volume fraction in inter-phase transport rates and the break-up of liquid elements. Experimental results show that drop break-up influences spray penetration, vaporization and mixing in high-pressure sprays [16, 22]. The spray drop size is the outcome of a competition between drop break-up and drop coalescence phenomena. In most sprays, the atomisation details at the injector are lost during this process. Atomisation process will be discussed in detail later in this chapter.

2.5.2 Dilute flow region

Next region is the dilute flow region. Dilute disperse flow contains well-defined dispersed-phase elements. It contains spherical or nearly spherical droplets and occupies a relatively small volume fraction (less than 1%) compared to the continuous phase. This leads to infrequent drop collisions. It can be argued that neighbouring droplets do not directly influence heat transfer, mass transfer or drag coefficients of individual drops. Therefore it can be assumed that each droplet has enough freedom and space to interact with the gas phase without having direct affect from other droplets [23]. This enable the use of single-drop formulas to describe transport rates in dilute flow regions. However this does not mean that droplets are in a totally isolated environment, because transport to and from the droplets could change the structure and properties of the continuous phase. This is known as two-way coupling between the phases.

The small liquid volume fractions in the dilute region enable experimental observations and allow the validation of mathematical models easily. As a result, many features of dilute sprays are understood reasonably well [24].

The liquid fraction requirement for this dilute phase assumption is not well defined. There are several phenomena that can be considered and the one, which consider the effect of inter-drop spacing on drop transport rates, is one of the best understood methods. Experimental work has shown that for mono dispersed droplets in a convective environment; the single droplet transport formula can be applied reasonably well if the centre to centre distances of droplets are greater than two droplet diameters. This requirement implies a liquid fraction less than 0.08 [25]. A method of characterizing the dilute flow region is particularly important in pressure atomised sprays, because they have larger dense spray regions than air atomised sprays due to the existence of unity liquid fraction at the injector exit.

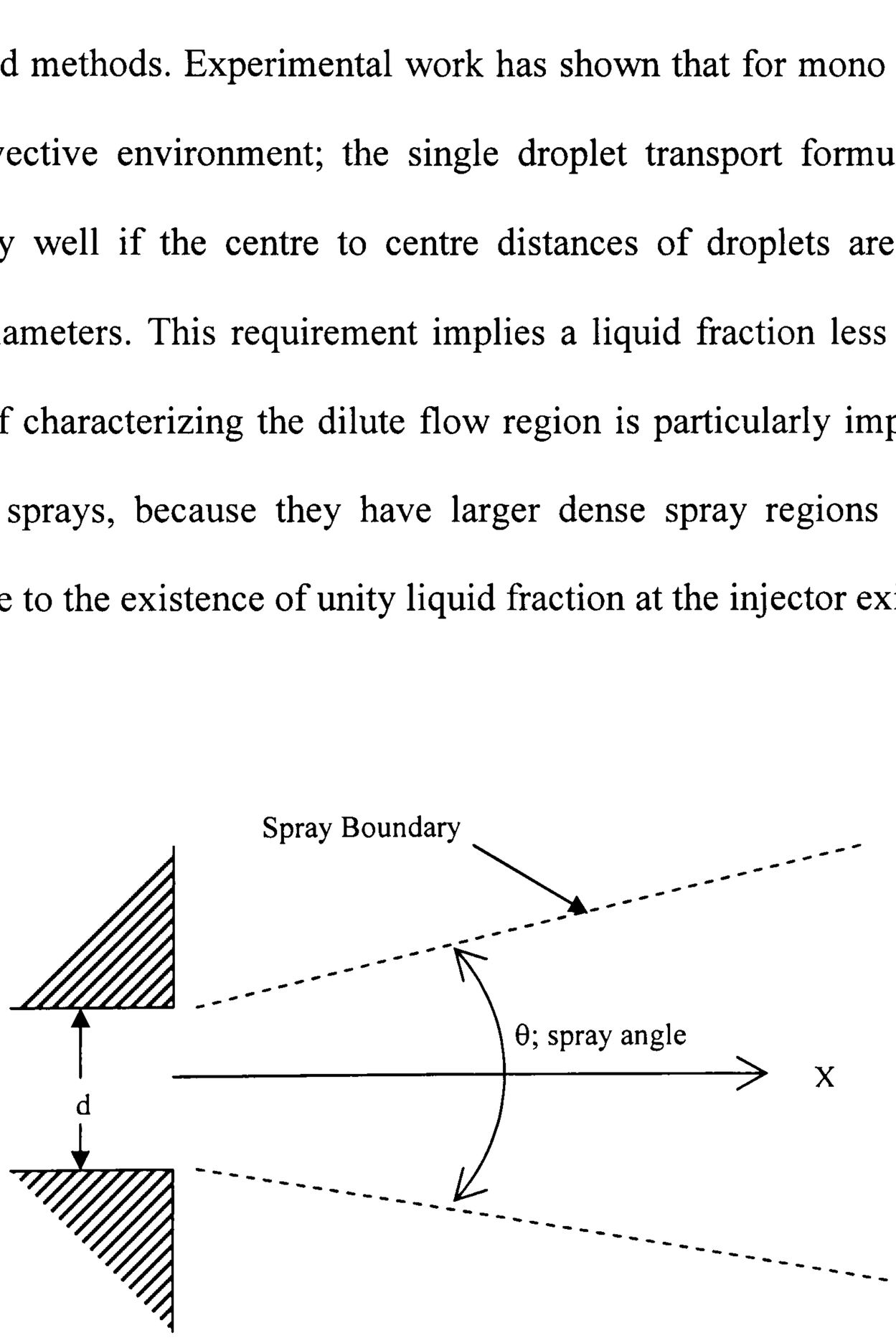

Fig. 2.3 Injector geometry of a pressure atomiser

According to Fig. 2.3 the total area of the two phase region could be defined by spray angle. For liquid fraction calculation, it is assumed that the liquid flow is uniformly distributed over the cross-section of the spray and the liquid flow velocity is equal to the injector exit velocity throughout the dense region. Then the liquid fraction for a one dimensional flow can be defined as the ratio of liquid and the total flow areas.

$$\alpha_{liquid} = A_{liquid} / (A_{liquid} + A_{gas}) \qquad (2.15$$

Based on above Fig. and using simple geometry, liquid fraction can be expressed as

$$\alpha_{liquid} = 1 \Big/ [1 + 2(x/d)\tan(\theta/2)]^2 \qquad (2.16)$$

It can be shown that for the spray angle range 12-25deg which is a common spray angle range for solid cone sprays, liquid fraction of less than 0.08 could be obtained at about 6-12 nozzle diameter distances from the injector exit.

Another phenomenon described by Crowe [22] is based on the way particles or droplets respond to gas phase variations. According to that, a dilute gas-particle flow is a flow in which the particle motion is controlled by local aerodynamic forces, whereas in a dense gas-particle flow particle motion is governed by particle-particle collisions. This phenomenon can be quantitatively established by the ratio of

aerodynamic response time (τ_A) to the time between collisions (τ_C). The aerodynamic response time is the time required for a particle, released from rest in a flowing stream, to achieve 63 percent of the free stream velocity. Thus, if $\tau_A / \tau_C < 1$, a particle has time to respond to the local gas velocity field before the next collision and that means its motion is dominated by aerodynamic forces. This flow is therefore considered as a Dilute Flow. On the other hand if $\tau_A / \tau_C > 1$, the particle does not have sufficient time to respond to aerodynamic forces before the next collision. This means particle motion is controlled by collisions. This represents a dense flow.

2.5.3 Fully mixed Region

The third region is the fully mixed region. In this segment of the flow, droplets are no longer present. All droplets have evaporated during the dilute flow region. Fuel is completely evaporated and move with air. This is a single-phase flow region having fuel vapour as a component of the air fuel vapour mixture.

2.6 Atomisation and Droplet break-up

The process of converting bulk fluid into a huge number of individual fragments or droplets is called liquid atomisation. Atomisation is fundamental to many industrial processes. When considering steady state spray combustion process as in a gas turbine, the combustion in the primary zone is influenced by the atomisation and also penetration of the liquid fuel spray. Characteristics of the fuel spray can also affect the NO_x and CO emissions. This results from the effects of atomisation on the rate of vaporisation and the subsequent rate of mixing of the fuel vapour with air. Also in large furnaces, used to heat or maintain constant temperature of liquid metals (e.g. liquid zinc bath used in hot-dip galvanizing), long flames are required to assist satisfactory heat transfer to the liquid metal. This is achieved by using atomisers designed to produce larger droplets to ensure good penetration. In fire safety systems, fire suppression by sprinkler system requires fine control of the atomisation process to produce droplets small enough to evaporate fast and large enough to penetrate into the fire. In waste incineration units burnout efficiency is known to depend on the width of the drop size distribution since large drops require considerably longer times to evaporate and burn completely.

According to the above it can be clearly seen that the characteristics of the spray is governed by the atomisation process. Therefore in spray combustion modelling it is very important to have clear understanding of fuel injection and atomisation processes in order to develop a realistic model. This is particularly

important in Separated Flow modelling approach because of the requirement of initial spray data.

Fig. 2.4 show a sketch of the near injector region of a pressure atomised spray which is based on the observations of Bracco and co-workers [26, 27]. As illustrated in the Fig. 2.4, all liquid flow at the beginning gradually develops to a dilute spray. When the dilute flow approximations are acceptable over the cross section of the flow, from that region onwards the spray is considered dilute. However, even in the dense spray region, a dilute region is exist near the periphery of the spray.

As the liquid leaves the injector, it enters a region called churn flow region which includes the liquid core and irregular shaped liquid elements. O' Rourke and Bracco [28] describes churn flows for sprays as a region where the volume fraction of the liquid is greater than that of the gas, so that the liquid cannot be considered as dispersed in gas phase. Since the gas density and volume fraction in this region is small, momentum exchange between the gas phase and liquid phase is relatively small. This leads to negligible relative velocity between the phases creating rather stable region for large liquid elements.

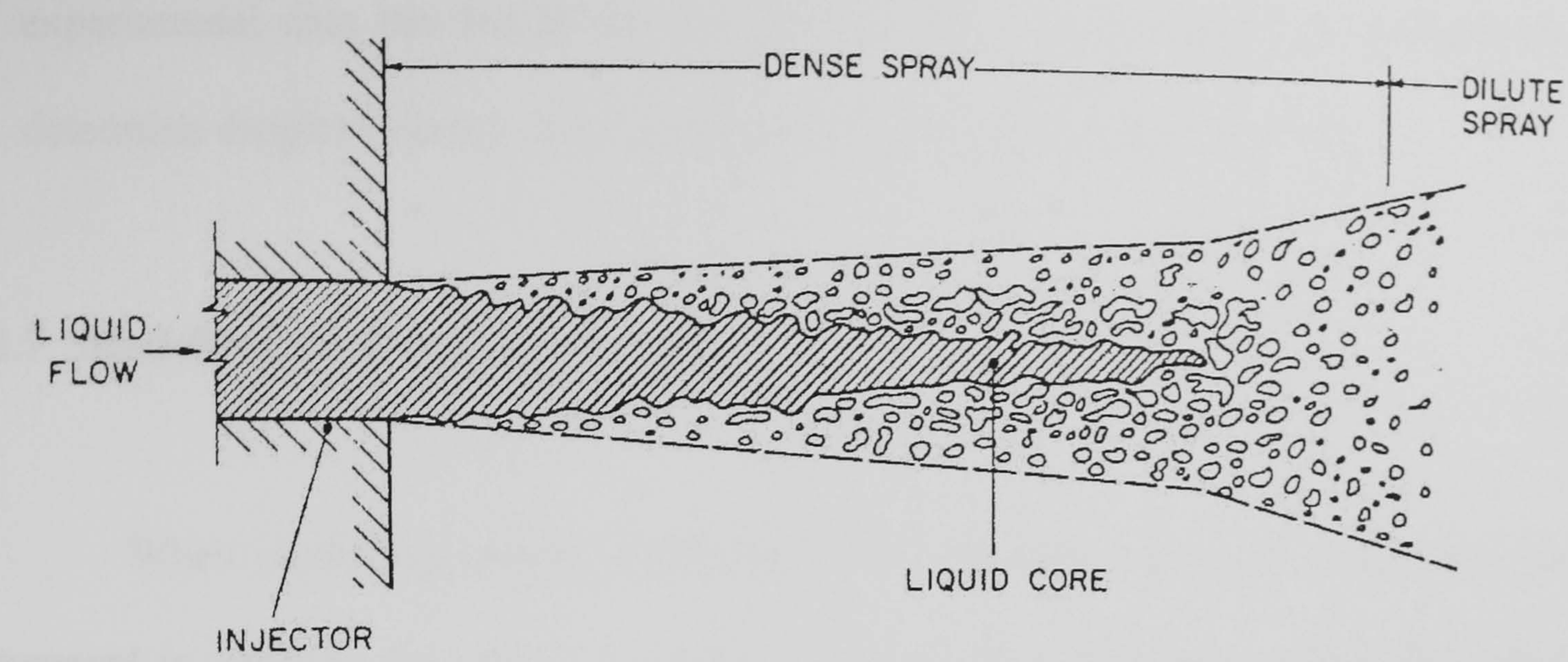

Fig. 2.4 Sketch of the near injector region of a pressure atomized spray

As liquid moves away from the injector the void fraction continuous to increase by mixing with slow moving air. When the large liquid elements move into the slow moving gas, the liquid elements become unstable (due to the velocity difference) and break up into rather small elements and droplets. This leads to various drop sizes with different shapes and velocities which ultimately increase the probability of drop collisions. Due to drop collisions droplets may break up into smaller drops or may collide and turn into even larger drops.

Nevertheless researchers are not able to get satisfactory experimental data at the spray inlet due to the dense flow structure near the injector. Even Laser Doppler Anemometry [29] has limited use because of the opaque nature of the flow. Solomon et al. [30] noted during his experimental analysis that, even for evaporating non burning sprays, it was not possible to determine droplet parameters at a distance closer than x/d=50 from the injector exit. This lack of reliable

experimental data has led to the use of empirical or semi-empirical methods to determine droplet velocity and size distributions with acceptable accuracy.

2.7 Modelling drop size distributions

When modelling sprays; particularly in Lagrangian approach, some way is required to describe the spray quantitatively. In general, a spray can be sufficiently described by its size and velocity distribution. As discussed earlier, the process of break-up of bulk liquid into a spray gives rise to drops with a range of sizes. These sizes are distributed from non zero minimum to a finite maximum diameter. Even so, for the mathematical ease, in most droplet distributions it is assumed that the diameters range from zero to infinity. This permits the use of probability density functions to describe size distributions.

Generally, a distribution; f(D) must be positive and normalized.

$$f(D) \geq 0$$

$$\int_0^\infty f(D)dD = 1 \tag{2.17}$$

when modelling a polydisperse phase like sprays it is often convinent to represent the distribution of droplets by a representative diameter and switch the problem to a mono-size dispersed phase case. Various representative droplet diameters can be calculated from the following equation:

$$D_{pq} = \left[\frac{\int_0^\infty D^p f(D) dD}{\int_0^\infty D^q f(D) dD} \right]^{\frac{1}{(p-q)}} \tag{2.18}$$

where p and q are positive integers. Commonly used representative diameters are

D_{10} = the arithmetic mean diameter

D_{30} = the volume mean diameter

D_{32} = the Sauter mean diameter

The traditional method of modelling drop size distributions is empirical; a curve is fitted to data collected from a particular atomizer nozzle. Most widely used methods are Nukiyama-Tanasawa, Rosin-Rammler, root-normal etc [31-33]. The problem with this approach is the difficulty of extrapolating the data outside the experimental [34] range. To overcome this, two analytical approaches have been developed recently; the Maximum Entropy (ME) method and the Discrete Probability Function (DPF) method. The ME method assumes that the most likely drop size distribution is the one which maximizes an entropy function under a set of physical constraints e.g. conservation of spray mass, minimization of surface energy. The DPF method, divides the spray formation process into deterministic and non-deterministic portions. The deterministic portion of the model describes the break-up of the initial fluid structure and non-deterministic portion describes the influence of fluctuating initial conditions on the resulting drop size distribution. It is assumed that the spray formation involves a series of break-up stages of the initial fluid structure. A fluid mechanic instability analysis can be used to describe the break-up process

[35]. The ME and PDF approaches require significantly large time and effort to model the drop size distribution, therefore in his work author has used the empirical methods to describe droplet distributions in his research and these are further discussed subsequently.

2.7.1 The root-normal distribution

This was proposed by Tate and Marshall [33] to express the volume distribution of drops in a spray. The root-normal distribution for droplet volume is

$$f_3(D) = \frac{1}{2\sigma_{RN}\sqrt{2\pi D}} \exp\left\{-\frac{1}{2}\left[\frac{\sqrt{D}-\sqrt{\overline{D}}}{\sigma_{RN}}\right]^2\right\} \tag{2.19}$$

where $\sigma_{RN} > 0$ and it represents the width of the distribution.

2.7.2 The Rosin-Rammler distribution

This was introduced by Rosin and Rammler [32] to describe the volume distribution of coal particles. The Rosin-Rammler distribution for droplet volume is

$$f_3(D) = q\overline{D^{-q}}D^{q-1}\exp\left\{-(D/\overline{D})^q\right\} \tag{2.20}$$

where $\overline{D}$ represents the mean and q represents the width of the distribution..

2.7.3 The Nukiyama-Tanasawa distribution

This was introduced by Nukiyama and Tanasawa [31] to describe the number distribution in sprays from a pneumatic atomizer.

$$f_0(D) = aD^p \exp(-bD^q) \tag{2.21}$$

where b, p and q are adjustable parameters. And $\boldsymbol{a}$ is a normalising parameter.

All the empirical distributions were proposed to describe experimental data sets. Therefore there is at least one experimental data set that is described well by a particular distribution. Also there may be some distributions which give admirable fit to a wide range of data. In order to find out which of those distributions is best fit for a wide range of data, Paloposki [36] et al compared data from these distributions with number of well known drop size distribution data provided by experimental studies. The results show that the Nukiyama-Tanasawa distribution provided the best fit. Log-normal distribution was reasonably accurate and Rosin-Rammler distribution performed poorly. Semiao et al. [37] has obtained a simplified equation of Nukiyama-Tanasawa type from the concept of entropy information, assuming spherical droplets and zero and infinity as limit sizes. The distribution function dependent solely on Sauter mean diameter, which is calculated from available correlations for pressure jet atomizers.

2.8 Mathematical techniques of analysing dilute disperse flows

Two-phase or multi-phase flow models can be broadly categorised based on the type of reference frame, **Lagrangian** or **Eulerian,** used. In the Lagrangian method, particles are tracked individually or in small groups as they travel through the flow field. The instantaneous position of a particle can be measured as a function of original particle location and the time spent. Lagrangian models are sometimes referred to as Discrete Droplet Models (DDM) because they treat particle phase as discrete, which is of course the natural way to treat the particles in dilute flows. These models are commonly used in applications such as spray and pulverized coal combustion systems. In Eulerian models, particles are treated as a continuum and properties of the particle phase are obtained solving partial differential equations of the particle phase in a given coordinate system. These models are also known as continuum models or two-fluid models. These models are popular when modelling dense flows [9, 38-40]. Also these are used in modelling dilute particle flows [9, 41].

This discussion of modelling multiphase flows will be divided into two sections, Eulerian models and Lagrangian models and the discussion will be focused mainly on modelling dilute flows using the Lagrangian approach. Turbulence modelling will also be discussed, since it is required in both Eulerian models and gas phase modelling in Lagrangian models.

It must be emphasised that it is essential to validate these models against experimental data. Experimental data for sprays with reacting and non reacting

conditions are essential not only to validate computational models but also to improve the understanding of the processes involved in two phase flows and thereby improve the computational models further. While there are sufficient number of resources from experimental data for non evaporating particles like (glass, copper and corn pollen etc), it is still very difficult to find experimental data with well-defined boundary conditions for liquid fuel sprays. The modelling of two-phase flows, specially using Lagrangian approach, it requires initial data such as; droplet size distribution, velocity distribution and mass fraction distribution. Parameters that can not be obtained from experimental data need to be assumed or arrived at using empirical or semi-empirical models.

2.9 Eulerian Models

In the Eulerian approach the particle or droplet cloud is treated as a continuous medium. Because of this, continuous medium properties like density and velocity, which are not the actual material properties for the particle phase, need to be defined. The particle material density is replaced with the bulk density which is the mass of particles in unit volume of the mixture. The particle velocity used is the average velocity of droplets over an averaging volume. Since the current turbulent models developed to model continuous phases are in Eulerian form, it was convenient to develop a method to model dispersed phase using Eulerian approach. As both phases are modelled using Eulerian approach these models often called Eulerian-Eulerian models [2].

According to the flow systems being modelled, Eulerian models have a number of different branches or levels. If the particles and gas phase have the same velocity and temperature and assumed to be in phase equilibrium at each point of the flow, then two–phase mixture could be regarded as a single phase with modified properties. On the other hand, if there is a significant velocity difference between gas and particle phases; (which is true for the most gas particle flows), then both phases must be considered separately and treated as two inter-penetrating continuous flows.

2.9.1 Turbulence modelling

Turbulence is the most difficult theoretical problem in fluid dynamics since turbulence makes the fluid flow problem unpredictable. However, when dealing with practical engineering problems some means of modelling is needed. The earliest and simplest method is to use turbulent viscosity or turbulent diffusivity as a constant property of the flow.

The fundamental approach to study turbulence is the direct numerical simulation using Navier-Stokes equations with the grid size in the order of Kolmogorov scales without using any turbulence models. However, the number of grid point required to resolve the details of the flow would be huge [42]. Therefore to deal with practical engineering applications, mathematical models are required to take into account the turbulence. Rather than relying on empirical experimental methods, techniques have been developed that allow turbulent flows to be analysed to obtain useful information. The most common method of analysing turbulent flows is to perform **Reynolds decomposition** and then average the set of governing equations over time. The resulting governing equations are called the **Reynolds-averaged** equations. The time averaged equation of the turbulent flow for a generic variable can be written as follows [2].

$$\frac{\partial(\rho\varphi)}{\partial t}+\frac{\partial(\rho v_j\varphi)}{\partial x}=\frac{\partial(\frac{\mu}{\sigma_\varphi}\frac{\partial\varphi}{\partial x_j})}{\partial x_j}-\frac{\partial(\rho\overline{v_j'\varphi'})}{\partial x_j}+S_\varphi \qquad (2.22)$$

where φ is the generalised dependent variable and S_φ is the source term. The superscript denotes the fluctuating components of the generalised variable (φ) and the velocity component (v_j).

However, this averaging process has two major consequences;

1. It eliminates the fine details of the flow. For example, the complex time dependent velocity at a point could not be predicted using time averaged equations.
2. Due to the averaging process some new terms appear in the time averaged equations which do not have similarity with the original equations

The dashed terms are the new terms arising due to the averaging process. For a two dimensional flow configuration, the generalised variable of the momentum equation at 'j' direction is a the tangential velocity v_i. Then the new term arising due to the averaging can be written as $-\rho\overline{v_i'v_j'}$. This represents additional momentum flux resulting from the turbulent fluctuations. These are called turbulent stresses or Reynolds stresses. Similarly, time averaged transport equations for scalar variables also add extra terms containing $\overline{v_j'\varphi'}$. The basic idea of turbulence modelling is to simulate these unknown higher order correlation terms that appear due to Reynolds averaging by using lower order correlations or mean flow properties. This treatment is acceptable, since in an engineering problem only time averaged quantities like velocity, temperature and turbulence characteristics are needed. But it has to be emphasised that even the simplest

turbulence models are complex when dealing with practical engineering problems. The most common turbulence models are

1 Zero equation model- mixing length model

2 Two-equation model- k-ε model

3 Reynolds stress equation model

4 Algebraic stress model

From these models the k-ε is the most widely used. The mixing length and k-ε models are based on the assumption that there is an analogy between the action of viscous stresses and Reynolds stresses on the mean flow. In 1877, Boussinesq proposed that Reynolds stresses could be related to mean rates of deformation [8]. This leads to the following relation between Reynolds stresses and mean properties of the flow.

$$-\rho v_i' v_j' = \mu_t \left(\frac{\partial U_i}{\partial x_j} + \frac{\partial U_j}{\partial x_i} \right) \tag{2.23}$$

where μ_t is turbulent or eddy viscosity.

Similarly, turbulent transport of a scalar property; Φ is taken to be proportional to the gradient of the mean value of the transported quantity (Φ).

$$-\rho v_i' \varphi_j' = \Gamma_t \frac{\partial \Phi}{\partial x_i} \tag{2.24}$$

where Γ_t is the turbulent diffusivity and φ' is the fluctuating component of the scalar property Φ . This can be related to the turbulent viscosity μ_t by introducing a Prandtl/Schmidt number as follows:

$$\sigma_t = \frac{\mu_t}{\Gamma_t} \tag{2.25}$$

Substituting (2.24) in equation (2.22) and rearranging, gives

$$\frac{\partial(\rho\varphi)}{\partial t} + \frac{\partial(\rho v_j \varphi)}{\partial x} = \frac{\partial(\Gamma_\varphi \frac{\partial \varphi}{\partial x_j})}{\partial x_j} + S_\varphi \tag{2.26}$$

where Γ_φ denotes the generalised transport coefficient given by

$$\Gamma_\varphi = \frac{\mu_e}{\sigma_\varphi}$$

and μ_e is called effective turbulent viscosity ($\mu_e = \mu_t + \mu_{laminar}$).

However, the introduction of the turbulent viscosity does not complete closure. Now the problem is transformed into determining a value or the functional form of turbulent viscosity which depends on the flow. Mixing length models attempt to solve this by means of a simple algebraic formula for turbulent viscosity as a function of position. The k-ε model is more advanced and allows for the transport of turbulence properties by mean flow and diffusion and for the production and destruction of turbulence.

2.9.1.1 Mixing length model

This is the simplest method used to model turbulence by using Prandtl's hypothesis. Prandtl's hypothesis states that the eddy viscosity is propotional to the product of the fluid density, a length scale called the mixing length and a characteristic turbulent velocity which is given by

$$\mu_t = \rho l_m v_t \tag{2.27}$$

also it is assumed that the turbulent velocity, v_t, is proportional to the product of the mixing length and the magnitude of the mean velocity gradient. For a two dimensional situation v_t can be taken as

$$v_t = l_m \left| \frac{\partial v_j}{\partial x_i} + \frac{\partial v_i}{\partial x_j} \right| \tag{2.28}$$

Combining the above equations, the turbulent viscosity can be expressed as

$$\mu_t = \rho l_m^2 \left| \frac{\partial v_j}{\partial x_i} + \frac{\partial v_i}{\partial x_j} \right| \tag{2.29}$$

in order to attain the closure of the problem, the mixing length has to be specified. Since the mixing length depends on the flow, different specifications are required for each kind of flow [43]. Therefore mixing length functions are given for a variety of flows and for a free axisymmetric jet, it can be given as:

$$l_m = 0.075L \tag{2.30}$$

where L is the half width of the jet.

Advantages and disadvantages of the mixing length model

- The model is simple and no additional differential equations need to be solved.
- If good choices are made for the mixing length, good predictions can be achieved.
- Incapable of handling recirculating flows
- The model takes no account of the effects of convection and diffusion on turbulence

2.9.1.2 *k*-ε model or two equation model

It is possible to express the influence of turbulence using mixing length if the turbulence convection and diffusion of turbulence properties can be neglected. But most of the practical flows contain regions with recirculation which makes the mixing length method inadequate. By considering the dynamics of turbulence, several models with two- equations have been developed such as k-kl model of Rodi and Spalding, k-W model of Spalding [44, 45] and the k-ε model by Harlow and Nakayama [46]. From these the k-ε model has become the most widely used model. This model can handle effects of transport of turbulence properties by mean flow and diffusion and for the creation and destruction of turbulence [8].

The general form of the k equation is as follows:

$$\frac{\partial}{\partial t}(\rho k)+\frac{\partial}{\partial x_j}(\rho v_j k)=\frac{\partial}{\partial x_j}\left(\frac{\mu_e}{\sigma_k}\frac{\partial k}{\partial x_j}\right)+G_k+G_b-\frac{C_D\rho k^{\frac{3}{2}}}{l} \qquad (2.31)$$

$$G_k=\mu_T\left(\frac{\partial v_i}{\partial x_j}+\frac{\partial v_j}{\partial x_i}\right)\frac{\partial v_i}{\partial x_j}$$

$$G_b=-\beta g_j\frac{\partial \mu_T}{\partial \sigma_T}\frac{\partial T}{\partial x_j}$$

where:

G_b buoyancy production term

G_k mean production term

β thermal expancivity

g the body force term

C_D drag coefficient

σ_k effective Prandtl number for turbulent kinetic energy (constant)

σ_T known constant

The general form of the ε equation is as follows:

$$\frac{\partial}{\partial t}(\rho\varepsilon)+\frac{\partial}{\partial x_j}(\rho v_j\varepsilon)=\frac{\partial}{\partial x_j}\left(\frac{\mu_e}{\sigma_\varepsilon}\frac{\partial \varepsilon}{\partial x_j}\right)+\frac{\varepsilon}{k}(c_1G_k-c_2\rho\varepsilon) \qquad (2.32)$$

where c_1, c_2 and σ_ε are constants and the term G_k is the one used in the k equation.

Advantages of the model:

The k-ε model is simple enough to model while being able to produce meaningful results for recirculating flows such as confined flows (pipe, channel and nozzle flows).

Disadvantages of the model:

This model is more complex than mixing-length model and the performance is poor for swirling flows.

2.9.1.3 Higher order turbulence models

Both turbulence models described above are for isotropic turbulent flows. But in practical, most of turbulent flows are non-isotropic, which require direct solution of the Reynolds stress equations by simulating the unknown third order terms in the equations with second order correlations (second order moment closure) [2], which is called Reynolds stress model. This has been applied successfully to predict strongly swirling and buoyant flows in combustors and furnaces and the predictions were better than that given by the k-ε model. The main drawback is that the model is too complex engineering predictions, because this method requires 11 equations to be solved whereas in the k-ε model only two equations are solved. Another model is Algebraic stress model, which is an economical way of accounting for the anisotropy without

solving the full length of Reynolds stress equations. The main idea is to reduce the stress equations into algebraic expressions by using some simplifications, while retaining the basic features of non-isotropic turbulence [8].

2.9.2 Locally Homogeneous Flow (LHF) analysis

LHF analysis implies that all phases are in dynamic and thermodynamic equilibrium. This implies that at each point in the flow, all phases have the same velocity and temperature and are in phase equilibrium. In reality this is not true; slip between the two phases is a significant factor. LHF analysis therefore only accurately represents two-phase flows, whose disperse phase elements are infinitely small. This leads to fundamental errors being present when LHF analysis is used for practical systems that contain relatively large droplets or higher droplet mass loading. However due to the uncertainties in required inlet parameters for more complete analysis, LHF analysis is presently a viable option [23].

With the above assumptions, properties at each point in the flow correspond to a thermodynamic equilibrium state is attained when liquid from the injector and ambient fluid (air), at their initial state, are mixed adiabatically at the ambient pressure. The equation of state provides the relationship between the mixture fraction, temperature and density of the mixture. The feature that distinguishes a two phase flow from a single phase flow when a LHF method is used, is the presence of liquid at high mixture fractions in control volumes. The liquid evaporation is accounted for via saturation vapour pressure function of the form [47]:

$$\log_{10} P_{fg} = a - \frac{b}{T} \tag{2.33}$$

where P_{fg} is the partial pressure of the fuel vapour in the control volume and ***a*** and ***b*** are known constants for a specific fuel. The mass fractions of the evaporated and the liquid parts of the fuel can be obtained by the following relationships (molar fractions of the gas phases; air and fuel vapour, are proportional to the partial pressures):

$$Y_{Fg} = Y_A P_{Fg} \frac{M_F}{P_A M_A} \tag{2.34}$$

$$Y_{Ff} = Y_F - Y_{Fg} \tag{2.35}$$

where Y_{Ff} and Y_{Fg} are the mass fractions of the liquid and the vapour parts of the fuel present in the control volume (P_A, Y_A, M_A are the partial pressure, mass fraction and molar mass of the air; Y_F, M_F are the mass fraction and molar mass of fuel in the gas phase control volume)

2.9.2.1 Advantages and Disadvantages of LHF method

Advantages of LHF analysis are as follows; relatively little information is required to specify initial condition for computations, because initial dispersed phase size and velocity distributions are not needed; the formulation is equivalent to a single-fluid flow analysis, which simplifies calculations and LHF can handle relatively complex flows involving appearance and disappearance of variety of phases [38]. LHF predictions for combusting flow by Mao et al [48, 49] using n-propane spray showed good agreement against experimental data for temperature and centreline mean velocity.

The performance of advanced SF models becomes very poor without accurate initial conditions at the injector exist. Since it is very difficult to obtain experimental injection properties for spray nozzles, LHF analysis has become an attractive modelling tool to provide a reasonable first approximation to the behaviour of the spray [41]. Faeth G.M. [23] suggested that LHF analysis might be effective for estimating the mixing and turbulent dispersion properties of the dense region of pressure atomised fuel sprays. Nazha and Rajakaruna [38] have presented an "effective property LHF model" that includes a droplet evaporation module to be used in this kind of complex modelling situations. This "Effective property LHF model (ELHF)" also demonstrated the applicability of the LHF method to model dense region of the spray.

In order to asses the applicability of LHF models to sprays with finite drop sizes, Shearer et al [47] predicted the drop life histories along the centreline of an evaporating Freon-11 spray. When gas and drop velocities were compared, it was observed that even the droplets as small as 10μm have significant relative velocities or slip up to some distance from the injector. This supports the previous researcher's claim that LHF predictions are satisfactory when particle or drop diameters are less than 10μm.

2.9.3 Eulerian-Eulerian approach or Two Fluid model

Eulerian approach treats both continuous and particle phases as continuous media. The method involves solving partial differential equations for both continuous and particle phases. The volume concentration of each phase needs to be introduced and the continuity, momentum and energy equations for both phases need to be solved. Then the influence of the liquid or solid particles on the continuous flow needs to be taken as proportional to the void fraction of the particle phase. Unlike the LHF model, the two-fluid model can account separately for large slip and particle diffusion with no direct relation between them and can fully account for particle mass, momentum and energy diffusion [50].

The basic idea of this model is to consider the particle phase as a continuum interpenetrating with the continuous phase. The basic assumptions used are [2]:

1. At each location of the flow field, both gas phase and particle phase coexist and interpenetrate into each other, each having its own velocity, temperature and volume fraction
2. Each particle phase has continuous velocity, temperature and volume fraction distribution in space.
3. Each particle phase has its own turbulent fluctuation resulting from particle turbulent transport of mass, momentum and energy.
4. Particle groups are identified by their initial size distribution.

Eulerian approach is good for mono-size dispersed flows. When the number of phases or numbers of particle size groups to be considered are high the number of continuous fields to be considered becomes high, leading to a high number of PDEs [51, 52]. This makes mathematical formulation more complex. Also the methods used to treat dispersed phase-turbulence interactions in this approach have not been evaluated to a great extent. Although the Lagrangian approach overcomes these difficulties, when particle loading is high, discrete formulation tend to have convergence problems. This is due to the fact that Lagrangian formulation does not take into account the volume occupied by the droplet or particles, when solving the gas phase flow field. On the other hand the Eulerian approach can easily handle this kind of dense flows and suspension flows with high void-fractions [53-55].

Gouesbet and co workers [52, 56, 57] done extensive predictions and experimental validations of solid particle sprays using an Eulerian approach. Predictions were compared with experiments from Snyder and Lumley [58] and Wells [59] and found that the predictions were in close agreement with experiments.

Perrell et al. [60] proposed a new method to over come the need to discretise the polydispersed phase into different sizes by using a continuous distribution of sizes. Parameterised functions are assumed for both the particle size and velocity. A one-dimensional nozzle flow calculation is performed and compared with standard Eulerian calculations and is shown close agreement.

2.10 Lagrangian approach or Trajectory method

Lagrangian approach treats the fluid phase as a continuum and predicts the trajectory of a single particle in the fluid flow as a result of various forces acting on the particle. By assuming different starting positions of the particles and following their trajectories, a particle-fluid flow can be simulated. As the locations of the particles are known, the mass, momentum, and energy transfers of the particles to the fluid phase and vice versa can be calculated [4].

In the discrete element formulation, the dispersed- phase is divided into a number of groups and then their motion and mass, momentum and energy transfers are tracked through the flow field using a Lagrangian formulation. An Eulerian formulation is used to solve the governing equations for the continuous phase as in LHF type analysis. However, due to the finite transport rate between the disperse phase and the continuous phase, source terms are introduced to the governing equations of the continuous phase [61].

Discrete-element formulations can be divided into two types as follows:

1) Deterministic Separated Flow (DSF) analysis, where finite inter-phase transport rates are considered without particle diffusions

2) Stochastic Separated Flow (SSF) analysis, where both finite inter-phase transport rates and particle diffusion are considered using random-walk computations for the motion and transport of the dispersed-phase [12].

In discrete formulation, which is well known as particle trajectory method, the following basic assumptions are used [2].

1) The particle phase is a discrete system, and there is a slip between the gas and the particle phases in both velocity and temperature, which leads to dynamic and thermodynamic non-equilibrium.

2) Particle diffusion is not taken into account in deterministic formulations.

3) Particle groups are identified by their initial size, each having the same size, velocity and temperature at any instant.

4) Each particle group moves along its own trajectory from a certain initial position, and the particle's mass, velocity and temperature changes are tracked along the trajectory.

5) Particle mass, momentum and energy sources (sinks) are used in gas-phase calculations [6].

The relative advantages and disadvantages of two-fluid and trajectory approaches to modelling gas-particle flow can be summarised as follows. The two-fluid models can easily incorporate particle diffusion effects (if data are available) and can be extended easily to multidimensional flows. However, numerical instabilities, numerical diffusion and large storage requirements for multiple particle sizes are inherent difficulties. The trajectory approach embodies the "natural" solution schemes for each phase and exhibits no numerical diffusion of the particle phase. Also, storage requirements for multiple particle sizes are not excessive. But particle diffusion must be incorporated through an empirical diffusion velocity or more expensive Monte Carlo methods. [4, 25]

2.10.1 Deterministic Trajectory Models

In particle trajectory models the particle phase is evaluated using Lagrangian coordinates. The method of the Lagrangian treatment for the particle phase combined with the Eulerian approach for the continuous phase was first proposed by Migdal and Agosta. They showed that particles could be treated as sources of mass, momentum and energy to the continuous flow field [2]. For this method the generalised gas-phase conservation equation for a variable φ in cylindrical coordinates takes the form given below in equation (1):

$$\frac{\partial}{\partial x}(\rho u\varphi)+\frac{1}{r}\frac{\partial}{\partial y}(r\rho v\varphi)=\frac{\partial}{\partial x}\left(\Gamma\frac{\partial\varphi}{\partial x}\right)+\frac{1}{r}\frac{\partial}{\partial y}\left(r\Gamma\frac{\partial\varphi}{\partial y}\right)+S_{\varphi}+S_{\varphi}^{p} \tag{2.36}$$

Equation (1) contains the additional source term S_{φ}^{p}, which represents the net efflux of φ into the fluid phase due to particle-fluid interaction. This source term is calculated by solving Lagrangian equations for the corresponding particle variable φ^{p}. Simplified particle momentum equation in Lagrangian coordinates can be written as (2.37):

$$m_d\frac{dv}{dt}=C_D\rho\frac{A_d}{2}(U-v)|U-v|+m_d g \tag{2.37}$$

details of how to deduce this equation from the complex nonlinear paticle momentum equation will be discussed in the next chapter.

The procedure begins by solving the gas flow field using a numerical scheme such as SIMPLE [8]. In most cases the standard two-equation k-ε turbulence model is employed for the prediction of turbulence transport of the gas phase [3, 62].

Initially the method assumes that there are no particles present in the flow field and a pure gas field is solved. Then using this flow field, particle trajectories, and the temperature and mass history of the particle, on each trajectory are calculated. Particle properties crossing the boundaries of computational cells yield the mass, momentum and energy source terms for the continuous phase in each cell. Then the continuous flow field is recalculated, incorporating these source terms. Based on these flow field properties new trajectories are calculated and source terms are then re-evaluated. This process is continued until the flow field is converged. One interesting feature of the trajectory approach is the absence of numerical diffusion of the particle cloud, which is a problem in the two-fluid method. This is the essence of the so-called PSI-cell (Particle-Source-In-Cell) approach, which was initially developed by C.T. Crow and co-workers at Washington State University [22, 63].

The method is represented in the flow chart given in Fig. 2.5.

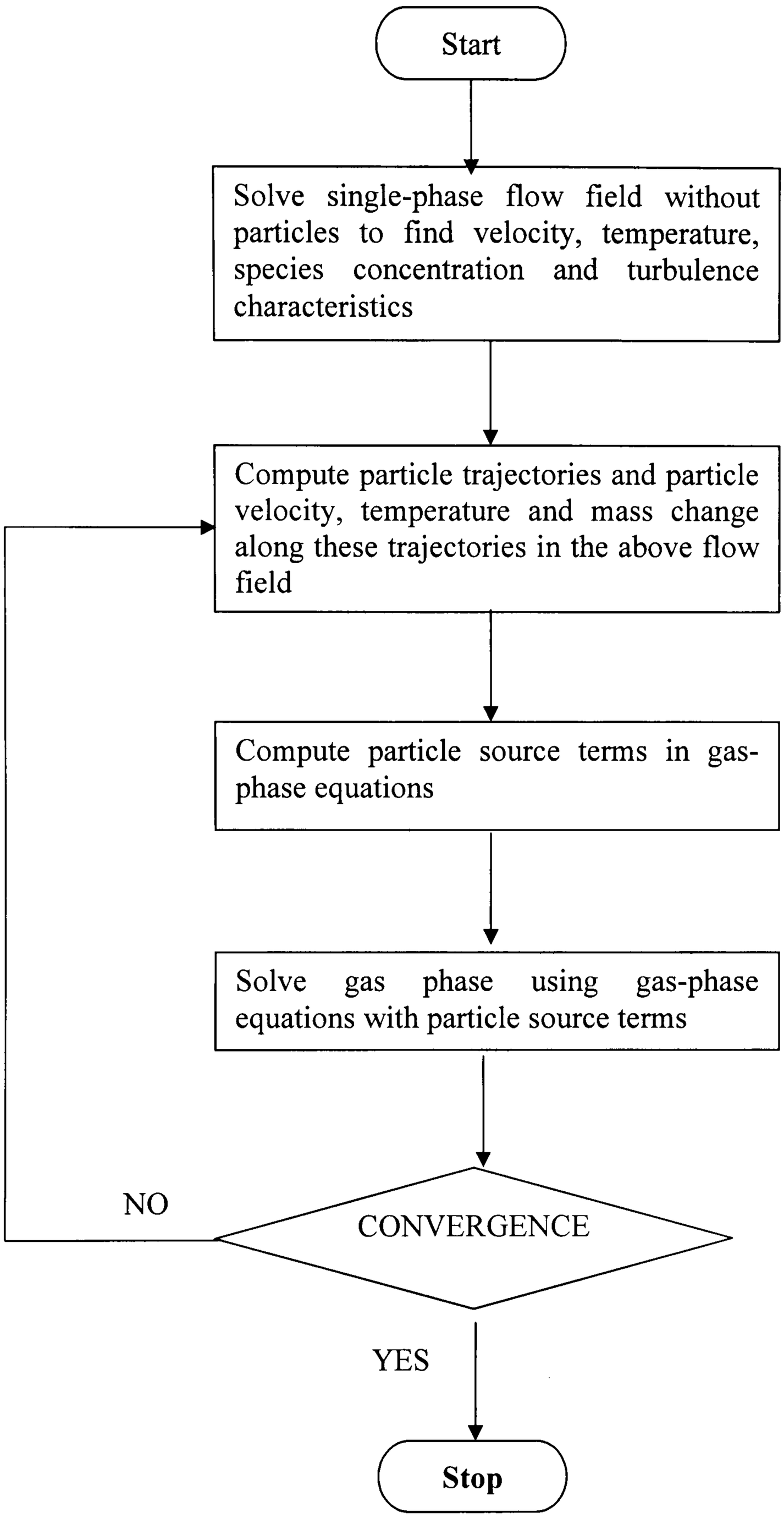
Start
Solve single-phase flow field without particles to find velocity, temperature, species concentration and turbulence characteristics
Compute particle trajectories and particle velocity, temperature and mass change along these trajectories in the above flow field
Compute particle source terms in gas-phase equations
Solve gas phase using gas-phase equations with particle source terms
CONVERGENCE
NO
YES
Stop

Fig. 2.5

2.10.1.1Modifications to particle turbulent diffusion

In the deterministic trajectory model it is assumed that the total particle number is constant along a trajectory with no particle diffusion due to turbulence in the flow. This means deterministic separated flow approach accounts only for the convection of the particles due to gas phase mean velocities and ignores the fluctuating component of the gas flow velocity present due to turbulence [64]. Experiments in this field have revealed that in many cases particle diffusion due to turbulence cannot be neglected [65]. In computational modelling of sudden-expansion gas–particle flows based on deterministic particle trajectory model, the predicted results showed that the particle trajectories were concentrated near the axis [66]. In reality, particles disperse almost throughout the flow field. Therefore certain modifications need to be carried out in the deterministic model in order to account for particle diffusion. This can be done by modifying the deterministic models by taking into account turbulent diffusion of droplets by approximating diffusive component of the particle velocity; $v_{p;k}^{d}$. Then the particle velocity at the trajectory 'k' is given by

$$v_{p;k} = v_{p;k}^{c} + v_{p;k}^{d} \tag{2.38}$$

where $v_{p;k}^{c}$ is the particle convective velocity due to mean gas phase velocity. $v_{p;k}^{d}$ is called **particle diffusive drift velocity**, which was first proposed by Smoot and Lockwood [2] and this is calculated using Fick's diffusion law

$$- \rho_k v_{p,k}^d = -n_k m_k v_{p,k}^d = D_k m_k \frac{\partial n_k}{\partial x_k} \tag{2.39}$$

This can be rearranged as

$$v_{p,k}^d = -\frac{D_k}{n_k}\frac{\partial n_k}{\partial x_k} \tag{2.40}$$

where D_k is particle diffusivity and n_k is particle number density.

Particle diffusivity can be evaluated using Hinze-Tchen formula.

$$\frac{\nu_{p;k}}{\nu_t} = \frac{1}{(1+\tau_{rk}^{'}/\tau_T)} \tag{2.41}$$

and

$$D_k = \frac{\nu_k}{\sigma_{kp}} \quad , \quad \sigma_{kp} = 0.35\sim0.7 \tag{2.42}$$

where ν_T is the gas turbulent viscosity, ν_k is the particle turbulent viscosity τ_T is the gas phase fluctuation time or Lagrangian fluid time scale and σ_{kp} is the turbulent particle Schmidt number. These can be obtained using the following formulas:

$$\nu_T = C_\mu \frac{k^2}{\varepsilon} \tag{2.43}$$

$$\tau_T = \sqrt{3/2}C_\mu^{3/4}\frac{k}{\varepsilon} \tag{2.44}$$

$\tau_{rk}^{'}$ is the particle relaxation time, which is determined by

$$\tau_{rk}^{'} = \frac{\overline{\rho}_p d_k^2}{18\mu} \tag{2.45}$$

After determining particle diffusivity using the above formulas, the task left is to determine particle number density. This is given by

$$n = \frac{\sum_k \dot{n}_k \Delta t_k}{V} \tag{2.46}$$

where Δt_k is the time required for the particles in the k^{th} trajectory to traverse the cell and V is the volume of the computational cell. When calculating particle number density; **n,** it is more realistic if normalised number density is used. Because in a spray there are various droplet sizes and effect from different drop sizes may not be the same. In order to obtain normalised number density Smoot et al [67] solved the particle diffusion equation in Eulerian approach along with the gas phase calculations

Another method proposed by Jurewicz and Stock et al [68] for turbulent diffusion, using a gradient **diffusion approximation** within the Lagrangian formulation for the motion and transport of the dispersed phase. This involves the defining of an effective diffusion velocity or diffusion force in the equation of motion of the dispersed phase [2, 23, 69-71]. This method can be described as follows:

Jurewicz and Stock [68] assumed that the turbulent diffusion can be treated as a body force acting on particles. Then the simplified particle motion equation can be written as

$$\frac{dv_p}{dt} = \frac{1}{\tau}(u - v_p) + f_B \tag{2.47}$$

integrating this over a small time step

$$v_p = v_{p_0} e^{-t/\tau} + (u + \tau f_B)(1 - e^{-t/\tau}) \tag{2.48}$$

where v_{p0} is initial particle velocity and f_B is the drift force which is defined as

$$f_B = \frac{v_{p;diff}}{\tau} \tag{2.49}$$

where $v_{p;diff}$ is called particle diffusion drift velocity, which can be obtained using Fick's law of diffusion. The mass flux relative to the mass-averaged velocity is

$$J_p = \rho_p (v_p - v^*) \tag{2.50}$$

where ρ_p is the particle mass concentration (particle apparent density) and v^* is the mass averaged velocity defined by

$$v^* = \frac{\rho_p}{\rho_m} v_p + \frac{\rho}{\rho_m} u \tag{2.51}$$

where ρ_m is mixture density. If the particle mass fraction is small, which is the case for dilute flows, and can be neglected, then the gas phase mass fraction becomes unity. This leads to

$$v^* \approx u$$

then the equation for mass flux due to diffusion becomes

$$J_p = \rho_p (v_p - u) \tag{2.52}$$

the term v_p-u is called diffusion velocity

According to Fick's law

$$J_p = -\rho_m \varepsilon_p \frac{d\omega_p}{dx} \tag{2.53}$$

where $\omega_p = \rho_p / \rho_m$ is the mass fraction of particles, and ε_p is the turbulent particle diffusivity. Therefore particle diffusion velocity can be written as

$$v_{p;diff} = -\frac{\varepsilon_p}{\omega_p}\frac{d\omega_p}{dx} \tag{2.54}$$

the particle eddy diffusivity (ε_p) is related to the fluid turbulence through the turbulent Schmidt number.

$$Sc_T = \frac{\varepsilon_{gas}}{\varepsilon_p} \tag{2.55}$$

where $\varepsilon_{gas} = \mu_{eff} / \rho$ (ε_{gas} is gas/air momentum diffusivity) and μ_{eff} is the effective gas viscosity.

Therefore

$$v_{p;diff} = -\frac{\varepsilon_{gas}}{Sc_T \omega_p}\frac{d\omega_p}{dx} \tag{2.56}$$

and the particle velocity can be written as

$$v_p = v_{p_0} e^{-t/\tau} + (u - \frac{\varepsilon_{gas}}{Sc_T \omega_p}\frac{d\omega_p}{dx})(1 - e^{-t/\tau}) \tag{2.57}$$

Dukowics et al. [61] proposed another method by employing estimated turbulent gas/particle exchange coefficients to compute particle dispersion. In this case, the turbulent exchange coefficient is related to the variance of the probability density function (Gaussian) of particle position at the end of each computational time step. Then the distribution is randomly sampled to obtain the change in particle position due to diffusion.

These diffusion models are easy to implement and incorporate in deterministic separated flow models. However, due to the simplifying assumptions involved, they are unable to account for the dispersion completely. For example trajectory calculated using the model proposed by Smoot [67] for pulveized-coal particles in an axisymmetric reactor, Shirolkar and Queiroz [66, 72] observed that the dispersion model only accounts for mean particle behaviour, which is against the experimental observations. However, experimental analysis and numerical predictions of Gosman and Ioannides [73] and also of Solomon at al [74] suggest that for rapid evaporating droplets it might be possible to ignore the effect of turbulent dispersion.

2.10.1.2 Deterministic method evaluation

There are numerous studies carried out by researchers using deterministic approach [75, 76] and some of these approaches will be discussed. Initially Crowe et al. [2, 6, 12, 77] and co-workers done some parametric studies and demonstrated the applicability of PSI-Cell to practical situations like fire sprinklers , spray drying and evaporating fuel sprays. Then Jurewicz and stock et al. [68] proposed a method to include turbulent particle dispersion to the deterministic method by assuming dispersion as a body force exerted on the particle. Also, they further improved the model to take account of electrostatic force on a particle and showed the applicability of the deterministic model to electrostatic precipitators. Zhou et al. [2] used the deterministic approach and k-ε gas turbulence model to model an evaporating spray-air two-phase flow caused by opposite injection of a swirl atomizer into a heated air flow. Predicted droplet trajectories showed fairly good agreement with experimental results. Also, the predicted velocity profiles were in good agreement with experiments. However, Zhou et al. noted that predicted droplet mass flux in the near axis region is lower than experimental values. Obviously, this is due to the exclusion of particle turbulent dispersion in the deterministic trajectory model.

2.10.2 Stochastic Separated Flow (SSF) methods

Stochastic separated flow methods have been proposed by a number of researchers, as a means of predicting dispersed-phase turbulence interactions without depending on empirical data to predict properties like turbulent diffusivity of the dispersed phase as used in gradient diffusion models. This method takes into account the instantaneous velocity, which include both mean and turbulent fluctuating parts of the velocity field of the flow to calculate particle or droplet trajectories. Since the particle momentum equation is solved with instantaneous velocity at each time step, the main challenge in SSF models is to determine the fluctuating velocity of the gas/fluid at the particle location. Depending on the modelling situation several different assumptions are made in order to estimate the gas phase fluctuating velocity at the particle location. The main distinguishing characteristic in SSF models is whether they account for the temporal correlations of the fluctuating velocity or not. Also, unless the flow approximates isotropic behaviour, the velocity fluctuations are directionally correlated. The gas phase solutions are obtained by solving time averaged Navier-Stokes equations, which provide time-averaged Reynolds stresses. So, if this time averaged turbulent properties of the gas/fluid flow field are used to obtain fluctuating velocity, it is obvious that the time dependent correlations are not satisfied. To avoid this problem it is assumed that the same fluctuating fluid velocity acts on the particle/drop for a time interval known as interaction time between the particle and a turbulent eddy. This interaction time is the minimum of the eddy lifetime and the eddy transit time. It is also assumed that the fluid velocities are independent of each other in successive interaction times. This is the essence of eddy lifetime method that is used in

SSF approaches to model turbulent dispersion. This approach used by Gosman and Ioannides [73] and proves its ability to handle particle dispersion more realistically. Shuen et al. [74]; Chen and Crowe [78] also used the same approach with some modifications.

Another approach called time-correlated dispersion models are developed to account for both fluctuating fluid time and cross-relations. These were first used by Ormancy and Martinon [79] and later refined by Berlemont [80] and Burry and Bergeles [81]. The time-correlated models overcome the disadvantages of the eddy lifetime models by including a fluid particle trajectory that runs directly along the particle trajectory. This is done in order to estimate the fluctuating fluid velocity at each time step, along the particle trajectory. The fluid particle trajectory is generated by using a Markov-chain model, which is capable of incorporating the time correlations in the fluid fluctuating velocity. The particle trajectory is obtained by solving paricle equation of motion between time steps. Therefore by following a fluid particle and a dispersed phase particle simultaneously, whilst marching down the flow field, it is possible to determine the fluid fluctuating velocity at the particle location. These two approaches are discussed in detail below.

SSF models require large number of particle calculations per particle size to correctly predict dispersion in turbulent flows. Therefore a new approach based on PDF propagation approach has been developed [82-84]. This was evaluated by Shirolkar et al [85] with the experimental data of Snyder and Lumley [58] and Wells and Stock [59], and showed that one ensemble calculation per particle size can provide good predictions for particle dispersion.

2.10.2.1SSF models based on eddy lifetime concept

The particle momentum equation (2.37) is a first order, non-linear differential equation, which can be solved analytically over small time steps (Δt) when the instantaneous fluid velocity and the particle relaxation times are assumed to be constant. Therefore by predicting the new particle velocity at the end of each time step, a particle trajectory can be obtained [86-89].

The main problem is to obtain the instantaneous fluid velocity along the particle trajectory and the time interval during which it can be assumed to be constant. Solution of the gas phase governing equations provides only the mean gas velocity. Thus the fluctuating velocity component is unknown. This unknown is estimated considering eddy-particle interaction. While particles pass through the flow, they are assumed to interact with a series of eddies as shown in Fig.2.6.

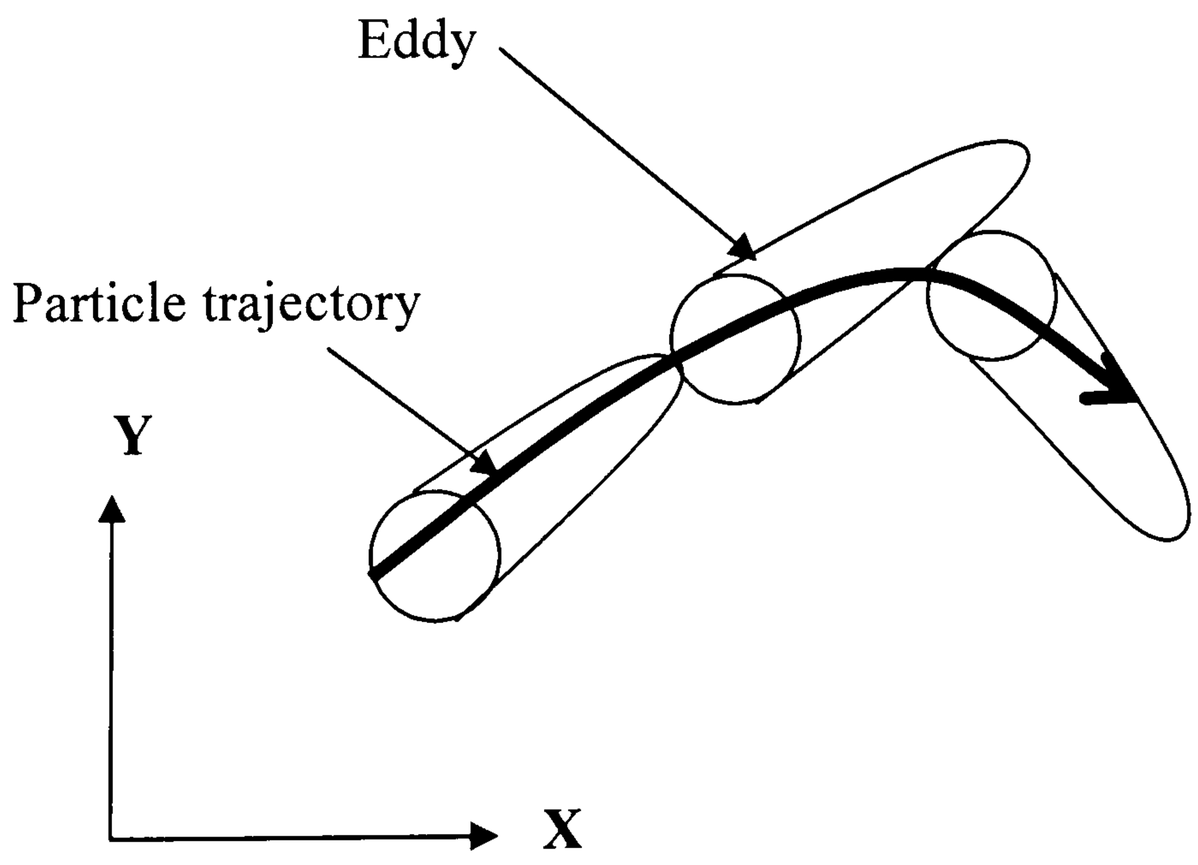

Fig. 2.6

Each eddy is characterised by a velocity (fluctuating), a time scale (eddy lifetime) and a length scale (size). The eddy size and the lifetime can be estimated using gas phase local turbulent properties (k and ε). The turbulence is assumed to be isotropic and fluctuating velocity components are assumed to have a Gaussian distribution. The standard deviation of the velocity distribution is taken as $(2k/\varepsilon)^{1/2}$. This distribution is randomly sampled when a particle enters to a particular eddy to obtain the instantaneous velocity required. In a particular eddy the associated fluctuating velocity is assumed to be constant during the interaction time. Any particle is assumed to interact until the end of the eddy lifetime t_e or the transit time t_r; required for the particle to travel thorough the eddy whichever is the smallest. The eddy lifetime and transit time are determined assuming that the characteristic size of the eddy is the dissipation length scale, L_e, given by

$$L_e = C_\mu^{3/4} k^{3/2} / \varepsilon \tag{2.58}$$

The eddy lifetime, t_e is then estimated as

$$t_e = L_e / |u'| \tag{2.59}$$

The transit time is determined from the following equation

$$t_t = -\tau \ln\left(1 - : L_e / \left(\tau |u - u_p|\right)\right) \tag{2.60}$$

where τ is the particle relaxation time given by

$$\tau = \frac{4}{3}\rho_f d_p / \left(\rho C_D \left| u - u_p \right|\right) \tag{2.61}$$

At the end of each time step, a new fluctuating fluid velocity is obtained from a new velocity distribution, which is generated using the local turbulence properties at the new particle position. This is the basic idea of the eddy lifetime concept

2.10.2.2SSF based on Time-correlated dispersion models

This method is similar to the eddy life time concept because both focus on how to determine the particle trajectory using the momentum equation given by (2.37). The difference is the method used to determine the fluctuating fluid velocity along the trajectory. If a particle and a fluid particle at the discrete particle location are followed simultaneously, then it is possible to determine where the fluid particle is relative to the discrete particle after a time interval (*dt*) and also the fluctuating velocity at that location. If the discrete particle is small and its density is close to the fluid density and the time step is sufficiently small, then the relative distance between the fluid particle and the discrete particle can be neglected. This is done in order to assume that the fluctuating fluid velocity vector at the fluid location is acting on the particle location for the next time step. This tracing of fluid and discrete particles is shown in Fig 2.7.

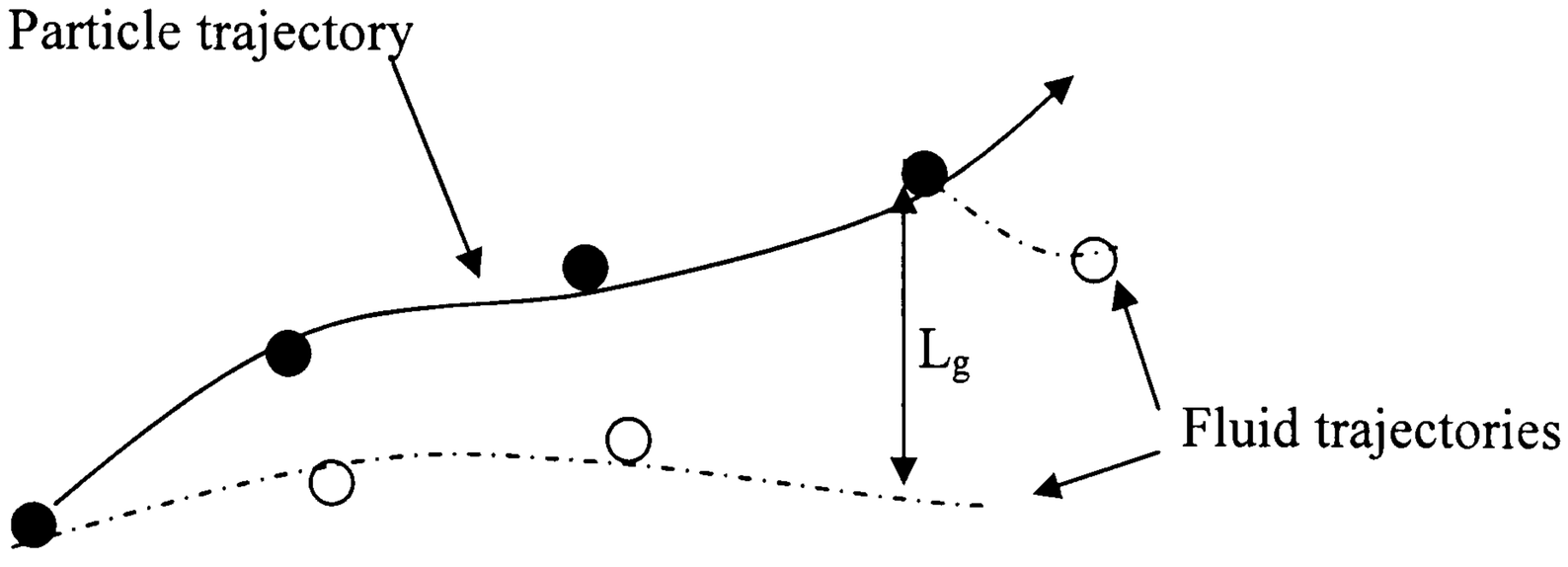

Fig. 2.7

Berlmont [80] followed the two particles, monitoring their relative separation between time steps and if the distance exceeded certain length scale (Lg), a new fluid particle trajectory was started from the discrete particle location. But Burry and Bergeles [81] adopted another methodology, they monitored a new fluid particle at each new time step at particle location, Fig 2.8. This was done in order to avoid the unknown length scale.

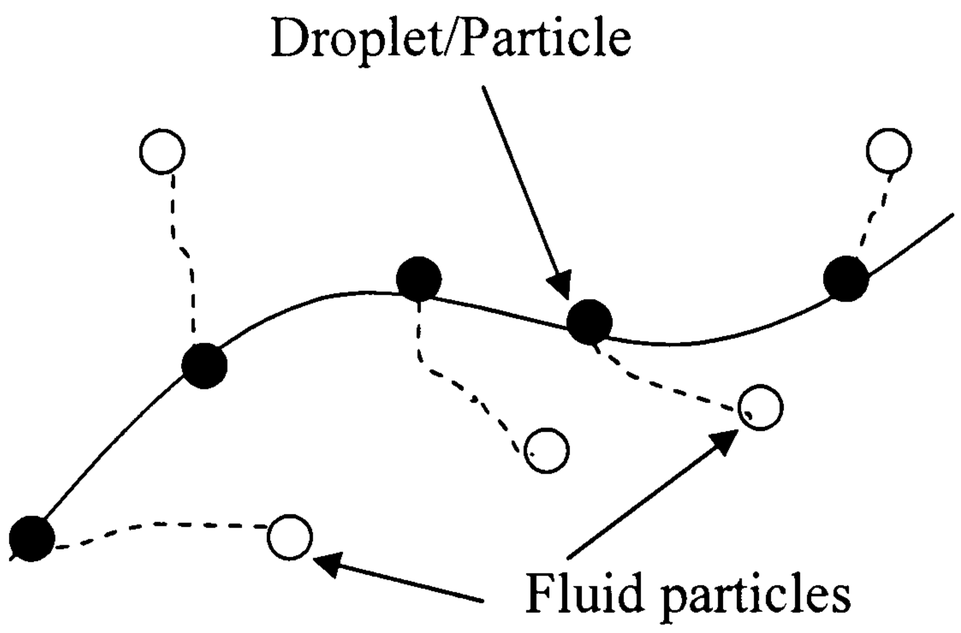

Fig 2.8 droplet trajectory and different fluid particle trajectories starting at different time steps

2.10.2.3 SSF Model Assessment

Since the introduction of the SSF model using eddy life time concept by Gosman and Ioannides [73], the Lagrangian stochastic model has been widely applied to predict a variety of dilute turbulent two-phase flows. Many encouraging applications have been reported by, among others, Shuen et al. [74], Chang and Wu [90], and Zhou and coworkers [2] for two-dimensional evaporating and nonevaporating [91] two-phase flows. A complete review of the stochastic trajectory models can be found in Faeth [23, 25], Crowe [3, 22], among others [92-95]. Even though the Lagrangian stochastic model has been successful in predicting various two-phase or multiphase flows [96], one problem persists due to the stochastic procedure used in the conventional Lagrangian trajectory computations, that is, when a discrete delta-function dispersion is used for the distribution of physical particles. Many authors have found it necessary to track a "large" number of particle trajectories to achieve stochastically significant solutions for two-dimensional flows;, Crowe *et al.* [1], Chang and Wu [90], and Chen and Pereira [97]. In these computations, a total number of particle trajectories, ranging from 3×10^3 to 10^5, were used to achieve stochastically significant or invariant solutions. Obviously, for industrial applications where three-dimensional computations are often encountered, it would be unacceptable, even for present supercomputers, to track such a large number of particle trajectories [98, 99].

The main disadvantage in these SSF methods is that to get reasonable accuracy for even a mono-dispersed flow thousands of trajectories have to be calculated. So obviously for a multiphase flow like a fuel spray, in order to get a

satisfactory result very large numbers of trajectories have to be obtained. Another shortcoming with the SSF method is that the velocity field established by adding the local turbulent fluctuational velocity and the mean gas flow velocity does not satisfy the continuity equation (MacInnes and Bracco [100]). Shirolkar et al. [66, 101] argued that it is possible to get a good agreement with experimental results by using the deterministic approach modified to include the particle diffusion effect. According to Gosman and Ioannides [73] and Solomon et al. [30], the effects of turbulent dispersion appear to be diminished in rapidly evaporating sprays. Therefore it may be possible to neglect turbulent dispersion for engineering calculations in some applications.

2.11 COMBUSTION MODELLING

Combustion flames can be mainly categorized into two as premixed flames and nonpremixed or diffusion flames according to the state of mixedness of reactants. In a premixed flame, the fuel and the oxidiser are mixed at the molecular level before the occurrence of any significant chemical reaction. The spark-ignition engine is an example where premixed flames occur. On the other hand, in a diffusion flame, the reactants are initially separated, and reaction occurs only at the interface between the fuel ant the oxidiser, where mixing and reaction both take place [102]. A good example of a diffusion flame is a candle. In most practical combustion systems both types of combustion may be present in various levels. It is considered that in diesel engine both premixed and diffusion combustion flames are present at various stages. Although it appears simple to define combustion flames, the underling chemical reactions during the combustion are so complex and the number of combustion by-products is huge

[103-104]. For example, over 40 elementary reactions are involved in the combustion of methane which is the simplest hydrocarbon fuel [8, 105]. Therefore modelling combustion of even a simple configuration is a very complex task [106-108].

Two main modelling approaches are used to model combustion process. One approach is to assume combustion has no effect on the mixing, hence the effect of combustion on turbulence is neglected. This allows the use of a mixing program to evaluate fuel spray evaporation and mixing with air and then the output of fuel vapour concentration data from this program is used to evaluate the combustion process. Although this may lead to errors on the micro-scale level, this allows a higher number of species to be taken into account in the combustion model without the addition of extra partial differential equations [109]. This type of combustion modelling is referred to in the literature as 'mixed-is-burnt' type. On the other hand turbulence combustion interaction methods can improve micro-scale mixing prediction but requires a use of a combustion model which is included within the main flow equations. But for each species considered it requires the use of an extra differential equation to solve along the gas flow equations. Therefore in this method the number of species considered has to be limited in order to have reasonable computation time. This leads to less informative global picture of the combustion data maps than the mixed-is-burnt type models.

Lots of research has been conducted on combustion using modelling methods and experiments [110-111]. Few best known combustion models are Simplified PDF fast reaction model and Simplified PDF local instantaneous equilibrium model etc. [2, 8, 112].

2.11.1 Simplified PDF (Probability Density Function) fast reaction model

For diffusion–controlled turbulent combusting flows such as fuel spray combustion flows the simplest model is the simplified PDF fast reaction model, which based the concept of mixture fraction, fast reaction and probability density distribution function. In this approach following assumptions are made [2]:

1. chemical reaction is sufficiently fast enough to be described by a single step reaction
2. two components; fuel and oxygen do not coexist instantaneously at the same time (one reactant which is locally in excess causes other reactants to be consumed stoichiometrically)
3. mass exchange coefficients ($\Gamma_{fuel} = \Gamma_{oxidiser}$) are equal

Then all the conserved scalars (mass fraction and temperature or enthalpy) can be related to a single normalised conserved scalar called mixture fraction, f . Then its instantaneous conservation equation is

$$\frac{\partial(\rho f)}{\partial t} + \frac{\partial(\rho u_j f)}{\partial x_j} = \frac{\partial}{\partial x_j}\left(\Gamma_f \frac{\partial f}{\partial x_j}\right) \tag{2.62}$$

The equation can be solved subject to boundary conditions of known values at inlet and zero flux across boundaries. Then the mass fractions of reactants and

products after combustion can be obtained by following algebraic equations based on the reaction stoichiometry.

$$when\ \ f_{st} < f < 1;\ \ m_{ox} = 0\ \ and \qquad m_{fu} = \frac{f - f_{st}}{1 - f_{st}} \tag{2.63}$$

$$when\ 0 < f < f_{st};\ \ m_{fu} = 0\ \ and \qquad m_{ox} = \frac{f_{st} - f}{f_{st}} \tag{2.64}$$

$$f_{st} = \frac{1}{s+1} \tag{2.65}$$

Where

m_{ox} = mass fraction of oxidiser in the cell

m_{fu} = mass fraction of fuel in the cell

s = mass of oxidiser needed for the stoichiometric combustion

The mass fraction of the combustion product can be obtained from the conservation of mass as follows

$$m_{pr} = 1 - (m_{ox} + m_{fu}) \tag{2.66}$$

However, in turbulent combusting flows the fuel stream breaks up into eddies with inter-diffusion at eddy boundaries. This causes the mixture fraction to fluctuate [113, 114], which leads to fluctuation of all the dependant variables of the mixture fraction. Therefore in order to predict realistic combustion temperature this

fluctuations need to be taken into account. This can be done by a statistical approach based on modelled equation of mixture fraction variance (g) and assuming the form of the probability density function of the mixture fraction [2, 113, 115].

$$g = (\hat{f} - \bar{f})^2 \tag{2.67}$$

$$\frac{\partial(\rho g)}{\partial t} + \frac{\partial(\rho u_j g)}{\partial x_j} = \frac{\partial}{\partial x_j}\left(\Gamma_f \frac{\partial g}{\partial x_j}\right) + C_{g1}\mu_t\left(\frac{\partial f}{\partial x_j}\right)^2 - C_{g2}\frac{\varepsilon}{k}g \tag{2.68}$$

Where C_{g1} and C_{g2} are modelled constants and μ_t is the turbulent viscosity.

The remaining problem is to find a probability density function (PDF). Although various PDF's such as top hat (rectangular wave) PDF [116], clipped Gaussian [117] and Beta function [118-119] used for combustion modelling, the clipped Gaussian and beta function PDFs gave best results. Jones and Whitelaw [120] compared results from models based on clipped Gaussian and beta function and found that the results were almost similar.

Predictions made by Spalding [114, 116] for a simple diffusion flame show general agreement with experiments. Smith and Smoot used a similar combustion model to compare experimental results from axisymmetric combustor and found the predictions were in reasonable agreement with experiments. Jones and Whitelaw [120] compared experimental results of Owen [121] with the results from a program developed by Jones and found that the results were in general agreement with some deficiencies in calculated mixture fraction values.

In general this model is a good option as the model is simple and therefore required computational resources are small still produce results with reasonable accuracy.

2.11.2 Equilibrium Model

The above model is appropriate only for the simple two-species reactions. For more complex diffusion combustion such as coal combustion many species and more than one-step reaction, Smoot et al. [112] proposed a local instantaneous equilibrium model. In this model, the gas mixture is assumed to be at chemical equilibrium. The equilibrium composition and temperature of the flame are calculated as a function of mixture fraction based on the minimisation of Gibbs free energy [ ]. An important advantage of the chemical equilibrium model is that it can provide information about the minor species without a detailed knowledge of the reaction kinetics. The chemical equilibrium model is valid if the reaction processes are faster than the convection and diffusion process of the flow. However, in many practical combustion systems all the combustion processes are not fast. Therefore these finite rate combustion processes lead to large quantity of species involved. Nevertheless, this model has been widely used and reasonable temperature and species concentrations were obtained.

2.11.3 Joint probability distributions and the Monte Carlo method

The above approach of describing the combustion system by the mixture fraction and its variance is limited to two species (fuel and air; oxidant). In joint probability distribution and Monte Carlo method, a more complete description of the flow field is achieved using a joint probability density function of the velocity and the composition variables (mass fractions and the enthalpy). This method was pioneered and extensively used to analysis combustion systems by Pope and co workers [122-124]. A detailed description of the formulation of this method can be found in the papers presented by Pope [125, 126].

PDF methods mainly gain their advantage from the more complete description of the turbulent combustion flow field. Consider a flow field involving three scalars such as fuel mass fraction, air mass fraction and enthalpy. With a two equation turbulence model, at each point the turbulent flow field is represented by 8 quantities (three mean velocities, three mean scalars and k and ε). On the other hand, in PDF method the flow field is described by the joint probability of the three velocities and three scalars (turbulence is modelled using gradient diffusion techniques). Therefore any point in the flow field is described by six independent variables. The equation governing the transport of the above joint probability density function is solved using Monte-Carlo methods [124, 126] due to the computational efficiency of this method compared to standard numerical techniques. Another important feature of this method is the ability to incorporate the complicated reaction terms without modelling approximations. In conventional turbulence models the mean reaction rate can be

determined only in special conditions- when the reaction rate is linear, or when it is fast or very slow compared with the turbulence time scales [122-124]. This permits PDF models to handle both diffusion and premixed combustion with minimal modifications.

2.12 Conclusion

Main advantage of SF method over LHF method is its ability to handle interphase transports. Although LHF method is easy to model and produce more realistic results at near injector region as argued by Nazha, Rajakaruna[38, 41], it is unable to produce detailed data of the dispersed phase. Due to the ability to take account of finite inter-phase transport rates SF analysis can handle relatively broader class of dispersed flow and produce more detailed results about the dispersed phase, such as drop life histories.

When comparing DSF and SSF although SSF is said to produce more accurate results due to its ability to handle turbulent dispersion of droplets or particles, it is necessary to calculate thousands of trajectories to conserve particle momentum and get overall particle behaviour. Furthermore its accuracy of predicting droplet/ particle dispersion depends on the accuracy of the turbulence model used in the gas phase calculation. On the other hand some researchers (Solomon [30], Gosman and Iliniads [73]) shown that the effects of turbulent dispersion appear to be diminished in rapidly evaporating sprays such as fuel spray combustion. Therefore it may be possible to neglect turbulent dispersion for engineering calculations in some applications.

Considering the above limitations and difficulties it can be argued that although DSF method can not treat for the turbulent droplet dispersion directly as SSF method, it would be useful as a design tool to get further insight about dispersed phase if it is used with an advanced droplet evaporation model and combustion model.

CHAPTER 3

Theoretical Formulation of the Trajectory Method

In this chapter the theoretical formulation of the trajectory method is discussed. First a brief introduction of the governing equation of the gas-phase is presented. This is followed by the droplet equations, derived from the general equations for droplet motion. Finally the discussion is focused on how to model the combustion process using a "mixed is burnt" type combustion model.

3.0 Numerical modelling of spray combustion

Spray combustion is a highly turbulent two-phase flow process involving mass, momentum and energy interactions between the phases. Therefore it is impossible to analyse these using analytical method and require numerical modelling based on computational fluid dynamics. But modelling of evaporating and burning sprays is also a complex process due to the diverse phenomena that must be considered, including: the hydrodynamic characteristics of injection and spray formation; the transport characteristics of individual droplets; the turbulent two-phase flow of the fuel spray, and chemical phenomena in a turbulent environment leading to the formation of product species and pollutants. Therefore when dealing with numerical modelling of complex flow problems understanding the underlying physical and chemical phenomena, which requires a great insight into thermo-chemistry, thermodynamics, fluid mechanics and numerical methods, is of paramount importance. This enables a better description of the actual processes mathematically [1, 2, 8].

The ideal numerical model for this kind of a flow would provide the properties of each particle in the flow field and the detailed properties of the carrier phase at any point in the fluid. Thus the motion of each particle, as well as the particle temperature and mass, would be obtained by integrating the particle equations using the local velocity, temperature, and density of the carrier flow and accounting for all particle-particle collisions. The model for the carrier phase would require the direct solution of the Navier-Stokes equations including the boundary

conditions imposed by all the particles in the field. However, such an exact model is still well beyond current computational capability. This has lead to the use of simplified models to carry out the numerical analysis [2,8].

Numerical models for two-phase flows can be based either on one-way or two-way coupling. In a model based on one-way coupling it is assumed that the presence of the particulate phase has a negligible effect on the carrier phase. Two-way coupled models include the effect of the particles on the carrier phase. For example, a two-phase turbulent flow model that includes the effect of the particles on the turbulent velocity fluctuations would be two-way coupled.

There are two different approaches that can be used to model spray combustion process; **Lagrangian** or **Eulerian**. In the Lagrangian method, particles are tracked individually or in small groups as they travel through the flow field. The instantaneous position of a particle can be measured as a function of original particle location and the time spent. Lagrangian models are sometimes referred to as Discrete Droplet Models (DDM) because they treat particle phase as discrete, which is of course the natural way to treat the particles in dilute flows. These models are commonly used in applications such as spray and pulverized coal combustion systems [2, 127-129]. In Eulerian models, particles are treated as a continuum and properties of the particle phase are obtained solving partial differential equations of the particle phase in a given coordinate system. These models are also known as continuum models or two-fluid models. These models are popular when modelling dense flows as well as modelling dilute particle flows [9, 38, 41, 130-132].

Considering the limitations and difficulties argued in the chapter two, in this research exercise spray combustion process is modelled using Lagrangian approach. For modelling simplicity, the spray combustion process is divided to three separate processes, which are droplet evaporation, mixing and combustion. For the analysis of the droplet evaporation and the mixing process a program was developed, which has two separate sub models; a sub model to model the droplet phase and another sub model to model the mixing process. These two sub-models run simultaneously passing data to each other. When convergence is achieved fuel vapour equivalence ratio data from this model is used in a separate "mixed is burnt" type combustion model to calculate combustion temperature and species mole fractions.

3.1 The basic Concept of the mathematical model

Consider a spray issuing into a moving gas stream, as droplets traverse the flow field, they exchange mass, momentum and energy with the gas phase due to two-way coupling. When modelling this type of a flow field using PSI-Cell method it is necessary to subdivide the flow field into a suitable grid or control volumes [12, 63, 68, 133]. Then finite difference equations for mass, momentum and energy conservation are written for each cell, incorporating the effects due to particle phase. The entire flow field solution is then obtained by solving the system of equations for each cell. The droplet trajectories, size and temperature histories are obtained by integrating the equation of motion in the gas flow field and utilising correlations for droplet-gas mass and heat transfer rates. The Lagrangian approach is used to solve the relevant equations

for droplet velocity, size and temperature histories. The mass, momentum and energy properties of droplets crossing the cells are used to calculate droplet source terms for the gas phase equations. This concept of regarding the particle phase, as a source of mass momentum and energy to the gas phase was first proposed by Migdal and Agosta [134].

The complete solution procedure can be briefly described as follows: first, the gas field is solved as if particles were not present. This flow field is used to calculate particle trajectories, size and temperature histories. Then the droplet source terms for each cell are calculated. The gas flow field is solved again incorporating these droplet source terms. The new gas flow field is used to determine new droplet trajectories that represent the effect of the gas phase on the droplets. This operation is carried out repeatedly until the gas flow field converges.

3.2 The Gas-Phase Equations:

The gas-phase equations in the separated flow approach are similar to those used in the locally homogeneous flow method, except for the addition of source terms to account for the mass, momentum and energy transfer between the two phases. For a two-dimensional flow field, the generalised gas-phase conservation equation [2, 8] in cylindrical coordinates has the form of:

$$\frac{\partial}{\partial x}(\rho u\varphi)+\frac{1}{r}\frac{\partial}{\partial y}(r\rho v\varphi)=\frac{\partial}{\partial x}\left(\Gamma\frac{\partial\varphi}{\partial x}\right)+\frac{1}{r}\frac{\partial}{\partial y}\left(r\Gamma\frac{\partial\varphi}{\partial y}\right)+S_{\varphi}+S_{\varphi}^{p} \tag{3.1}$$

Where φ is the generalized dependent variable, Γ_φ is the transport coefficient, S_φ is the source term of the gas-phase itself and S_φ^p is the source term due to gas-particle interaction. The terms φ, Γ_φ, S_φ and S_φ^p are explicitly given in table 3.1:

Equation	φ	Γ_φ	S_φ	$S_{p\varphi}$
Gas Continuity	1	0	0	S_{mass}
Gas Momentum	u_i	μ_e	$-\frac{\partial p}{\partial x_i}+\Delta\rho g_i+\frac{\partial}{\partial x_i}\left(\mu_e\frac{\partial u_j}{\partial x_i}\right)$	$S_{momentum}$
Gas Turbulent Kinetic Energy	k	$\frac{\mu_e}{\sigma_k}$	$G_i-\rho\varepsilon$	0
Turbulent Kinetic Energy dissipation rate	ε	$\frac{\mu_e}{\sigma_\varepsilon}$	$\frac{\varepsilon(c_1G_k-c_2\rho\varepsilon)}{k}$	0
Gas species conservation	Y_s	$\frac{\mu_e}{\sigma_Y}$	$-w_s$	Fuel species diffusion from droplets
Gas enthalpy	h	$\frac{\mu_e}{\sigma_h}$	$-q_r$	S_{energy}

Table 3.1

where G_k is as follows:

$$G_k = \left[2\left(\frac{\partial u_i}{\partial x_i}\right)^2 + 2\left(\frac{\partial u_j}{\partial x_j}\right)^2 + \left(\frac{\partial u_i}{\partial x_j} + \frac{\partial u_j}{\partial x_i}\right)^2 \right] \quad (3.2)$$

Table 3 parameters of the generalised equation

The variables in the above set of equations are as follows:

u_i = velocity in i^{th} direction

μ_e = viscosity (turbulent + laminar) = $\mu + \mu_T$

$\Delta\rho g_i$ = the body force in the i^{th} direction

P = pressure

k = turbulent kinetic energy

ε = turbulent dissipation rate

$\sigma_{(k, e, Y, h)}$ = turbulent Prandtl or Shemidt numbers (taken as modelled constants)

$\sigma_K = \sigma_h = \sigma_Y = 0.9$ and $\sigma_\varepsilon = 1.3$ [2]

c_1 , c_2 = constants in the turbulent dissipation rate equation [2]

$c_1 = 2.8$ and $c_2 = 2.0$

Y_s = mass fraction of the species

h = enthalpy of the gas phase

w_s = reaction rate (for an evaporation problem this is equal to zero)

q_r = heat flux

S_{mass} = mass source term

$S_{momentum}$ = momentum source term

S_{energy} = energy source term

The turbulent viscosity can be calculated using the formula given below

$\mu_T = C_\mu \rho k^2 / \varepsilon$, where $C_\mu = 0.09$ [2]

The above set of equations can be solved using a finite volume discretisation method. In order to accommodate the non-linear nature of the underlying flow phenomena and the linkage between the pressure and velocity in a variable density fluid, the SIMPLE (Versteeg & Malalasekara[8], and Patankar & Spalding [135, 136]) algorithm developed by Patankar and Spalding is used as the core of the solution procedure. For more detailed description of SIMPLE algorithm, the reader may refer the works of Patankar & Spalding [135, 136] and Versteeg & Malalasekara [8]

3.3 Droplet phase Equations

The starting point of particle tracking is the particle motion equation. To date, there is no definitive formulation available to describe the particle motion. Various formulations have been given, initially by Basset (1888) and Boussinesq (1903), then recently by Maxey and Riley [10]. Although the discussion is still open, the particle motion equation accepted by researches at present is the modified Riley [10, 11] equation and this can be written as follows:

$$\rho_p \frac{\pi d^3}{6}\frac{dV}{dt} = \frac{\pi d^2}{8}\rho_g C_D (U-v)|v-U| - \rho_g \frac{\pi d^3}{6} C_A \frac{d(v-U)}{dt} + \frac{\pi d^3}{6}(\rho_p - \rho_g)g$$
$$+\rho_g \frac{\pi d^3}{6}\frac{DU}{Dt} - \frac{\pi d^2}{4} C_H \sqrt{\frac{\rho_g \mu}{\pi}} \int_{-\infty}^{t} \frac{d(v-U)}{dt}(t-\tau)^{-1/2} d\tau \tag{3.3}$$

where ρ_p and ρ_g are the particle and fluid (gas) densities, d is the particle diameter; v and U are the instantaneous velocity vectors of the particle and gas phase respectively. In the above equation, d/dt is the temporal derivative along the discrete particle trajectory and D/Dt is the temporal derivative along the fluid motion, g is the gravity vector and μ is the fluid's viscosity. Coefficients C_D, C_A and C_H are correction factors applied to the drag term, added mass term and Basset term (also called "history term accounts for the viscous effects) respectively to account for non-small particle Reynolds numbers and acceleration numbers. For dense particles in turbulent flows ($\rho_p >> \rho_g$), the particle motion equation can be simplified to drag and gravity force terms [12, 21, 137-139].

$$\rho_p \frac{\pi d^3}{6}\frac{dV}{dt} = \frac{\pi d^2}{8}\rho_g C_D (U-v)|v-U| + \frac{\pi d^3}{6}(\rho_p - \rho_g)g \qquad (3.4)$$

This can be rearranged as

$$m_d \frac{dv}{dt} = C_D \rho_g \frac{A_d}{2}(U-v)|U-v| + m_d g\left(1-\frac{\rho_g}{\rho_p}\right) \qquad (3.5)$$

Since $\rho_p >> \rho_g$, it can be further simplified as

$$m_d \frac{dv}{dt} = C_D \rho_g \frac{A_d}{2}(U-v)|U-v| + m_d g \qquad (3.6)$$

Where m_d is the mass of the droplet, A_d is the droplet cross sectional area.

According to the above equations, it can be seen that in analysing gas particle flows the particle drag coefficient is an important basic property. The particle drag term for a particular range of Reynolds number can be given as follows:

Newton's Formula [2]

$$C_D = 0.44 \qquad (\mathrm{Re_p} > 1000) \qquad (3.7)$$

Clift's formula [2,12]

$$C_D = \frac{24}{\mathrm{Re}_p}(1+0.15\,\mathrm{Re}_p^{0.687}) \qquad (1 < \mathrm{Re_p} < 1000) \qquad (3.8)$$

Stock's formula

$$C_D = \frac{24}{\mathrm{Re}_p} \qquad (\mathrm{Re_p} < 1) \qquad (3.9)$$

where $\mathrm{Re_p}$ is droplet Reynolds number. Clift's formula will be used in this work due to the fact that in general, the droplet Re number in these studies falls between the limits given by Clift's equation.

It can be seen that the drag coefficient of a droplet primarily depends on the Reynolds number based on gas droplet relative velocity.

$$\mathrm{Re} = \rho \frac{|U - v| d}{\mu} \qquad (3.10)$$

where d is the droplet diameter.

Evaporation can reduce the drag coefficient due to mass flux from the surface, for which Bailey [8] suggested the following correlation:

$$C_D = \frac{C_{D0}}{1 + B} \qquad (3.11)$$

Where B is the transfer coefficient (Spalding transfer number) [12], given by

$$B = C_v \frac{\Delta T}{L} \qquad (3.12)$$

With C_v being the specific heat of the diffusing vapour, ΔT the temperature difference, and L the enthalpy of evaporation.

Significant saving in computing time can be realised if the droplet trajectory equation is integrated analytically. First, the above equation for droplet motion can be re-written in the following form:

$$\frac{dv}{dt} = \left(\frac{18\mu f}{\rho_d d^2}\right)(U - v) + g \qquad (3.13)$$

Where $f = C_D Re/24$ and ρ_d is the density of the droplet substance. When modelling axi-symmetric flow, it is also possible to neglect gravity term $\boldsymbol{g}$, which is negligibly small compared to the drag term.

The above equation could be integrated assuming the gas velocity is constant over a small time interval. Then the new droplet velocity at the end of the time interval Δt is

$$v = U - (U - v_0)\exp\left(\frac{-\Delta t}{\tau}\right) \qquad (3.14)$$

where v_0 is the initial droplet velocity, Δt is the time interval and τ is the characteristic time defined as:

$$\tau = \frac{\rho_d d^2}{18\ \mu f} \qquad (3.15)$$

Once the new droplet velocity after a time increment Δt is obtained, the droplet position at this time is determined by using:

$$x_d = x_{d,0} + (v + v_0)\frac{\Delta t}{2} \tag{3.16}$$

where $x_{d,0}$ is the droplet position at the beginning of the time increment.

The rate of decrease of droplet mass is given by

$$\frac{dm}{dt} = -Sh(\rho D)\pi d(x_v - x_\infty) \tag{3.17}$$

where ***Sh*** is the Sherwood number, D the diffusion coefficient, $\boldsymbol{x_v}$ the mass fraction of vapour at the droplet surface, and x_∞ the mass fraction of vapour in the free stream. The ***Sh*** can be expressed as [12, 63]

$$Sh = 2 + 0.6\,\mathrm{Re}^{0.5}\,Sc^{0.33} \tag{3.18}$$

where **Sc** is the Schmidt number. Using equation (23), the rate of decrease of droplet diameter with time can be written as [63]

$$\frac{d(d)}{dt} = -2Sh(\rho D)\frac{(x_v - x\infty)}{\rho_d d} \tag{3.19}$$

and the droplet size history is obtained from

$$d = d_0 - \frac{d(d)}{dt}\Delta t \tag{3.20}$$

where d_0 is the initial droplet diameter and Δt is the time step along the trajectory. The mass fraction of the vapour at the droplet surface is given by

$$x_v = \frac{P_v m_v}{m_g - (m_g - m_0)P_v} \tag{3.21}$$

where P_v is the partial pressure of the vapour and m_g and m_v are the molecular masses of gas and vapour, respectively.

The heat balance equation for the droplet can be stated as:

$$m_d C_D \frac{dT_d}{dt} = \dot{q} + L\left(\frac{dm_d}{dt}\right) \tag{3.22}$$

where $\dot{q}^{\circ}$ is the heat transfer rate to the droplet, L is the enthalpy of evaporation, and C_D is the specific heat capacity of liquid fuel of the droplet. The rate of heat transfer to the droplet is obtained from

$$\dot{q} = Nu\pi kd(T_g - T_d) \tag{3.23}$$

where k is the thermal conductivity of the gas phase (air and fuel vapour mixture) and Nu is the Nusset number, which is taken to vary with Reynolds number and Prandtl number as [63]

$$Nu = 2 + 0.6\,\mathrm{Re}^{0.5}\,\mathrm{Pr}^{0.33} \tag{3.24}$$

Dividing equation (3.22) by the droplet mass and specific heat and using equation (3.19) for the rate of mass decrease results in

$$\frac{dT_d}{dt} = \frac{T_g - T_d}{\theta} - \frac{Q_L}{\theta} \tag{3.25}$$

where Q_L and θ are defined as

$$Q_L = \frac{L.Sh.(\rho D)(x_v - x_\infty)}{Nu.k} \tag{3.26}$$

$$\theta = \frac{\rho_d d^2 c_d}{6.Nu.k} \tag{3.27}$$

Integrating the heat balance over a small time interval Δt and assuming the gas temperature is constant over the time interval of integration results in

$$T_d = T_g - (T_g - T_{d,0}).\exp\left(\frac{-\Delta t}{\theta}\right) - Q_L\left[1 - \exp\left(\frac{-\Delta t}{\theta}\right)\right] \tag{3.28}$$

3.4 Droplet Source Terms

The entry of the droplets to the gas flow field is represented by a finite number of entry positions. The mass of droplet size $d_{i,}$ which enters per unit time at port j is given by

$$\dot{m}_{pj}(d_i) = \dot{m}_p X_j Y_i \tag{3.29}$$

where $\dot{m}_p$ is the total droplet mass inflow rate, X_j is the fraction of the droplet mass, which enters at port j, and Y_i is the fraction of droplet mass with initial diameter $d_{i.}$ If droplets are assumed to be spherical and the number flow rate of droplets of a given initial size can be taken as constant along a trajectory, the number flow rate of droplets of initial diameter d_i along a given trajectory is determined by

$$\dot{n}_j(d_i) = \frac{6\dot{m}_p X_j . Y_i}{\pi \rho_d d_i^{\,3}} \tag{3.30}$$

The source term [106, 140] in the continuity equation, S_{mass}, is the net efflux rate of droplets mass for a given cell (control volume). The efflux rate of droplet masses due to droplet trajectory "i" which traverse a given cell is

$$\Delta S_{mass} = \pi \rho_d \dot{n}_i \frac{d_{i,out}^3 - d_{i,in}^3}{6} \tag{3.31}$$

The net efflux rate of droplet mass is obtained by summing over all droplet trajectories, which traverse a given cell:

$$S_{mass} = \sum_{i,cell} \Delta S_{mass} \tag{3.32}$$

Similarly the momentum source terms ($S_{momentum}$) and the energy source terms (S_{energy}) are evaluated in the same way as the mass source terms.

$$S_{momentum} = \sum_{i,cell} \left(\pi \rho_d \dot{\eta}_i \frac{v_{i,out} d_{i,out}^3 - v_{i,in} d_{i.in}^3}{6} \right) \tag{3.33}$$

$$S_{energy} = \sum_{i,cell} \left(\pi \rho_d \dot{\eta}_i \frac{h_{d,out} d_{i,out}^3 - h_{d,in} d_{i.in}^3}{6} \right) \tag{3.34}$$

These source terms are added to the gas phase calculations by modifying source terms in gas phase equations.

3.5 Combustion model

In order to simulate the combustion process, a standalone combustion model, which is of type '*mixed-is-burnt*' [9, 109] is used with the data obtained by running the above discussed droplet evaporation and mixing program. The module is based on the minimisation of Gibbs free energy of the system. It is assumed that the combustion system is adiabatic and the combustion is governed by the steady flow energy equation.

3.5.1 Flame temperature calculation

Fuel vapour map of the flow field obtained from the mixing program was fed to the combustion program. Then the flame temperature is initially calculated assuming stoichiometric combustion. Depending on the local fuel air equivalence ratio of the control volume, air fuel mixture in the control volume may be lean, stoichiometric or rich which leads to complete or partial combustion, yielding a combustion temperature that may or may not be the stoichiometric temperature. Therefore the enthalpy balance equation needs to be modified to calculate the correct temperature. These equations can be summarized as follows:

Stoichiometric combustion equation for initial guess:

$$C_Z H_S + b\, O_2 + f\, N_2 \rightarrow a\, H_2O + d\, CO_2 + f\ N_2 \tag{3.35}$$

Where a, b, d and f are the number of moles of each species and z, s are the number of carbon and hydrogen atoms in the fuel molecule.

Flame temperature [109]:

$$T_f = \frac{HC + n_p C_{P_p T_r} T_r + \frac{n_{as}}{\phi_v} C_{P_a T_g} + C_{P_v T_g} T_g - \frac{n_{as}}{\phi_v} C_{P_a T_r} T_r - C_{P_v T_r} T_r}{n_p C_{P_p T_r}} \tag{3.36}$$

where

$HC = (CV)_{fuel}$ for the lean and stoichiometric mixture

CV = Lower calorific value

$HC = \frac{(CV)_{fuel}}{\phi_v}$ for rich mixture

$C_{Pp} = \sum_p \frac{n_i}{n_p} C_{P_i}$ mean product isobaric heat capacity

$C_{P_a} = C_P$ of air

$C_{P_v} = C_P$ of fuel vapour

$\phi_v = \frac{\frac{Fuel\ mass\ fraction}{Air\ mass\ fraction}}{(Fuel / Air)_{stoichiometric}}$ fuel air equivalence ratio

T_r = reference temperature (298K)

T_g = initial temperature of reactant species

T_f = flame temperature

n_{as} = number of moles of air required for stoichiometric combustion

n_p = total number of moles of products

Since C_p is temperature dependent, an iterative method must be used to evaluate the flame temperature. However, in a practical situation combustion is not always stoichiometric and the combustion produces extra products such as CO and H_2. Therefore the accuracy of the above mentioned flame temperature can be increased if more accurate equilibrium equation is used for the chemical reaction as follows:

$$C_Z H_S + j\, O_2 + f\, N_2 \rightarrow a\, H_2O + b\, CO_2 + d\, CO + e\, H_2 + f\, N_2 \qquad (3.37)$$

Where a, b ,d ,e, f and g are the number of moles of various products taking part in the combustion process. Therefore a more accurate flame temperature can be obtained using equation 4.6, and a corrected value for the heat of combustion HC as follows:

$$HC = (CV)_{fuel} - d(CV)_{CO} - e(CV)_{H2} \qquad (3.38)$$

3.5.2 Prediction of Combustion products

The molar fractions of the combustion products are evaluated by taking into account the Gibbs free energy of the various combustion products. The equilibrium solution is obtained by minimising the total free energy of the system. The mathematical solution of this is obtained based on the FORTRAN routines developed by Nazha [109]. To improve accuracy of results, a fifth order polynomial function is used to obtain Gibbs energy for a given temperature and species. In this model 12 product species (CO_2, CO, H_2O, H_2, N_2, O_2, CH_4, NO, HO, O, N and H) are considered and these are supplied to the minimisation module with the appropriate Gibbs functions based on the previously calculated flame temperature. The minimisation program then works in an iteration loop to obtain the minimum Gibbs free energy value. This is then sent to the flame calculation routine with the product species to obtain the temperature. The final values of the product matrices and temperature matrix are passed to the driver unit, which then print output data files. The calculation procedure of the combustion model can be shown in a flow chart as in Fig 3.1.

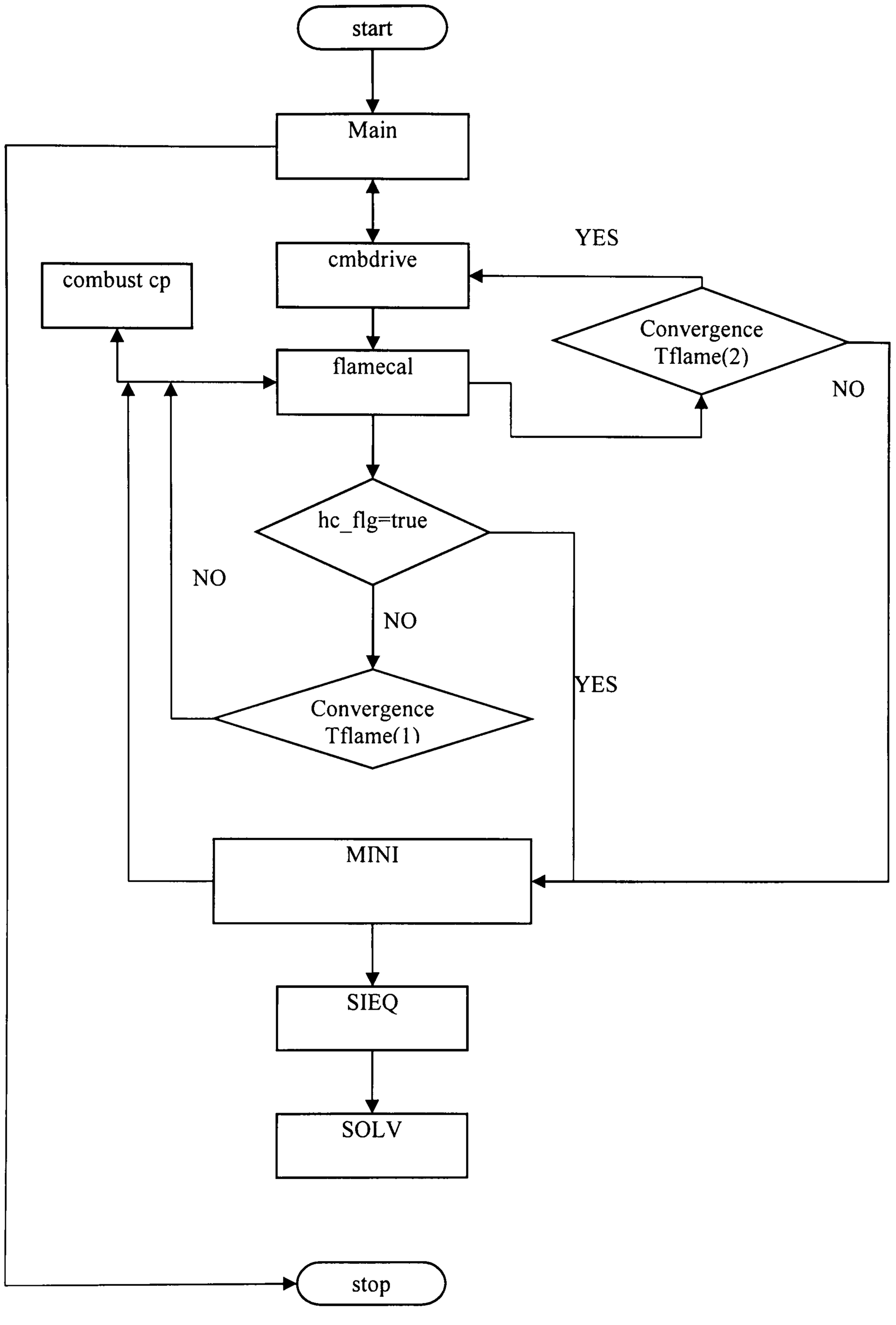
start
Main
cmbdrive
combust cp
flamecal
Convergence
Tflame(2)
YES
NO
hc_flg=true
NO
NO
YES
Convergence
Tflame(1)
MINI
SIEQ
SOLV
stop

Fig. 3.1

CHAPTER 4

Computational Formulation of the Trajectory Method

In this chapter the computational formulation of the separated flow model based on trajectory method is discussed. First a brief introduction of how to address the problem is presented and then the structure of the in-house built LHF code is discussed. This is followed by a detailed description of how to change and modify the LHF code in order to obtain a deterministic separated flow model is presented. Then computational formulation of trajectory subroutine is then discussed. Finally the problems faced during the computational treatment and how they were resolved is presented in detail.

4.1.1 Numerical implementation

As stated in the previous chapter the governing equations of the gas and the droplet phases are highly complex and non linear, which can not be solved analytically. Therefore a numerical method, which is a reliable, accurate enough and computationally efficient, has to be used to solve those equations. First, droplet evaporation and mixing of fuel vapour with gas phase will be modelled. Then the data from the gas phase solution will be used in a mixed is burnt type combustion model to obtain the temperature and species mole fractions. The gas phase will be solved using finite volume method and the droplet phase will be solved using particle trajectory technique, while the interaction between the phases will be accounted through source terms.

4.1.2 Discretisation and solution procedure for the gas phase equations using Finite Volume method

The general form of all partial differential equations (except the continuity equation) presented in previous chapter can be written in a combination of generalised convective, diffusive and source terms as,

$$\frac{\partial(\rho u_i \phi}{\partial x_i} - \frac{\partial}{\partial x_i}\left(\Gamma_\phi \frac{\partial \phi}{\partial x_i}\right) = S_\phi \qquad (4.1)$$

Where ϕ is the generalised flow variable and subscript i represent the x, y, z directions. To solve these partial differential equations numerically, they need to be reduced to a set of algebraic equations (finite difference equations) by integrating over a

domain (control volumes or cells). In order to derive the finite difference equations, the calculation domain (flow field under consideration) is divided into a finite number of control volumes or cells to form a computational grid system. The positions of the variables that are computed, are given by the grid points, which are the points of intersection of the grid lines. In a two dimensional calculation domain, grid lines are parallel to the two axis of the domain and volume surrounded by the grid points form the finite difference cells. The size of the grid should be selected depending on the accuracy needed for the solution of the partial differential equation set, storage capacity and computational time in implementing the solution. Thus the grid size will influence the accuracy and the computational cost.

In this research the knowledge of grid design and selection is important because the same grid system will be used for the solution of the droplet phase (trajectory calculation).

4.1.3 Grid system in 2-D calculation Domain

In order to solve the gas phase equations, the computation domain is divided into smaller cells using grid lines which are parallel to the axes of the coordinate system used. The sizes of the differencing cells are decided based on the required precision of the solution. The grid size influences both the accuracy and the convergence of the iterative scheme. In general, the smaller the grid size the more accurate the solutions up to a certain grid size, then the accuracy of the solution becomes independent of the grid size.

4.1.4 Staggered Grid system

The scalar variables and the two velocity values are stored in staggered positions as shown in Fig.4.1. This ensures the stability of the solution [135, 137]. The scalar variables are evaluated at the nodal points. The velocities (u and v) are defined at the faces of the scalar cell (mid point between the nodal points). Fig.4.1 shows this grid arrangement for a two dimensional Cartesian co-ordinate system.

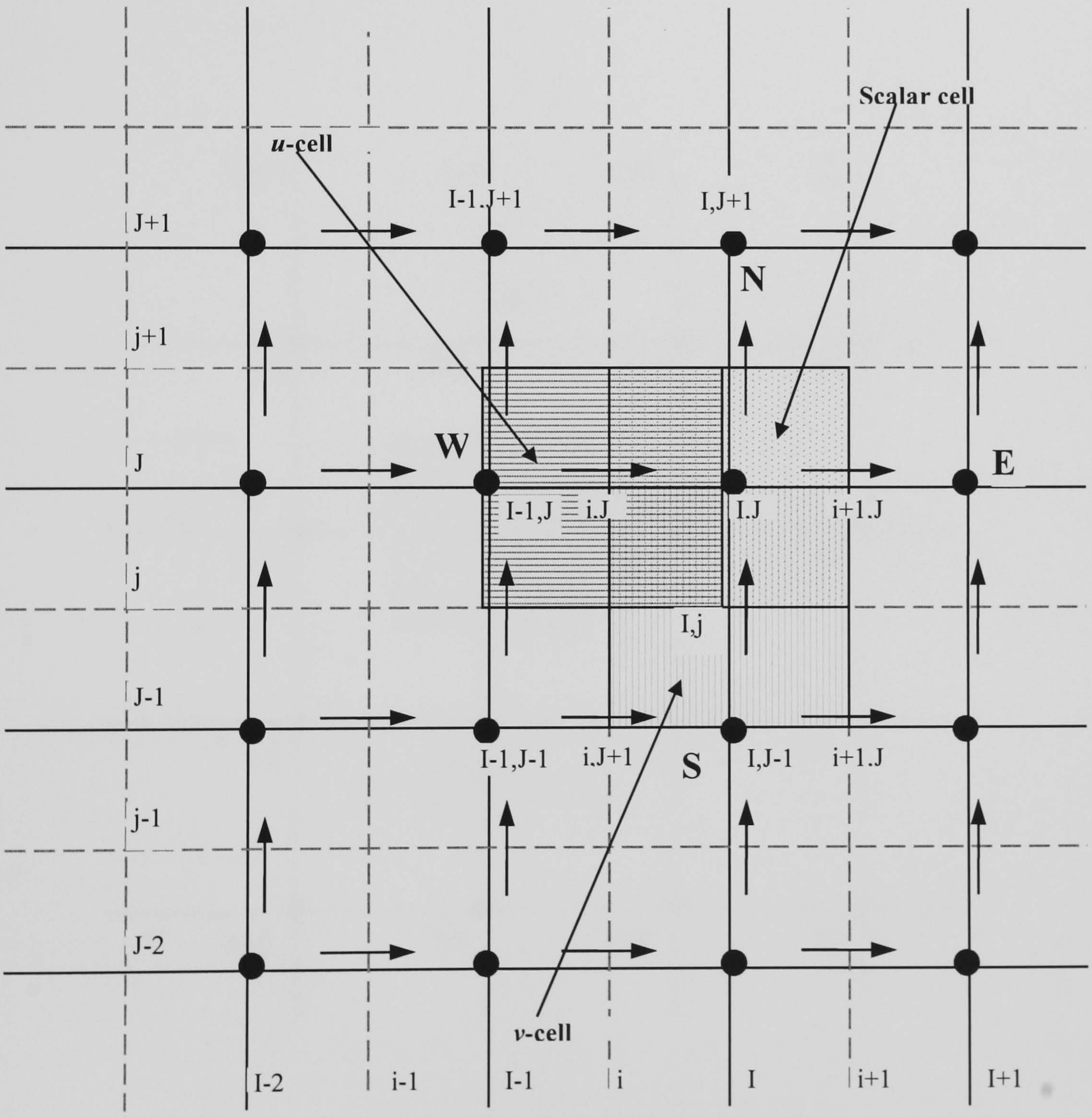

Fig. 4.1 Staggered 2-D Grid System

Arrows in Fig.(4.1) represent the locations where velocities are calculated

If the velocity and pressure were both defined at the nodes of an ordinary control volume, even a highly non-uniform pressure field would act like a uniform pressure field for the discretised momentum equations. This can be demonstrated with an assumed checker-board type pressure field in two-dimensional situation as shown in Fig.4.2.

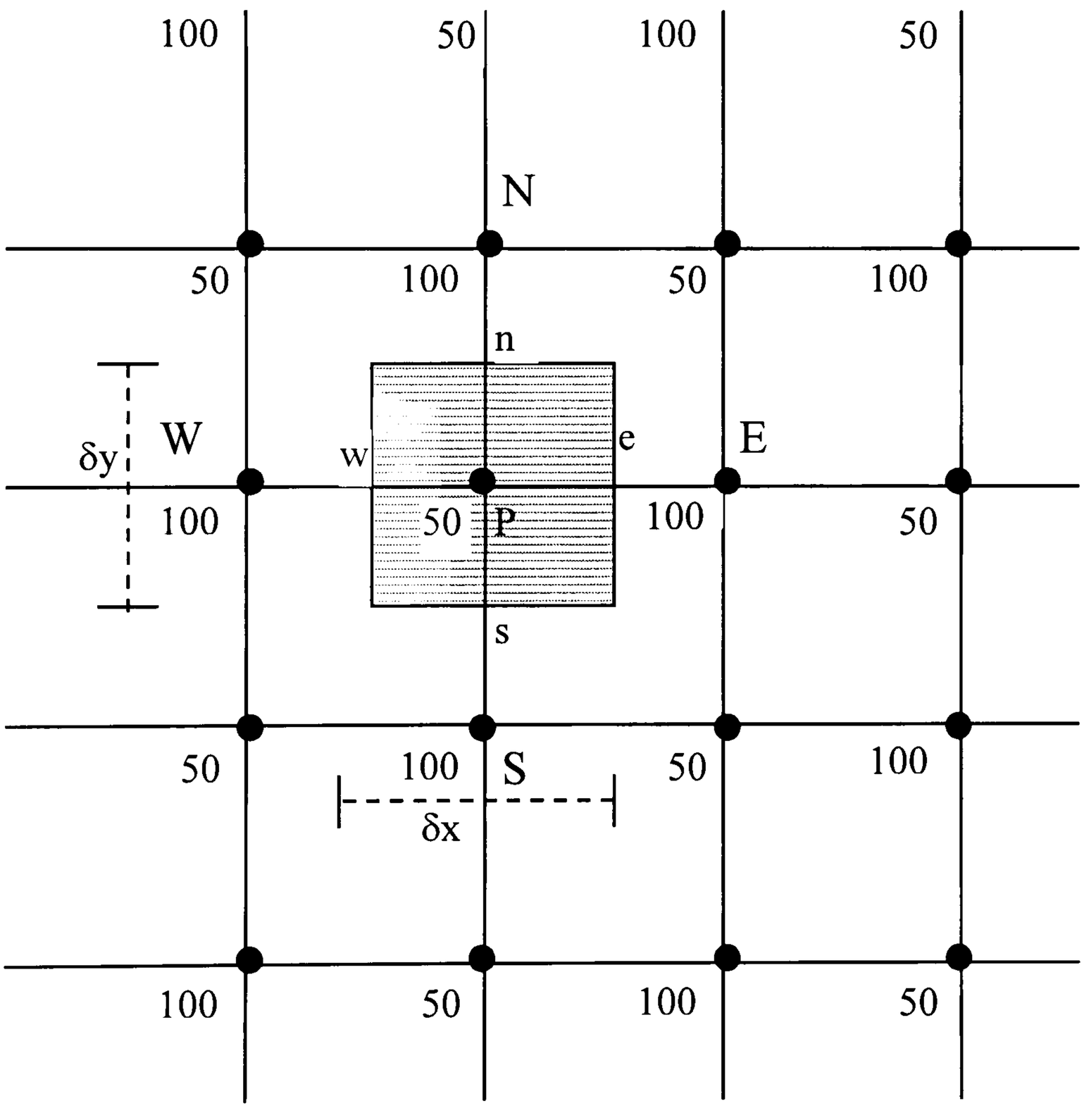

Fig.4.2 Non-uniform pressure field

First consider a grid arrangement where pressure and velocities are represented at nodal points. The pressure gradient for the *u*-momentum and *v*-momentum equations at nodal point *P* can be given by:

$$\frac{\partial P}{\partial x} = \frac{P_e - P_w}{\delta x} = \frac{\left(\frac{P_E + P_P}{2}\right) - \left(\frac{P_P + P_W}{2}\right)}{\delta x} = \frac{P_E - P_W}{2\delta x} \tag{4.2}$$

Similerly,

$$\frac{\partial P}{\partial y} = \frac{P_N - P_S}{2\delta y} \tag{4.3}$$

In the above expressions the pressure at node P does not appear in discretised form of the pressure gradients. Therefore when the above pressure field is substituted to the above equation (4.2) results in a zero pressure gradient at the node ***P*** in both *x* and *y* directions, although the pressure field is highly non-uniform. Thus, the momentum equation sees this as a uniform pressure field which is obviously not true.

In the staggered grid arrangement the pressure nodes coincide with the cell faces of the *u* and *v* control volumes. Therefore if staggered grid system is used, pressure gradients for the two momentum equations are as follows:

$$\frac{\partial P}{\partial x} = \frac{P_P - P_W}{\delta x} \tag{4.4}$$

$$\frac{\partial P}{\partial y} = \frac{P_P - P_S}{\delta y} \tag{4.5}$$

It can be seen that when appropriate values are substituted the resulting pressure gradient terms are non-zero. Thus the staggered grid of the velocity circumvents the unrealistic behaviour of the discretised momentum equations. Another advantage of this grid system is that the calculated velocities are at the exact location where they are required for convection-diffusion computations [8].

4.1.5 Finite Difference Equations; a brief description

The integration of the equation (4.1) over the corresponding control volume (refer Fig.4.1) for the variable ϕ, lead to the algebraic equation of the form;

$$a_P \phi_P = \sum_{i=E,W,N,S} a_i \phi_i + S_u \tag{4.6}$$

where, P is the central node and E, W, N, S are the neighbour nodes of the control volume. The source term; S_ϕ is linearised as:

$$S_\phi = S_P \phi_P + S_u \tag{4.7}$$

where S_P is selected in a way that it is always negative. Then the coefficient of the central node P is given by:

$$a_P = \sum a_i - S_P \tag{4.8}$$

The coefficients a_i contain the influence of the convective and diffusive fluxes through the cell faces. The Peclet number is used as a measure of the relative strength of convection and diffusion.

$$Pe = \rho u \frac{\delta x}{\Gamma} \tag{4.9}$$

For pure diffusion *Pe* is zero and *Pe* increases convection increases. The influence becomes increasingly bias towards upstream direction of the flow with larger values of Pe. Therefore, this phenomenon must be taken into account when selecting a differencing scheme. For practical flow problems with convection and diffusion, the hybrid differencing scheme has been used widely. This uses central differencing for low Peclet number ($Pe<2$) situations and upwind differencing for high Peclet numbers ($Pe>2$) [136]. The coefficients of the discretised equation (4.1) which result from applying the hybrid scheme are given in tables 4.1 and 4.2.

a_W	$\max[F_w, (D_w + F_w/2), 0)]$
a_E	$\max[-F_e, (D_e - F_e/2), 0)]$
a_S	$\max[F_s, (D_s + F_s/2), 0)]$
a_N	$\max[-F_n, (D_n - F_n/2), 0)]$

Table 4.1 coefficients of the general finite volume equation

In the above expressions F and D are calculated using following formulae:

Face	w	e	s	n
F	$(\rho u)_w A_w$	$(\rho u)_e A_e$	$(\rho u)_s A_s$	$(\rho u)_n A_n$
D	$\frac{\Gamma_w}{\delta x_{WP}} A_w$	$\frac{\Gamma_e}{\delta x_{PE}} A_e$	$\frac{\Gamma_s}{\delta y_{SP}} A_s$	$\frac{\Gamma_n}{\delta y_{PN}} A_n$

Table 4.2 convective and diffusive terms

4.1.6 Boundary conditions

For the solution of partial differential equations require information to be provided at all points on a closed boundary surrounding the solution domain. The specifications of these boundary conditions are vary according to each problem. The treatment and implementation of boundary conditions in general are given in detail in Versteeg and Malalasekera [8]. Also the boundary conditions for the problem under consideration are given in detail in Rajakaruna [9].

4.1.7 Solution methodology of the finite difference equations

In order to accommodate the non-linear nature of the underlying flow phenomena and the linkage between the pressure and velocity in a variable density fluid, the SIMPLE algorithm developed by Patankar and Spalding [135, 138] is used as the core of the solution procedure. For more detailed description of SIMPLE algorithm, the reader may refer the works of Rajakaruna [9] and Versteeg & Malalasekara [8]. The set of resulting algebraic equations are solved by repeated sweeps of line by line application of the well known Tri-Diagonal Matrix Algorithm (TDMA) [8, 136].

As a starting point to the development of the separated flow model the author has used an in-house LHF code [9]. The solution procedure of this code is based on the above described simple algorithm. Main contribution is the modification of this code to change it to a separated flow code capable of modelling the two phase flows accounting for transfer of mass, momentum and energy between the two phases.

4.2 The in-house two-phase evaporation model based on LHF approach

The program is designed to simulate droplet evaporation and mixing process involved in steady state turbulent gas-liquid flows inside a cylindrical combustion chamber. A cylindrical combustion chamber type as shown in Figure 4.3 with fuel and air inlets placed concentrically at one end of the chamber is considered.

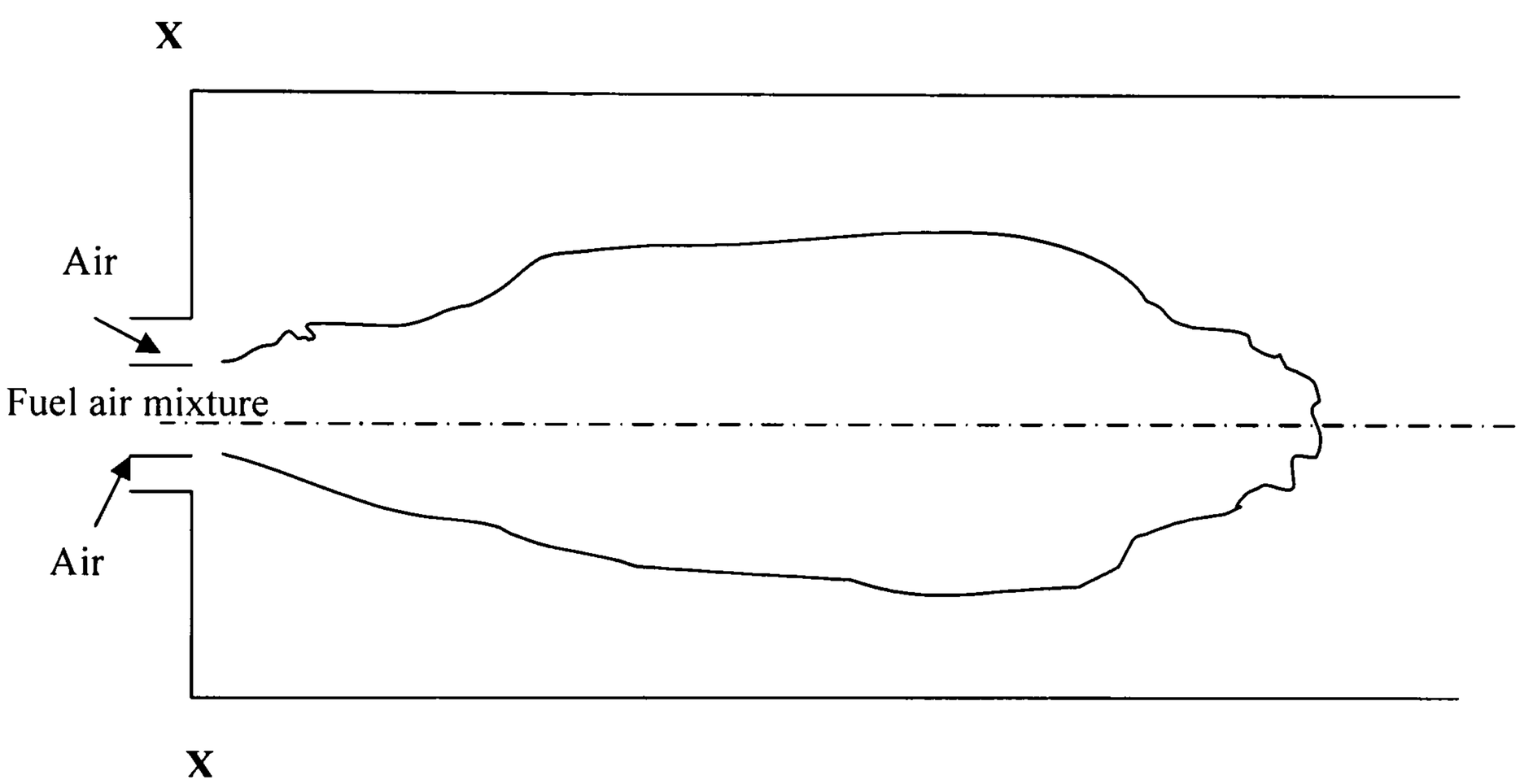

Fig. 4.3 cross sectional view of the chamber configuration

The length and diameter of the chamber and the radius of each inlet port could be varied by the user. The partial differential equations governing the flow are discretised using finite volume method, which are then solved numerically. The structure of the program is based on the TEACH-T code of Gosman et al [139].

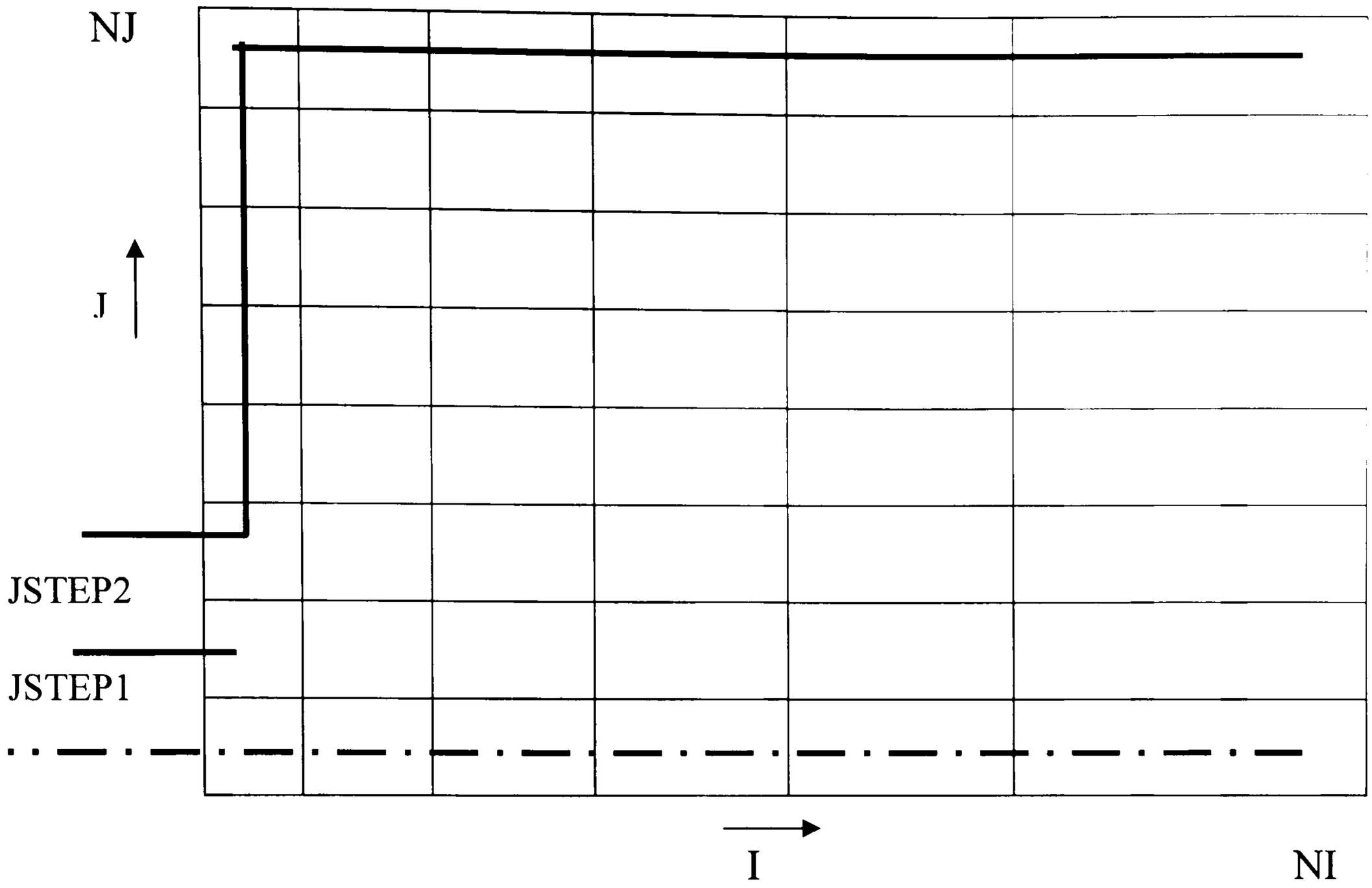

Fig 4.4 Grid system

For the finite volume formulation the flow field is divided into NI grid points in the axial direction and NJ grid points in the radial direction (Fig. 4.6). The terms JSTEP1 and JSTEP2 in the figure denotes the last grid point inside each of the two inlet ports supplying air and fuel. The thick lines represent the physical geometry of the cylindrical chamber and the dashed line is the axis of symmetry.

4.2.1 LHF model general overview

In the LHF formulation, the velocity and temperature differences between the two phases are neglected in the mixing program. The presence of the dispersed phase (droplet phase) is accounted for via the mixture density. The mixture density is a linear combination of the densities of liquid fuel, fuel vapour and air. In most LHF formulations the dispersed phase evaporation is calculated using saturation vapour pressure of the fuel in each control volume [47-48]. But in this model a droplet evaporation program is used in parallel to the mixing program with facility for passing data between the two modules. The droplet program obtains the information regarding the droplet residence time and position from the mixing program and work out the evaporation rate. The mixing program then uses the evaporation data from the droplet module to calculate the local density for each control volume.

The droplet evaporation is modelled as follows; a single droplet evaporating along the flow axis is assumed to represent the entire droplet phase evaporation. The start of the evaporation is at the first X-grid location inside the computational domain. Once the evaporation rate has been derived the liquid to gas ratio of the fuel is calculated. Based on this information, the density and the specific heat capacities of that particular cell are derived. The droplet evaporation is activated from a single call to the droplet module, which contains all the necessary subroutines for the evaporation model to work independently.

4.2.2 Mixing and evaporation temperature approximations

In this LHF model, droplet evaporation module and the mixing module uses two different temperatures, which are arrived at empirically. The way this temperature levels are arrived can be described as follows: In this model the transfer of energy between the two phase is based on the change of properties of the gas phase due to the droplet evaporation process. The changes occur in the control volumes traversed by the droplet is propagated to other control volumes via the mixing process. Therefore this model is described as an "Effective Property" type LHF model. There are two processes that cause local gas temperature to change; evaporation and combustion. That is due to the enthalpy of evaporation of fuel droplets and the enthalpy of combustion of fuel air mixture. Since the combustion module is run at the end of the mixing program as a "mixed is burnt" type module, it is necessary to set the mixing temperature by taking into account both of the above processes. In order to simulate mixing process, this temperature should be close to combustion temperature. Thus a mean temperature value of 1500K has chosen as the initial inlet temperature based on experimental findings [109]. The inlet air velocity and density are calculated based on this temperature and the inlet fuel mass flow rate. Although this causes the gas velocities and densities in the near injector region to differ substantially from the actual, this allows the theoretical values of the velocities and densities in the second half of the chamber to be more representative of the actual situation.

If the droplet evaporation is simulated at the above discussed gas phase mixing temperature, it will be a seriously over estimation during the early part of the

droplet evaporation and it will be a under estimation of the temperature during later part of the evaporation where combustion takes place. Therefore the evaporation is masked from the gas phase cell temperature and the evaporation is carried out using an empirically determined temperature function, which is base on the axial distance traversed by the droplet. The form of the temperature function was arrived at by comparing theoretically predicted values of temperature with that of the experimental values observed of Nazha [109].

4.2.3 Turbulence modelling approximation

It is assumed that the flow is fully turbulent. Therefore the viscosity of the flow is calculated as a fully turbulent viscosity μ_t. The standard exchange coefficients (σ_x) used in gas flows are used as exchange coefficients for the calculation of diffusion terms.

$$\mu_e = \mu + C_\mu \rho k^2 / \varepsilon \tag{4.10}$$

4.2.4 Structure of the LHF code

The programme layout of this LHF code is modular in nature allowing additions and modifications of specific routines as required. The solution procedure is based on the SIMPLE method and it is coded using FORTRAN77 programming language. The structure and layout of this code is shown in the flow diagram in Fig. 4.5. The sequence of operation of the programme is as follows.

First, the input variables are read from the data files and then the grid system is arranged based on user specified conditions. Next, the flow and property variables are initialised. The program then proceeds into an iteration loop, wherein the solution of flow variables and updating of property matrices and the boundary conditions are carried out. The iteration proceeds until convergence is achieved or until a pre-determined maximum number of iteration steps are reached. The number of iteration steps and the convergence criteria are given with the initial data.

All flow variables; U, V, T etc. are solved using respective subroutine modules. The subroutine modules are structured in such a manner that for each variable the generic part of the partial deferential equation and the terms other than the boundary condition source terms are evaluated in one routine (with starting letters 'CALC', i.e. CALCU,CALCV CALCT etc.). The remaining source terms are dealt in a separate common subroutine for all flow variables with multiple entry and exit points for each variable (PROMOD).

All gas phase thermodynamic and chemical properties [141] are calculated by a separate property module (PROPS) which sets up the property matrices before transferring control to the main program. This module calls for a set of routines to calculate properties such as molar volume, specific heat capacities and laminar viscosity etc..

All output results are directed to files written in a format accessible to MATLAB for data processing and visualisation.

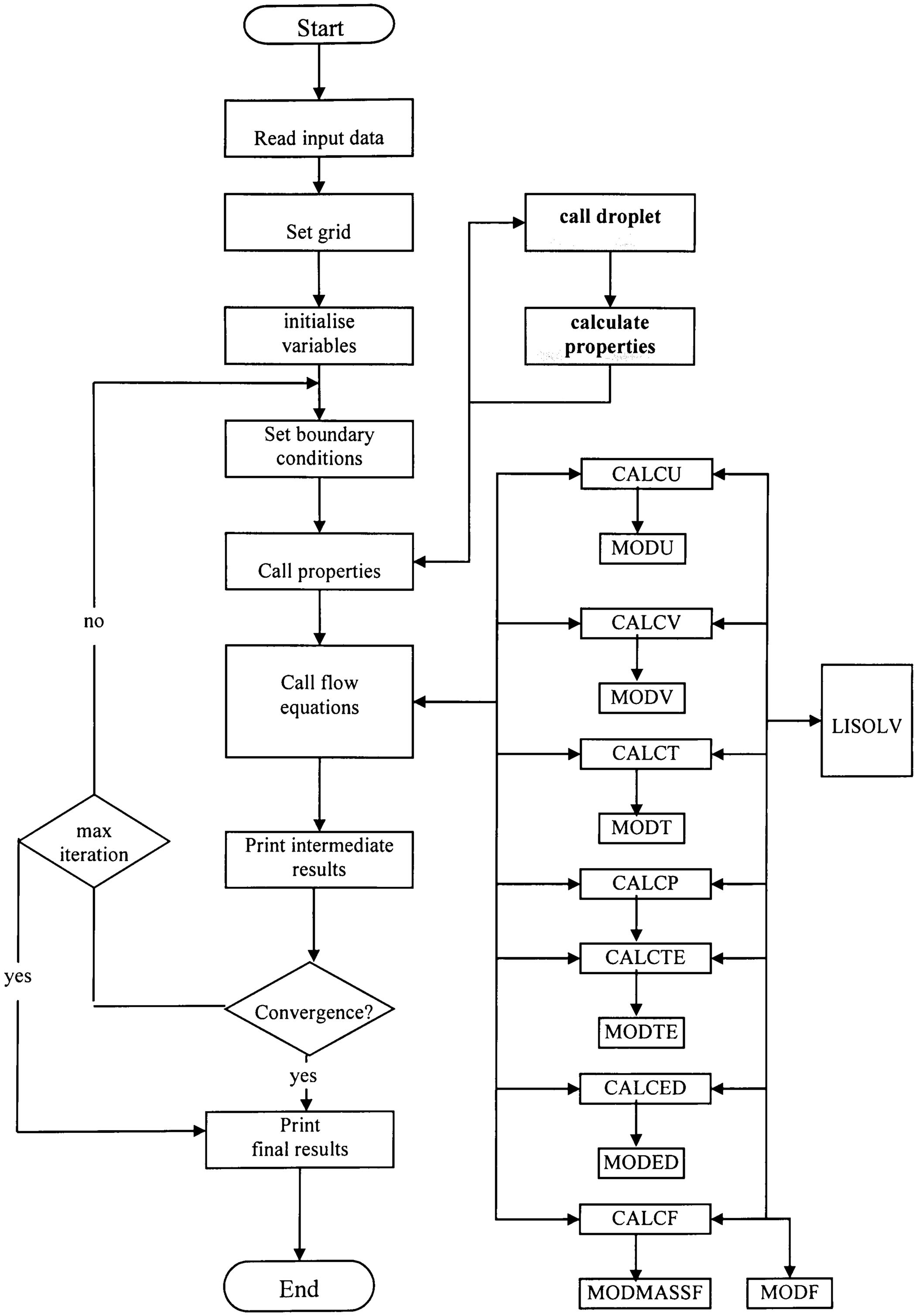
Start
Read input data
Set grid
initialise variables
Set boundary conditions
Call properties
Call flow equations
max iteration
no
yes
Print intermediate results
Convergence?
yes
Print final results
End
call droplet
calculate properties
CALCU
MODU
CALCV
MODV
CALCT
MODT
CALCP
CALCTE
MODTE
CALCED
MODED
CALCF
MODMASSF
MODF
LISOLV

Fig. 4.5

4.2.5 Definition of Subroutines and Functions

CALCU	discretised u-momentum equation
CALCV	discretised v-momentum equation
CALCT	discretised energy equation
CALCP	discretised pressure correction equation
CALCF	discretised fuel mass fraction equation
CALCED	discretised turbulent energy dissipation rate equation
CALCEK	discretised turbulent kinetic energy equation
PROPS	module that co-ordinates all the property subroutines, calculation of the necessary turbulent parameters and setting up of property matrices
PROMOD	unit that calculate the boundary condition source terms of each 'CALC' routine.
LISOLV	TDMA routine for line by line iteration method for the solution of the finite volume equations
BWR	Benedict Web Rubin equation for molar volume calculation
CPCVIDL	ideal gas C_p (T), C_v(T) calculation routine
VISCTHRM	laminar viscosity and thermal conductivity calculation routine
PRINT	routine to print all flow variables of the computational domain at user specified iteration level
PRINTVEL	routine to print data in a format accessible by MATLAB

4.3 Modifications made to convert the LHF code to a Separated Flow code

When converting the LHF code into a deterministic separated flow code, a number of modifications have been carried out in most of the subroutine modules. These subroutines are INIT, CALAU, CALCV, CALCT, CALCF CALCP and PROPS. Apart from the subroutines INIT and PROPS, all the others were modified mainly to accommodate the source terms from the dispersed phase.

4.3.1 Modification to the Property Routine (PROPS) ;

This is the subroutine which updates the mixture properties after each iteration. Mixture density (fuel vapour and air), C_p and C_v calculations are modified. The above quantities are now evaluated as follows:

Mixture density

$$\rho_{mix} = \frac{P_{absolute}}{(\alpha_{fuel} R_{fuel-vap} + (1-\alpha_{fuel}) R_{air}) T} \tag{4.11}$$

Specific heat capacities

$$C_{p_{mixture}} = \alpha C_{p_{fuel\_vap}} + (1-\alpha) C_{p_{air}} \tag{4.12}$$

$$C_{v_{mixture}} = \alpha C_{v_{fuel\_vap}} + (1-\alpha) C_{v;air} \tag{4.13}$$

4.3.2 Modification to the velocity (CALCU and CALCV);

To take into account of the momentum exchange between gas phase and droplet phase in x-direction, a momentum source term (momenx) is added to the subroutine CALCU. This is passed to the main gas phase program from the trajectory module through a common variable.

As discussed in chapter 3, when solving droplet phase equations all the calculations are carried out in the scalar grid of the staggered grid system. Therefore all the source terms obtained are valid only for this scalar grid (Fig.4.6). Thus, in order to add these momentum source terms (smomenx), a correction has to be made. So, if momentum source term of U velocity cell (i,J) is Umomentum, then this is given by

$$Umomentum(i,J)=0.5*(smomenx(I,J)+smomenx(I-1,J)) \quad (4.14)$$

Similarly, to take in to account the momentum exchange in the Y-direction, a source term (momeny) is added to the subroutine CALCV and this is given by

$$Vmomentum(I,j)=0.5*(smomeny(I,J)+smomeny(I,J-1)) \quad (4.15)$$

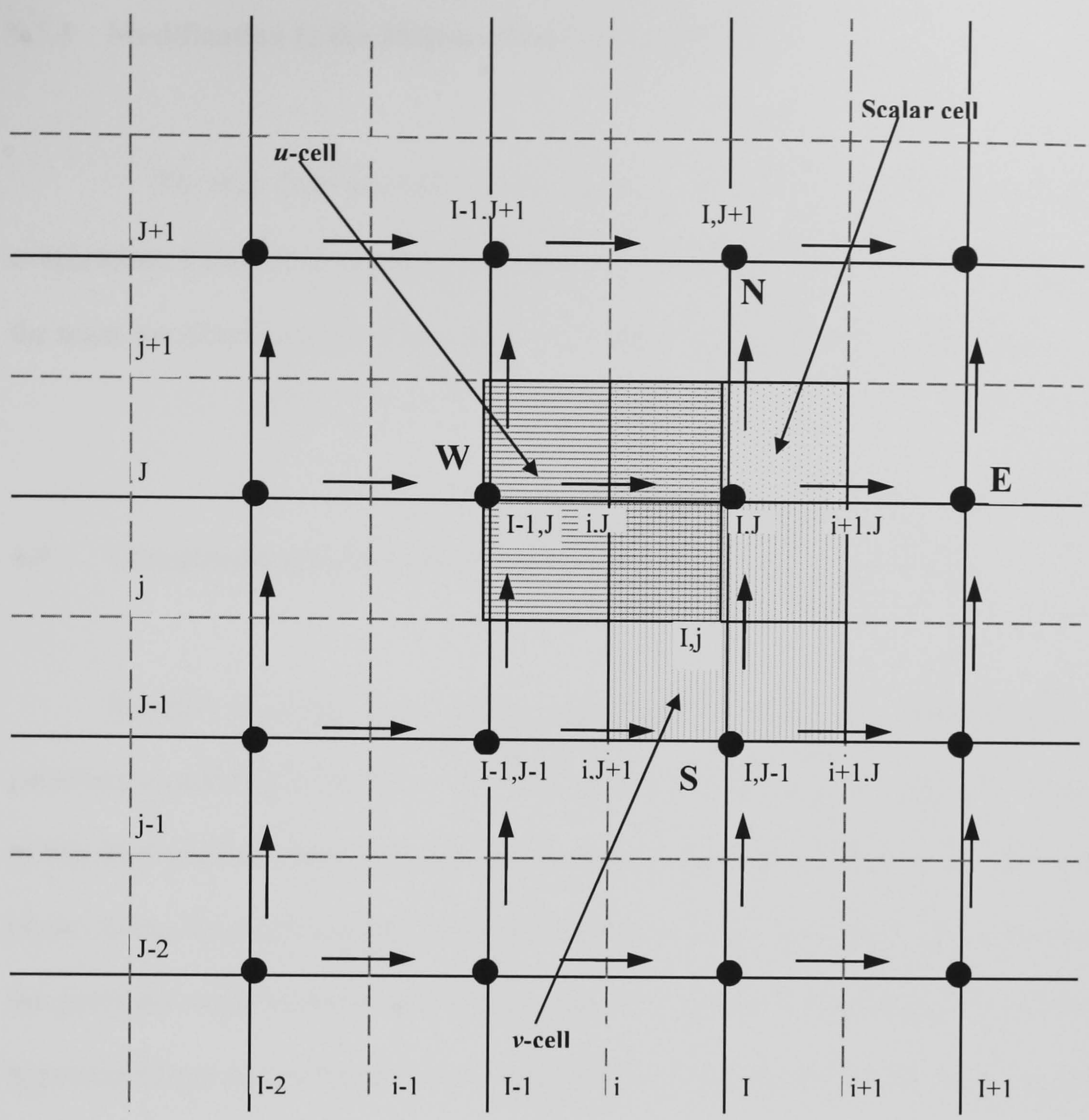

Fig.4.6

4.3.3 Modification to the Temperature (CALCT) and the Continuity (CALCP) equation.

In order to take into account of the energy exchange and mass exchange between gas phase and droplets due to droplet evaporation, respective source terms (senergy, smass) are added to the subroutines CALCT and CALCP. These source terms are passed to the main gas phase program from the trajectory module through a common variable.

4.3.4 Modification to the Mixture fraction (CALCF);

To take into account of the change in mixture fraction due to droplet evaporation, a source term (smass) is added to the subroutine CALCF. This is passed to the main gas phase program from trajectory module through a common variable.

4.4 Computational (treatment) Formulation of Trajectory module

In order to apply the trajectory approach to model the droplet phase, it is necessary to subdivide the flow field into a series of cells as in the figure 4.7. Each cell in this flow field is regarded as a control volume or a computational cell for the gaseous phase. Since the gas phase and droplet phase both interact with each other, scalar grid of the gas phase calculations is used as the computational grid of the trajectory model. This approach allows to use the gas phase properties without modifications when calculating droplet trajectories and life histories. And also this will enable easy application of the droplet source terms in gas phase calculations.

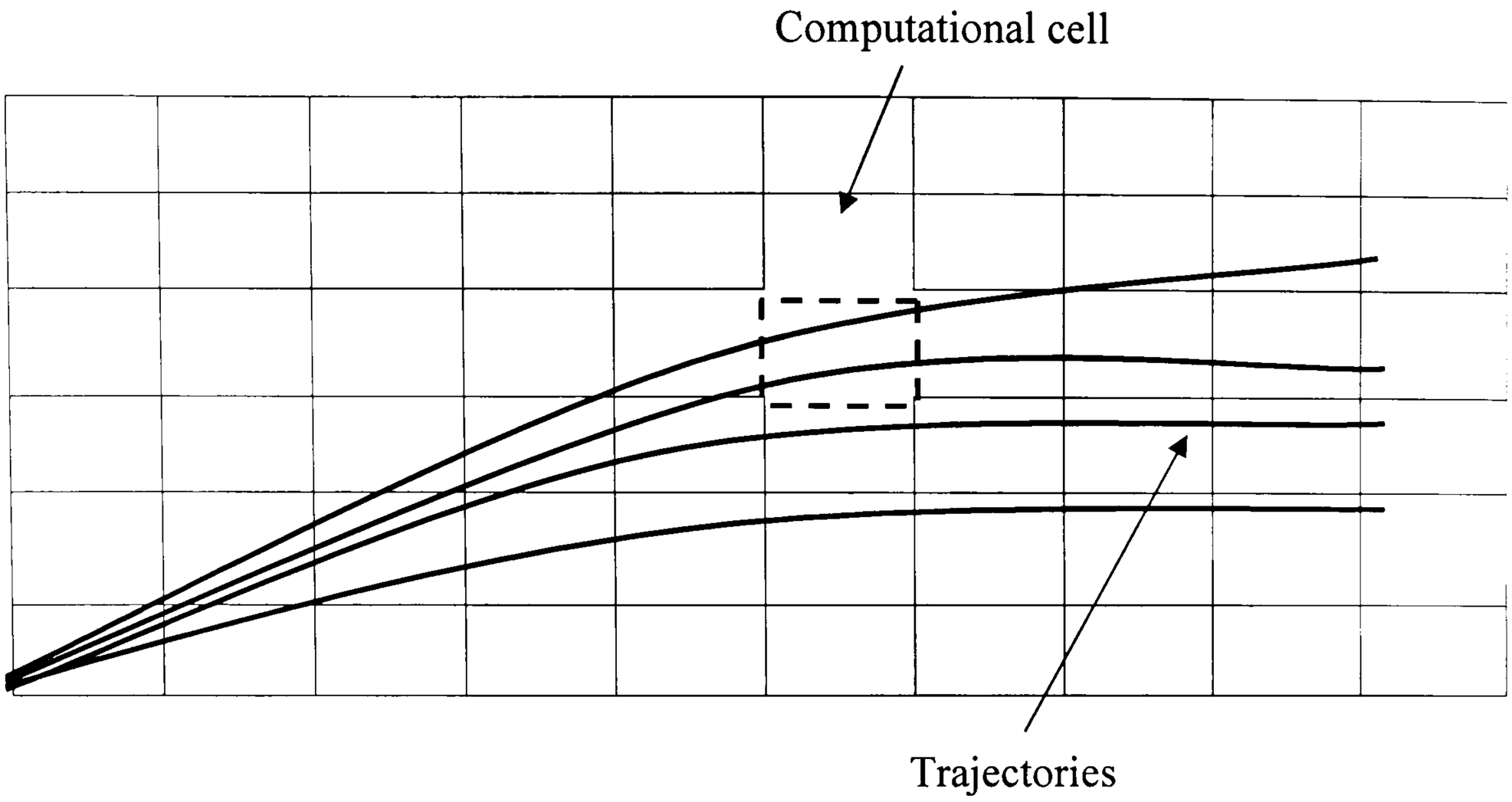

Fig. 4.7

Consider a cell in two dimensional flow field, through which a droplet is moving, (fig. 4.8). The four faces of this cell can be identified as N, S, E and W to denote North, South, East and West faces respectively. A droplet entering the cell from the west face, can exit through any of the four faces of the cell (as indicated by the four trajectories in fig.4.8.

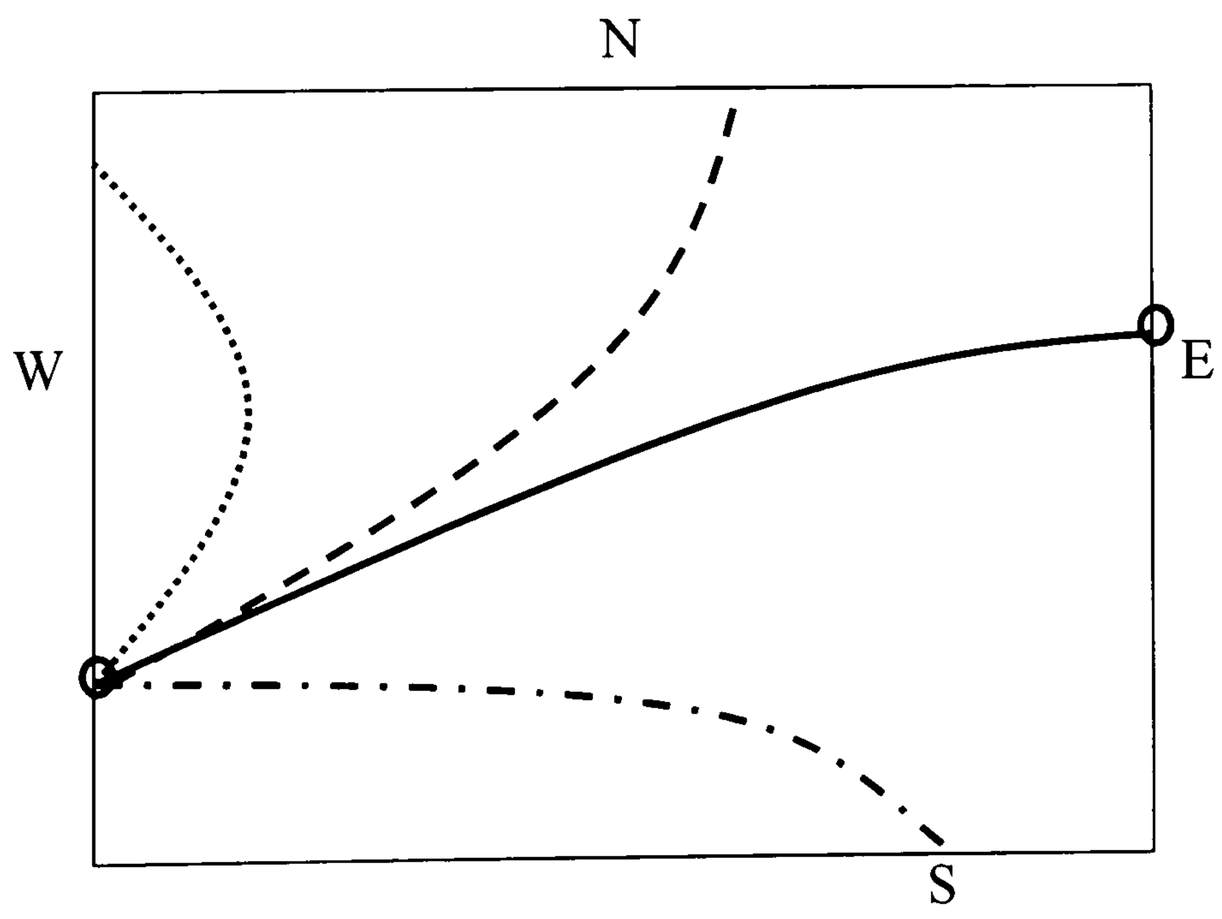

Fig. 4.8

Next, it is necessary to find out how many droplets are needed to model the droplet phase. If 20μm diameter droplets are injected from the nozzle at a rate of 5.4g/s [109], then there will be about $1.5*10^9$ droplets. Since it is impractical to model all these droplets individually, a smaller number of computational droplets were chosen to represent the actual droplet phase. Each computational droplet is regarded as a parcel of droplets. And also, the entry of the droplets to the gas flow field is represented by a finite number of entry positions. The mass of droplet size d_i, which enters per unit time at port j is given by

$$\dot{m}_{pj}(d_i) = \dot{m}_p X_j Y_i \tag{4.16}$$

where m_p is the total droplet mass inflow rate, X_j is the fraction of the droplet mass, which enters at port j, and Y_i is the fraction of droplet mass with initial diameter d_i. If droplets are assumed to be spherical and the number flow rate of droplets of a given initial size can be taken as constant along a trajectory, the number flow rate of droplets of initial diameter d_i along a given trajectory is determined by

$$\dot{\eta}_j(d_i) = \frac{6\dot{m}_p X_j . Y_i}{\pi \rho_d d_i^{\,3}} \tag{4.17}$$

As described previously, the combustion system under consideration is an axi-symmetric system. Therefore the number of droplets that need to be tracked can be reduced if symmetry is taken into account. For the gas phase calculation a sector of

angle 1radion is used to calculate gas phase properties. Therefore the number of droplets whose trajectories are needed to be calculated, are $1/2\pi$ of the total number of representative droplets of the spray.

4.5.1 Droplet injecting area diameter

In this work the author has modelled fuel spray evaporation with dilute dispersed flow assumptions. In the literature review it was shown that fuel spray could be taken as dilute dispersed except in the near injector region where droplet break-up and coalescence occur. Also it must be pointed out that void fraction is not taken into account (effect due to the volume occupied by droplets) for gas phase flow solution. Since the effect of void fraction becomes significant in the near injector region due to the high liquid fuel mass fraction, if the dispersed phase modelling started some distance away from the injector exit it is possible to safely assume that the droplets are sufficiently remote and void fraction is unity. This leads to a larger droplet inlet area compared to actual injector exit diameter. The outcome is the use of fuel inlet region with radius of about 5mm, which was determined empirically.

4.5.2 Droplet size distribution

For the two phase separated flow approach more rigorous description of fuel spray inlet characteristics such as droplet size and velocity distribution and also radial distribution of droplet mass fraction in each size category are required. However, it is difficult to find relevant experimental data on these characteristics therefore the author

has used empirical models to determine drop size distributions. In literature the most common models used to determine size distribution are log-normal, Rosin-Rammlar and Nukiyama distributions. During this work all these three models were taken in to account and these were calibrated to produce distributions of 20μm sauter mean diameter. Then the two-phase model has been solved with all these three distributions. After that the resulting flow predictions have been compared against available experimental data, which has shown that for the conditions used in this modelling situation the use of Nukiyama size distribution has produced results more close to the experimental data. Therefore, Nukiyama distribution has been selected to describe the spray size distribution. The calibrated Nukiyama size distribution (shown in Fig. 4.9) for 20mm sauter mean diameter can be written as:

$$f_3(D) = aD^p \exp(-bD^q) \tag{4.18}$$

where $a = 2.2002*10^5$

$b = 0.302$

$p = 5$

$q = 0.95$

D is droplet diameter in μm

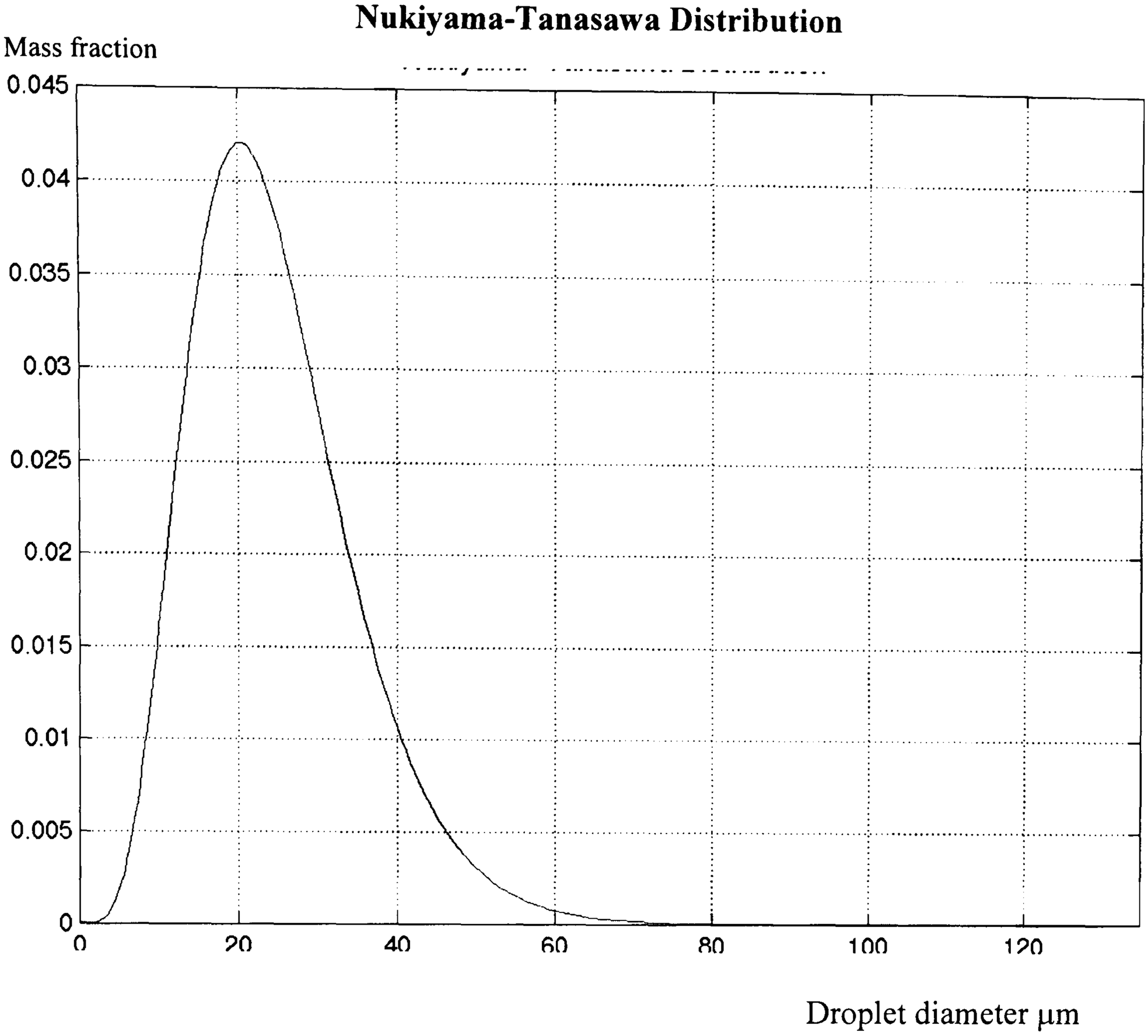

Fig. 4.9

This is a continuous distribution having droplet diameters from starting close to zero diameter to some maximum size as in the case of actual fuel spray. In the current model the maximum is about 125μm. However, it is not computationally realistic to use all those possible diameters when solving dispersed phase equations and predicting droplet trajectories. Therefore, this distribution is divided into six size groups (as shown in Fig.4.10) and arithmetic mean diameter of a particular size group is used as the representative diameter for that group.

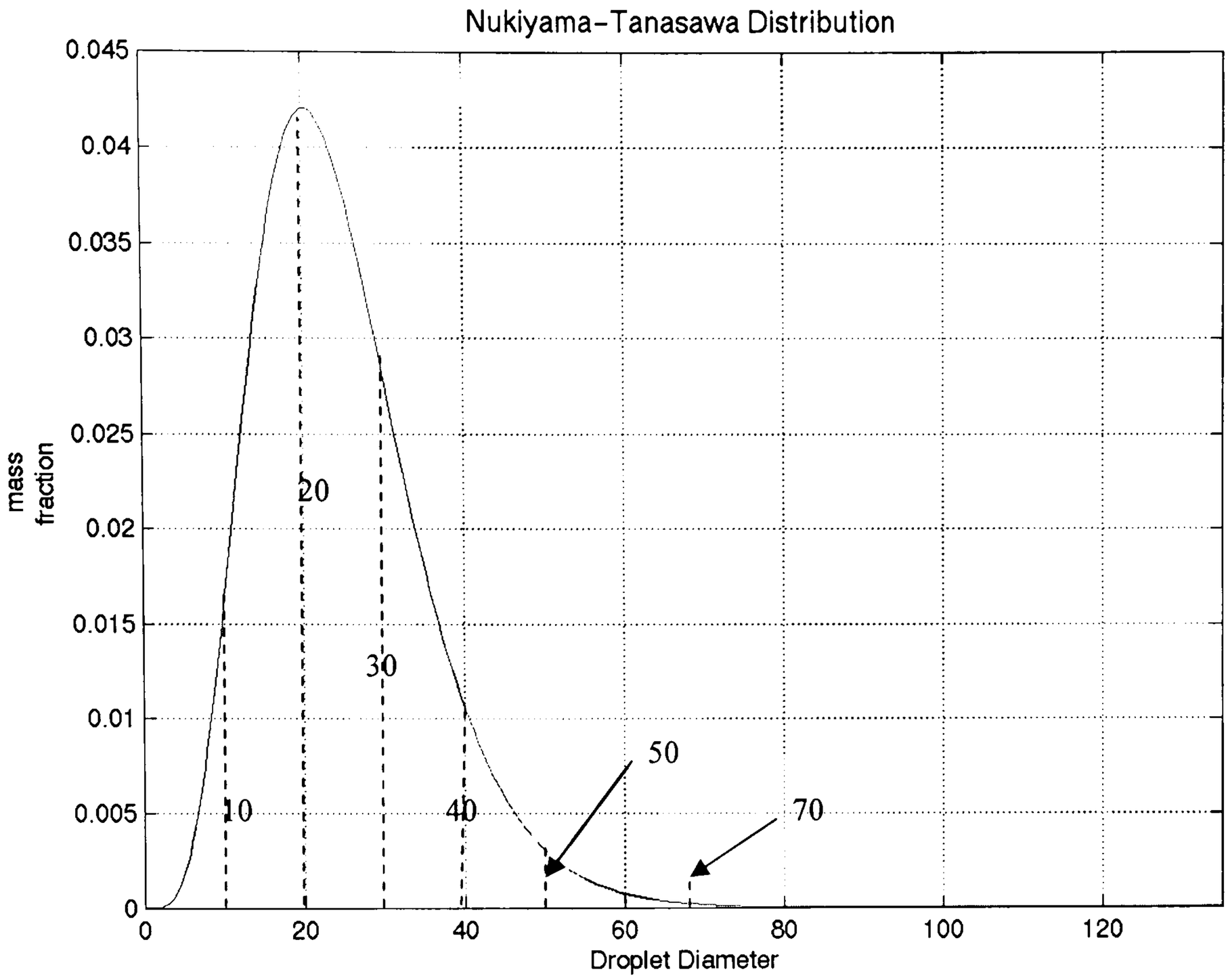

Fig.4.10

The six diameter groups shown above are selected as representative diameters to cover the whole extent of the size distribution. Then the distribution is divided into six sectors (as shown in the table 4.3) to include those six diameters such that the mean diameter of the sector is equal to the representative diameter of that section. Then the distribution function is integrated over the limits of each sector to obtain fuel mass fraction represented by that particular droplet size group.

Droplet size	Drop Diameter Range	Mean diameter(μm)
D1	0- 15.0	10.0
D2	15.0 – 25.0	20.0
D3	25.0 – 36.5	30.0
D4	36.5 – 45.0	40.0
D5	45.0 – 65.0	50.0
D6	65.0 – 125.0	70.0

Table 4.3

4.5.3 Radial distribution of droplets

Droplets in a spray are distributed over the span of the spray angle in varying proportions according to their sizes. It is known that large droplets travel mainly close to the centre line, while smaller droplets tend to move near the edge of the spray cone. However, this does not mean that large droplets are present only near the centre line or there are no smaller droplets near the centre line, but the proportion is less. When distributing droplets among the trajectories, it is therefore required to take this fact into account [1].

As discussed previously, it is assumed that the droplets start some distance away from the injector. Therefore it is possible to assume that the droplets start from a circular cross sectional area. However, since various drop trajectories starts from this cross section, it needs to be divided to allocate positions for each drop trajectory. This

has been done by partitioning this area by concentric circles [1] with equal separation (Δr) as shown in Fig. 4.11.

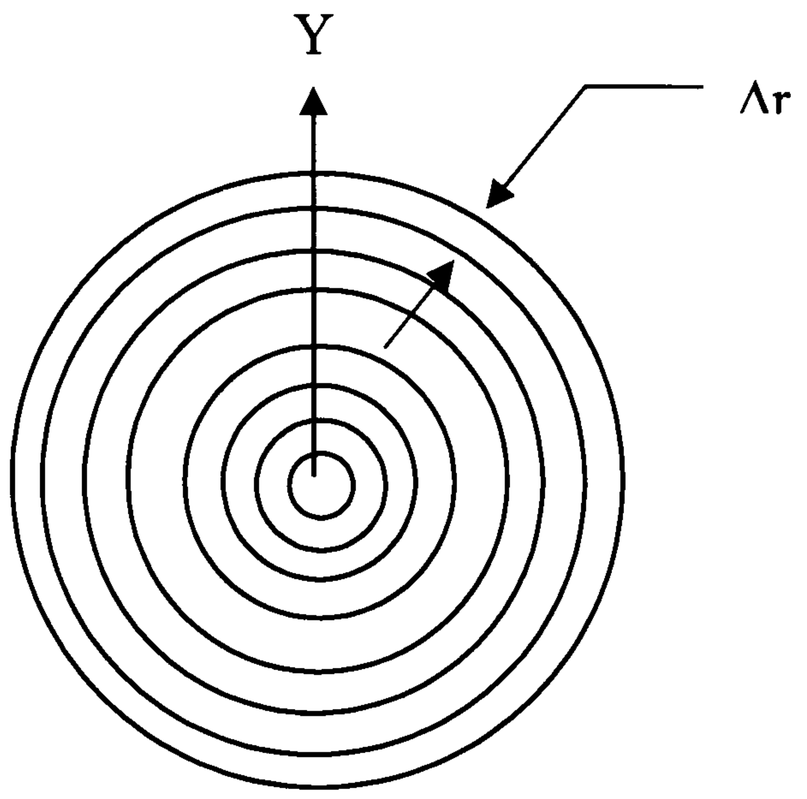

Fig. 4.11

Consider the sectional elevation OY of Fig. 4.11, these represent the droplet starting positions which started from a point upstream of the flow (injector exist) as shown in Fig.4.12. To represent the angle of separation between trajectories, previously described drop starting angle has been used.

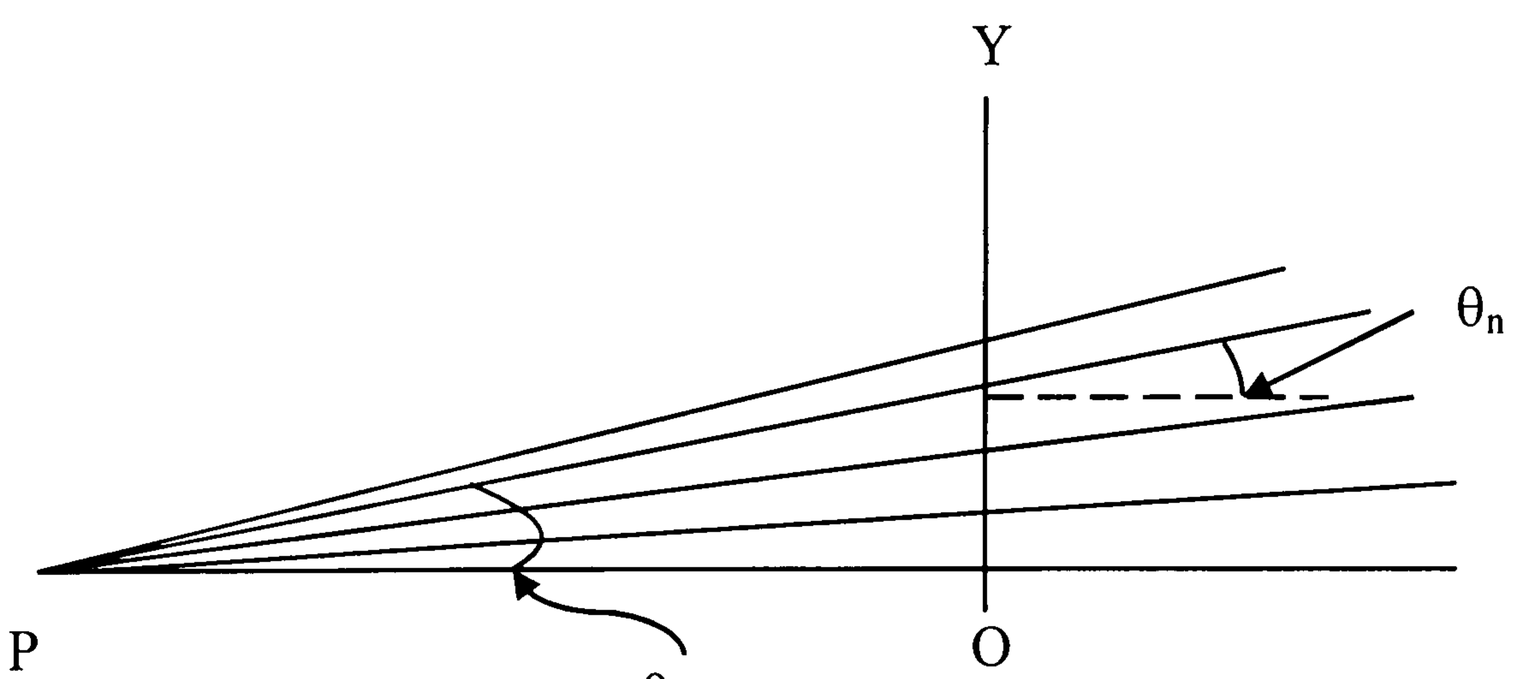

θ_n

Fig.4.12

It is also assumed that the droplet velocity and diameter at'O' is equal to that of point P. this can be justified, because

1. Droplet temperature will not change while it is travelling this small distance (due to the high velocity), hence small time interval and droplet evaporation is negligible during this time interval.

2. This portion of spray mainly contains liquid fuel and the mass fraction of air is very small compared to that of the fuel. Therefore very negligible amount of momentum of fuel spray will be lost due to drag. It is therefore reasonable to assume that the fuel droplet velocity is the same at both points.

After taking into consideration all the above facts, two functions are formulated to represent droplet number distribution over the trajectories. It is found by experimental observations that in outer boundary of the spray mainly smaller droplets are present and larger droplets move more close to the centre line [24, 142] (due to their high inertia larger droplets tend to move in the direction of the injector). In order to take into account this phenomenon, a distribution function is used and it can be written as

$$N_{drop} = \frac{N_{total\_drop} * ntraj(ntraj^2 - (ntraj-1)^2) * 6}{nt * (nt+1)(4nt-1)} \tag{4.19}$$

Where ntraj n^{th} Trajectory in the size group

nt number of trajectories in a size group

4.5.4 Velocity distribution

In this study the injection process is assumed to be pressure atomized. The span, over which the fuel spray is distributed, is called the spray angle (α). In a pressure atomising injector, this angle is normally between 5 – 25 degrees.

Therefore, inlet velocity of a droplet trajectory with θ starting angle to centre line and with x-direction starting velocity of ***vxd*** can be defined as

X-direction velocity = *vxd*

Y-direction velocity = $vxd^{*}.tan\theta$

Since only half spray angle ($\alpha/2$) is considered due to symmetry of the flow configuration, all the droplet trajectories concerned are to be distributed over the half spray angle. Therefore, for a particular droplet size group with ***'nt'*** number of trajectories, starting angle of n^{th} trajectory can be given as

$$\theta_n = \frac{\alpha}{2}\frac{n}{nt} \tag{4.20}$$

Since initial velocity of droplets could not be obtained from experimental data, an approximate value has been determined based on Nazha et al's [109] experimental setup parameters (given in chapter 5.4). Using nozzle diameter and fuel mass flow rate and simple geometry the droplet starting velocity (*vxd*) of 200m/s obtained and used in calculations. This same value is used in all tests and comparisons.

4.6.1 Particle Trajectory calculation

After choosing the necessary governing equations for the particle phase, the main difficulty is to find a method to track the intersecting position of the droplet trajectory with the computational cell walls of the gas phase. This is vital because when the particle moves out from the present control volume to another, local gas phase properties of the new location have to be used in the calculation. If an arbitrary value is used for the time increment (Δt), the particle may not be within the same cell at the end of that interval. In the literature most authors used trial and error methods to find an approximate Δt in order to determine this intersecting point. This method can be described as follows:

First consider the equations for droplet velocity and position, and assume that a droplet with velocity (u_0,v_0) is at the location (x_i,y_i) as shown in the fig. 4.13.

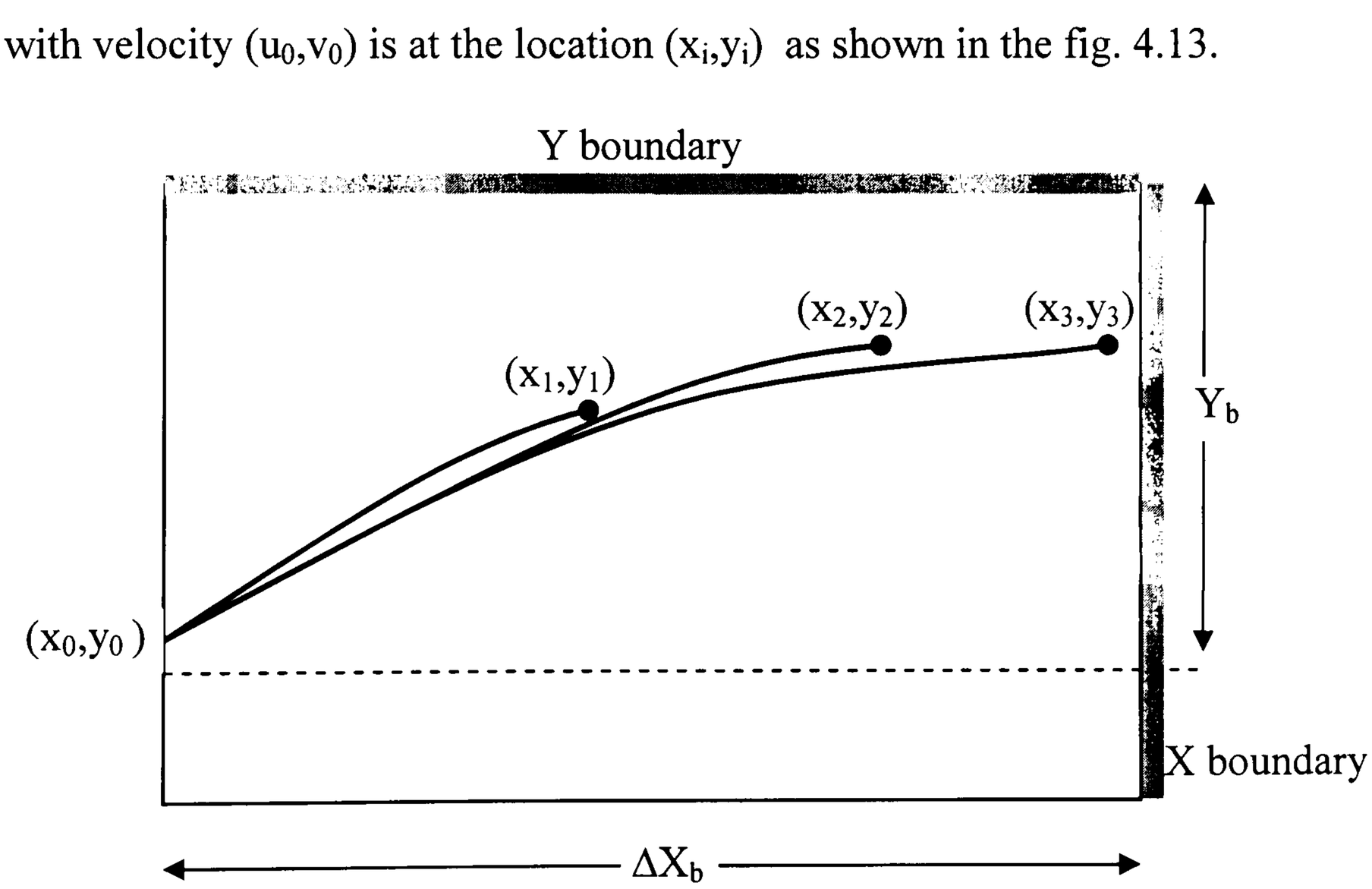

Fig. 4.13

In order to find Δt required for the droplets to reach either one of these boundaries of the cell, the initial guess may be taken as

$$\Delta t_1 = \min\left[\frac{\Delta X_b}{u_0}, \frac{\Delta Y_b}{v_0}\right] \tag{4.21}$$

and then (x_1,y_1) can be evaluated using the equation (3.14). If $x_0-x_1 < \Delta X_b$ and $y_0-y_1 < \Delta Y_b$, a new time increment Δt_2 is assumed which is larger than Δt_1 and this is then used to calculate (x_2, y_2). This process is repeated until x_i or y_i reaches their respective boundary values ΔX_b or ΔY_b. Hence, the final position of the droplet in this cell is determined. This will be a rather time consuming process, if it is used to predict the droplets final position on the boundary of the cell with a close tolerance (for example to reach the grey coloured area of figure 4.13 which indicates the acceptable tolerance level). Thus the droplet position is not easily predictable in this manner. Therefore the author has devised an indirect method to over come this problem and it will be discussed in the next section.

4.6.2 Methodology to predict droplet position

Using this method it is possible to obtain the exact time increment required for the droplet to travel from entering a cell, to the boundary of that cell, with a reasonable tolerance. Consider the computational cell shown in fig. 4.14 (the velocity and position marked have their usual meanings).

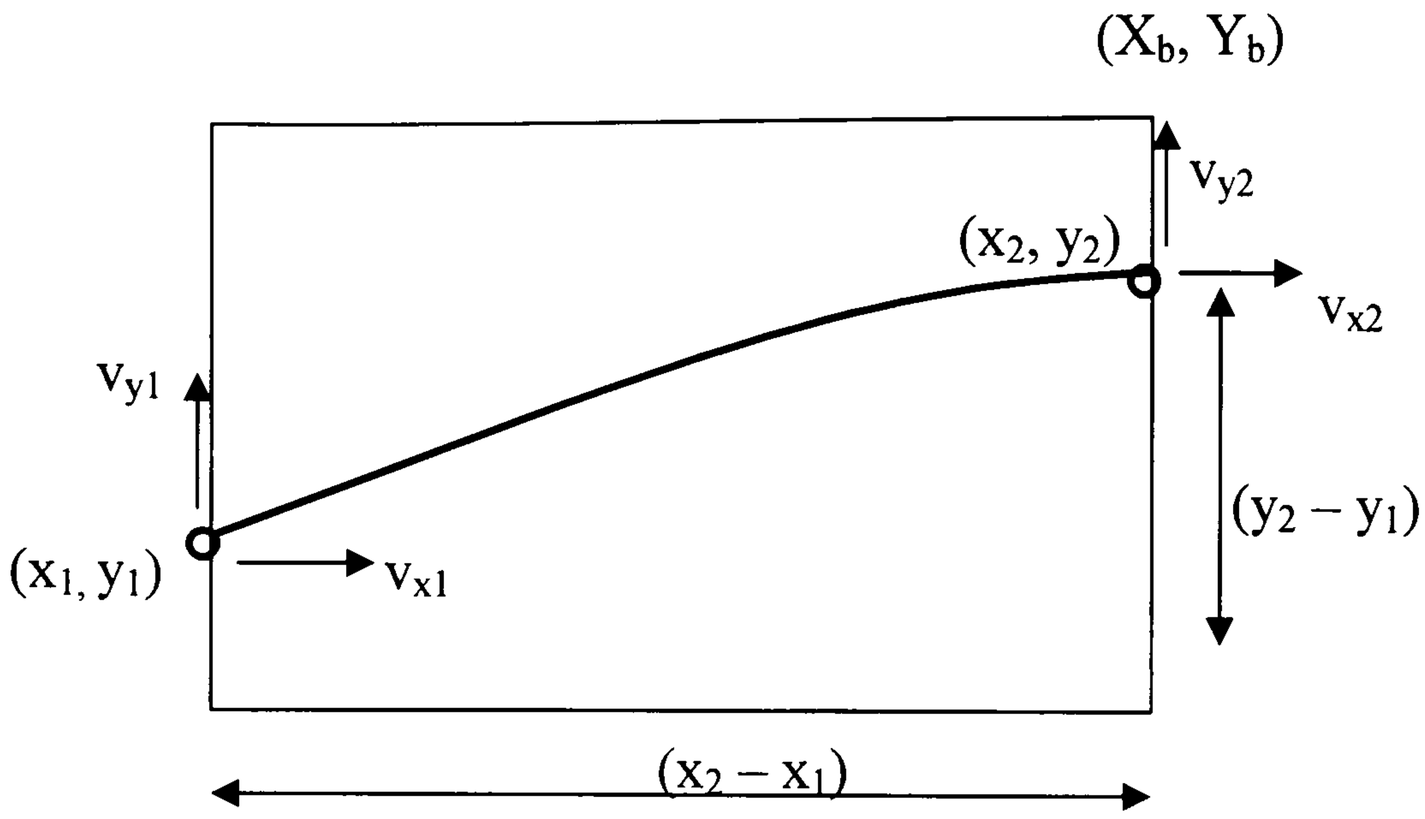

Fig. 4.14

Assume that the droplet trajectory crosses the cell boundary at $X=X_b$. Then the droplet velocity and position in x-direction can be written as

$$v_{x2} = U_{gas} - (U_{gas} - v_{x1}) \exp\left(\frac{-\Delta t}{\tau}\right) \tag{4.22}$$

$$x_2 = X_b = x_1 + (v_{x2} + v_{x1}) \frac{\Delta t}{2} \tag{4.23}$$

If the time increment is known, droplet velocity components in the X-directions at the next boundary can be calculated as follows:

$$v_{x2} = 2 \frac{(X_b - x_1)}{\Delta t} - v_{x1} \tag{4.24}$$

Substituting v_{x2} in the velocity equation (4.22) and rearranging, following equation can be obtained.

$$U_{gas} + v_{x1} - (U_{gas} - v_{x1}) \exp\left(\frac{-\Delta t}{\tau}\right) - 2\frac{X_b - x_1}{\Delta t} = 0 \tag{4.25}$$

This equation is a function of Δt, which is the only unknown in the equation and it can be stated as

$$f(\Delta t)=0 \tag{4.26}$$

And one of the roots of this equation is the time increment of interest. Since the equation is non-linear, it can only be solved numerically. Therefore to solve this equation an iteration technique based on the Newton-Rapson method is used in the present study.

If the initial guess for the time interval is Δt_{x0}, according to Newton-Rapson method is possible to approximate Δt_{x1} by

$$\Delta t_{x1} = \Delta t_{x0} - \frac{f(\Delta t_{x0})}{f'(\Delta t_{x0})} \tag{4.27}$$

Since the method converges rapidly with an appropriate first approximation, Δt_{Xb} (time to reach the X-boundary) can be obtained with a small number of iterations. Using the same method Δt_{Yb} can also be evaluated.

first approximations of Δt_{x0} and Δt_{y0} may be taken as

$\Delta t_{x0} = (X_b - x_1)/v_{x1}$ and $\Delta t_{y0} = (Y_b - y_1)/v_{y1}$

Now, these two time intervals (Δt_{Xb} and Δt_{Yb}) are compared and the smallest time increment is selected as Δt_b.

$$\Delta t_b = \min\left[\Delta t_{Xb}, \Delta t_{Yb}\right] \tag{4.28}$$

This is because the droplet is going to reach the boundary in the direction, which requires smallest time increment. Knowing Δt_b it is possible to calculate the droplet velocities and distances travelled in each direction. Then droplet temperature and mass histories can be calculated. When the above steps have been completed droplet source terms for that cell due to this particular droplet trajectory can be calculated.

After the droplet has reached the cell boundary, the local gas phase properties seen by the droplet are changed to those of the next cell. This would be the cell into which the droplet is about to enter. The above procedure is re-applied for the new cell to calculate the new droplet properties. This tracking procedure is then continued until the droplet has fully evaporated. After that a new droplet is tracked using the above procedure, which continues until all the droplets are tracked. The whole technique is shown in the flow diagram given in fig.4.15.

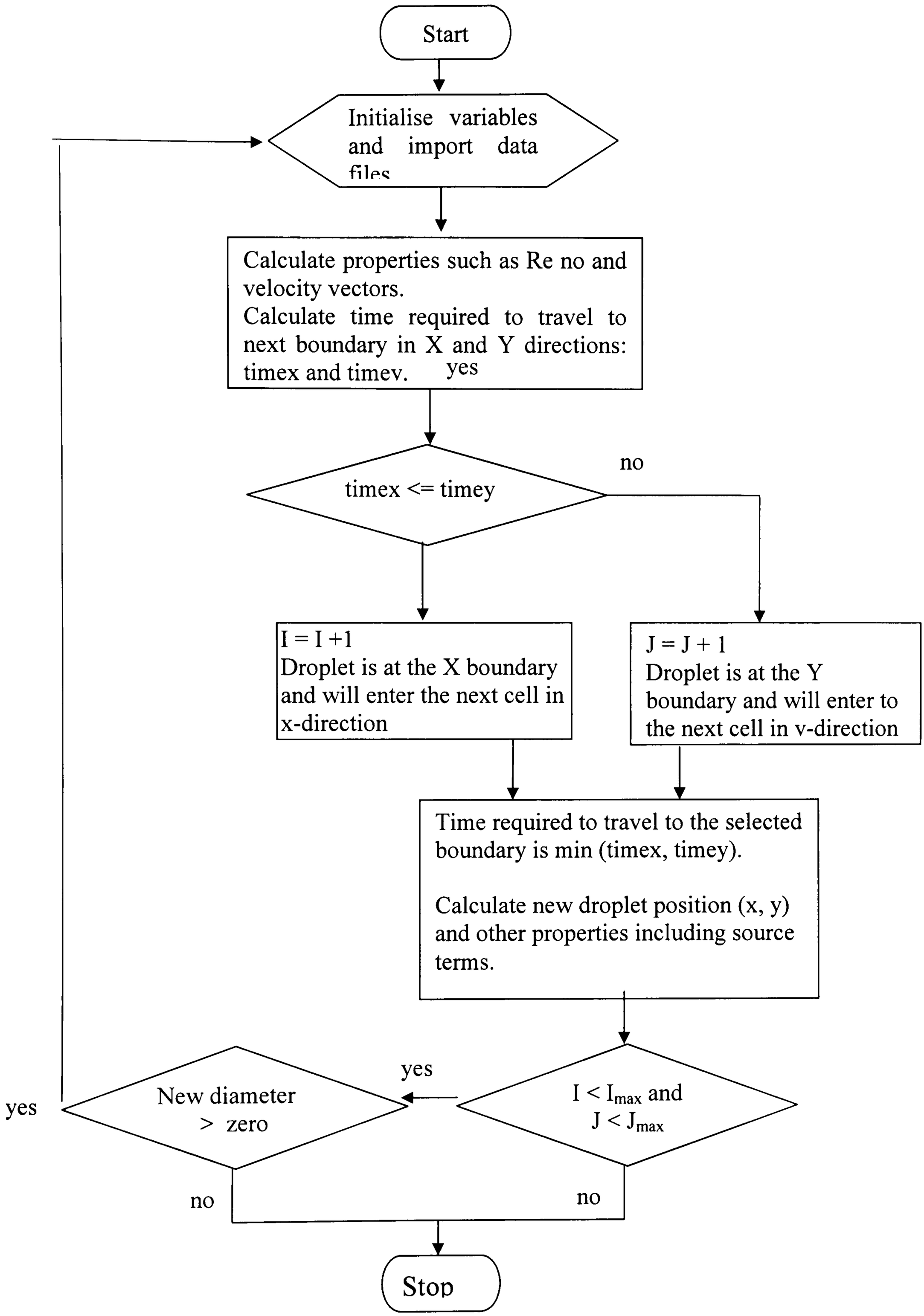
Start
Initialise variables and import data files
Calculate properties such as Re no and velocity vectors.
Calculate time required to travel to next boundary in X and Y directions: timex and timev.
yes
timex <= timey
no
I = I +1
Droplet is at the X boundary and will enter the next cell in x-direction
J = J + 1
Droplet is at the Y boundary and will enter to the next cell in v-direction
Time required to travel to the selected boundary is min (timex, timey).
Calculate new droplet position (x, y) and other properties including source terms.
I < Imax and J < Jmax
yes
no
New diameter > zero
yes
no
Stop

Fig. 4.15

4.6.3 Method of accounting for the change in droplet diameter due to evaporation whilst traversing a cell

It is obvious that if larger time increments are used for droplet tracking and evaporation calculations the resulting trajectories and droplet properties are less accurate. This mainly due to two reasons;

1 **Change in droplet velocity during the time step**: this is particularly important during the first part of the trajectory where most of the momentum of droplet is lost due to drag effect. In order to take into account of this effect, droplet calculations need to be done in small time intervals which enable the use of more accurate values for Reynolds number and droplet drag coefficient calculations.

2 **Change in droplet diameter during the time step:** this is important during the later part of the trajectory where most of the droplet mass loss occur due to evaporation. During this period droplet Reynolds number and drag coefficient will change rapidly which reduce the evaporation rate and droplet velocities significantly. This shows that it is vital to use small time intervals to account for the rapid change in droplet diameter.

To take into account above phenomenon's much smaller time increments have to be used which is taken as Δt_{evap}. Then the appropriate time increment for the trajectory calculation could be obtained from the following relation.

$$\Delta t_{traj} = \min\left[\Delta t_{Xb}, \Delta t_{Yb}, \Delta t_{evap}\right] \tag{4.29}$$

In this relation, if the minimum time interval selected is Δt_{evap} then the droplet position after that time increment will be somewhere within the cell. On the other hand, if either Δt_{Xb} or Δt_{Yb} is selected that means the droplet is crossing the cell boundary

4.7.1 Structure of the trajectory computation module

The trajectory computation module is written using FORTRAN language [143-144] and it can be depicted by a flow chart as in fig. 4.16.

The computation procedure can be described as follows: gas phase properties and droplet initial data files are read from the main program and relevant variables are initialised. Then initial drop size category and trajectory (drop starting position and angle) is then selected. Next, the trajectory calculation is carried out at the current computational cell, and resulting source terms due to this particular group of droplets are estimated. If the estimated new droplet diameter is positive (i.e. not fully evaporated), then the program moves to the next computational cell and evaluates the trajectory for this cell and it proceeds until droplet is fully evaporated. If the droplet is fully evaporated, computation is moved to the next trajectory. When all the trajectories of a particular size category are evaluated the program moves to the next size category and re-implement the calculation procedure for this size group and this continue until the trajectories of all size groups are evaluated.

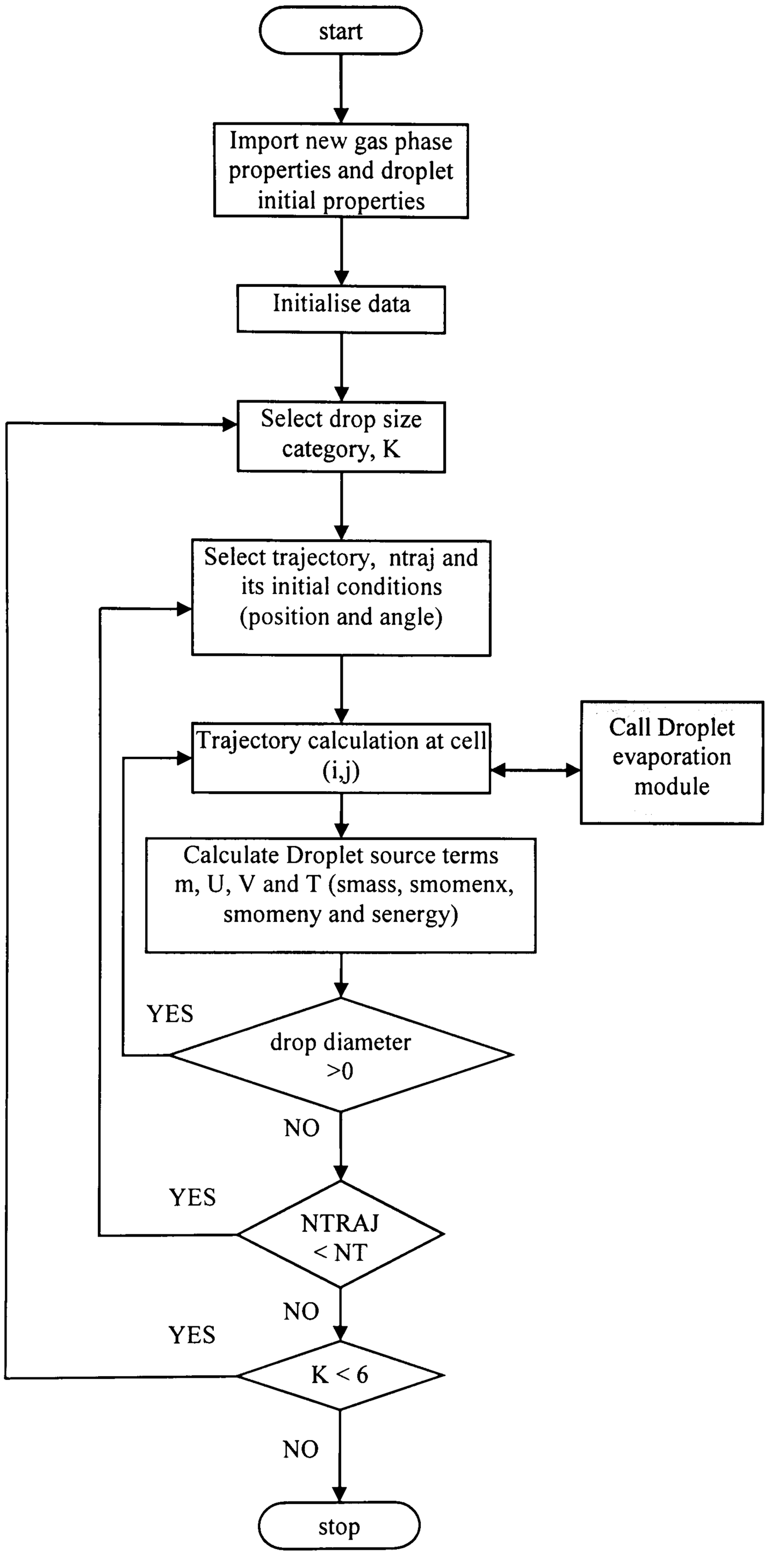
start
Import new gas phase properties and droplet initial properties
Initialise data
Select drop size category, K
Select trajectory, ntraj and its initial conditions (position and angle)
Trajectory calculation at cell (i,j)
Call Droplet evaporation module
Calculate Droplet source terms m, U, V and T (smass, smomenx, smomeny and senergy)
YES
drop diameter >0
NO
YES
NTRAJ < NT
NO
YES
K < 6
NO
stop

FIG 4.16

4.7.2 Definitions of functions and main variables of the program

ren	evaluate droplet Reynolds number
ft	evaluate the droplet velocity function
fdash	evaluate the derivative of the droplet velocity function required for Newton Raphson method
smass	this is a double precision array which stores mass source terms due to droplet evaporation. This is linked to main gas phase program using COMMON variable
smomenx	this is a double precision array which stores momentum source terms due to droplet in X-direction
smomeny	this is a double precision array which stores momentum source terms due to droplet in Y-direction
senergy	this is a double precision array which stores energy source terms due to droplet evaporation

4.8 Droplet evaporation module

There are two main modifications to the droplet evaporation module [9]. First, to supply the droplet velocity, this is required to evaluate relative droplet velocity needed. The second is to supply droplet evaporation time interval required. This time interval is selected as described earlier.

$$\Delta t_{traj} = \min\left[\Delta t_{Xb}, \Delta t_{Yb}, \Delta t_{evap}\right] \tag{4.30}$$

4.9 Description of the two-phase separated flow program

The two-phase separated flow program is a deterministic separated flow model formulated to simulate the droplet evaporation and the mixing process of a turbulent spray. Unlike the previous in-house built LHF model, this model is capable of taking into account the interphase transport effects. The effect (on the gas phase) due to the presence of the dispersed phase is accounted for via source terms added to the gas phase governing equations. The source terms locally modify the properties of the gas phase control volumes. This property change of the gas phase propagated on to other parts of the computational field as a result of diffusion and convection. The complete solution procedure of the separated flow model based on Lagrangian Trajectory approach can be represented by a flow diagram as in Fig. 4.17. With the exception of the property changes due to interphase transports, the gas phase modelling part is almost the same as LHF model of Rajakaruna [9]. The common parts include the cylindrical co-ordinate system, expanding and staggered grid system, convergence criteria for the

mixing analysis, subroutine arrangement for the flow variables u, v, T, $P`$, k, ε and f (mixture fraction). Therefore the discussion will be focussed on additional features used to develop the deterministic separated flow model. These consist of inlet conditions, trajectory model.

This two phase separated flow model is intended to simulate a steady state flow configuration. Therefore it is assumed that the gas flow enters the combustion chamber through both inner and outer tubes and the injected liquid fuel spray enters the combustion chamber through the inner tube.

As discussed in the literature review, accuracy of modelling by two phase separated flow method depends heavily on the accuracy and validity of the inlet boundary conditions used. Therefore special care has been taken when determining and setting inlet boundary conditions for both continuous (gas) and dispersed (fuel spray) phases. Inlet parameters for the droplet phase available from experimental data are mainly limited to equivalence ratio, sauter mean diameter of fuel droplets and fuel inlet temperature. This necessitates, all the other parameters needed for modelling to be obtained either from empirical methods or by intuition.

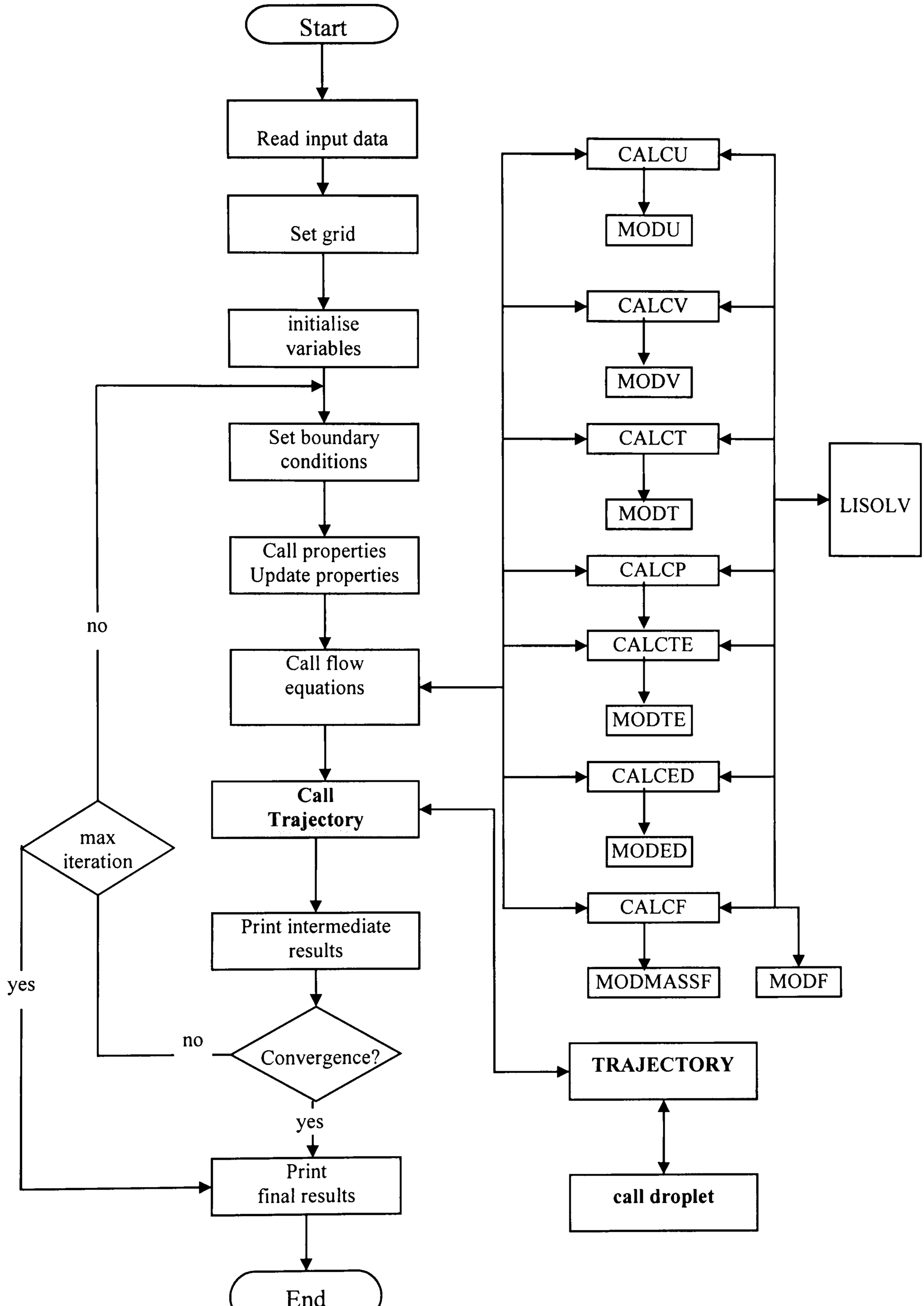
Start
Read input data
Set grid
initialise variables
Set boundary conditions
Call properties
Update properties
Call flow equations
Call Trajectory
Print intermediate results
Convergence?
no
yes
max iteration
no
yes
Print final results
End
CALCU
MODU
CALCV
MODV
CALCT
MODT
CALCP
CALCTE
MODTE
CALCED
MODED
CALCF
MODMASSF
MODF
LISOLV
TRAJECTORY
call droplet

Fig. 4.17

CHAPTER 5

Analysis of the program and Experimental validation

In this chapter parametric study and experimental validation of the program are discussed. The chapter is divided into three main sections. In section one, evaluation of the particle tracking module and its behaviour for various entry conditions is carried out. Here, the stability and capabilities of the trajectory subroutine is tested, by varying flow field parameters and droplet properties.

An extensive parametric study has been carried out in order to find out the response of the separated flow model to varying flow parameters, which is described in the second part of this chapter. The considered parameters are droplet diameter, droplet velocity, mixing temperature, droplet mean diameter, equivalence ratio, and system pressure. The data plot relevant to this discussion is given in appendices B -G. Finally in section three, the separated flow program results are compared against LHF results and Experimental data (appendices H-I).

5 Trajectory Program structure

The particle tracking module is written in FORTRAN 77 [40, 41]. This program includes several sub-routines [39], which can be called via the main program to calculate the desired parameters.

5.1 Input data to the program

The gas phase velocity field, grid structure and all other required data are supplied to the main program via data files.

Supplied data are as follows:

Gas phase	Variable
Local temperature	tair / [K]
X and Y direction velocity	uxgas ; uygas / [m/s]
Molar mass	molair / [kg/kmole]
Density	denair / [kg/m^3]
Thermal conductivity	kair / [W/mK]
Viscosity	visair [Pas]
Droplet phase	
Fuel droplet inlet temperature	tdst / [K]
Boiling temperature	tdb / [K]
Diameter	diam / [m]
Molar mass	mold / [kg/kmole]

Inlet angle	n	[deg.]
Inlet velocity	vxyd	[m/s]
Enthalpy of vaporization of fuel	lh	[kJ/kg]
Density of fuel at 15.6 C	dend	[kg/m^3]
No. of droplets in the group	ndrop	

5.2 Testing of the Trajectory module

After successful compilation of the program, a series of runs were carried out to check the numerical accuracy by comparing data obtained from the program with that of data obtained by manual calculation. Then, three tests were carried out by changing different parameters to check the response of the program to different flow conditions. The first test was carried out to observe the behaviour of the droplets injected into a stagnant environment by setting the gas flow velocity to zero in both X and Y directions. The test two and three were carried out to see the response of the droplet phase to a unidirectional and multi-directional velocity fields respectively. These tests are described below:

5.2.1 Test one (zero gas velocity field or stagnant environment)

Parameters modified for this test were:

Droplet /particle diameter (μm)		10, 20, 50,100 and 200
Droplet inlet velocity (m/s)		vxyd = 200.0
Gas Velocity (m/s)	X-direction	uxgas = 0.0
	Y-direction	uygas = 0.0

In this test the gas velocity was taken as zero to observe how the droplets react, when traversing still air. To find out the effect due to variation in droplet diameter, this program was run for several droplet diameters, 10 –200μm.

An interesting observation can be made from the result of these runs (appendix-A2); the particle trajectories are curved upwards. This is because the particle X-direction velocity decreases more rapidly than its Y-direction velocity due to the drag force. The drag force is nonlinearly (exponentially) proportionate to velocity difference. Therefore the higher the velocity difference between droplet and gas flow, higher the drag force exerted on the droplet. Since the droplet X-direction velocity is very large compared to that of Y-direction velocity, the drag force exerted on the droplet in X-direction is much higher compared to that of Y-direction.

5.2.2 Test two (X directional constant gas velocity field)

Parameters modified for this test were:

Droplet /particle diameter (μm)		10, 20, 50,100 and 200
Droplet inlet velocity (m/s)		vxyd = 200.0
Gas Velocity (m/s)	X-direction	uxgas = 3.0
	Y-direction	uygas = 0.0

This test was carried out to observe how droplets react to a unidirectional gas flow field by giving 3.0m/s gas velocity in the X-direction. In this case the droplet

diameter was varied from 10μm to 200μm in order to find out the effect due to droplet diameter variation. The results obtained are shown in Appendix A3.

From the graphs shown in appendix A3, it can be clearly identified that the particle trajectories are curved upwards for a certain time interval. Then the trajectories follow the gas flow field. At this point the particle has almost the same velocity as the gas field. When comparing graphs obtained from test two (appendix A3) against test one (appendix A2), it is clearly identified that there is a noticeable difference in distance travelled by droplets before they evaporate completely. This is due to the fact that the droplets in test two receive significant amount of momentum from the gas phase (in other words, momentum loss due to drag along the trajectory is less since the velocity difference is less).

It is also observed droplets with relatively large diameters (appendix A3 graph 4) penetrate or move through the flow field further than the small diameter particles (appendix A3 graph 2). This is mainly due to initial high momentum and long evaporation time of larger droplets. Smaller particles tend to change or loose their inlet characteristics in the flow field more rapidly due to low momentum and high surface area to mass ratio. This is because the effect due to drag force on the droplet is increased with increase in surface area to mass ratio.

5.2.3 Test three (Two dimensional constant gas velocity field)

Parameters modified for this test were:

Droplet /particle diameter (μm)		10, 20, 50,100 and 200
Droplet inlet velocity (m/s)		vxyd = 200.0
Gas Velocity (m/s)	X-direction	uxgas = 3.0
	Y-direction	uygas = 0.3

In order to find out how droplets respond to a complex two-dimensional flow field, a gas flow field with both X and Y direction velocities was used in this test. For ease of comparison with test two, the Y-direction velocity was set to 0.3m/s uniformly throughout the flow field. The post-processed data are shown in Appendix A4.

These graphs are also somewhat similar to graphs obtained from test two. Particles follow the flow field after loosing their initial high momentum. Compared to test two, in this test the droplet trajectories (appendix 4 graphs 3-5) seems to be moving slightly upwards. This is due to the addition of Y-direction velocity to the flow field. Also similar to previous tests, heavy particles travel further than smaller particles before loosing their momentum.

5.3 Parametric study of the two-phase program

A parametric study was carried out to examine the response of the model to changes in various parameters such as system pressure, equivalence ratio and droplet size. These are described next with the help of the graphs presented in appendices B-F.

5.3.1 Effect of droplet diameter

In order to evaluate the effect of changes in droplet diameter on droplet phase as well as on gas phase development, the program was run with an inlet equivalence ratio of 1.08 and 5 different initial droplet diameters (10, 20, 30 50 and 100μm). In each test fuel mass flow rate was kept constant at 7 g/s. The fuel parameters used in these tests were assumed to have the properties of gas oil (*n*-dodacane) and air temperature for all runs was set to 1500K (explained in chapter 4). The results obtained from these runs are given in Appendix B.

It can be seen by examining figures (B1-B3) obtained using droplet phase data, that trajectory plots (B2) are similar to those in appendix A1. Larger droplets move further down stream before complete evaporation due to high momentum and low evaporation rate. Although it appears to be that droplets with the same diameter attain complete evaporation at almost same axial distance, it can be seen from plot B3 that droplets near the centre line evaporate more rapidly than the droplets away from the centre line. The reason may be because the velocity difference between the gas phase

and droplets are higher near the centre line. This high velocity difference causes the droplets to evaporate faster.

When comparing velocity plots presented in (B4), it can be seen that the high velocity region (contour plot for 30m/s velocity) becomes small with the increase in diameter. On the other hand the moderate velocity region (contour plot for 10m/s velocity) becomes longer and wider with the increase in droplet diameter. The reason for this is as follows:

As discussed previously, smaller droplets loose their momentum more rapidly than larger ones due to drag force as well as evaporation. This momentum loss is a gain for the local gas flow field and the flow field changes accordingly. On the other hand larger droplets release momentum slowly due to comparatively low drag and of course due to slow evaporation. Also larger droplets move further down stream and move further away from the centre line (B2). This is the reason for near the injector small high velocity region and then later long and wider moderate velocity regions.

Another interesting feature is that the recirculation region (B6) moves down stream and diminishes with the increase in droplet diameter. Around the near injector region droplets are still heating up and the droplet evaporation is negligible, therefore in early part of the spray the momentum lost by droplets is mainly due to drag force. But the small droplets release their momentum to the gas phase through drag rapidly compared to larger droplets. Therefore near injector region momentum gain by the gas phase due to small droplets is higher than larger droplets. This higher momentum

addition close to injector causes recirculation to become larger and closer to the injector end. On the other hand, larger droplets initially loose momentum slowly and later part of the droplet life, they loose momentum due to drag as well as due to evaporation (this evaporation also reduce the drag force). But due to this evaporation gas phase gain considerable volume of fuel vapour which reduces the air needed for entrainment. Thus the cause for formation of recirculation region is less. This may be the reason for larger unmixed area with the increase in droplet diameter.

Equivalence ratio[1] plots (B5) show similar trends. As droplet diameter increases, the beginning of significant evaporation is shifted down stream from the injector. Since small droplets evaporate completely before moving away from the centre line, equivalence ratio near the centre line is higher for small droplets and peak equivalence ratio become smaller with the increase in droplet diameter. As the droplet diameter increases there is enough residence time for the droplet to reach high temperature and when it reaches critical temperature the droplet evaporates instantaneously. This is clearly demonstrated in the plot for 50μm drop diameter.

5.3.2 Effect of fuel injection velocity

The effect of changes in droplet injection velocity on the flow field properties was assessed by running the program for a set of different injection velocities (V=150, 200, 250 and 300m/s). A number of plots and contour maps was produced

[1] Vapour equivalence ratio

using these results and the graphs, which show significant differences, are presented in appendix C and discussed in the following paragraphs.

An increase in droplet injection velocity increases the injected momentum addition to the gas phase, which clearly changes the gas phase local velocity distribution as shown in fig. C3. It can be seen that with the increase in droplet velocity, recirculation in the gas phase becomes larger and the recirculation region moves close to the injector.

According to the equivalence ratio iso-contours C4, it can be seen that an increase in droplet injection velocity moves the maximum fuel vapour concentration point away from the injector. It also reduces the value of the maximum equivalence ratio and full mixing is achieved in a relatively shorter distance from the injector. This may be due to the occurrence of larger and much closer recirculation zone with the increase in droplet injection velocity.

Using the fuel vapour concentration data, the combustion program was executed and contour maps were obtained for temperature, CO_2 and CO concentrations (C5-C7). These plots further support the above evidence and especially the contour maps of CO concentration shows a decrease in CO concentration with the increase in drop velocity, which proves that increase in drop velocity, improves the fuel vapour mixing (reducing the fuel vapour rich pockets).

Figures; C8 and C9 show the axial and radial variation of the above properties with change in droplet injection velocity. From these figures it can be seen that increasing the injection velocity decreases the maximum fuel vapour equivalence ratio. That means increase in fuel momentum assist the fuel vapour mixing. From CO_2 and CO graphs it shows that better mixing enables better combustion therefore decrease the CO concentration near the centre line.

5.3.3 Effect of change of injector (droplet size distribution at various mean diameter)

The two-phase separated flow model developed make use of a droplet size distribution based on Nukiyama-Tanasawa distribution function [4.18], which can create various size distributions with different mean diameters by changing the function parameters. In order to asses droplet size distributions produced by different injectors, the program was run with three different droplet size distributions with mean diameters of 10, 20 and 30μm. Results obtained were used to plot several different graphs, which are presented in appendix D.

The equivalence ratio plots (D4) obtained are some what similar to those obtained with different droplet diameters in section 5.3.1. The portion with significant equivalence ratio values are moving away from the injector with the increase in droplet mean diameter. A similar trend can be identified from the graphs for temperature and, CO_2 and CO concentrations obtained by using combustion program output data.

5.3.4 Effect of inlet air temperature

The two-phase separated flow model was run for different inlet air temperatures (800, 1000, 1200 and 1500K) to observe the effect of temperature variation on flow field properties. All the runs were carried out at a pressure of 6.5bar and at an overall equivalence ratio of 1.08. Since a decrease in air temperature results in an increase in air density, the air inlet velocity was reduced in order to have constant mass flow rate for all tests. All the other properties were kept constant. The figures obtained, using the above computational data, are presented in appendix E.

Observing the velocity contour plots (E1) it can be seen that the decrease in air temperature increases the size of the recirculation zone of the gas flow field and also the recirculation zone moves towards the injector. This change in the recirculation region causes the fuel vapour to mix better, which shows clearly in the equivalence ratio contour maps of E2. This point is further established by the other plots obtained for temperature, CO_2 and CO data.

From these results and previous ones about droplet injecting velocity, it can be clearly stated that the recirculation increases when the momentum difference between the phases is higher.

5.3.5 Effect of inlet equivalence ratio

The program was run for four inlet equivalence ratios (E=0.8, E=0.9, E=1.0 and E=1.08). In order to have desired inlet equivalence ratio, fuel mass flow rate was changed. The system pressure and properties of fuel and gas were kept unchanged. The contour maps and other significant data plots are presented in appendix F.

It can be seen from the fig F2 that an increase in inlet equivalence ratio helps complete mixing. The reason may be that the increase in fuel mass flow rate increase momentum of the droplet phase, which is later absorbed by the gas phase, causing the recirculation region (F1) to become more significant. Similar trend is visible in the plots obtained for temperature and CO_2 and CO contour maps (F3-F6).

Axial plot of the above properties (F7) shows that final maximum temperature occurs with E=0.9 test. This is because in this case fuel burns completely with little excess air, which gives maximum increase in temperature. In the test with E=0.8 also fuel burns completely but it has more excess air, which absorbs a significant amount of heat energy and reduces the overall temperature. Since the complete combustion in tests of E=0.8 and E=0.9, there is very little or no CO present at the exit of the chamber. On the other hand E=1.0 and E=1.08 studies show high CO concentration at the exit, which indicates partially burnt fuel.

5.3.6 Effect of system pressure

The program was run for various ambient pressures to verify the model sensitivity to these pressures and four of those tests (P=11bar 21bar 31bar and 51bar) are presented. In all these tests equivalence ratio was kept constant at 1.08 and this was done by changing the fuel mass flow rate while keeping the inlet air velocity constant. Also the properties of gas and fuel were kept constant. Using the data obtained from these runs, various graphs were plotted and are presented in appendix G.

It can be seen from Fig.G1 that there is no significant change in velocity distribution with the increase of ambient pressure. This can be explained as follows: since the air inlet velocity is kept constant, the density of air increases proportionately with the increase of pressure. This yields proportionate increase of air mass flow rate and inlet air momentum. On the other hand fuel mass flow rate was increased to keep the air fuel ratio constant. Therefore the inlet fuel momentum increased proportionately with the increase of pressure. Thus the momentum ratio of air to fuel was constant. Therefore the velocity distribution of the flow field is constant even though the ambient pressure is varied.

Graphs in Fig.G2 were plotted to compare the effect of ambient pressure on local equivalence ratio distribution. It can be seen from the graphs that with the increase of ambient pressure, beginning of significant evaporation moved downstream from the injector. This is because as the ambient pressure increases the droplet evaporation rate decreases. When the droplet temperature increases with time, droplet evaporation rate

also increases. This is the reason for more tightly packed pressure contours at later stage. Another significant difference is that even though the overall fuel inlet equivalence ratio is kept constant, the peak local vapour equivalence ratio increases with pressure which can be clearly seen from the P=31bar and P=51 bar plots. The reason for this can be explained as follows: as the temperature of the fuel droplet reaches its critical temperature droplet evaporates instantaneously. Since both higher pressure tests are super critical (i.e. droplet temperature reaches the critical value causing instantaneous evaporation). This sudden evaporation of fuel droplets lead to increase in local vapour equivalence ratio.

The decrease in fuel evaporation rate due to pressure can also be shown by considering droplet evaporation time. A 20μm diameter droplet moving through the centre line evaporates completely after $6.563*10^{-2}$s at 11bar, but at 51bar pressure it takes $8.435*10^{-2}$s to evaporate completely.

Fig.G3 shows effect on combustion temperature distribution due to increase in ambient pressure. As in equivalence ratio plot G2, with the increase of pressure combustion temperature contours are moved downstream from the injector. And also due to the existence of high peak vapour equivalence ratio, the combustion temperature at the peaks has dropped. Similar changes are visible in the plots obtained for CO_2 and CO; Fig.G4 and G5. Due to presence of high peak equivalence ratio at higher pressure, fuel vapour burn partially at these locations. Therefore local CO_2 mole fraction has deceased considerably while increasing the CO mole fraction.

Axial variation of properties with the change in pressure is shown in Fig. G6. Also the radial variations of properties are presented in Fig.G7 (at the cross section through the peak local equivalence ratio of respective pressures).

5.4 Experimental validation

The experimental data were obtained by Nazha [109] at Queen Mary College using a purpose build high pressure combustion facility. This consists of a 800mm long cylindrical combustion chamber with an inner diameter of 150mm. The air and fuel enters the chamber co-axially. And the fuel was injected continuously at a pressure of 17300kPa via an injector with nozzle diameter of 0.2mm giving 5.4g/s. The spray was ignited by a spark igniter and the results were obtained at constant pressure of 653kPa and an input equivalence ratio of 1.08. Further details of the facility and the method of sample extraction and analysis are given in references [109].

The model was run for a theoretical chamber with the same dimensions as the experimental one. The inlet air temperature was taken as 1500K (reason given in chapter4) with a constant velocity of 3.7m/s. The fuel was supplied at a temperature of 300K with a nozzle exit velocity of 212m/s. The radius of the fuel air stream at entry to the computational chamber was taken as 5mm. The properties of gas-oil with the chemical formulae and molecular mass of n-dodacane were used as representative of the test fuel (shell gas-oil). Also the in-house built LHF code was run with the same conditions. The results of these test runs using the new two-phase code and the LHF code are shown in appendix H.

Figure H-1 shows the predicted spatial distributions of the vapour equivalence ratio, flame temperature and concentrations of CO_2 and CO of the new two-phase code. Figure H-2 shows the surface plots of the predicted vapour equivalence ratio, flame temperature and concentrations of CO_2 and CO of the new two-phase code. The rest of the graphs in this appendix H show trajectory model, LHF and experimental data plotted axially and radially at maximum equivalence ratio position of the respective axial data.

The figure H1 shows that a peak vapour equivalence ratio of 1.5 present at around 0.375m from the injector exit. The axial plot H3 show that the experimental peak vapour equivalence ratio is about 0.393mm from the injector. This axial equivalence ratio plot clearly show that the trajectory model closely follows the experimental data and this is an advancement compared to that of LHF model. The theoretical temperature plot of trajectory model shows an axial trend as with the experiment with a maximum axial value around 2000K for temperature at about 0.240m from injector. Temperature then reduces gradually to about 1700K and then increases to a maximum of about 2000K. The reason is that in this region (in local vapour equivalence ratio plot the region where E > 1) fuel vapour is rich causing partial combustion which leads to lower gas temperature.

The radial plot of trajectory model (H4) of vapour equivalence ratio very closely matches that of the experiment which is a significant improvement over the LHF model. However the radial temperature plot of the trajectory model shows a high peak value of about 2100K which corresponds to the local equivalence ratio of 0.85 (at radial

distance of 0.03m). Then the temperature gradually decreases with the radial distance and follow the experimental data. The radial plot of CO_2 concentration also shows similar trend. Although the CO_2 concentrations initially deviate from the experimental data, from about 0.03m radial distance it start to follow the experiment. CO plot of trajectory model initially slightly deviates from experiment then start to follow the experiment closely.

For the above analysis it was taken that the sauter mean diameter of the droplet size distribution as 20μm. Therefore in order to observe the behaviour of the model to another diameter, the program was run for 30μm sauter mean diameter and the results are shown in the plots H-5 and H-6.

In all these radial plots the LHF model shows very little or no property variation with the change in radial distance. This is because the LHF model does not account fully for the radial variation of fuel vapour distribution as only one droplet is tracked along the centre line. On the other hand the trajectory model fully account for the radial variation by modelling droplet phase using large number of trajectories.

5.5 Experimental comparison at higher pressures

Nazha et al [109] obtained further data at higher pressures; at 16bar and 21bar. At each pressure tests were conducted at three different fuel vapour equivalence ratios; 0.8, 1.0 and 1.2. The fuel used and combustion setup were the same as before.

In order to compare these data, the trajectory model was run with the same boundary conditions. Then the calculated fuel vapour equivalence ratio data were plotted against experimental data. These are presented in appendix I.

5.5.1 Ambient pressure P=16bar

Fig.I1. shows axial variation of equivalence ratio at 16bar pressure for the three inlet equivalence ratios. There are only three experimental data points at each case and no data points for the early stage. Therefore it is not possible to compare the region close to the injector. But for the available data, it seems that the trajectory model predict the equivalence ratio fairly well. Peak equivalence ratio occurs at around 0.37m in all the test cases.

Fig.I2 shows predicted axial variations of equivalence ratio, combustion temperature, CO_2 and CO. Combustion temperature for the test with E=1.2 is notably less than the others. The reason for this is partial combustion of fuel vapour due to high vapour equivalence ratio. The test with E=0.8 shows highest CO_2 mole fraction and

virtually zero CO at the end of the tube. Also the Combustion temperature of test; E=0.8, is the highest at around X=0.45, it continuously decreased with X distance. This is due to the heat absorbed by the excess air in the flow.

5.5.2 Ambient pressure P=21bar

Fig.I3. shows axial variation of equivalence ratio at P=21bar. Predicted equivalence ratio data are fairly closely matched with experimental data in each test. The axial distance where peak equivalence ratio occurs has slightly moved downstream (at around X=0.375) relative to that of the 16bar pressure.

Fig.I4. shows predicted axial variation of properties; equivalence ratio, combustion temperature, CO_2 and CO. This also show similar trend as with 16bar pressure.

CHAPTER 6

Conclusions and Recommendations for future work

6.1 Conclusions

The development of a two phase turbulent flow model using separated flow approach based on trajectory method has been demonstrated. This model was tested parametrically and validated against available experimental data. According to the results obtained during this research work, the following points can be concluded:

1. A droplet tracking module has been formulated and it was tested for various flow conditions to asses its ability to produce realistic droplet properties and life histories from droplet injection to complete evaporation.
2. The effect of drag force on droplet movement through the gas flow field was demonstrated. The main features were:
   - When droplets are injected to a stagnant environment, droplet trajectories which are away from the centre line tend to curve upwards due to the difference in magnitude of drag forces acting on droplets in X and Y directions.
   - Droplets with relatively large diameters penetrate or move across the flow field in initial injection direction further than the small diameter particles
3. A mathematical model, which is applicable to high pressure combustion flows has been formulated using the separated flow method based on deterministic trajectory approach. The main advantage of this model over the previous in-house-built LHF model is its ability to account for the full

interaction (two way coupling) between the dispersed phase and the gas phase via the source terms.

4. The ability of the model to capture recirculation regions has been demonstrated.

5. The applicability of the model over a wide range of pressure, temperature, input equivalence ratio and various droplet parameters has been analysed in the parametric study.

6. The effect of change in droplet diameter on the overall process of droplet evaporation, mixing and combustion has been examined.

7. The effect of change in droplet inlet velocity, mixing temperature and inlet equivalence ratio on the overall process performance has been demonstrated and found that increase in momentum difference between the two phases assist the mixing of fuel vapour and air.

8. The response of the model to changes in pressure on overall process of mixing, evaporation and combustion has been studied and found that the increase in pressure causes the significant evaporation region to move away from the injector.

9. The experimental data comparison with two phase model has shown its ability to predict axial and radial distributions of combustion products, temperature and equivalence ratio with reasonable accuracy.

6.2 Recommendations for future improvements

During the present research study, areas in need of further investigation and improvements have been identified. These are summaries below:

- When the model was run for experimental conditions relatively high vapour equivalence ratios were predicted near the centre line. This is clearly the result of neglecting turbulent dispersion of the droplet phase. Therefore as a first step of improvement, some method needs to be implemented to account for turbulent dispersion of the droplet phase. Thus the effect of turbulence can be incorporated in the deterministic trajectory model using a method such as gradient diffusion approximation.
- The turbulent interaction of both the gas phase and the droplet phase can be fully accounted for if the model is modified and transformed to a stochastic separated flow model as described in chapter 2.
- The model uses a empirical function based on experimental data to calculate the ambient temperature for droplet evaporation. Instead of using this function if the combustion temperature predicted from the combustion program is used as droplet evaporation with some parametric adjustment, the resulting droplet evaporation and the entire two-phase separated model as a whole will produce more accurate predictions.
- The major disadvantage of separated flow type two-phase models specially models that use trajectory approach, is their limited applicability to dense region (near injector region) of the spray; which is normally not the case for

LHF model. It has been shown by many researchers that LHF type models predict better results in the near injector dense region and also they require very little information about the spray. Therefore the author suggests that if it is possible to model the dense region of the spray using LHF approach and the dilute region using separated flow approach, then it may produce better predictions with less computational cost.

Appendix A

A1 Test one (zero gas velocity field or stagnant environment)

A2 Test two (X directional constant gas velocity field)

A3 Test three (Two dimensional constant gas velocity field)

Gas temperature: 600k
Gas Flow Velocity X direction: 0.0m/s
Droplet diameter: 10 μm
Droplet inlet Velocity: 200m/s
Droplet inlet angle: degree 1-5

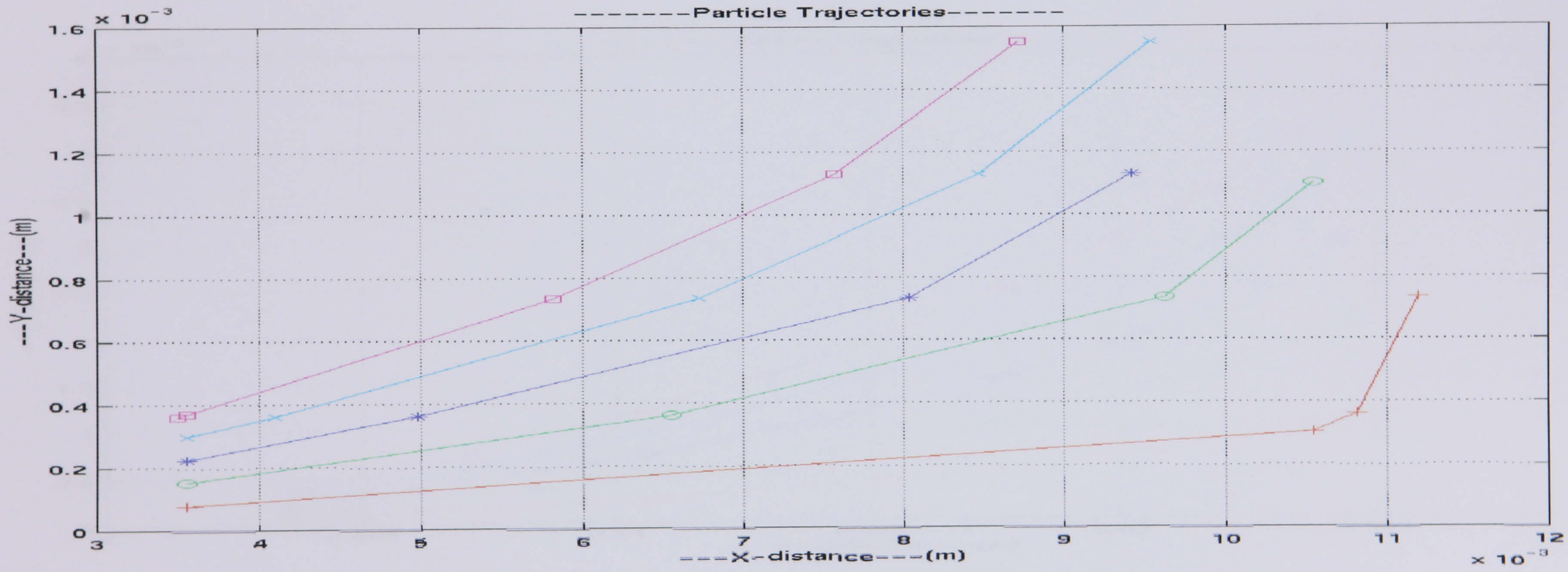

Gas temperature:	600k
Gas Flow r Velocity X direction:	0.0m/s
Droplet diameter:	20 μm
Droplet inlet Velocity:	200m/s
Droplet inlet angle:	degree 1-5

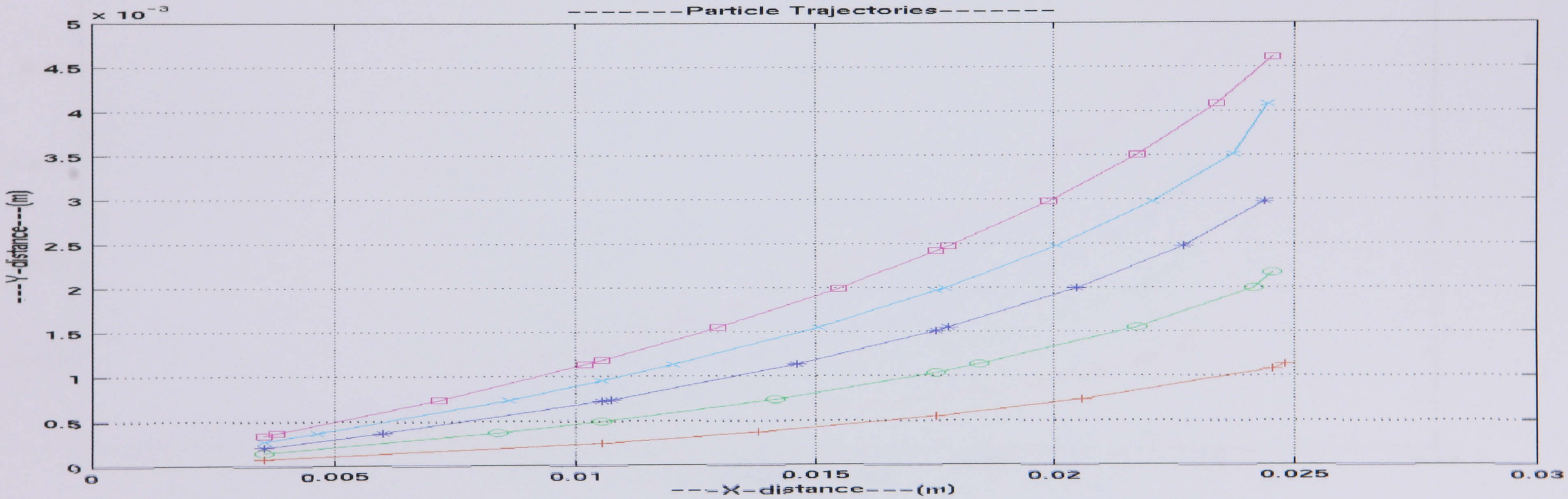

Gas temperature: 600k
Gas Flow Velocity X-direction: 0.0m/s
Droplet diameter: 50 μm
Droplet inlet Velocity: 200m/s
Droplet inlet angle: degree 1-5

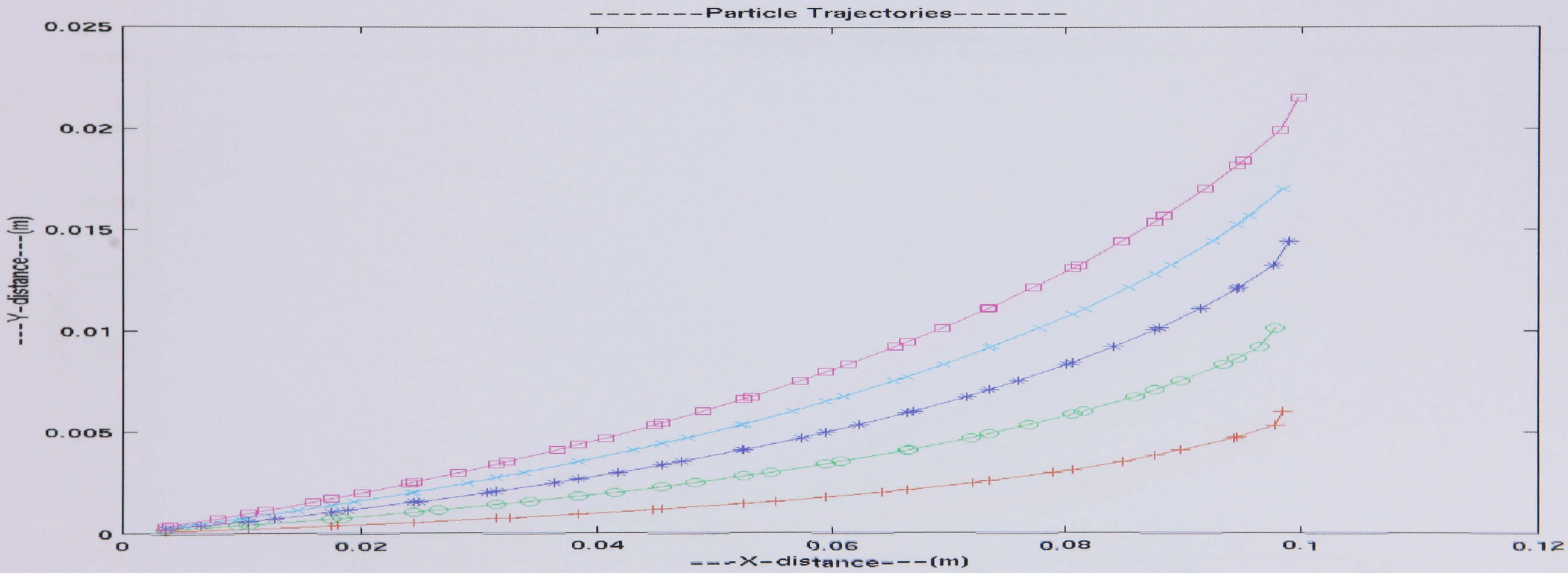

Gas temperature: 600k
Gas Flow Velocity X direction: 0.0m/s
Droplet diameter: 100 μm
Droplet inlet Velocity: 200m/s
Droplet inlet angle: degree 1-5

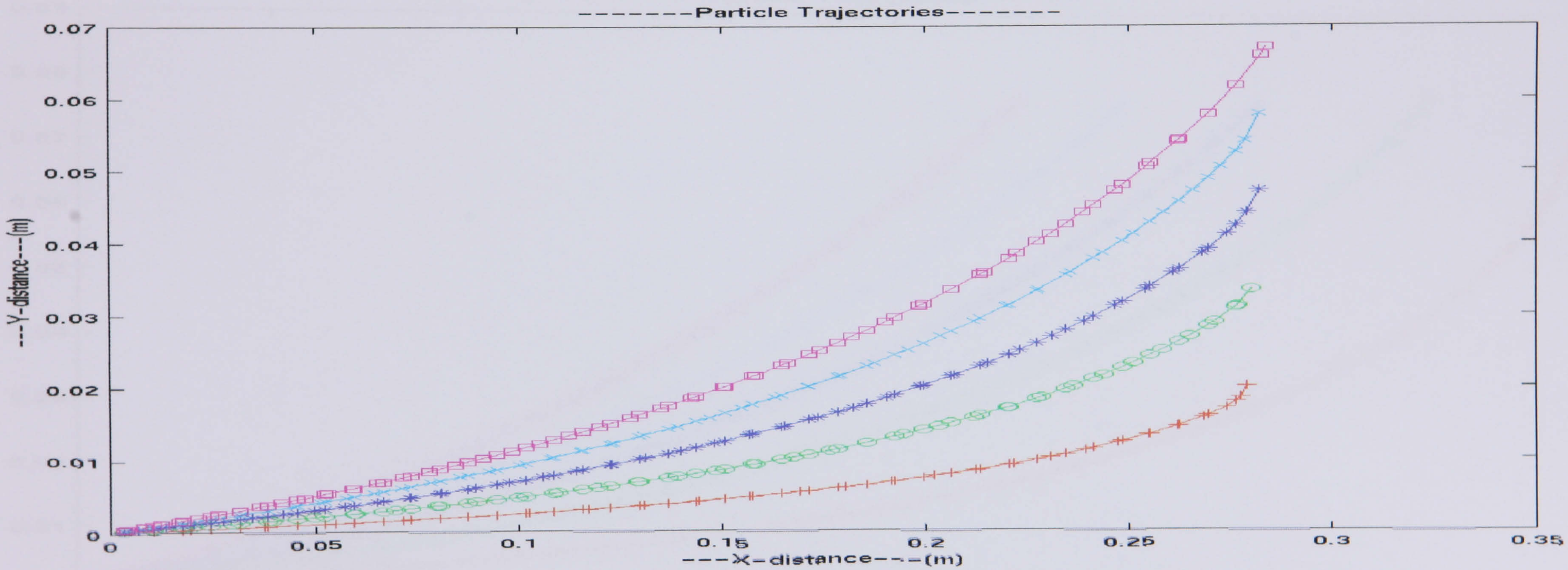

Gas temperature: 600k
Gas Flow Velocity X direction: 0.0m/s
Droplet diameter: 200 μm
Droplet inlet Velocity: 200m/s
Droplet inlet angle: degree 1-5

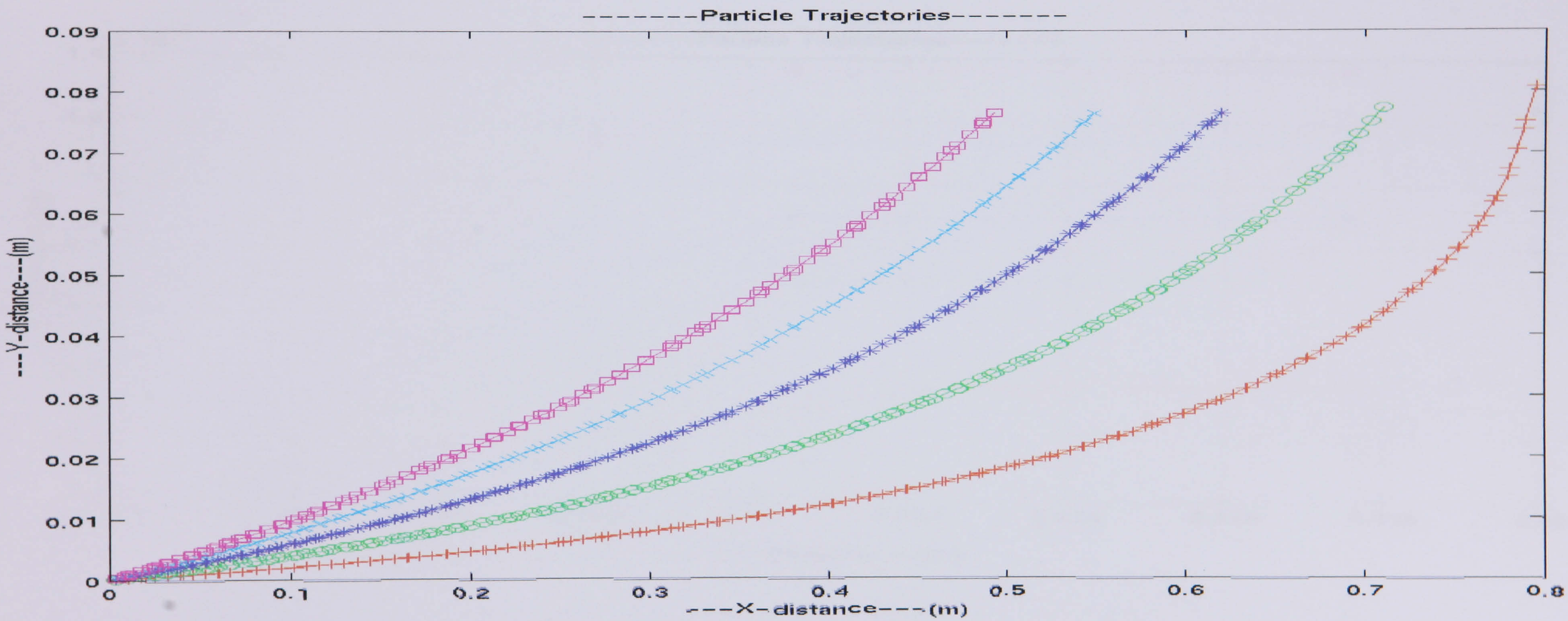

Gas temperature: 600k
Gas Flow Velocity X direction: 3.0m/s
Droplet diameter: 10 μm
Droplet inlet Velocity: 200m/s
Droplet inlet angle: degree 1-5

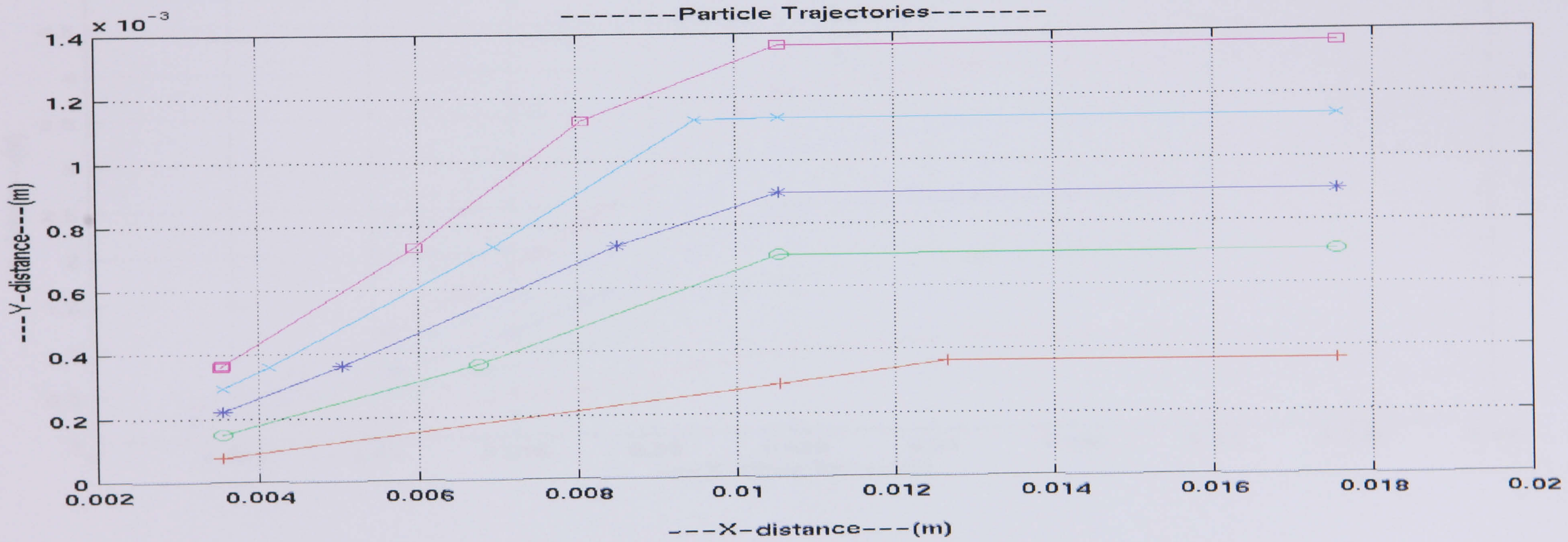

Gas temperature: 600k
Gas Flow Velocity X direction: 3.0m/s
Droplet diameter: 20 μm
Droplet inlet Velocity: 200m/s
Droplet inlet angle: degree 1-5

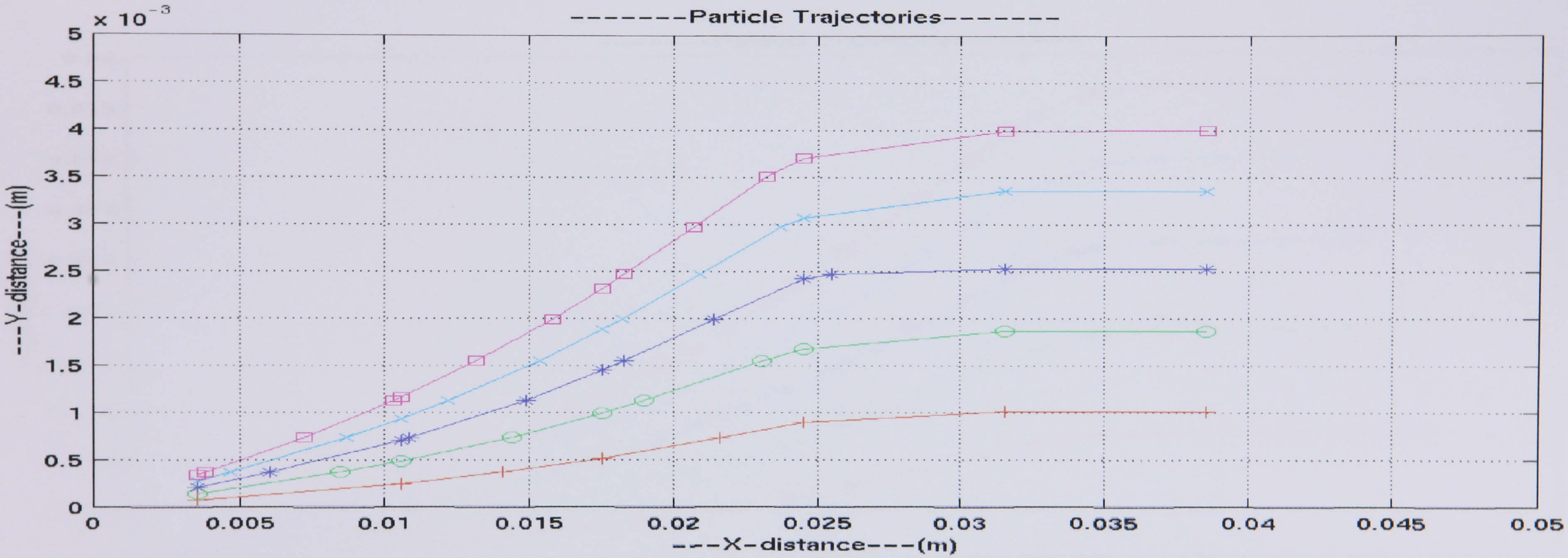

Gas temperature: 600k
Gas Flow Velocity X direction: 3.0m/s
Droplet diameter: 50 μm
Droplet inlet Velocity: 200m/s
Droplet inlet angle: degree 1-5

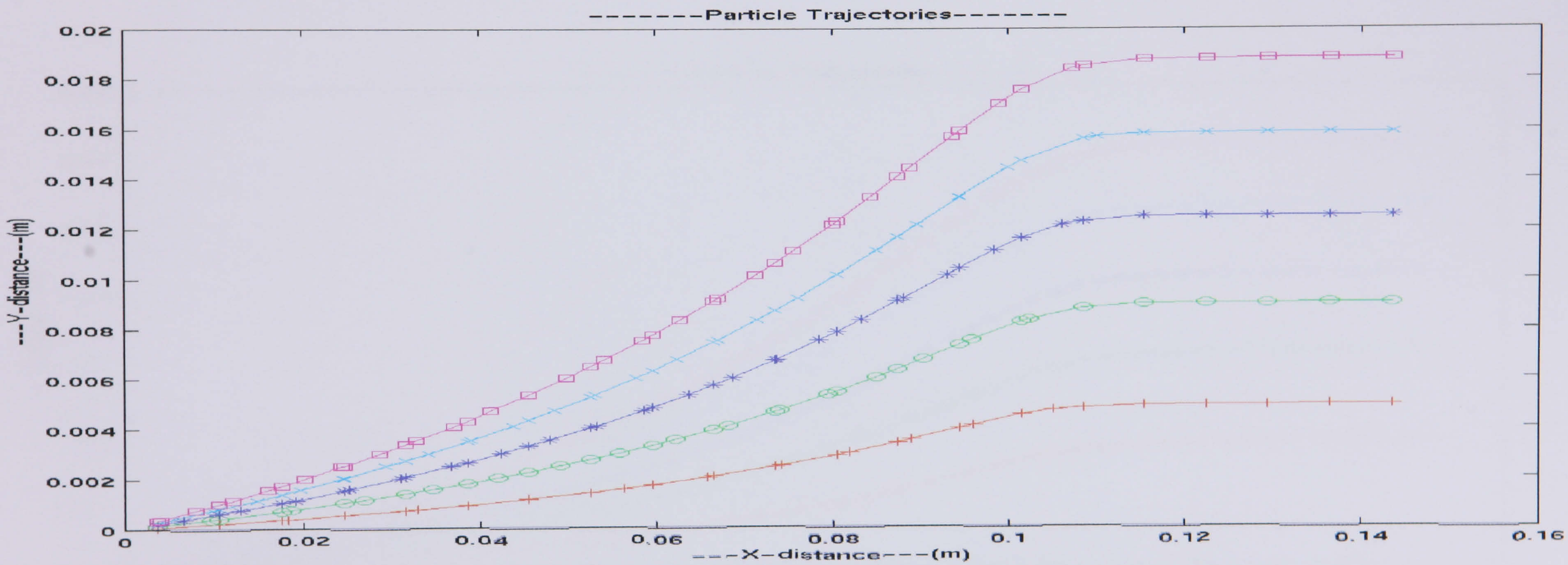

Gas temperature:	600k
Gas Flow Velocity X direction:	3.0m/s
Droplet diameter:	100 μm
Droplet inlet Velocity:	200m/s
Droplet inlet angle:	degree 1-5

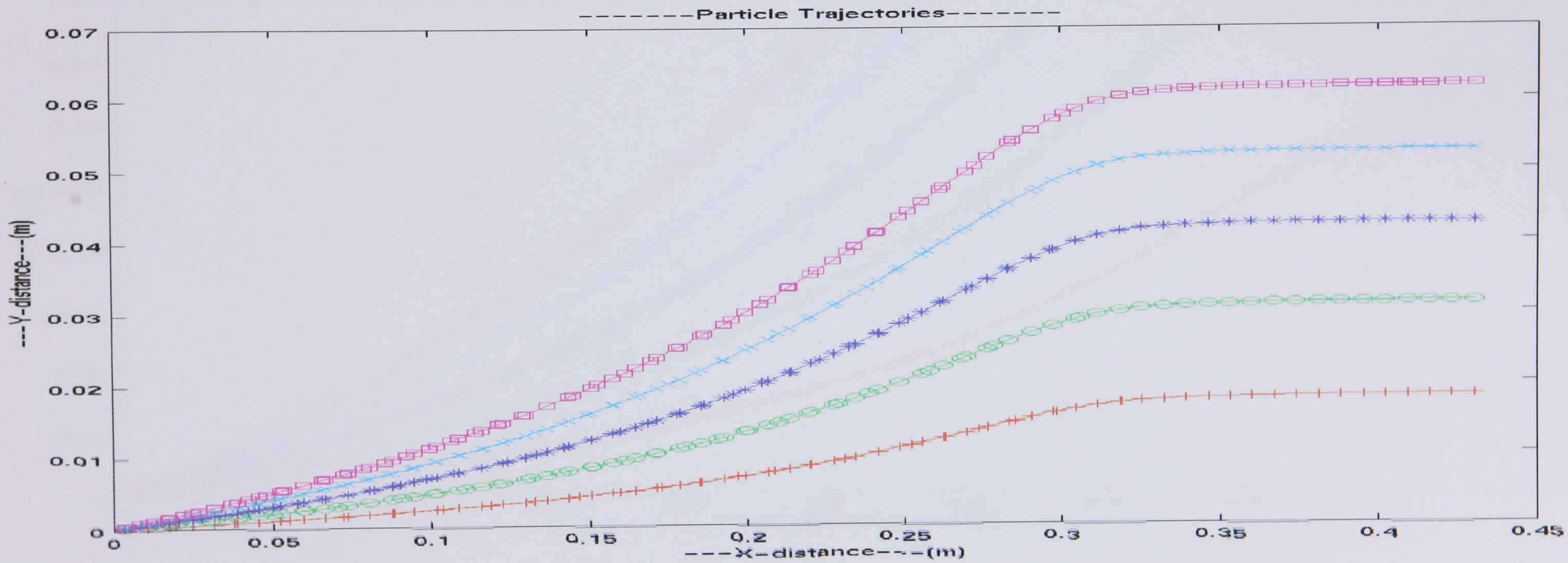

Gas temperature:	600k
Gas Flow Velocity X direction:	3.0m/s
Droplet diameter:	200 μm
Droplet inlet Velocity:	200m/s
Droplet inlet angle:	degree 1-5

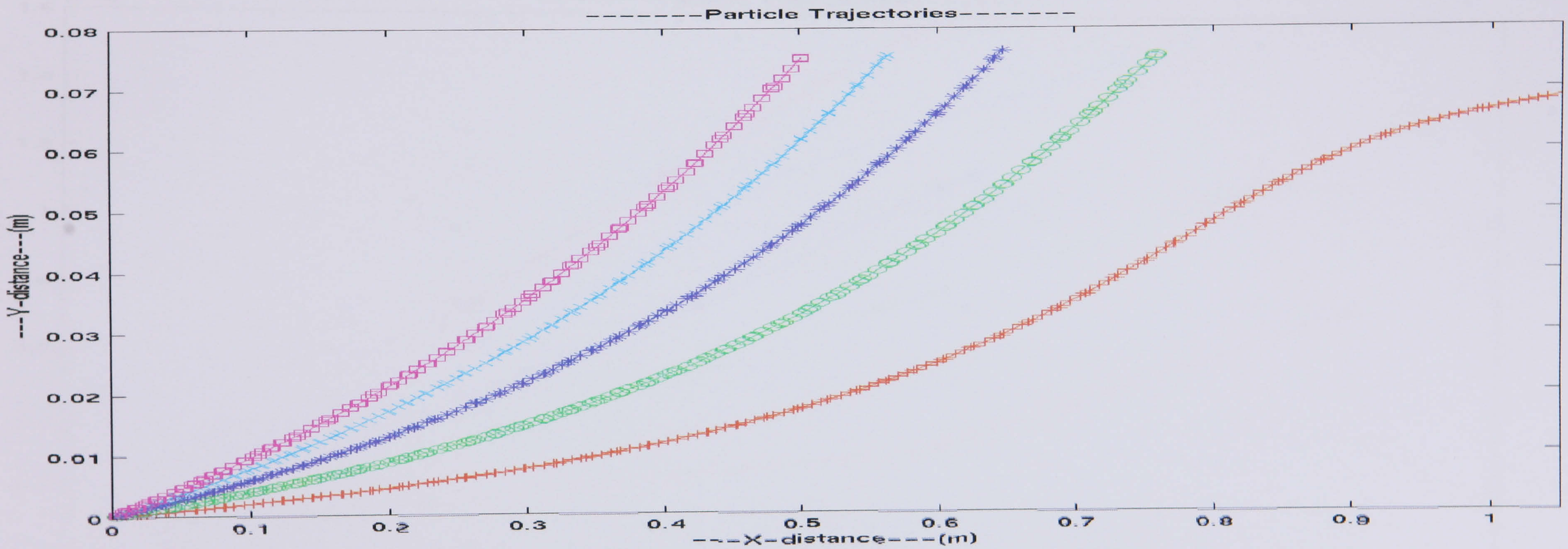

Gas temperature:	600k
Gas Flow Velocity X direction:	3.0m/s
Gas Flow Velocity Y direction:	0.3m/s
Droplet diameter:	10 μm
Droplet inlet Velocity:	200m/s
Droplet inlet angle:	degree 1-5

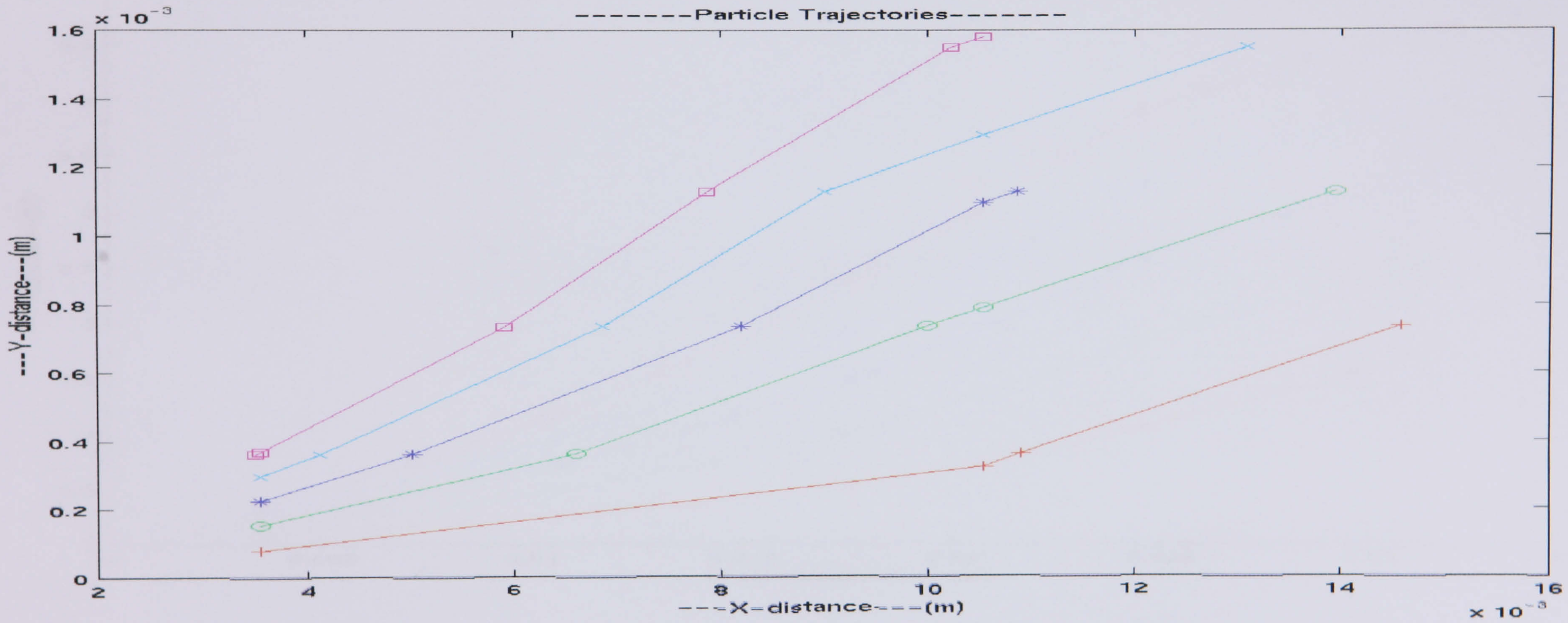

Gas temperature:	600k
Gas Flow Velocity X direction:	3.0m/s
Gas Flow Velocity Y direction:	0.3m/s
Droplet diameter:	20 μm
Droplet inlet Velocity:	200m/s
Droplet inlet angle:	degree 1-5

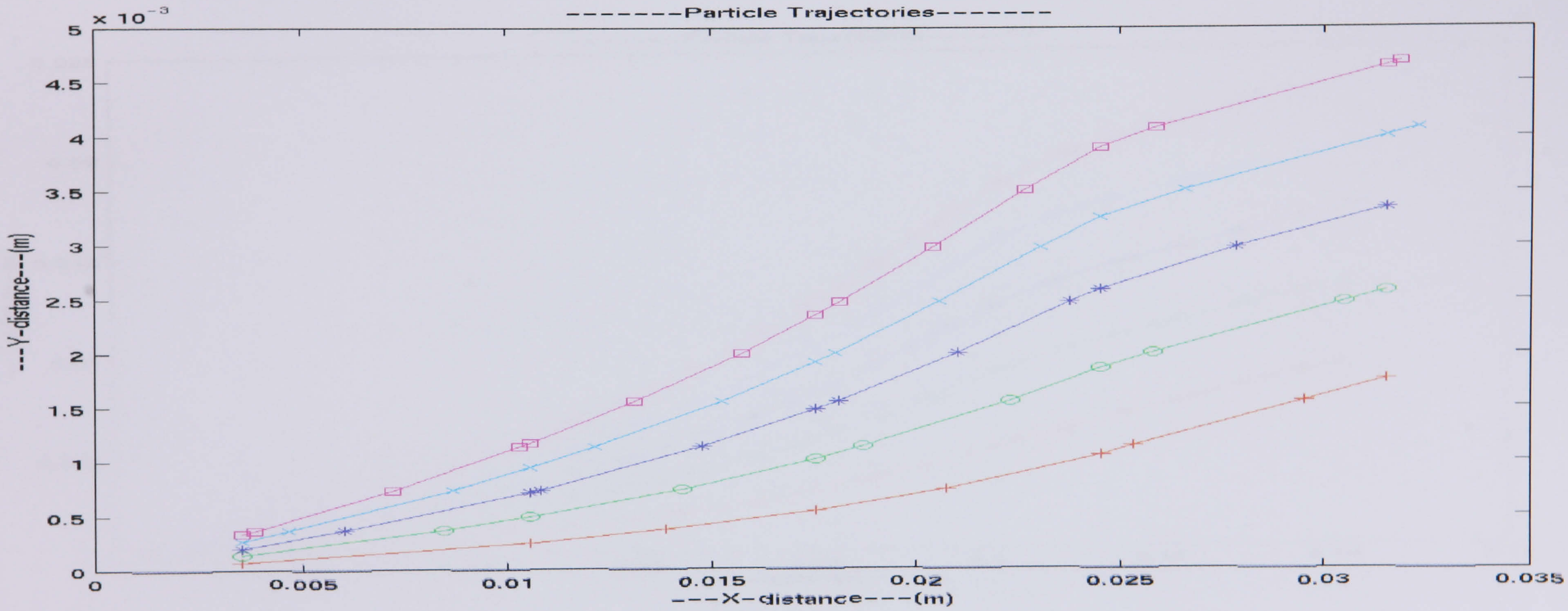

Gas temperature:	600k
Gas Flow Velocity X direction:	3.0m/s
Gas Flow Velocity Y direction:	0.3m/s
Droplet diameter:	50 μm
Droplet inlet Velocity:	200m/s
Droplet inlet angle:	degree 1-5

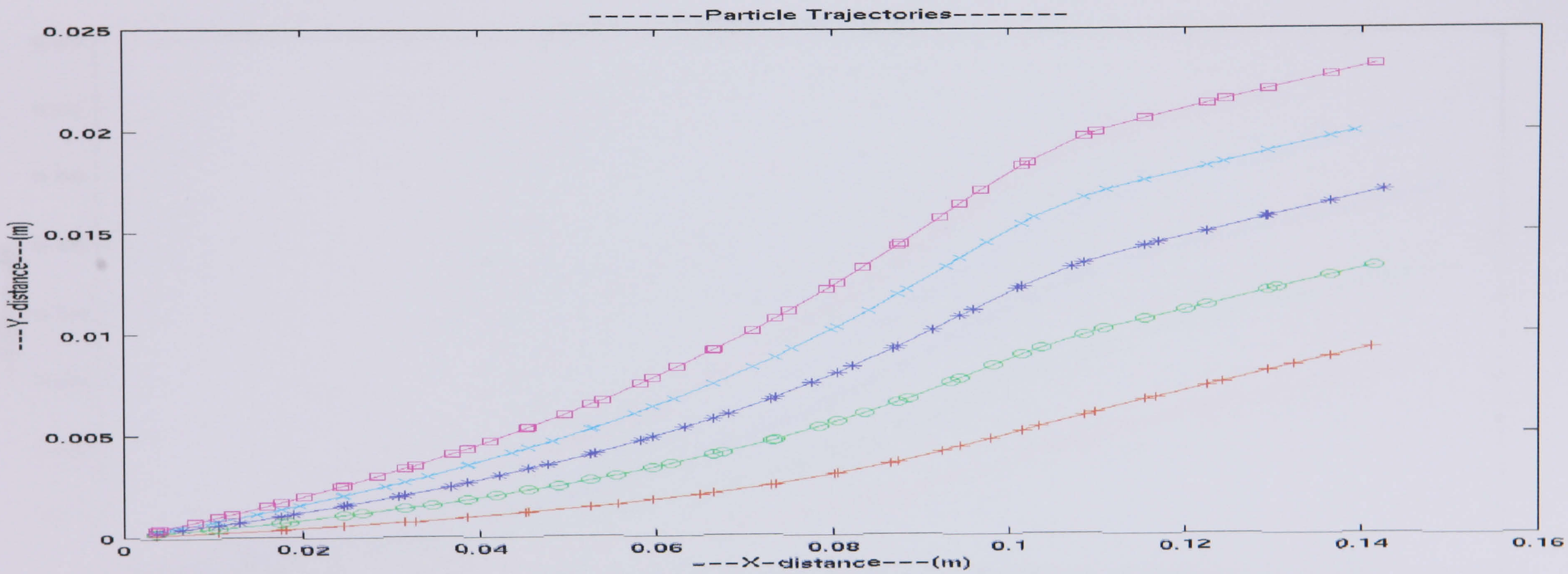

Gas temperature:	600k
Gas Flow Velocity X direction:	3.0m/s
Gas Flow Velocity Y direction:	0.3m/s
Droplet diameter:	100 μm
Droplet inlet Velocity:	200m/s
Droplet inlet angle:	degree 1-5

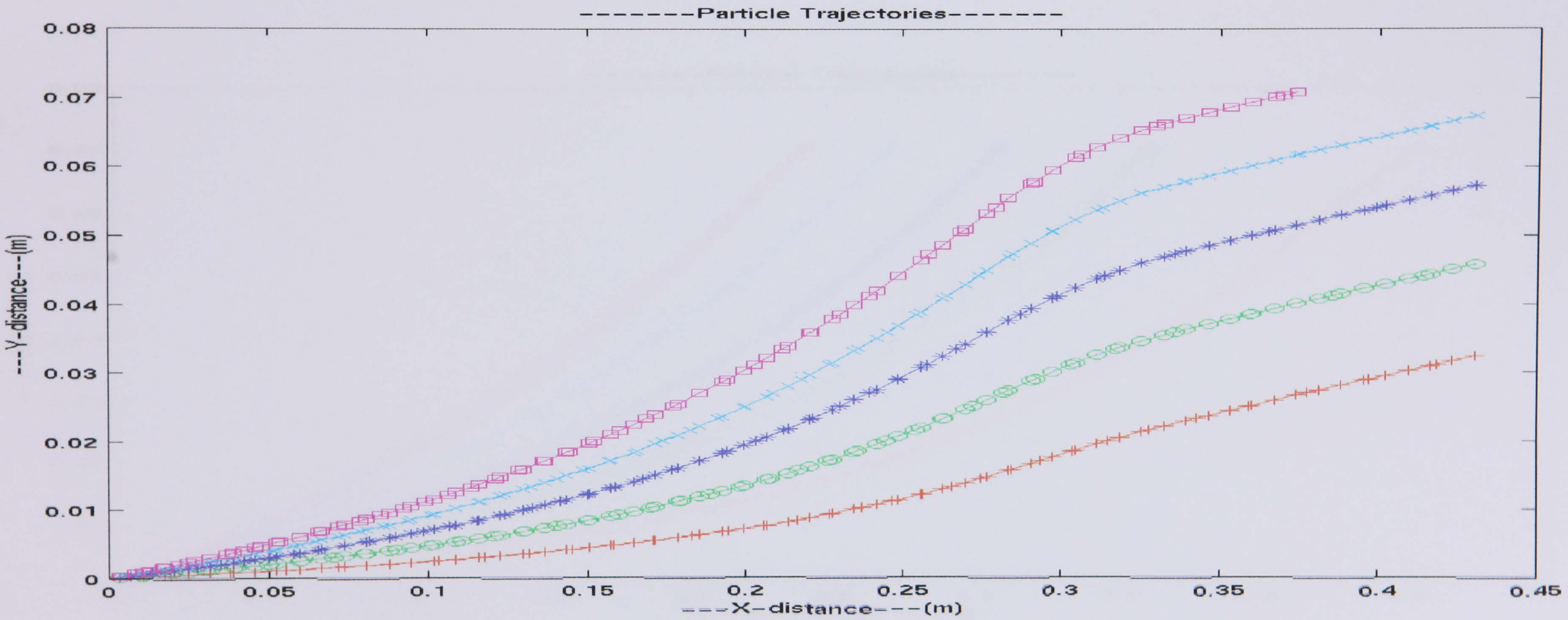

Gas temperature:	600k
Gas Flow Velocity X direction:	3.0m/s
Gas Flow Velocity Y direction:	0.3m/s
Droplet diameter:	200 μm
Droplet inlet Velocity:	200m/s
Droplet inlet angle:	degree 1-5

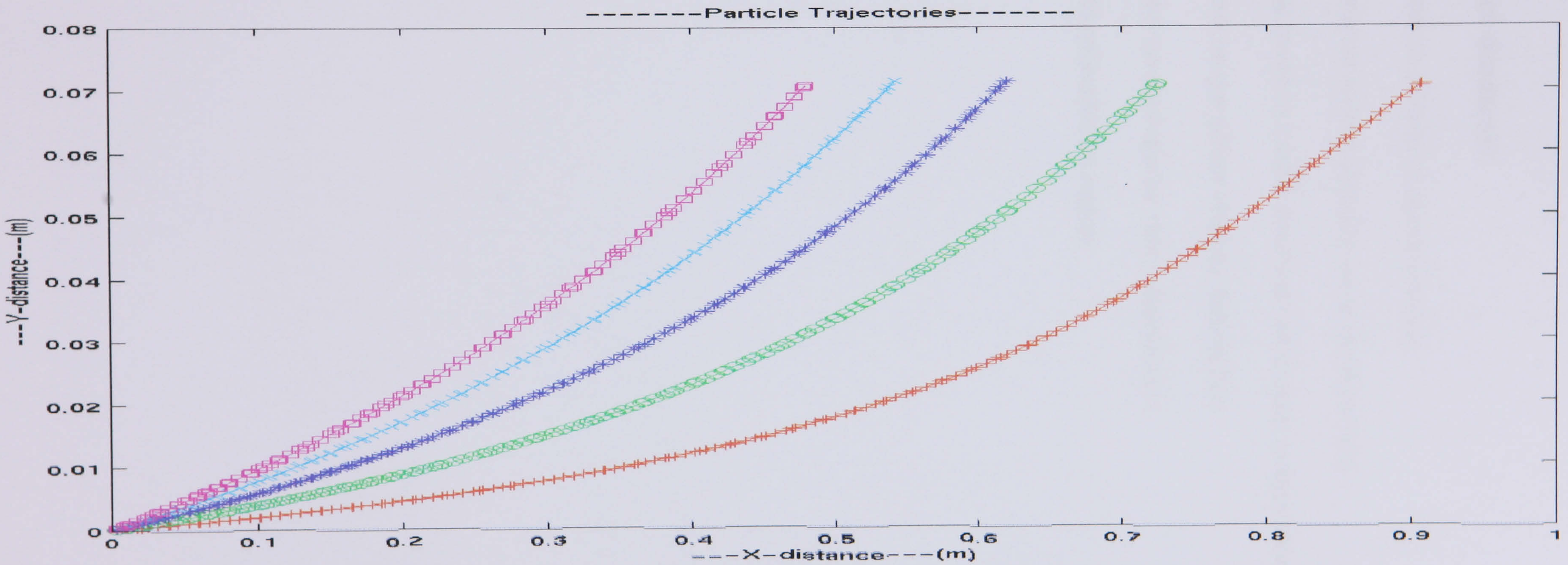

Appendix B

Parametric study: Droplet diameter

1. Effect of droplet diameter on droplet evaporation time
2. Effect of droplet diameter on droplet distribution in the flow field
3. Effect of droplet starting position (radial direction) on droplet evaporation
4. Effect of droplet diameter on gas phase velocity distribution
5. Effect of droplet diameter on equivalence ratio[1] distribution
6. Velocity distribution and recirculation region

---

[1] Vapour equivalence ratio

1. Effect of droplet diameter on droplet evaporation time

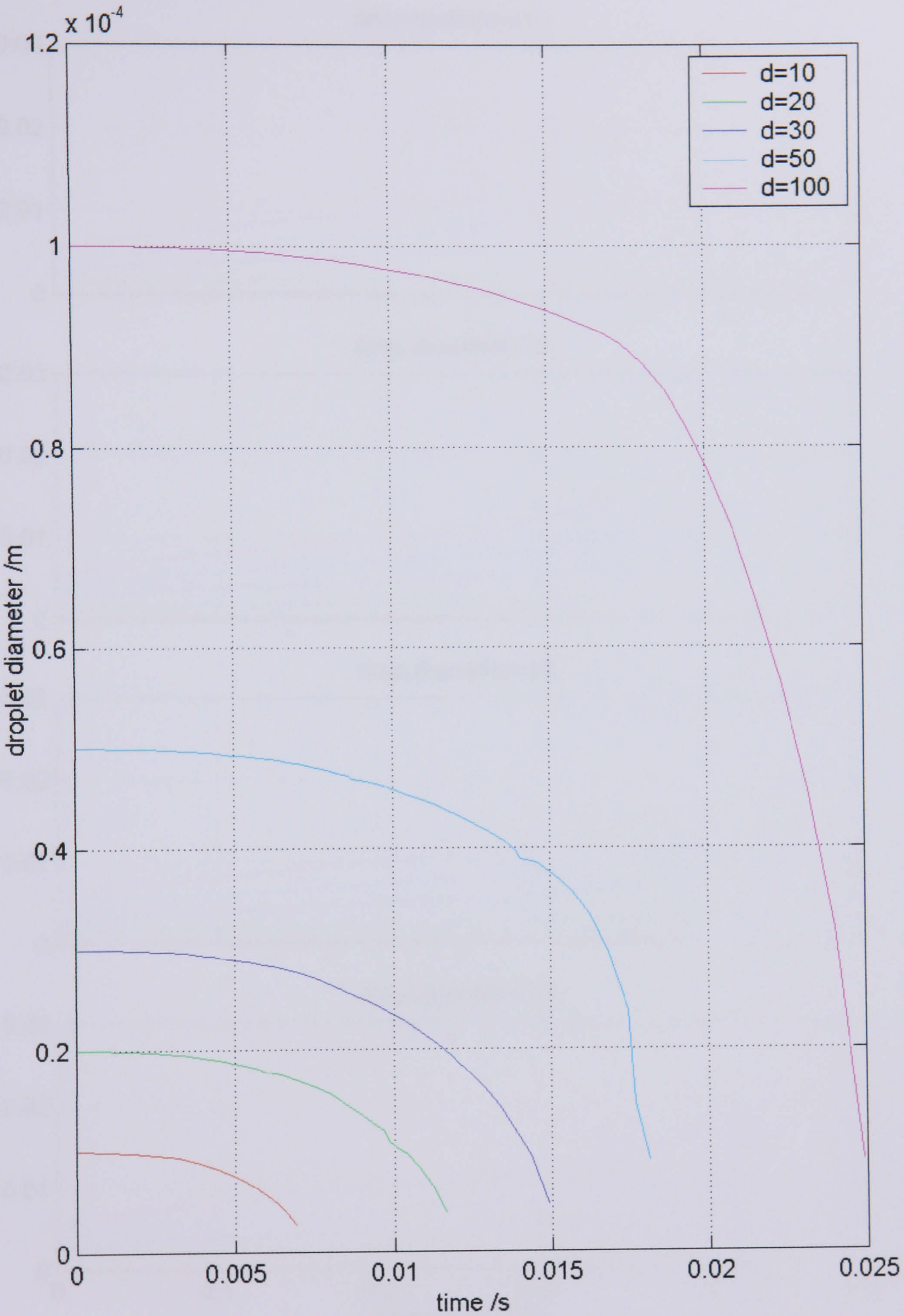

2. Effect of droplet diameter on droplet distribution in the flow field

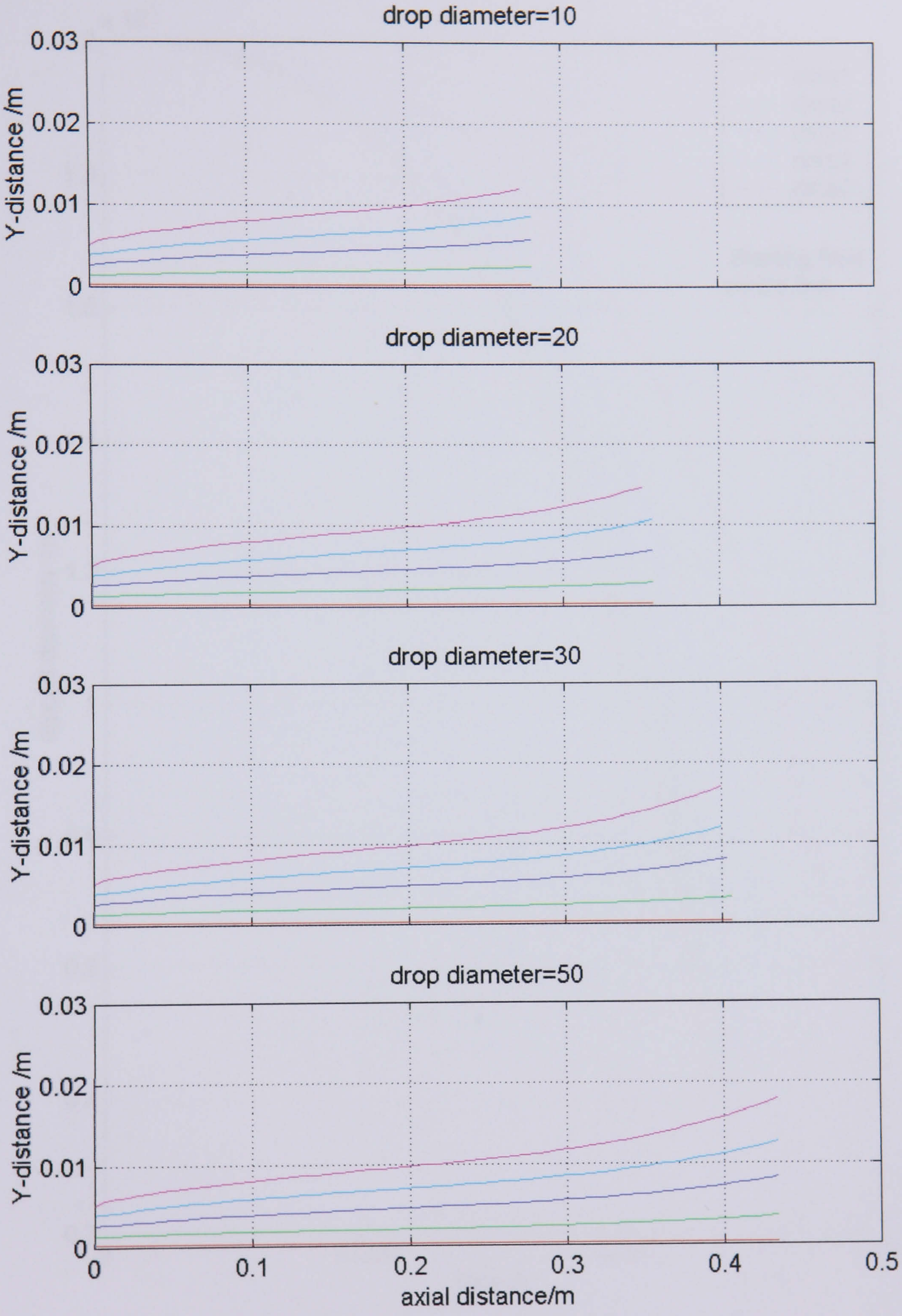

3. Effect of droplet starting position (radial direction) on droplet evaporation

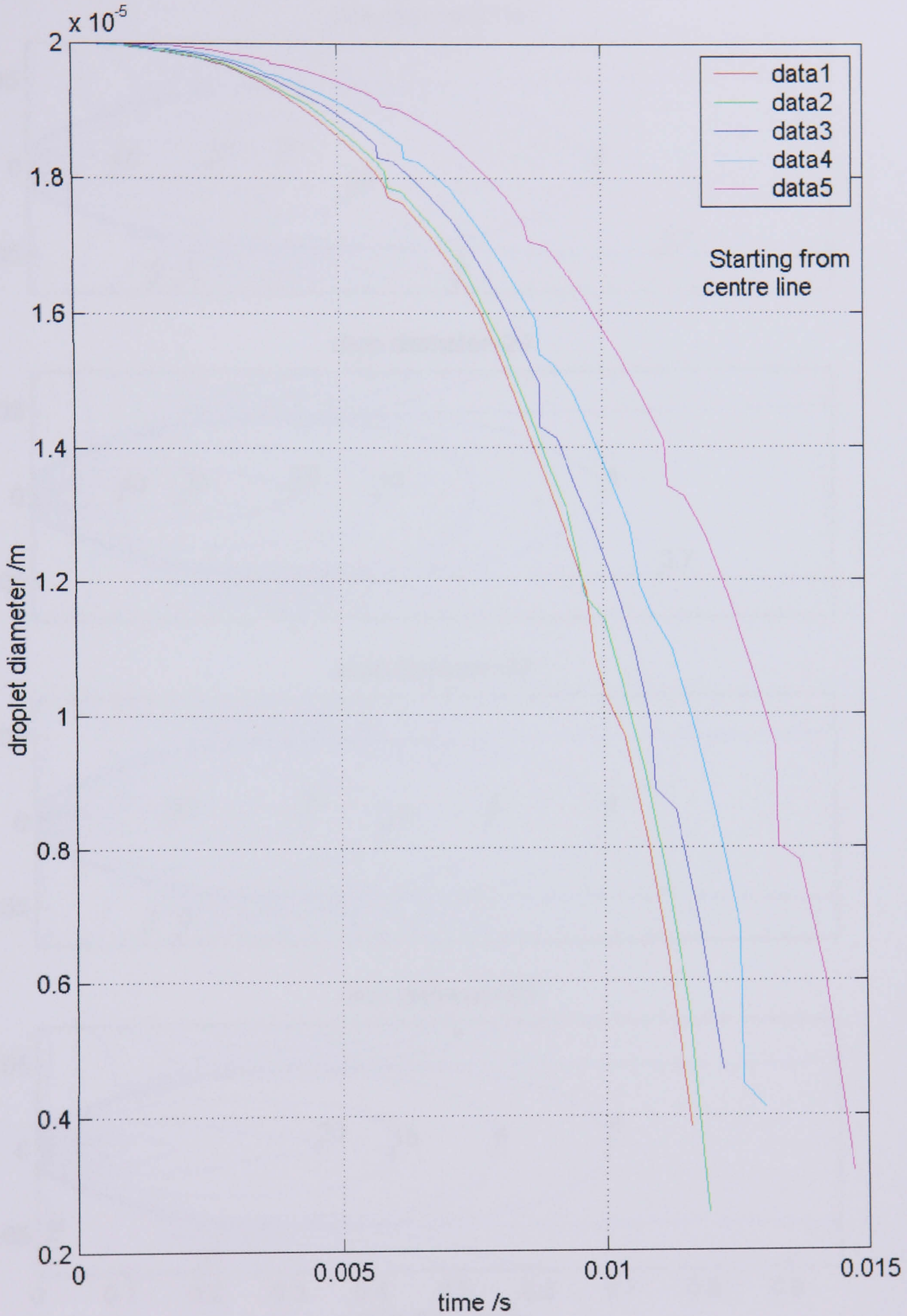

4. Effect of droplet diameter on gas phase velocity distribution

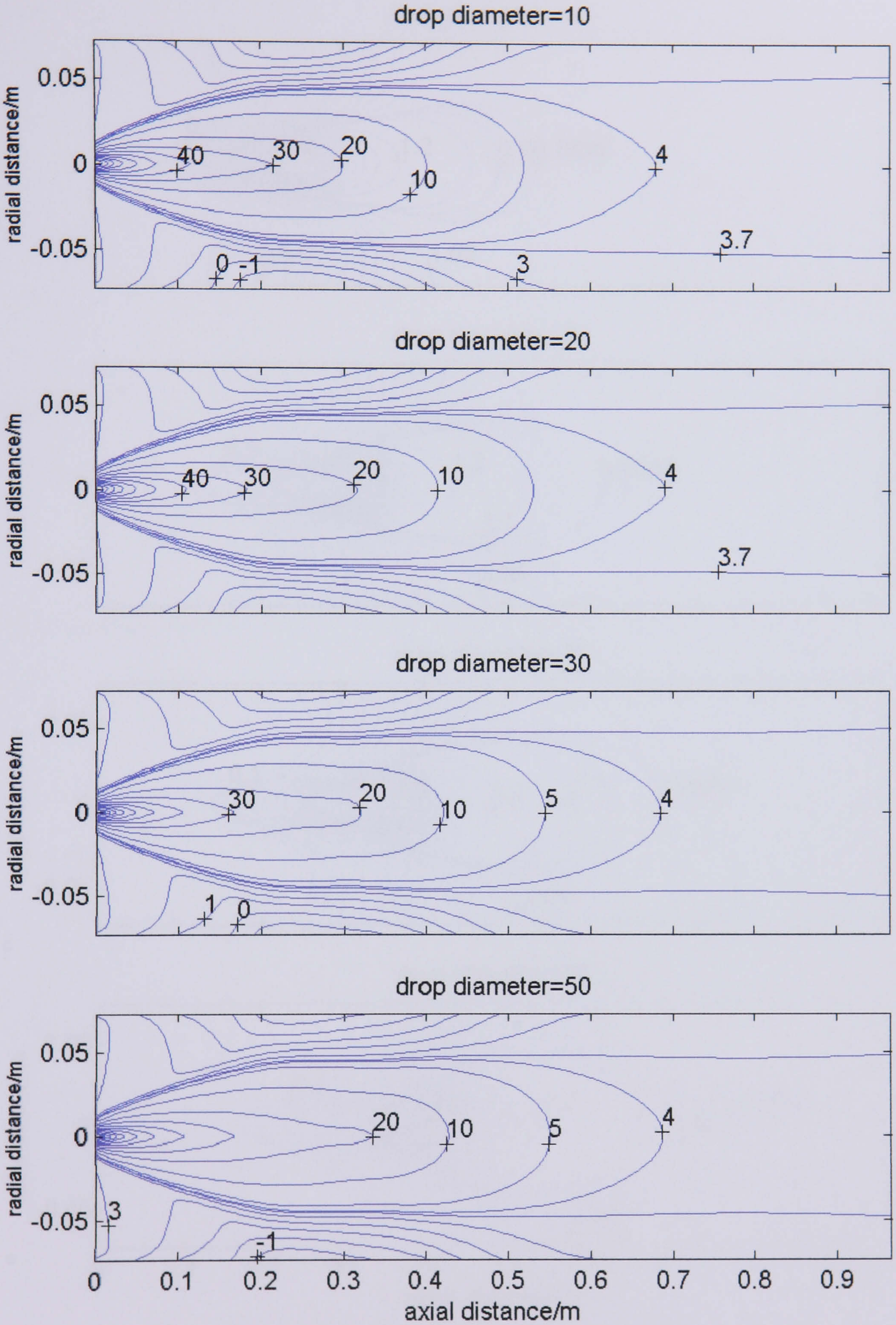

5. Effect of droplet diameter on equivalence ratio distribution

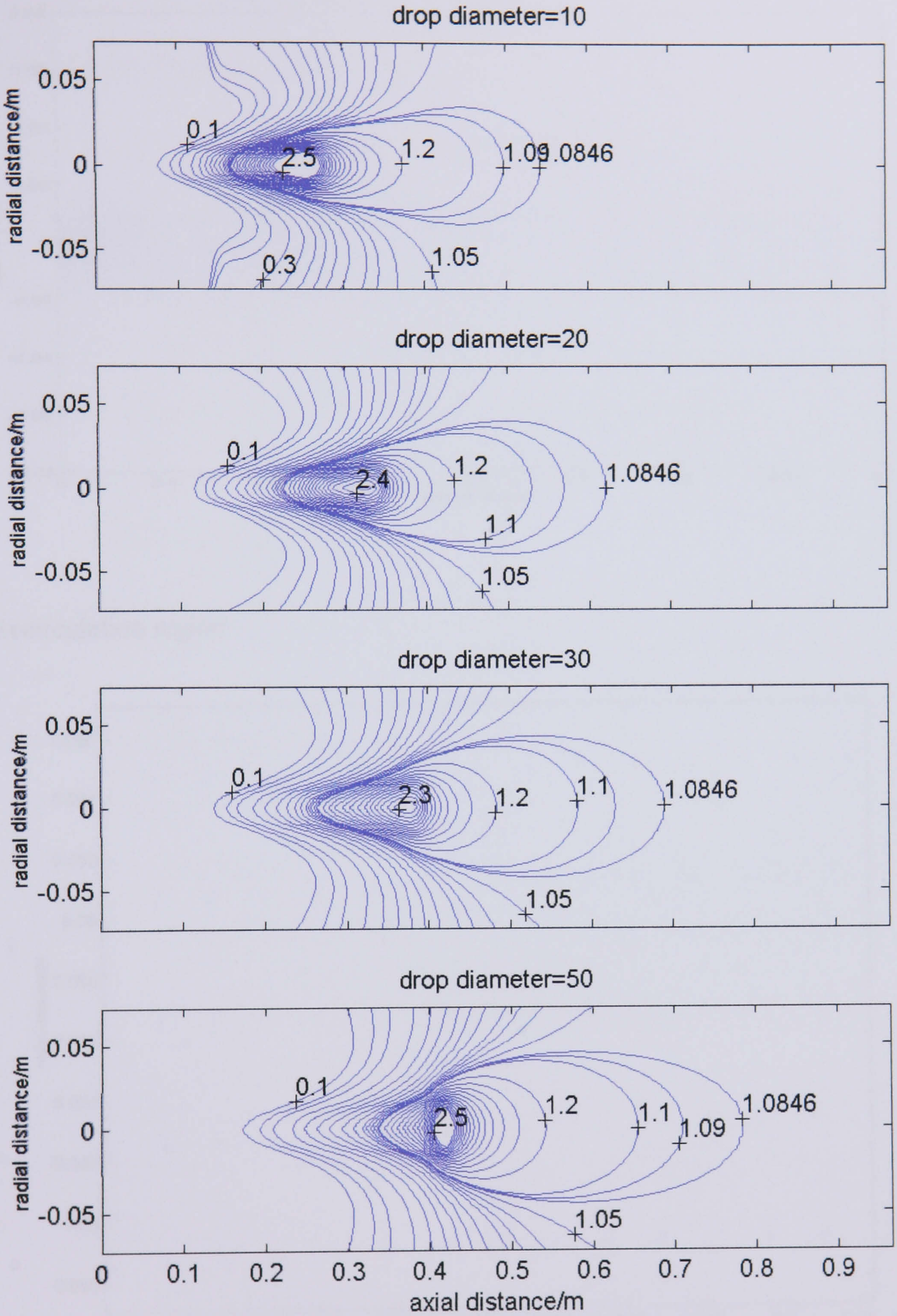

6 Velocity Distribution

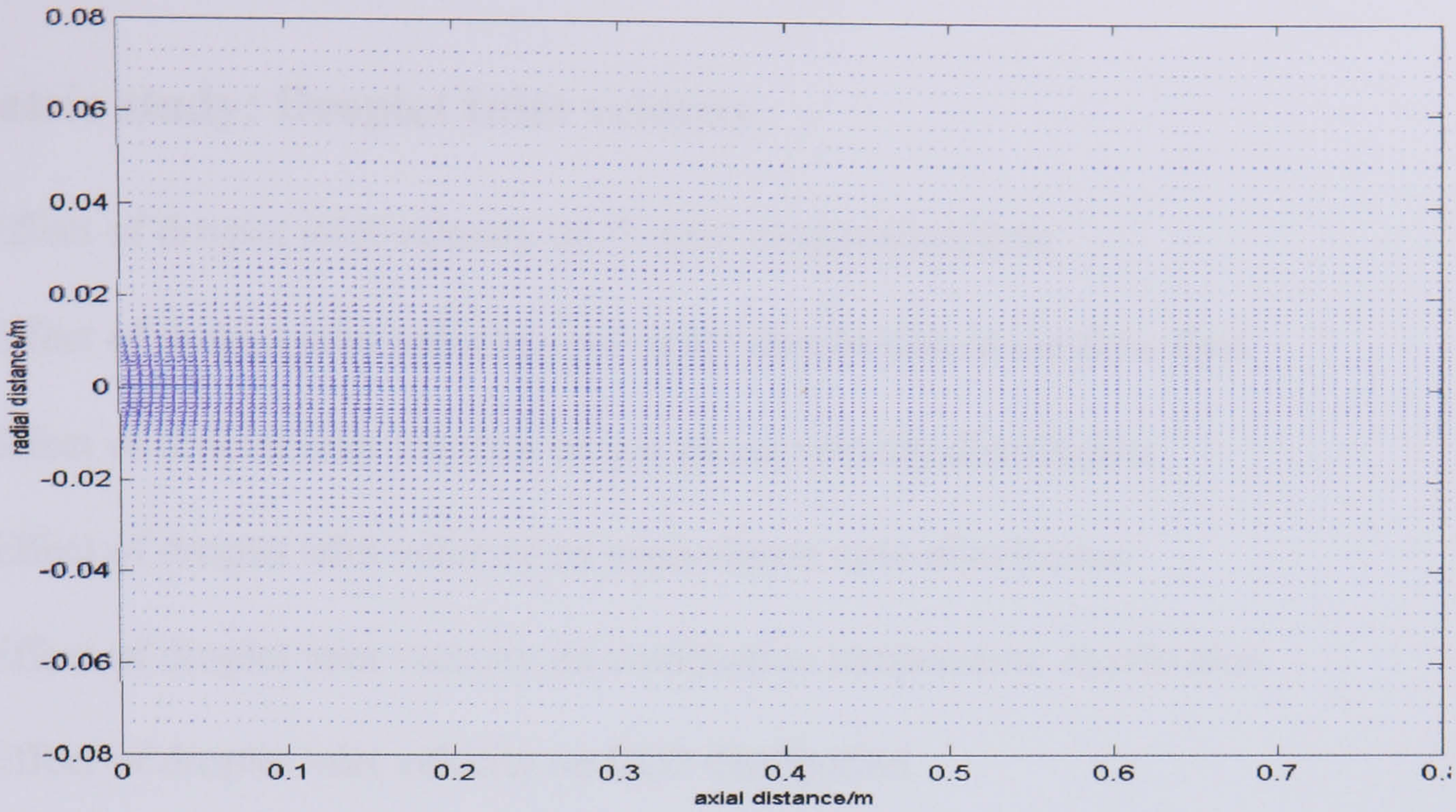

7 Recirculation region

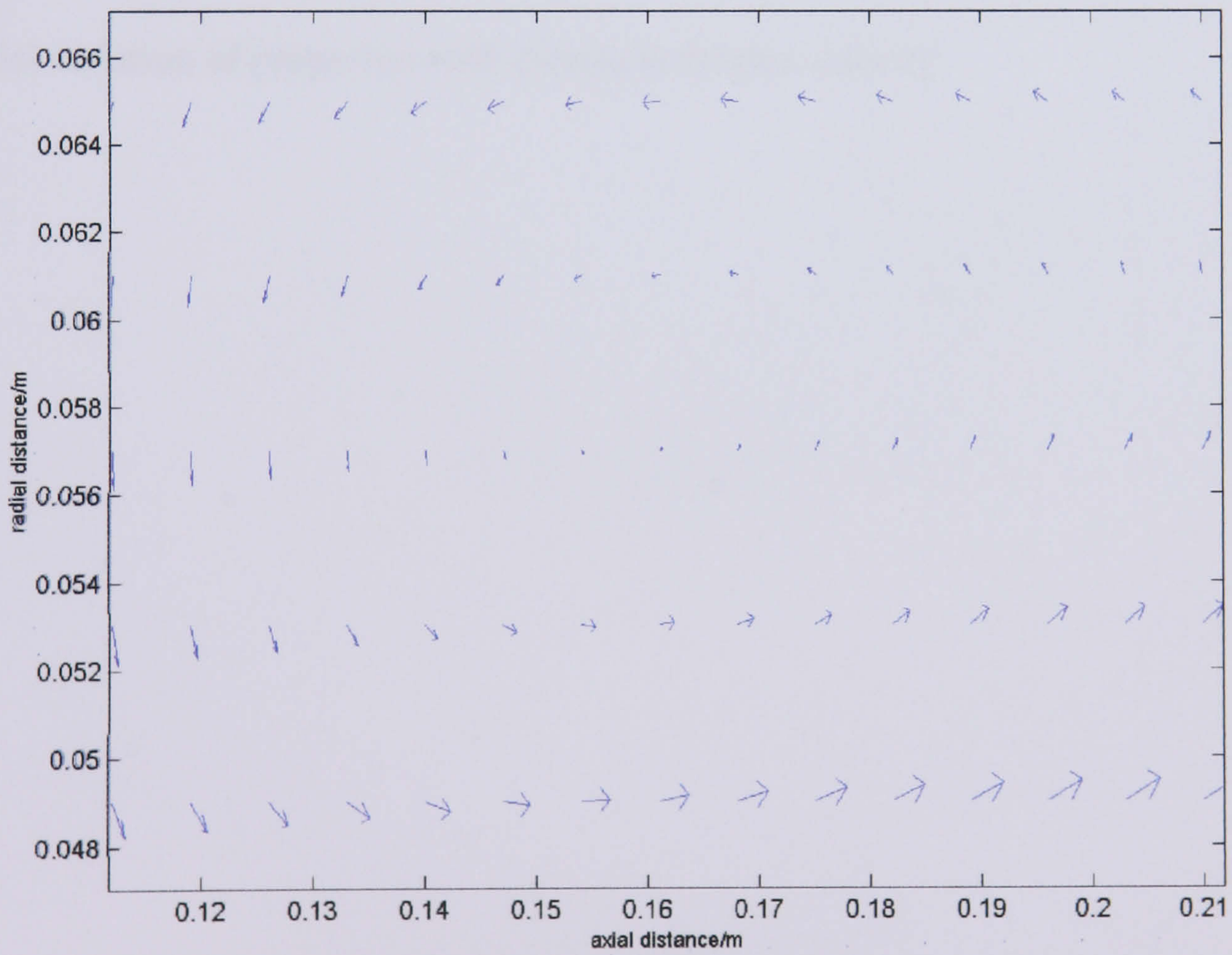

Appendix C:

Parametric study: Droplet Inlet velocity

1. Effect of droplet inlet velocity on droplet evaporation time
2. Effect of droplet inlet velocity on droplet distribution in the flow field
3. Effect of droplet inlet velocity on gas phase velocity distribution
4. Effect of droplet inlet velocity on equivalence ratio distribution
5. Effect of droplet inlet velocity on combustion temperature distribution
6. Effect of droplet inlet velocity on CO2 distribution
7. Effect of droplet inlet velocity on CO distribution
8. Axial variation of properties along the centre line with change in droplet velocity
9. Radial variation of properties with change in droplet velocity

1. Effect of droplet inlet velocity on droplet evaporation time

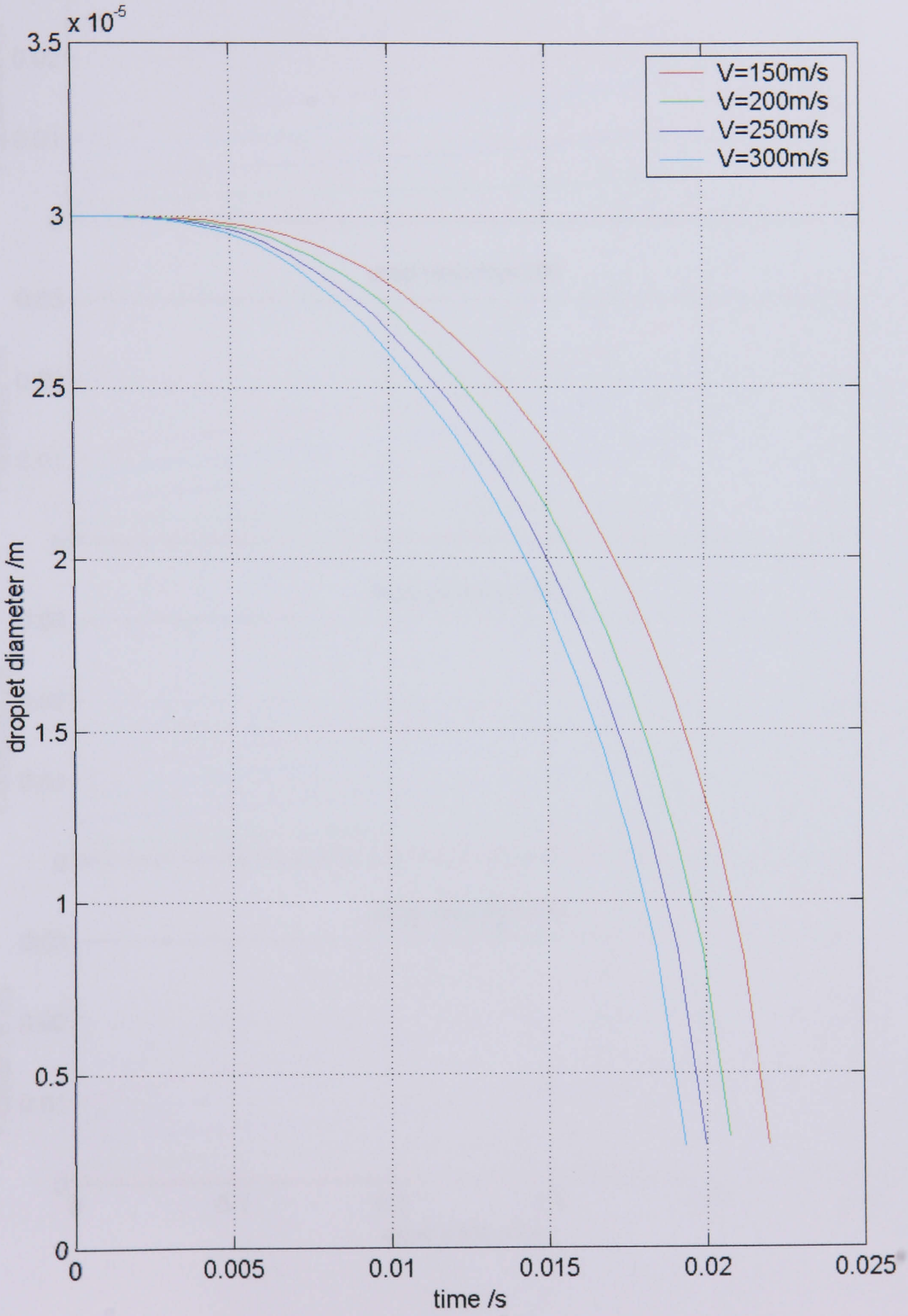

2. Effect of droplet inlet velocity on droplet distribution in the flow field

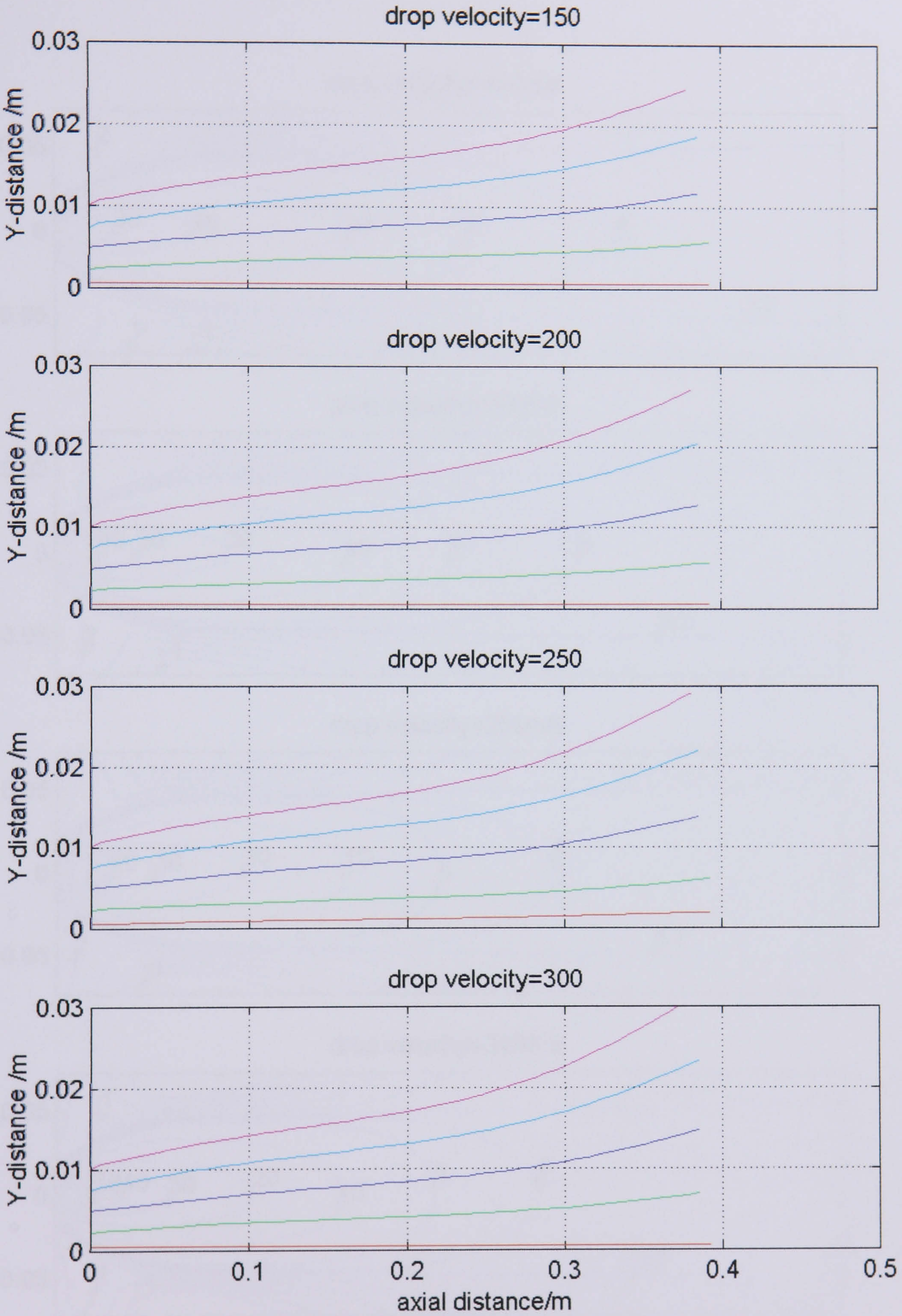

3. Effect of droplet inlet velocity on gas phase velocity distribution

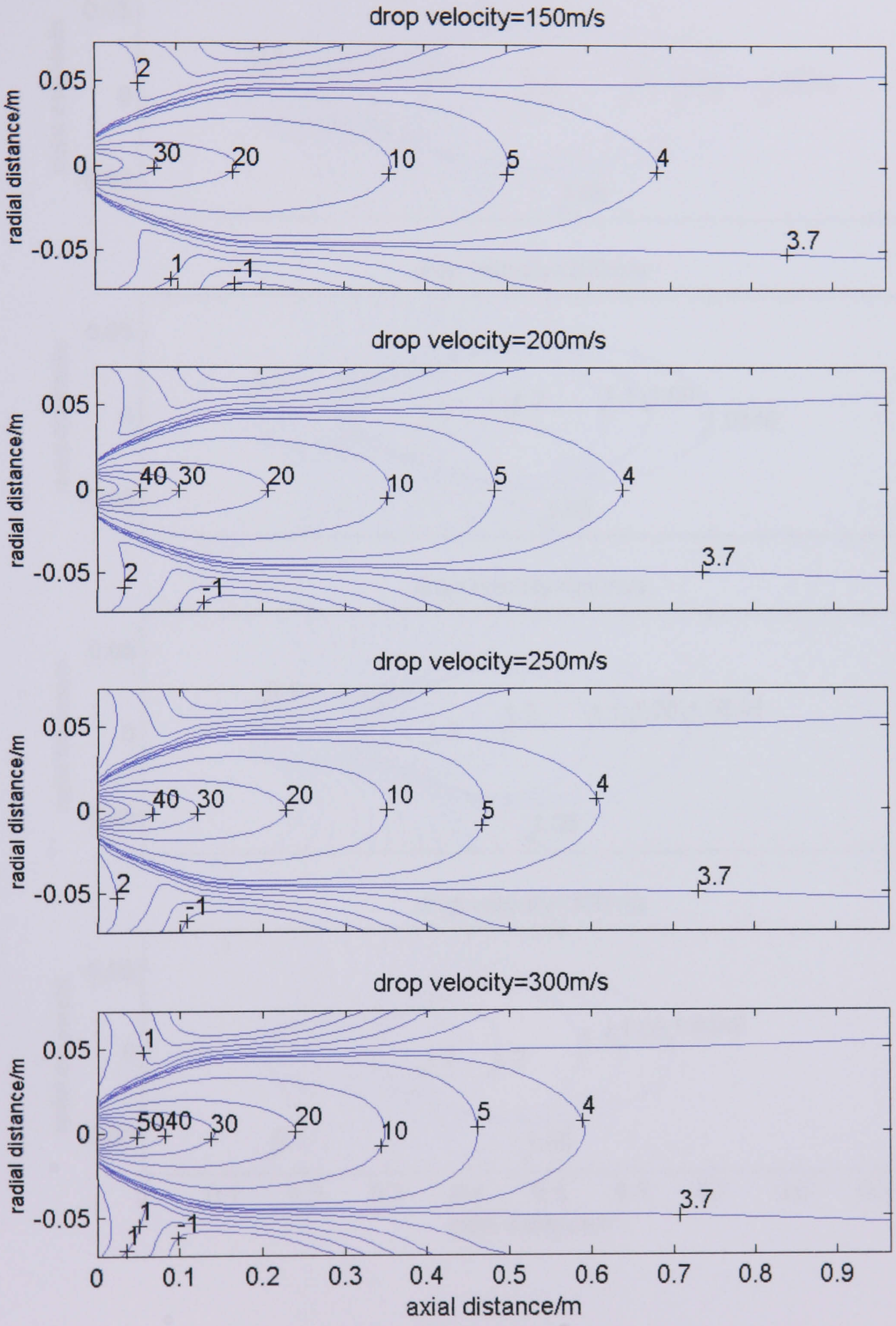

4. Effect of droplet inlet velocity on equivalence ratio distribution

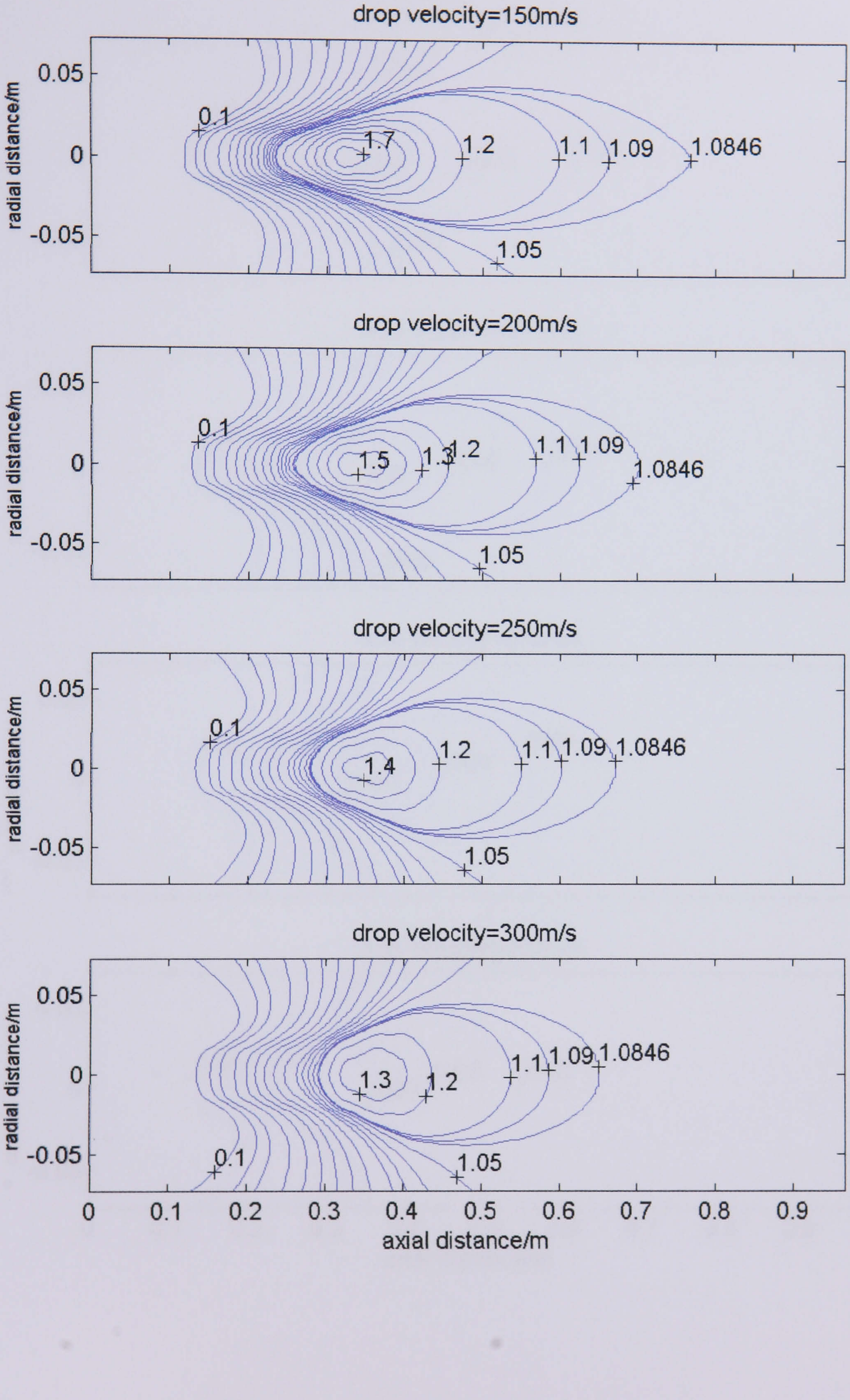

5. Effect of droplet inlet velocity on combustion temperature distribution

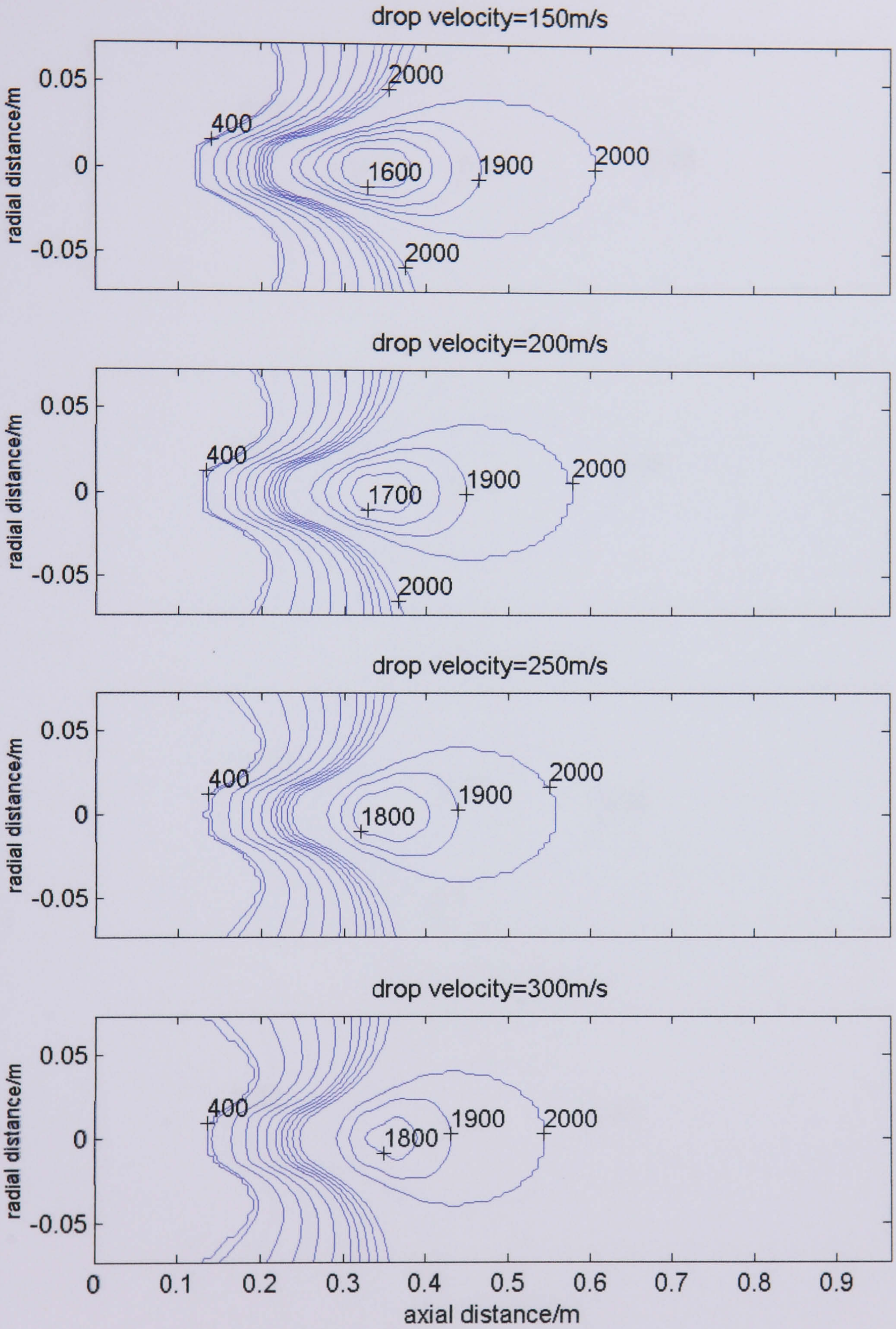

6. Effect of droplet inlet velocity on CO2 distribution

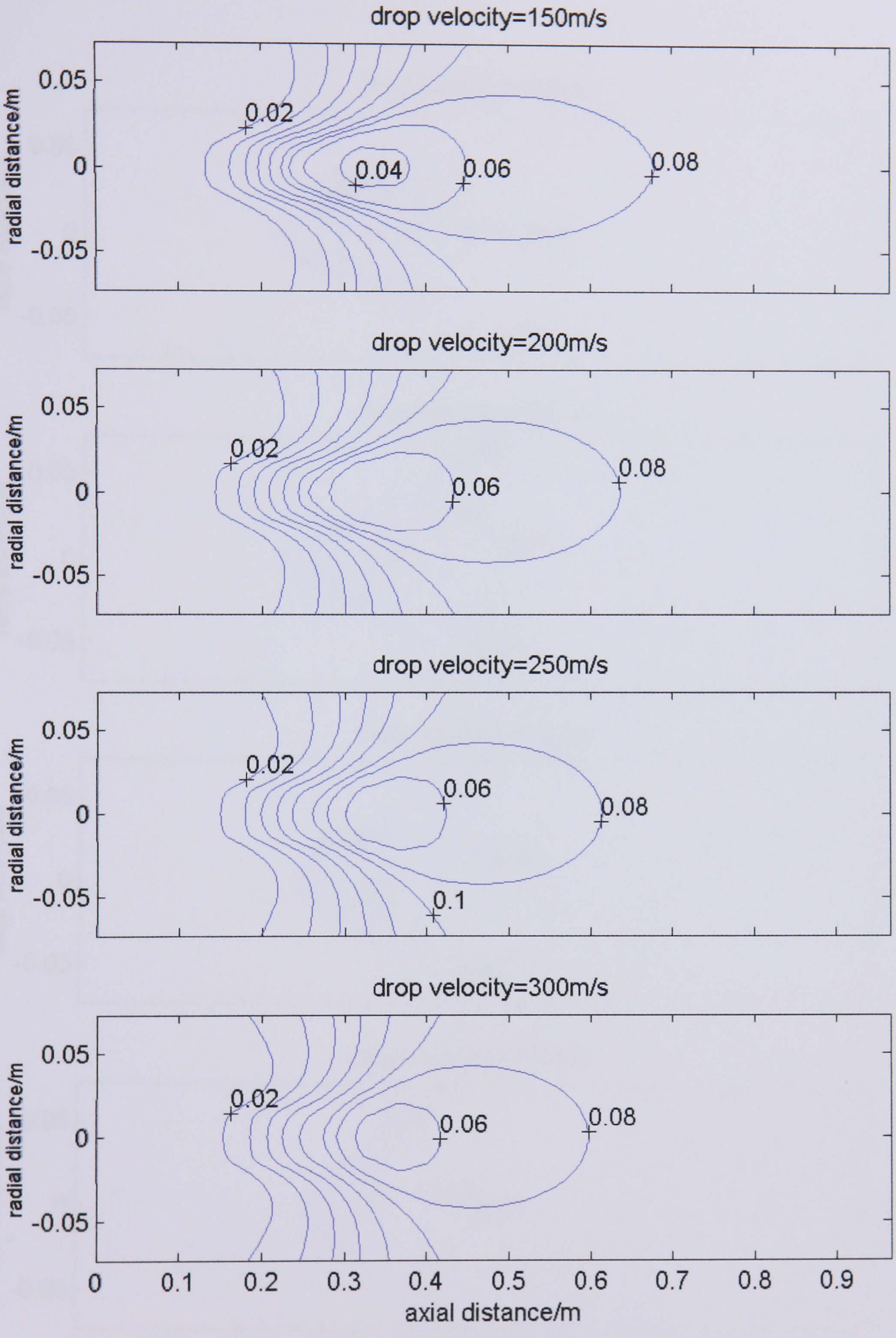

7. Effect of droplet inlet velocity on CO distribution

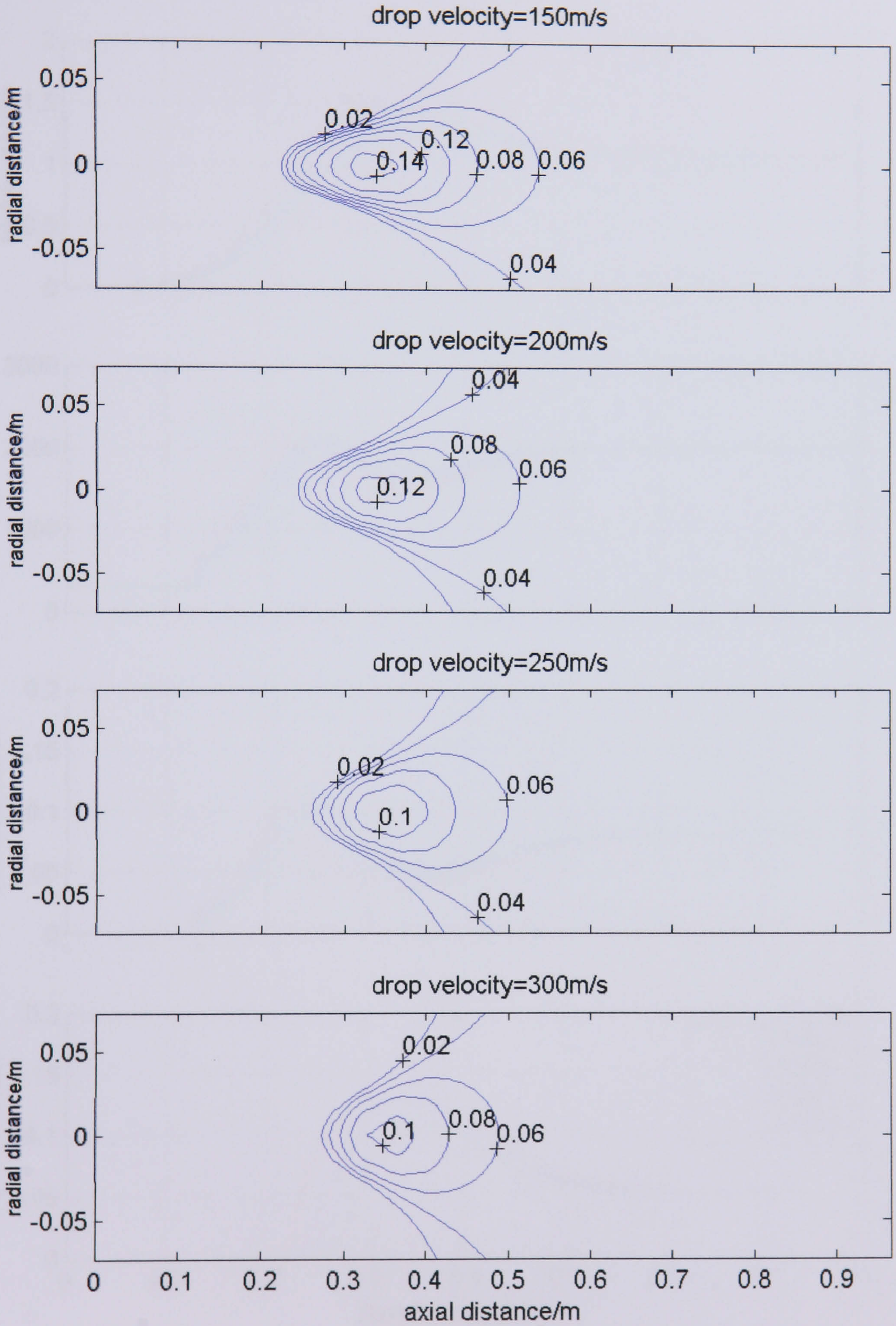

8. Axial variation of properties along the centre line with change in droplet velocity

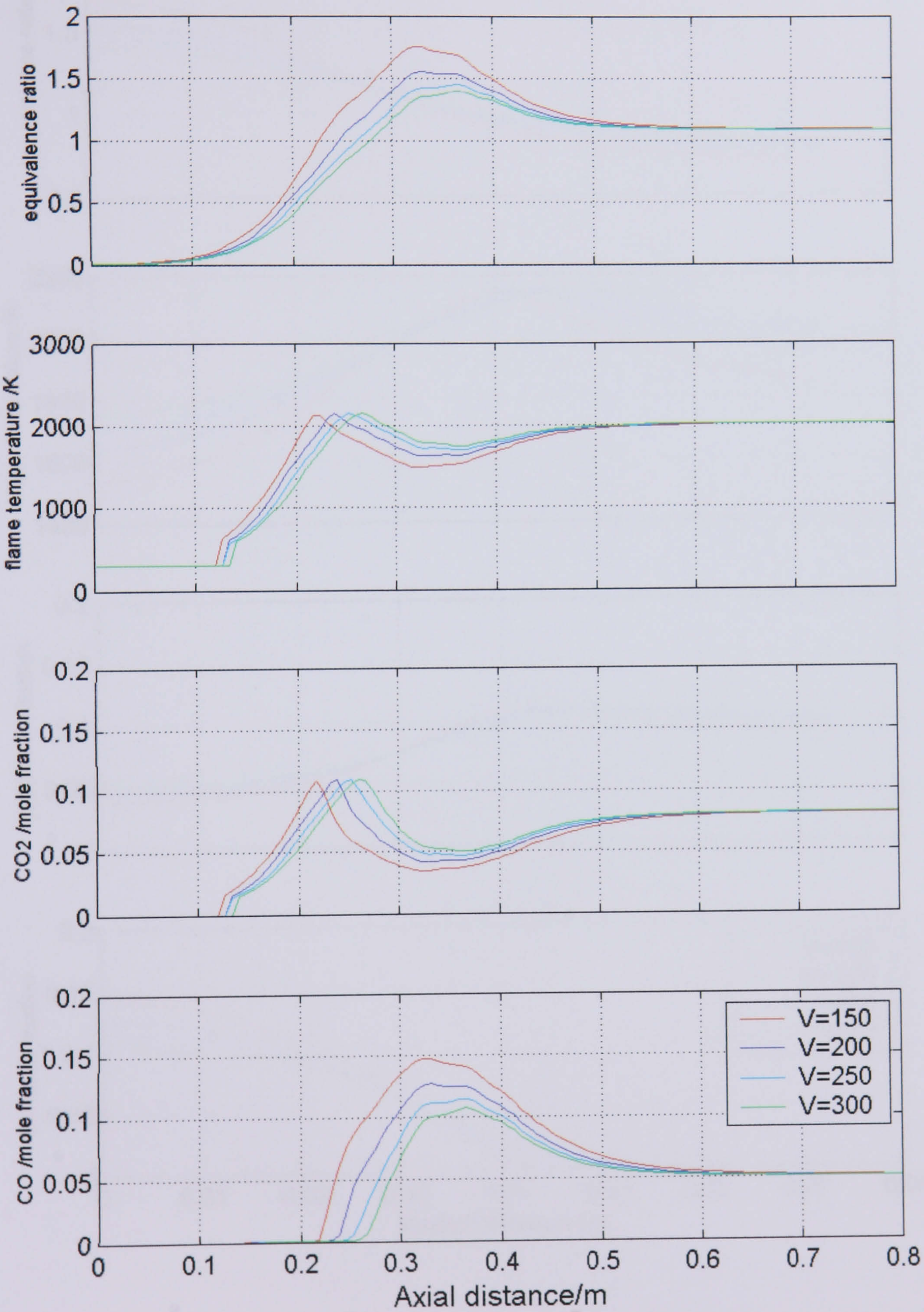

9. Radial variation of properties with change in droplet velocity

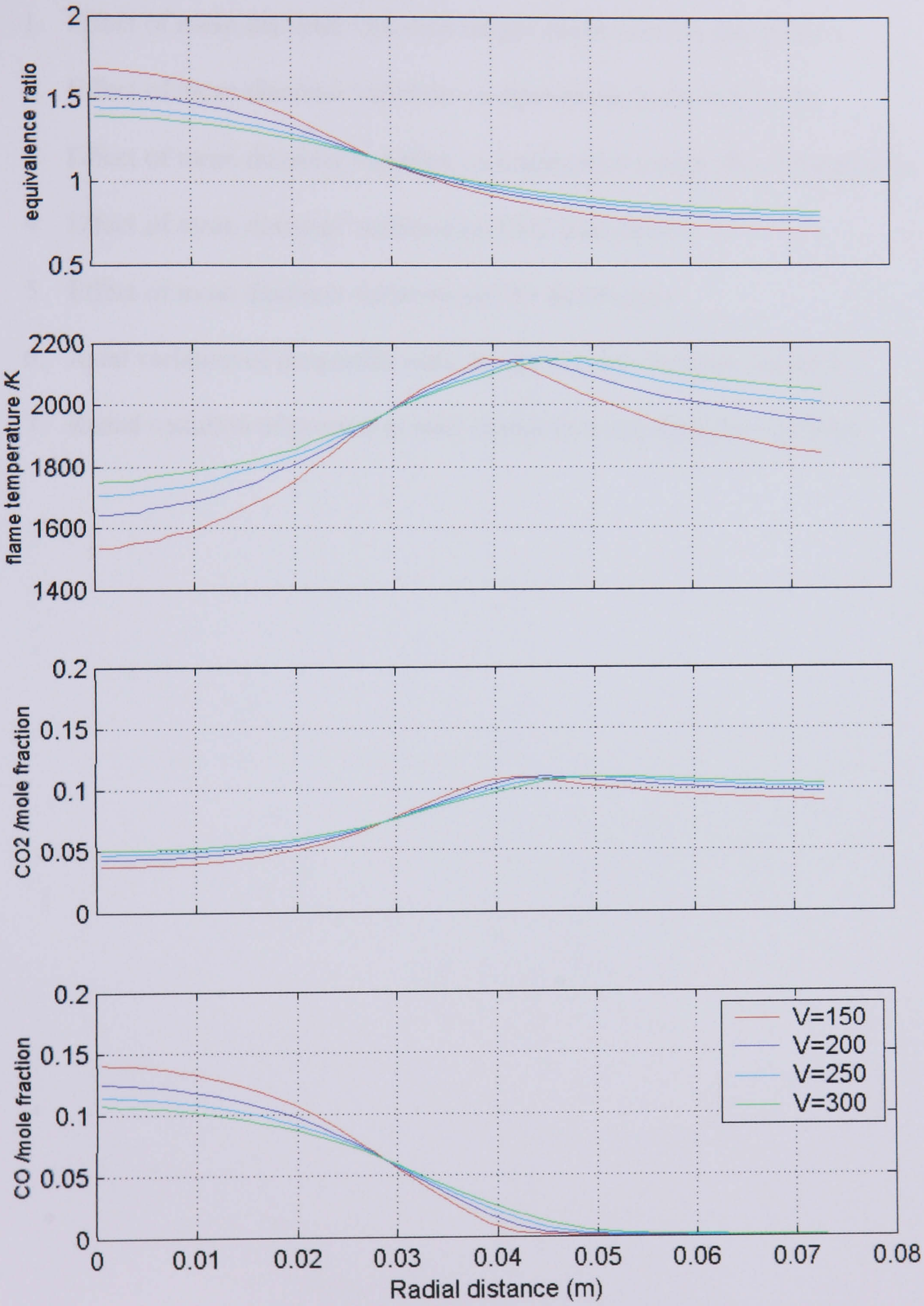

Appendix D

Parametric study: Mean Diameter variation

1. Effect of mean diameter variation on gas phase velocity distribution
2. Effect of mean diameter variation on equivalence ratio distribution
3. Effect of mean diameter variation on combustion temperature distribution
4. Effect of mean diameter variation on CO2 distribution
5. Effect of mean diameter variation on CO distribution
6. Axial variation of properties with change in mean diameter variation
7. Radial variation of properties with change in mean diameter variation

1. Effect of mean diameter variation on gas phase velocity distribution

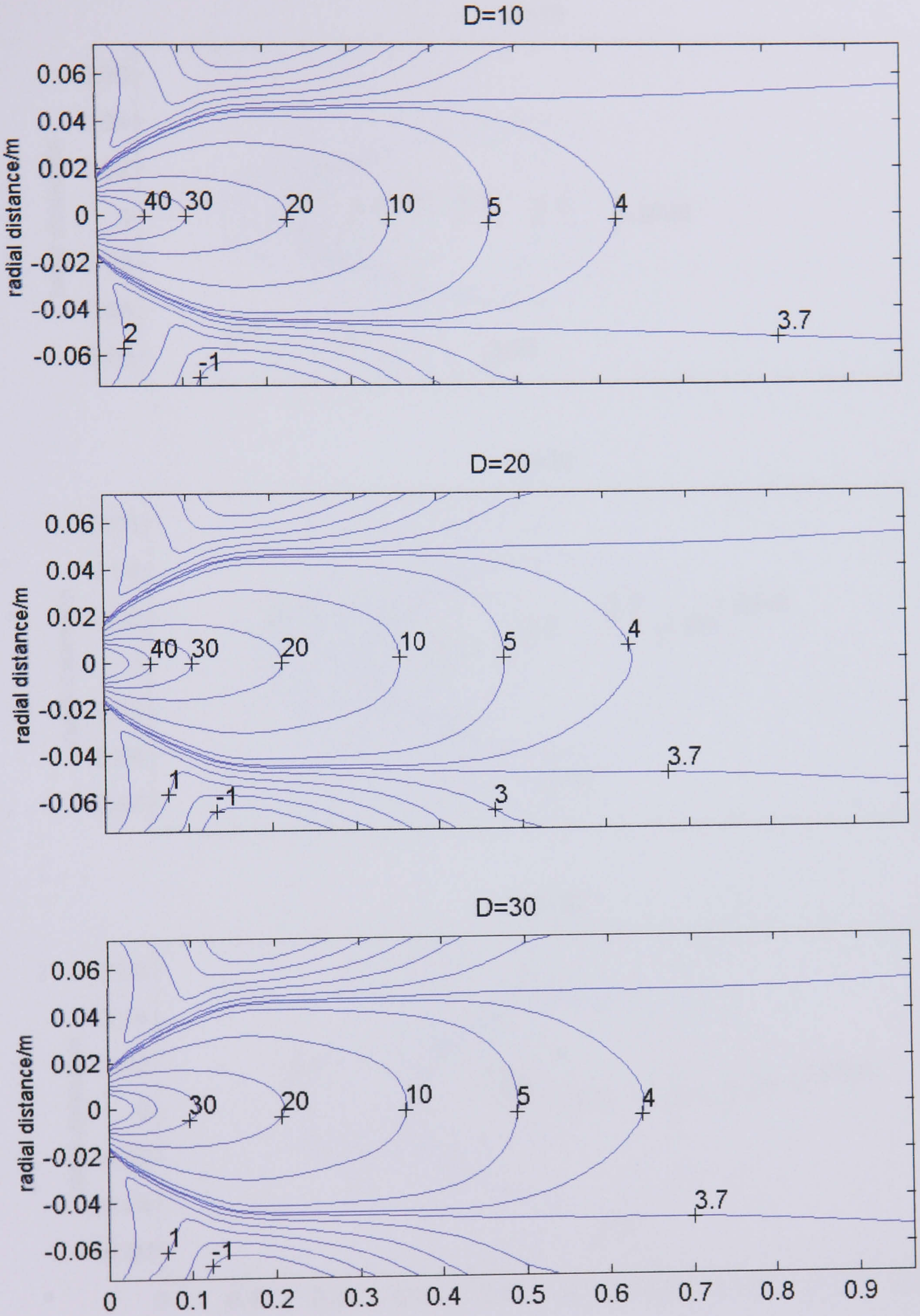

2. Effect of mean diameter variation on equivalence ratio distribution

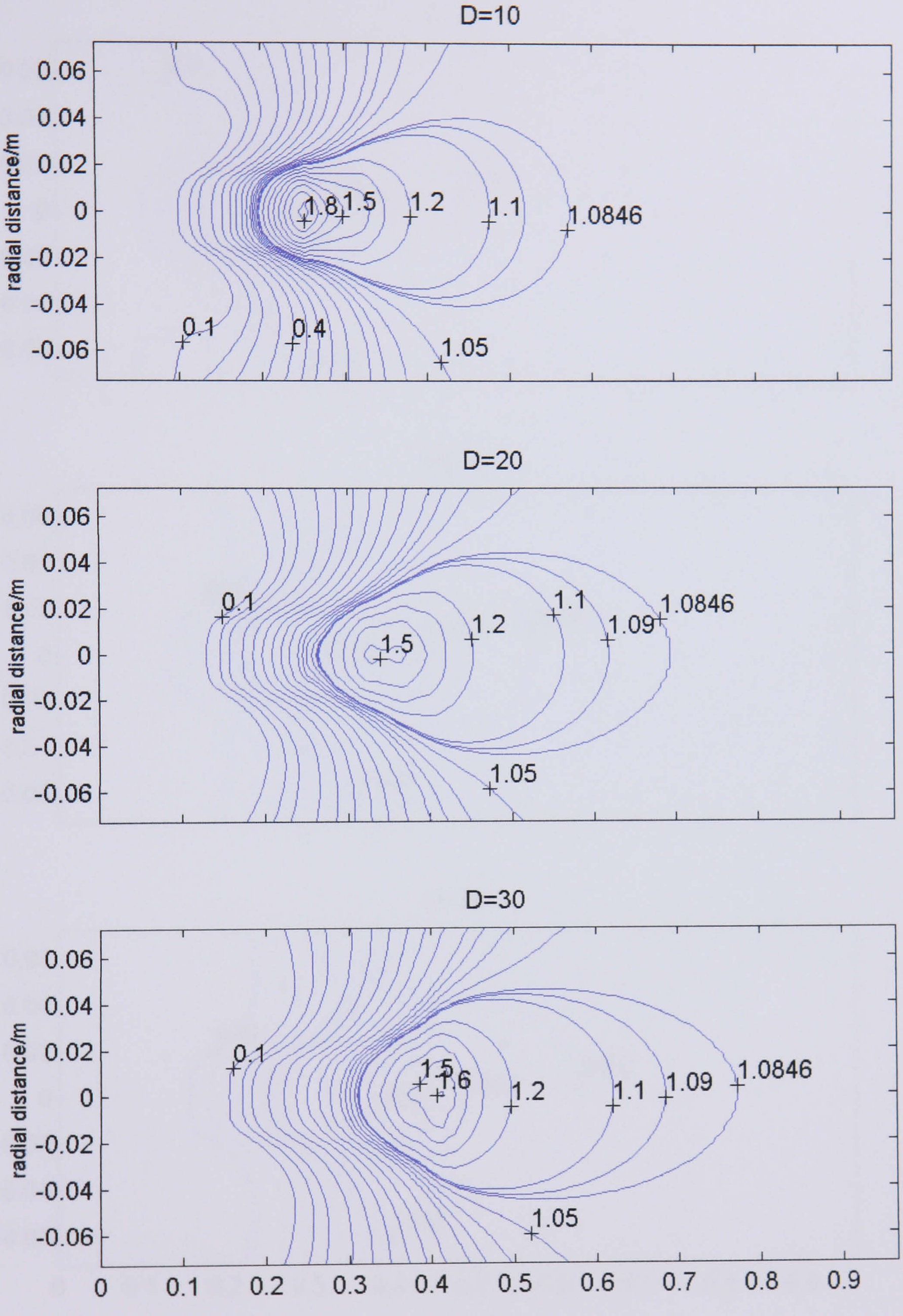

3. Effect of mean diameter variation on combustion temperature distribution

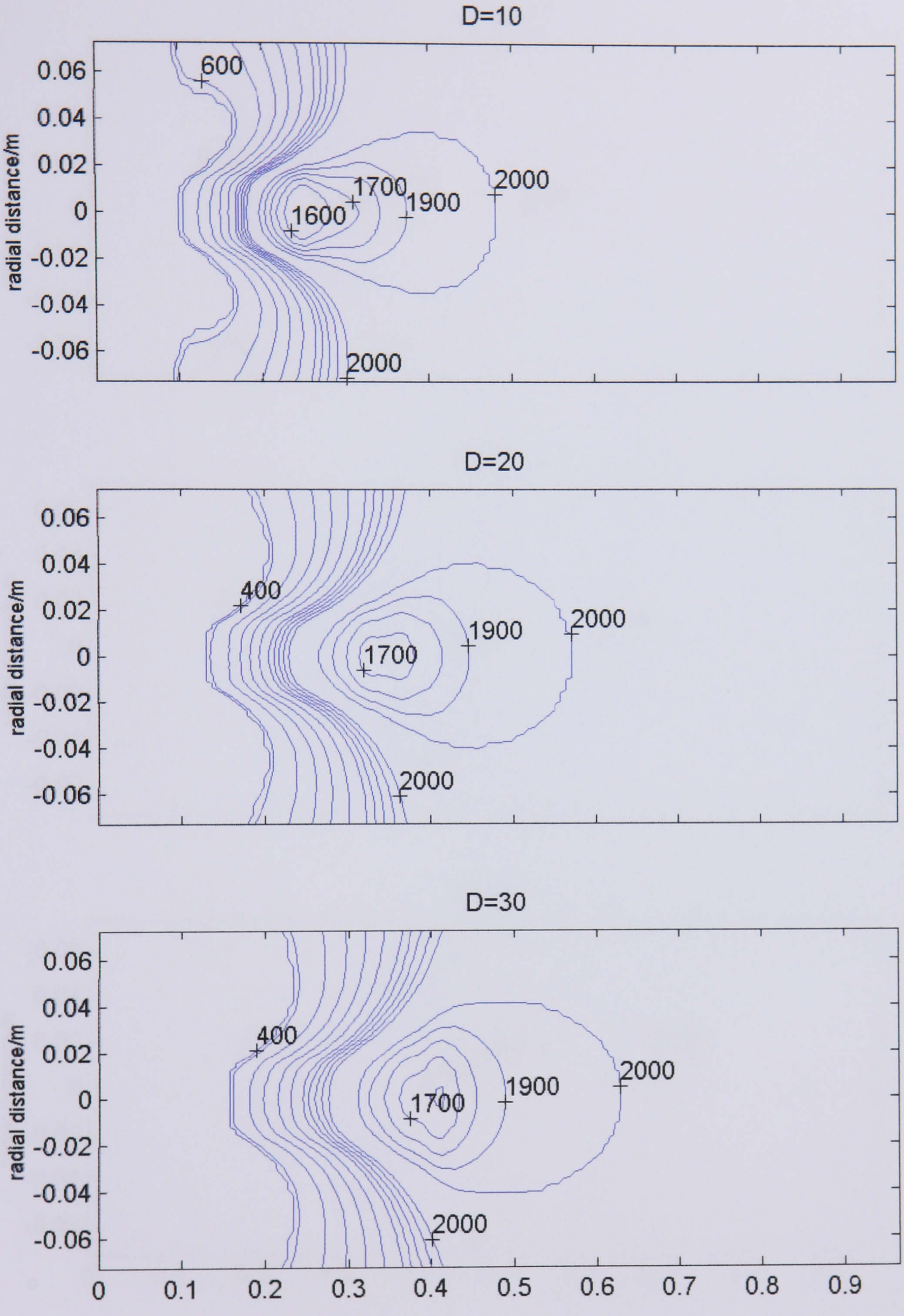

4. Effect of mean diameter variation on CO2 distribution

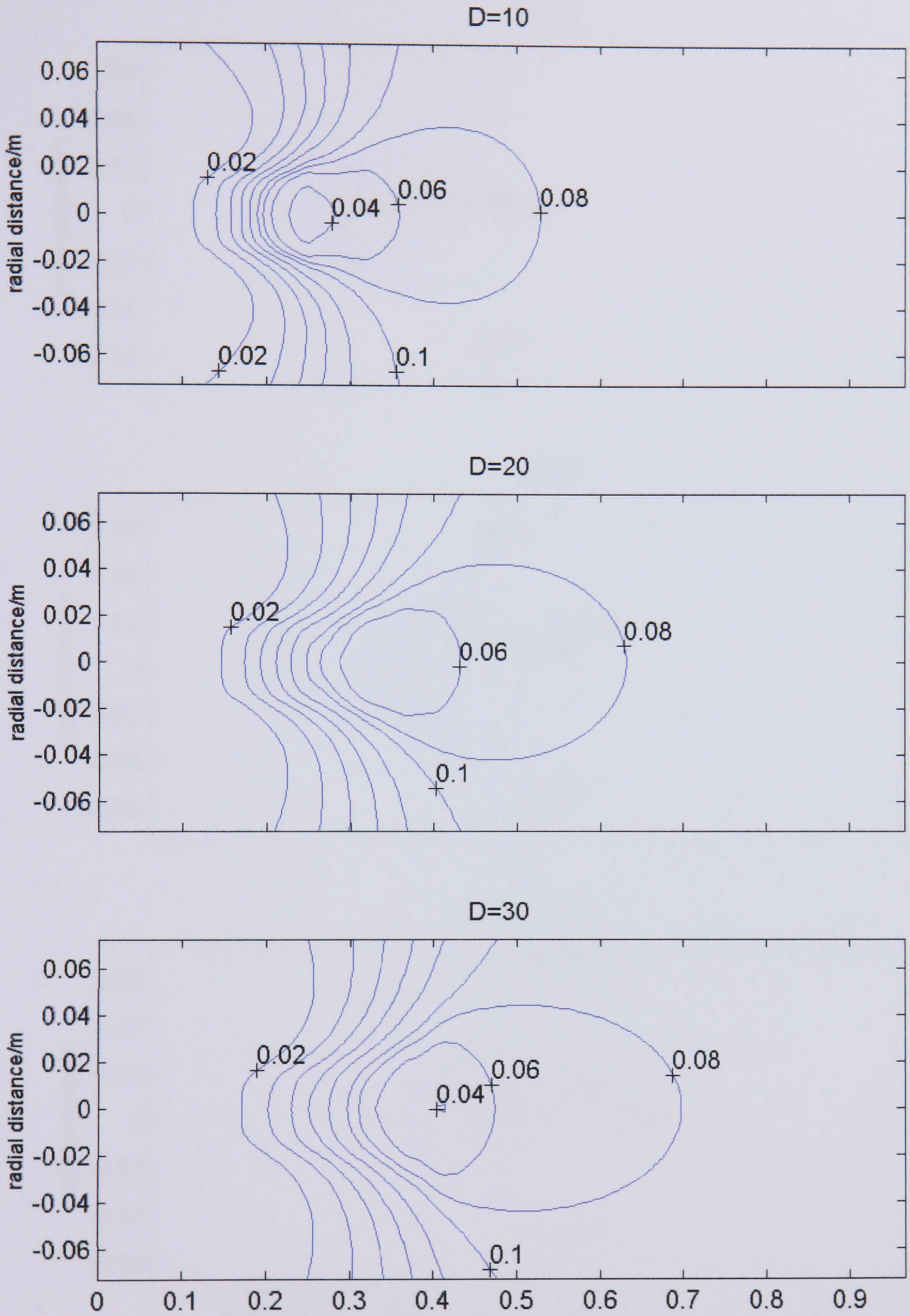

5. Effect of mean diameter variation on CO distribution

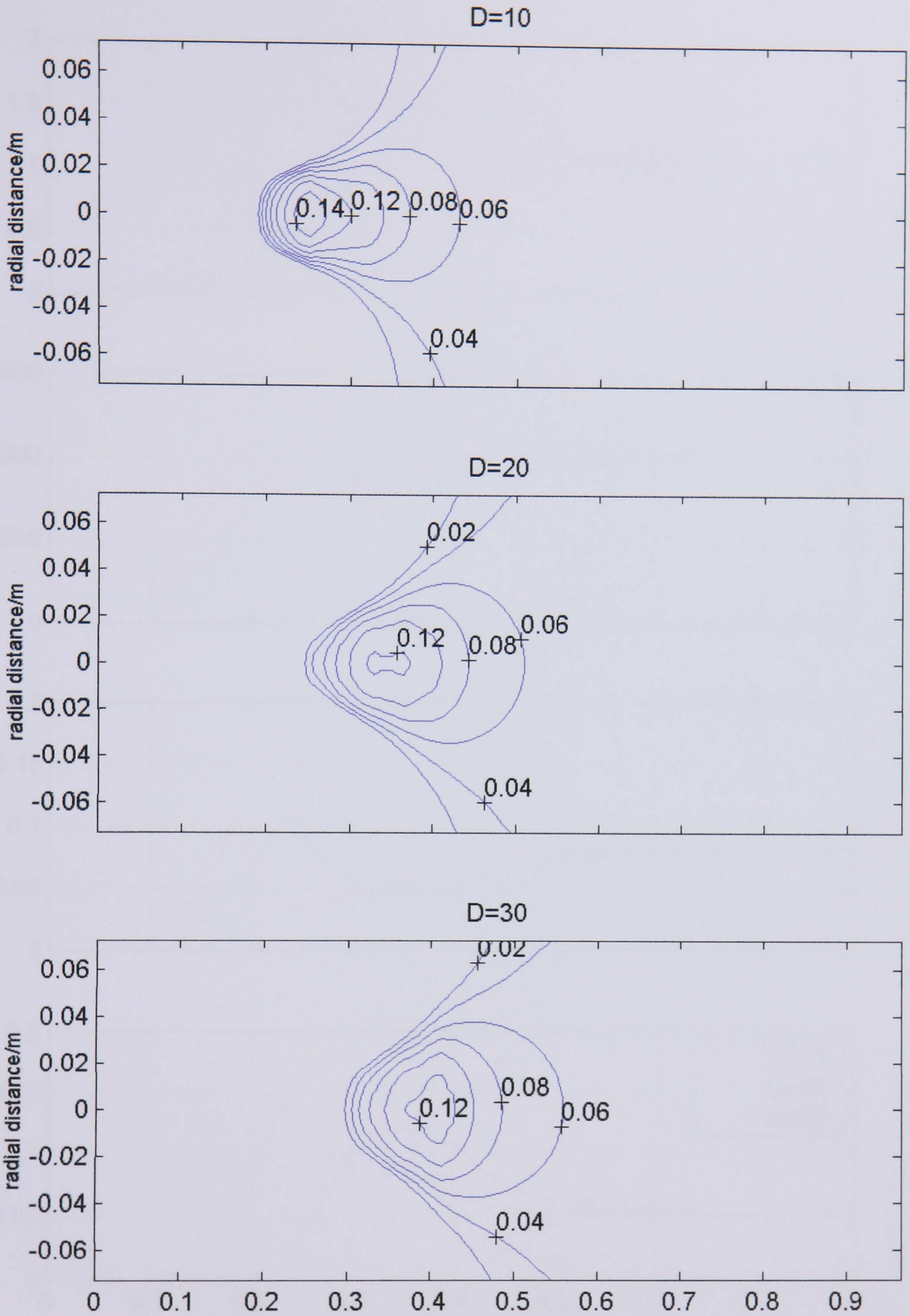

6. Axial variation of properties with change in mean diameter variation

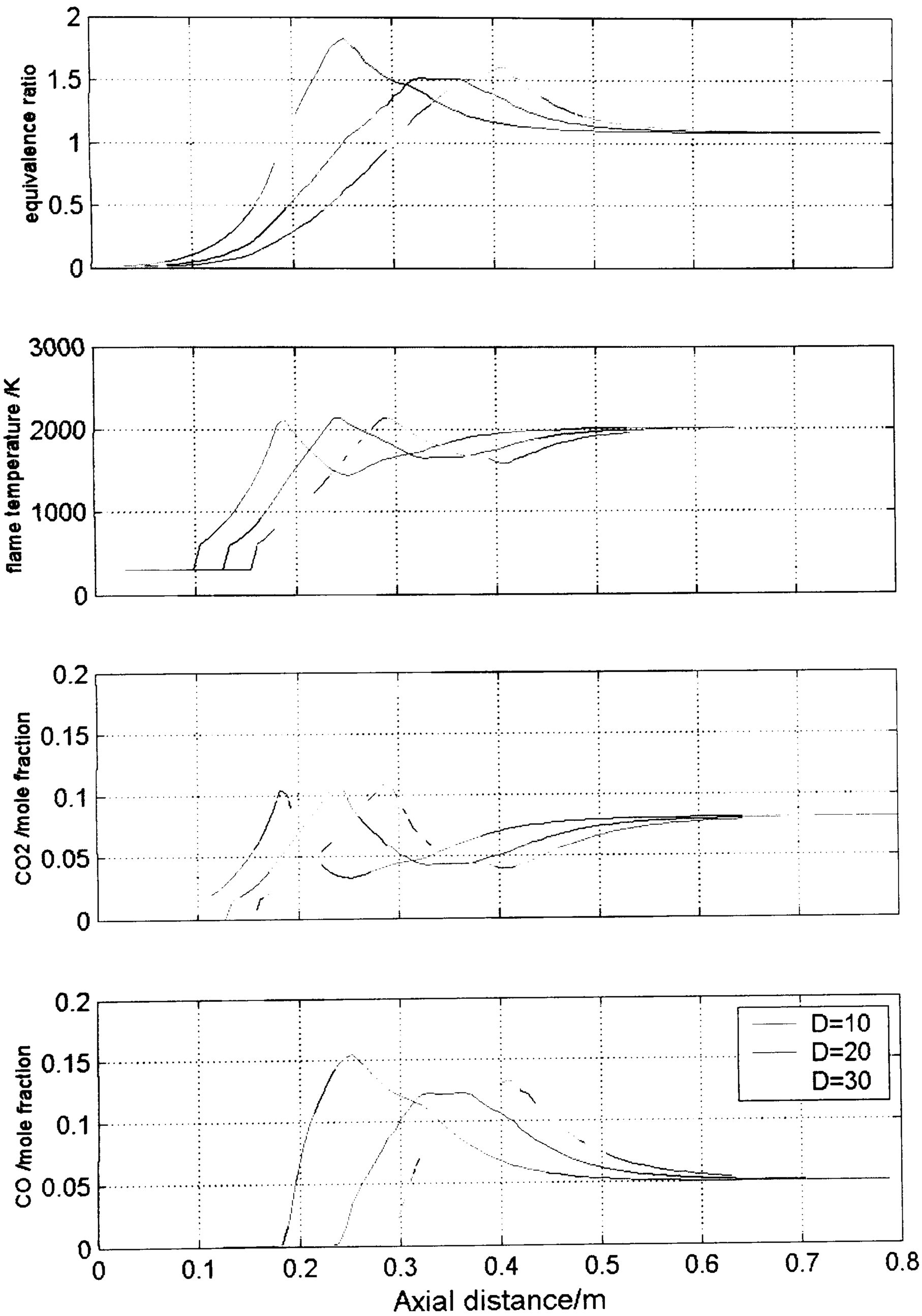

7. Radial variation of properties with change in mean diameter variation

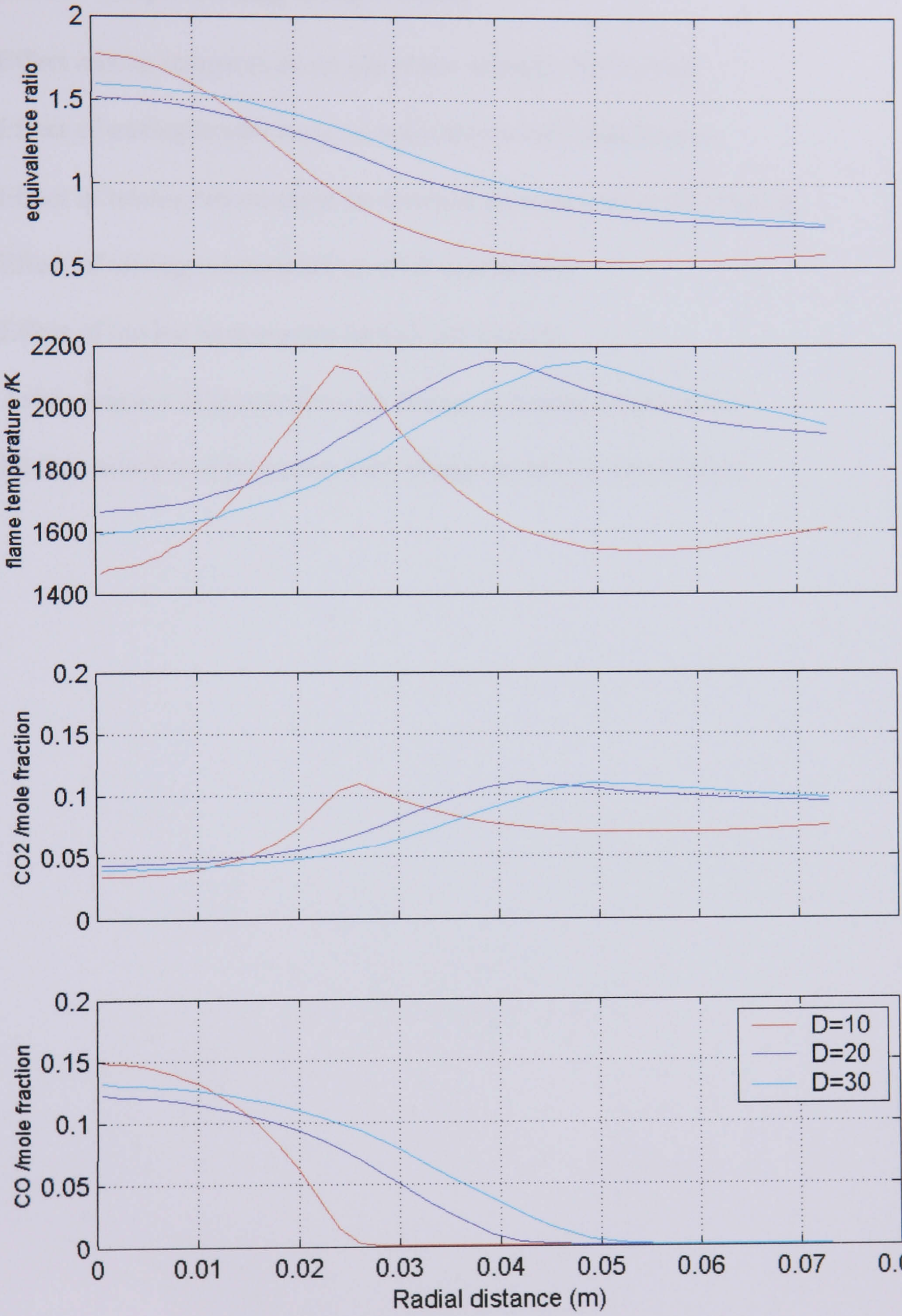

Appendix E

Parametric study: Mixing temperature

1. Effect mixing temperature on gas phase velocity distribution
2. Effect of mixing temperature on equivalence ratio distribution
3. Effect of mixing temperature on combustion temperature distribution
4. Effect of mixing temperature on CO2 distribution
5. Effect of mixing temperature on CO distribution
6. Axial variation of properties with change in mixing temperature
7. Radial variation of properties with change in mixing temperature

1. Effect mixing temperature on gas phase velocity distribution

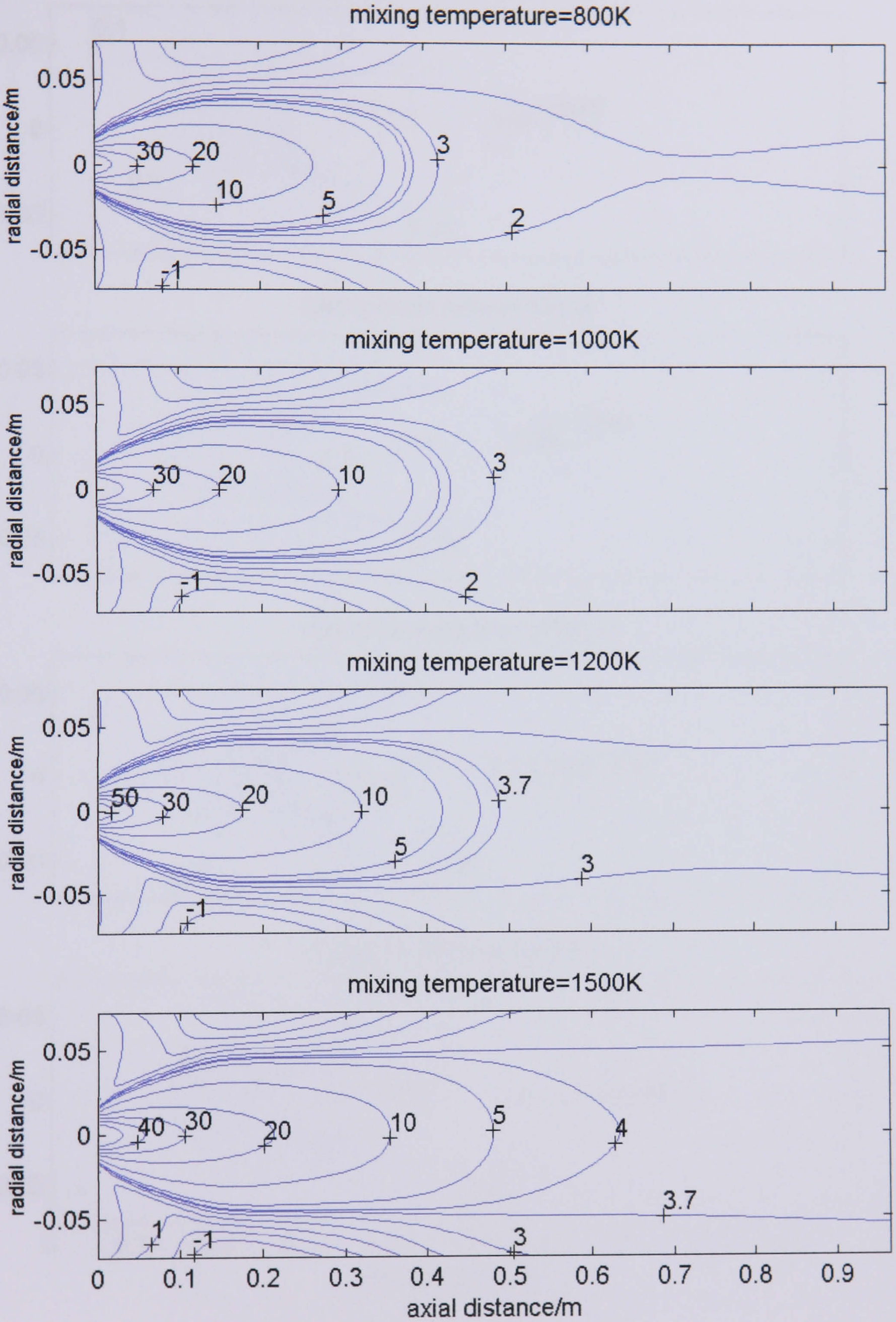

2. Effect of mixing temperature on equivalence ratio distribution

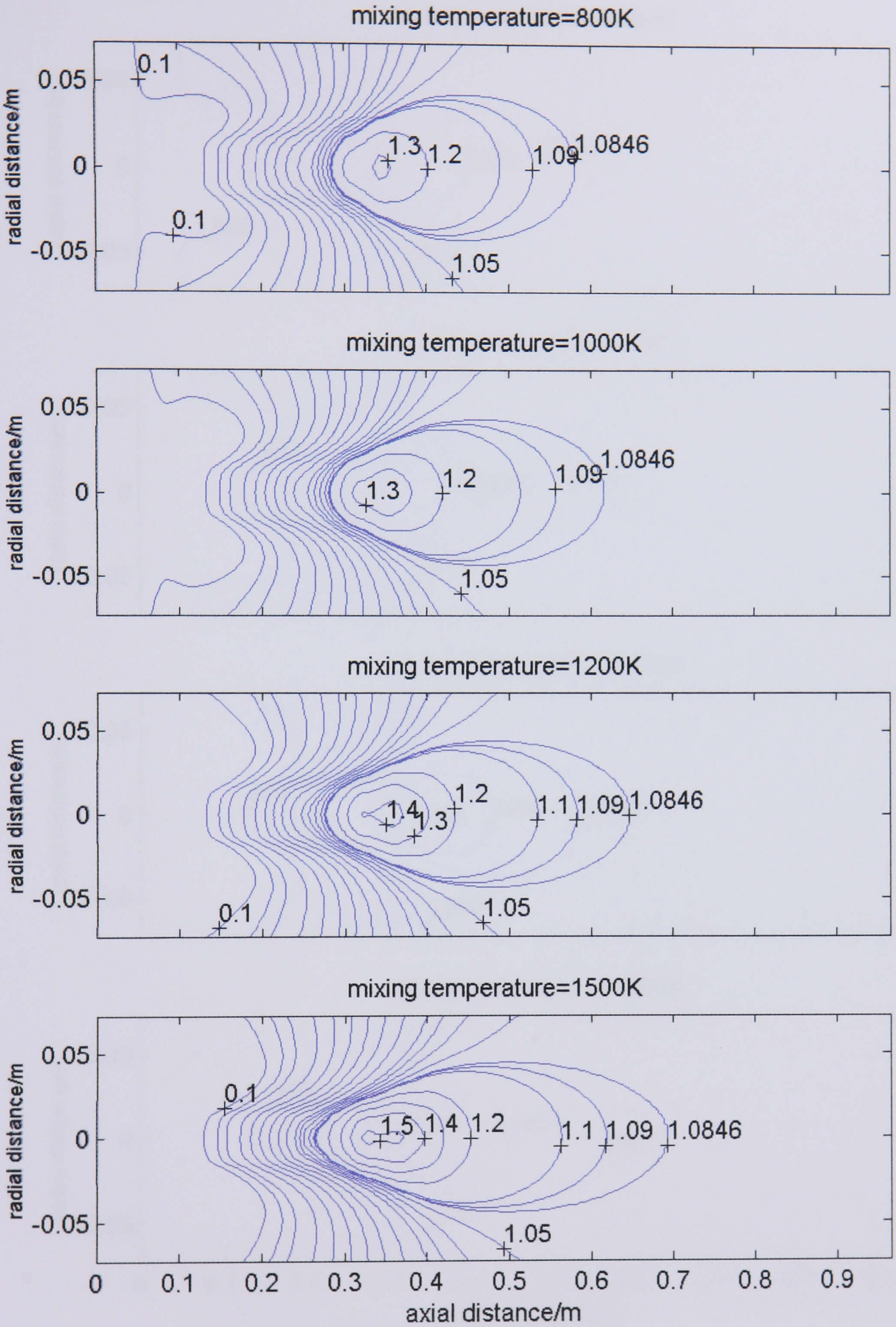

3. Effect of mixing temperature on combustion temperature distribution

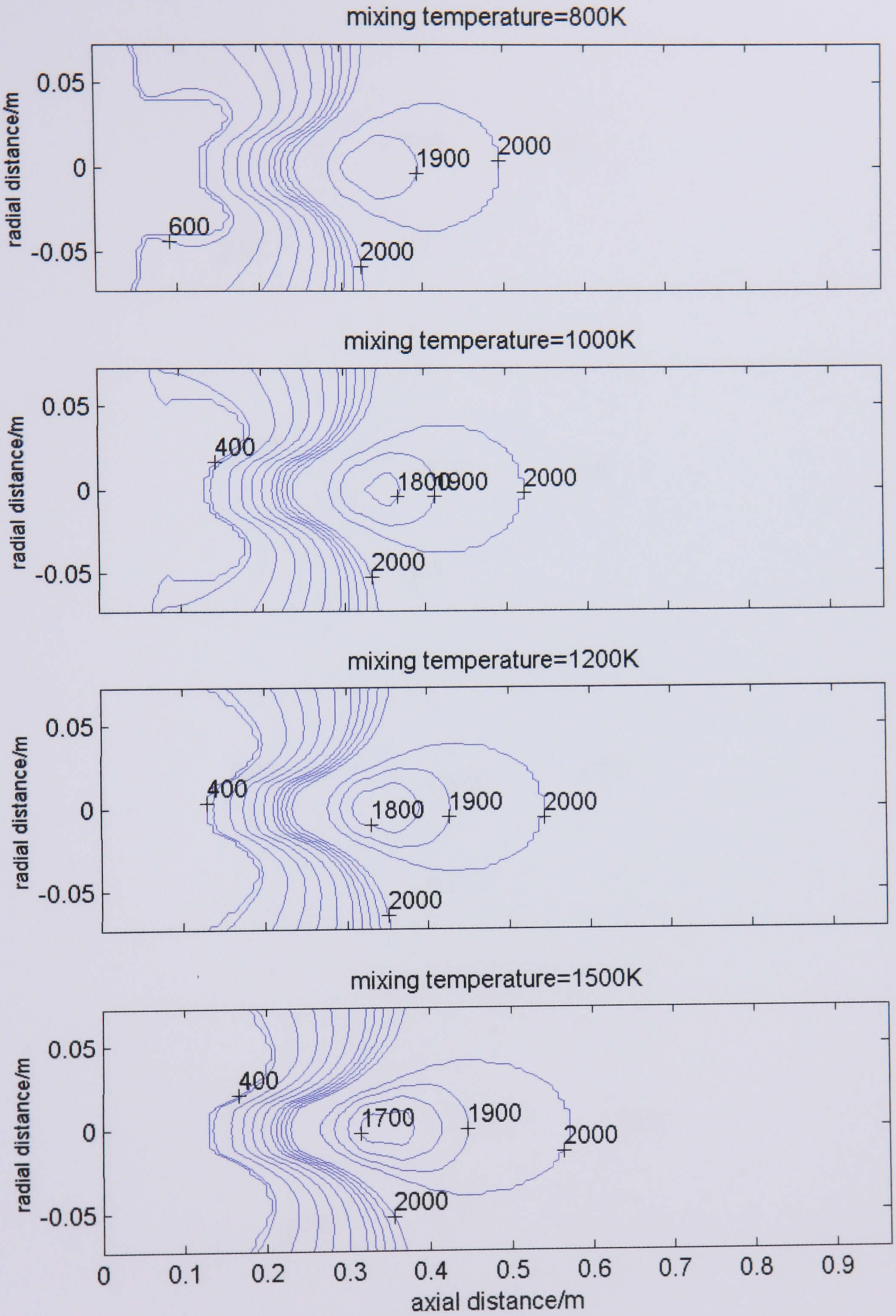

4. Effect of mixing temperature on CO2 distribution

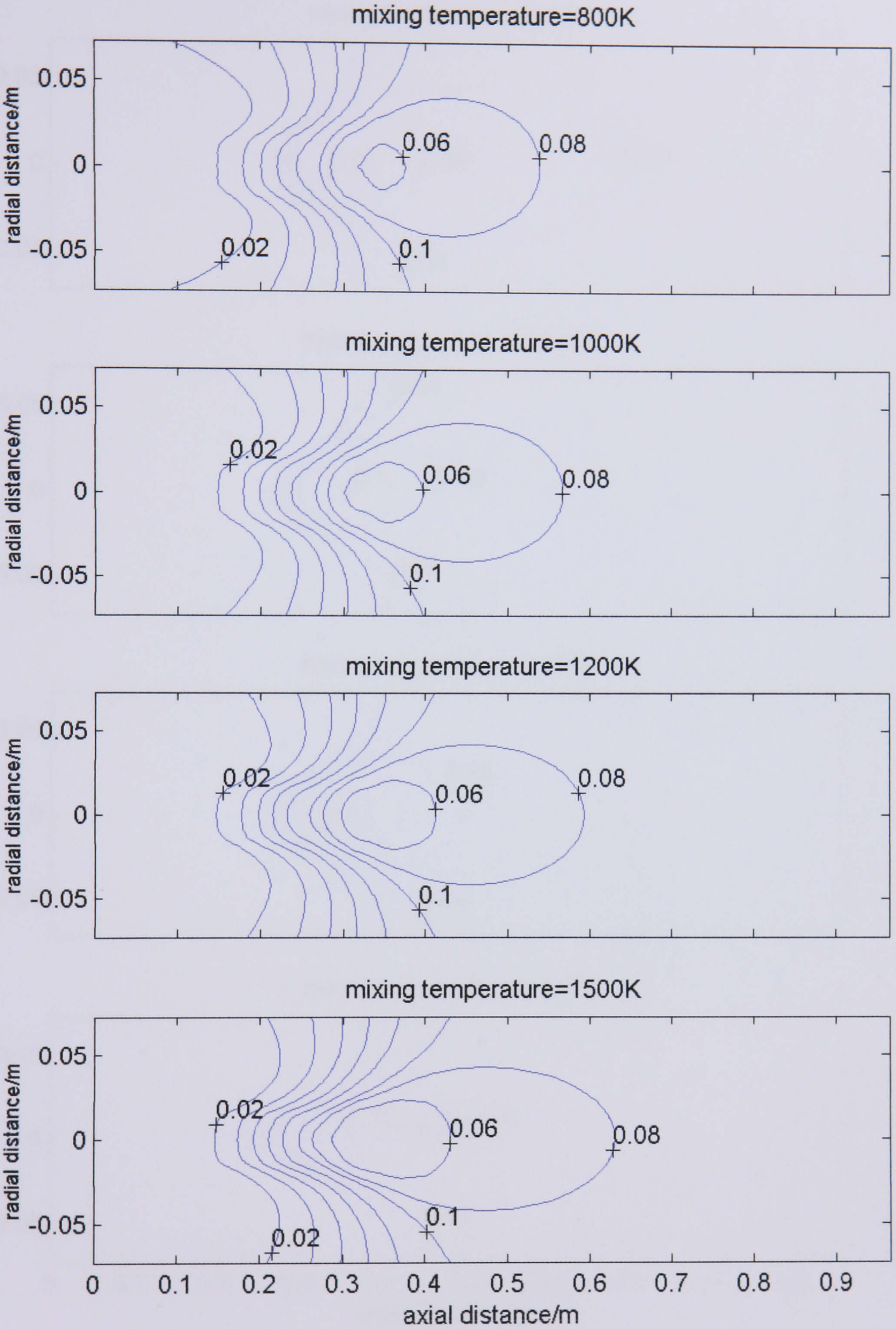

5. Effect of mixing temperature on CO distribution

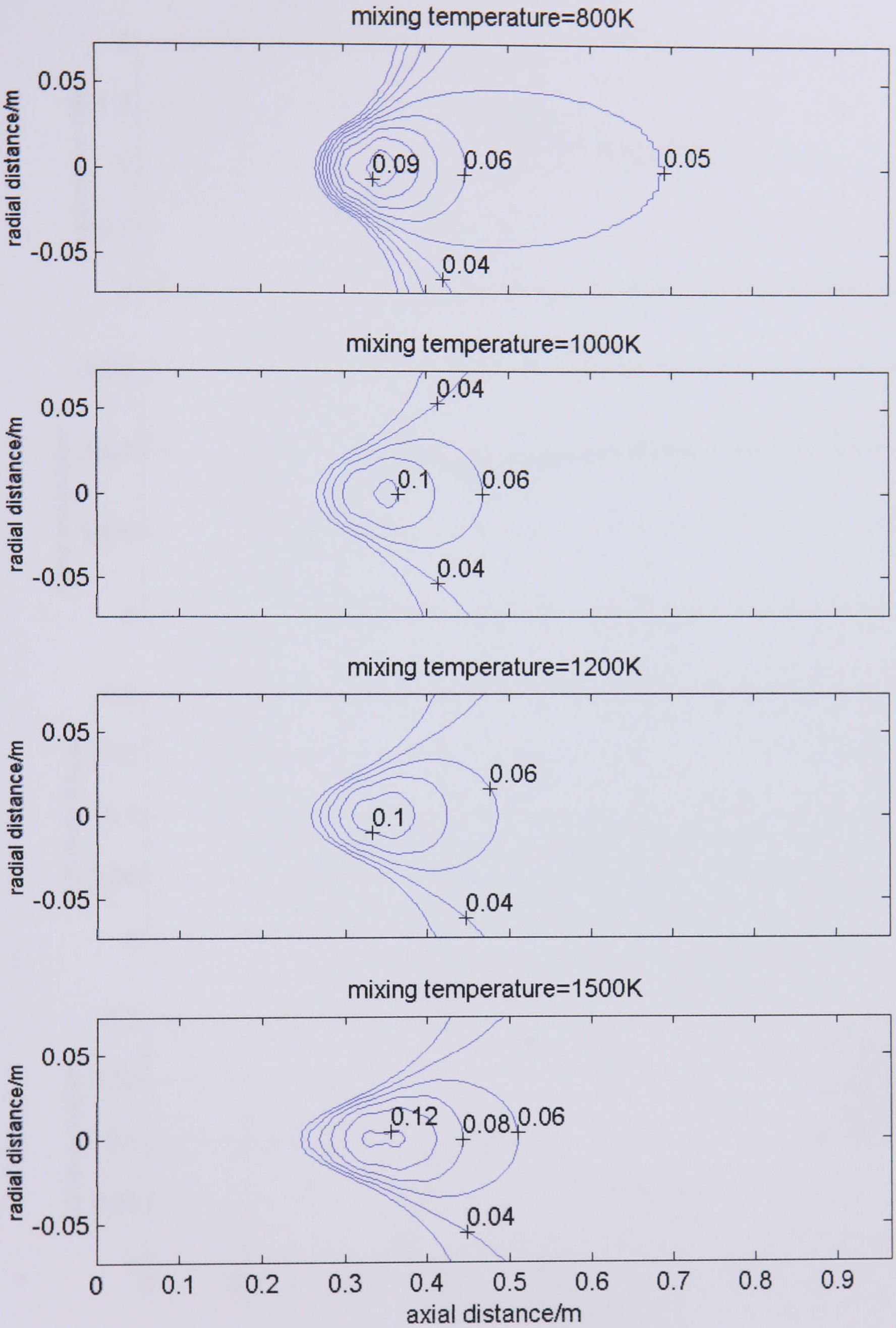

6. Axial variation of properties with change in mixing temperature

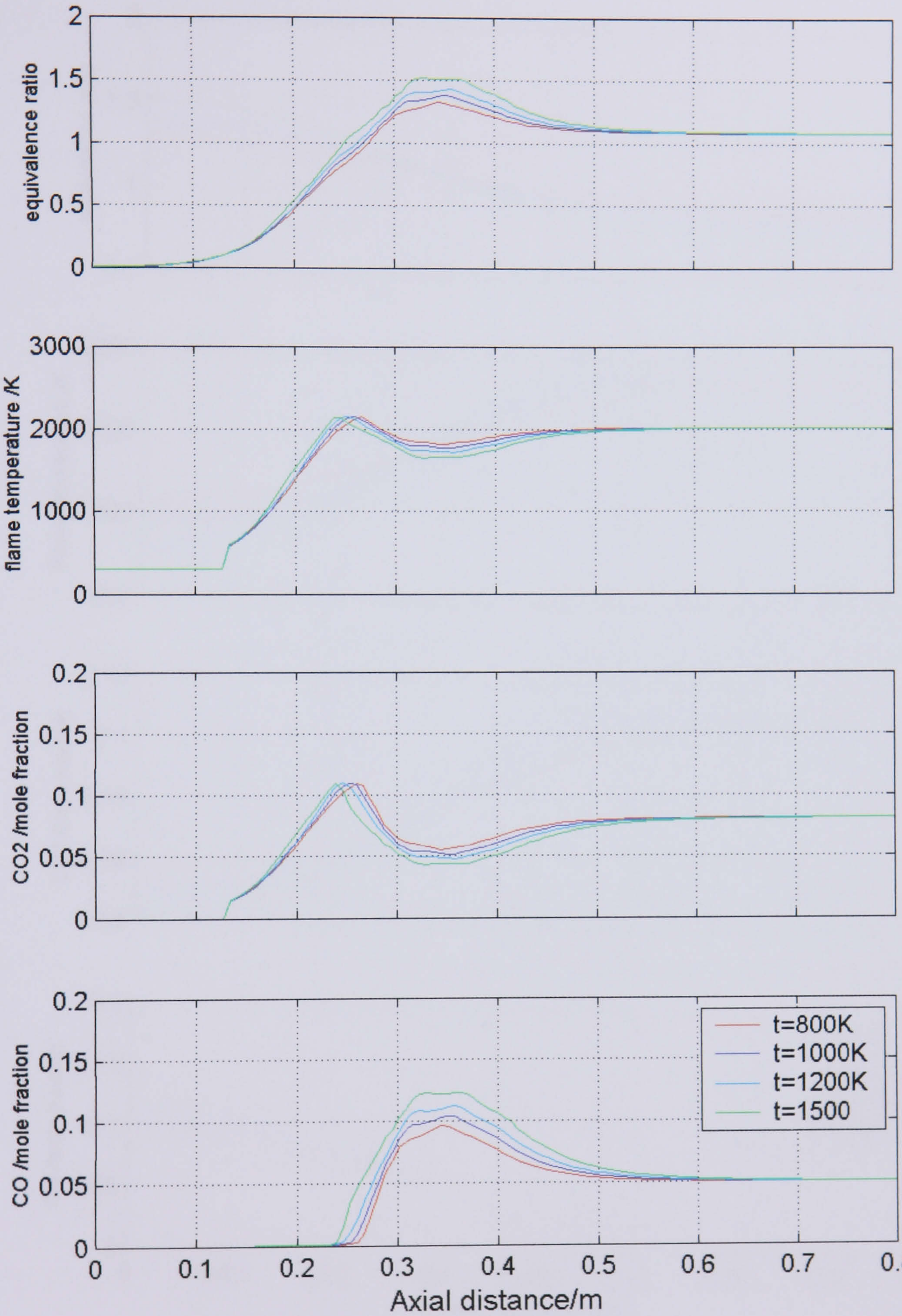

7. Radial variation of properties with change in mixing temperature

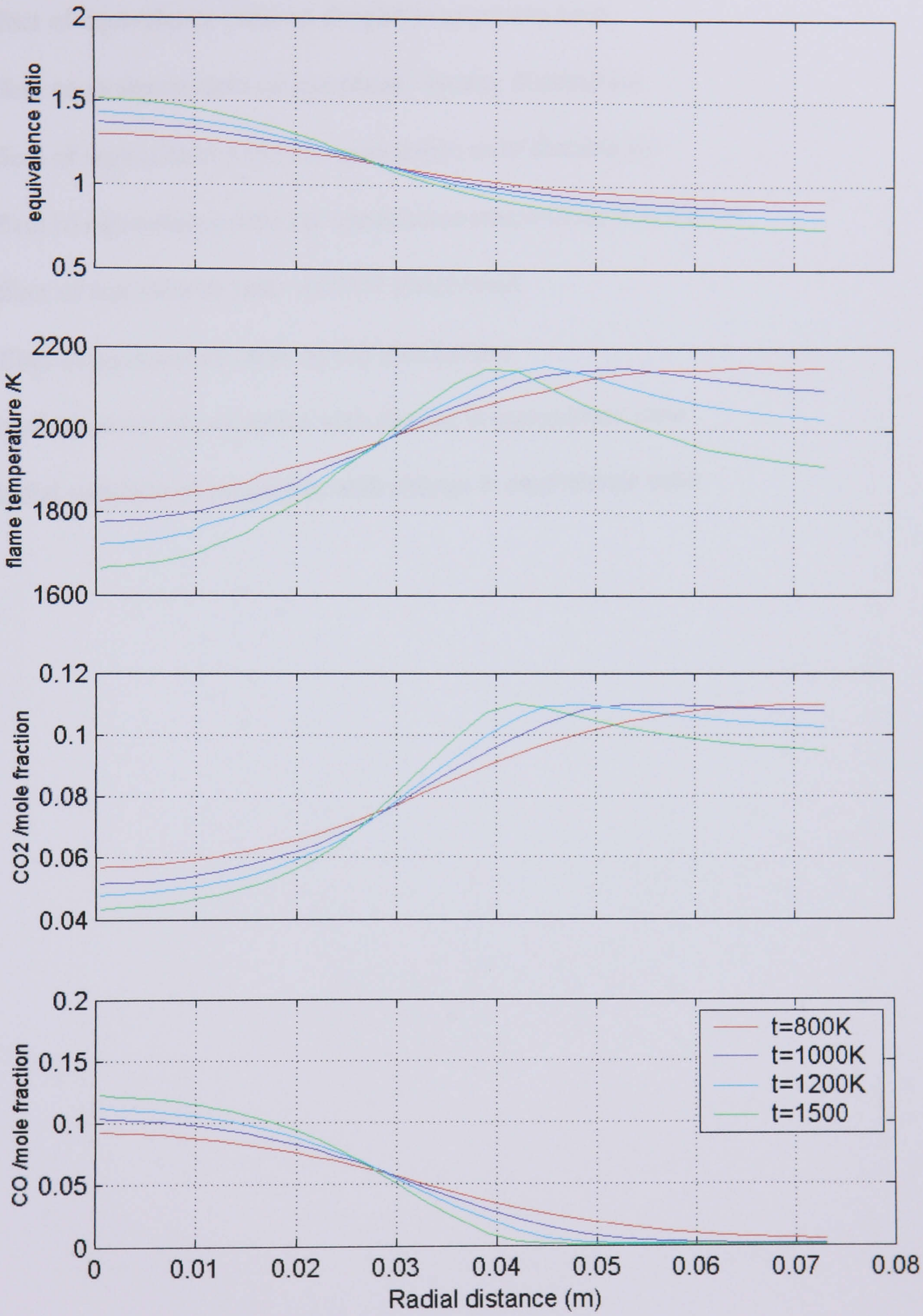

Appendix F

Parametric study: Equivalence ratio

1. Effect of equivalence ratio on droplet evaporation time
2. Effect equivalence ratio on gas phase velocity distribution
3. Effect of equivalence ratio on equivalence ratio distribution
4. Effect of equivalence ratio on combustion temperature distribution
5. Effect of equivalence ratio on CO2 distribution
6. Effect of equivalence ratio on CO distribution
7. Axial variation of properties with change in equivalence ratio
8. Radial variation of properties with change in equivalence ratio

1. Effect of equivalence ratio on droplet evaporation time

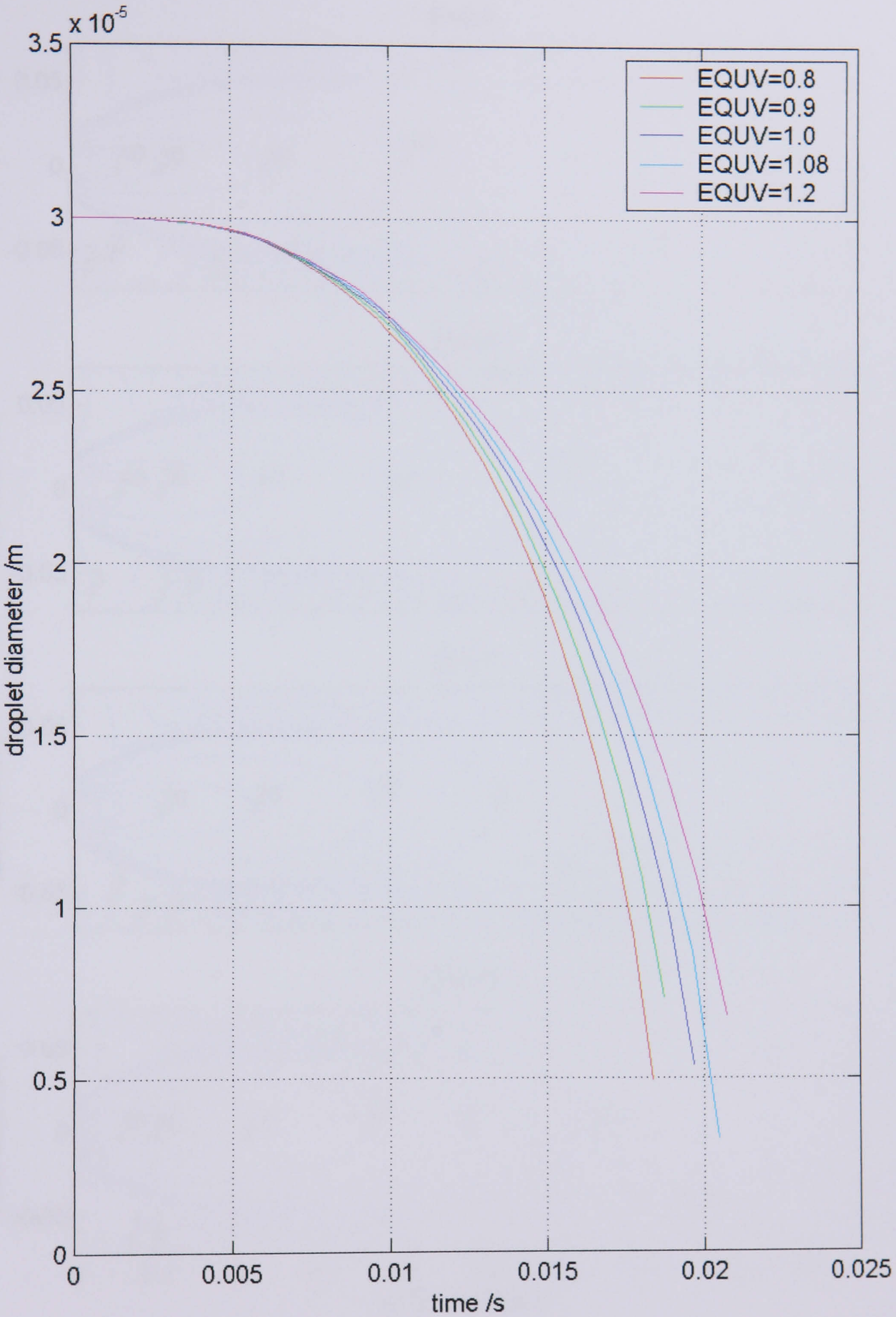

F 1

2. Effect equivalence ratio on gas phase velocity distribution

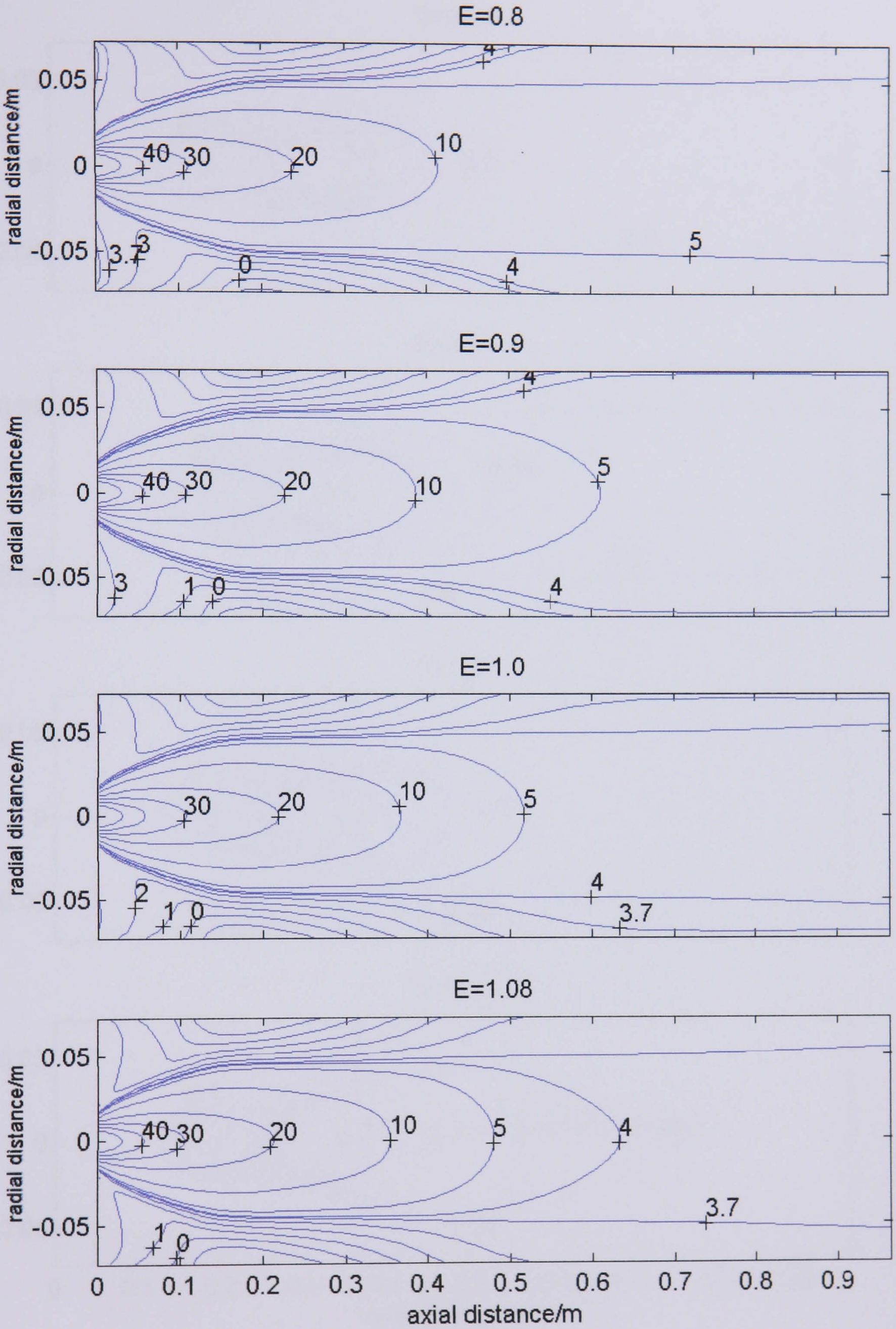

3. Effect of equivalence ratio on equivalence ratio distribution

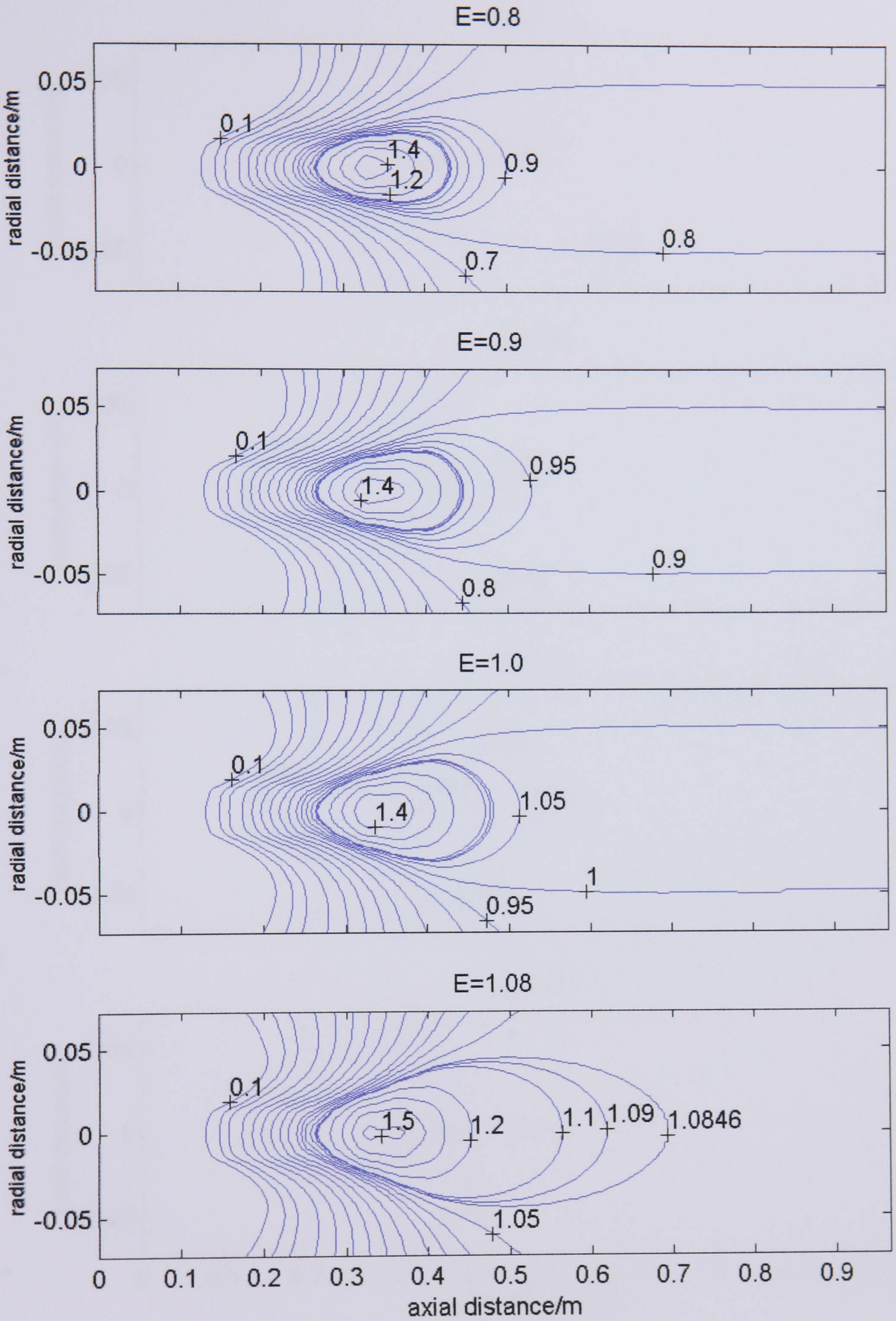

4. Effect of equivalence ratio on combustion temperature distribution

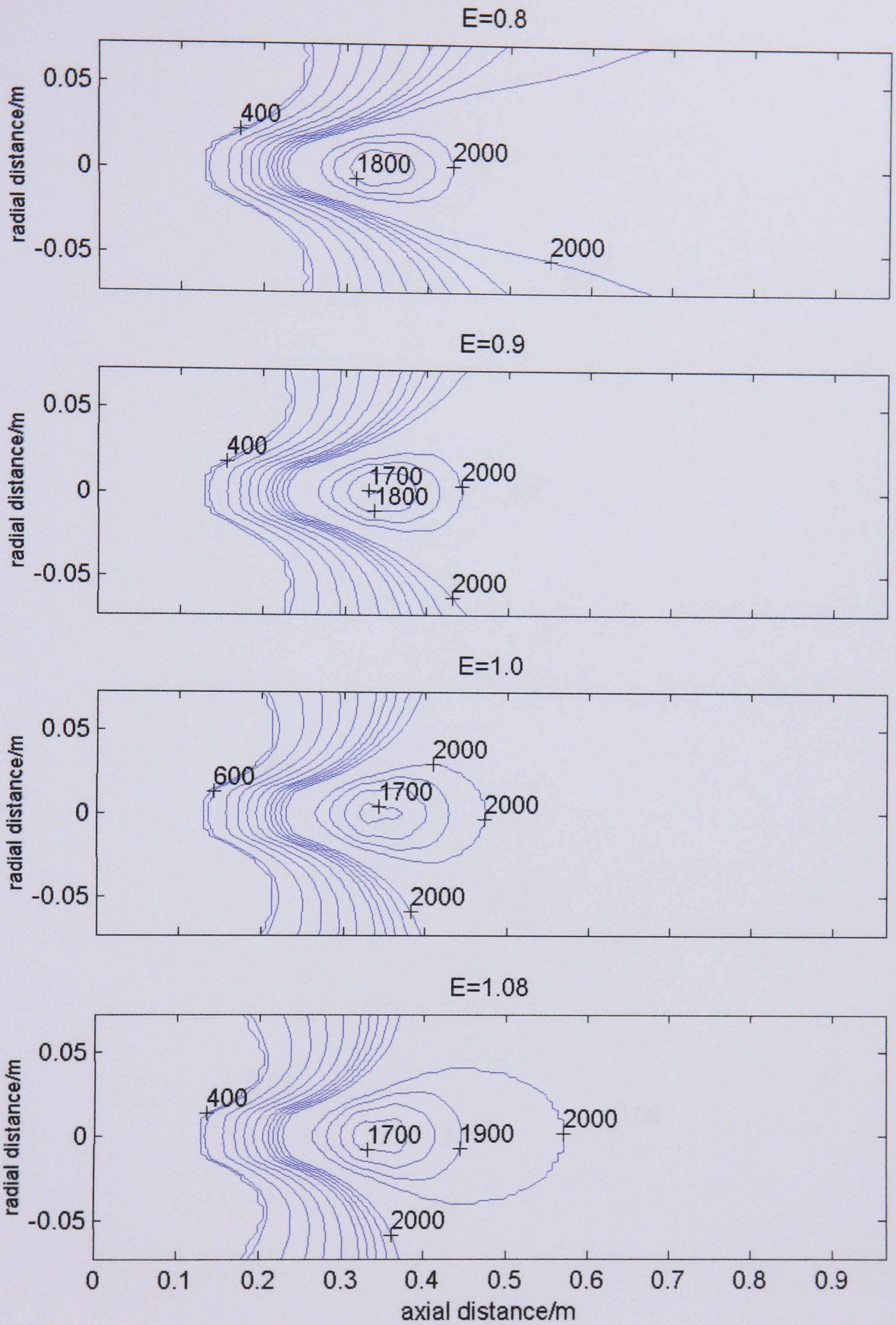

5. Effect of equivalence ratio on CO2 distribution

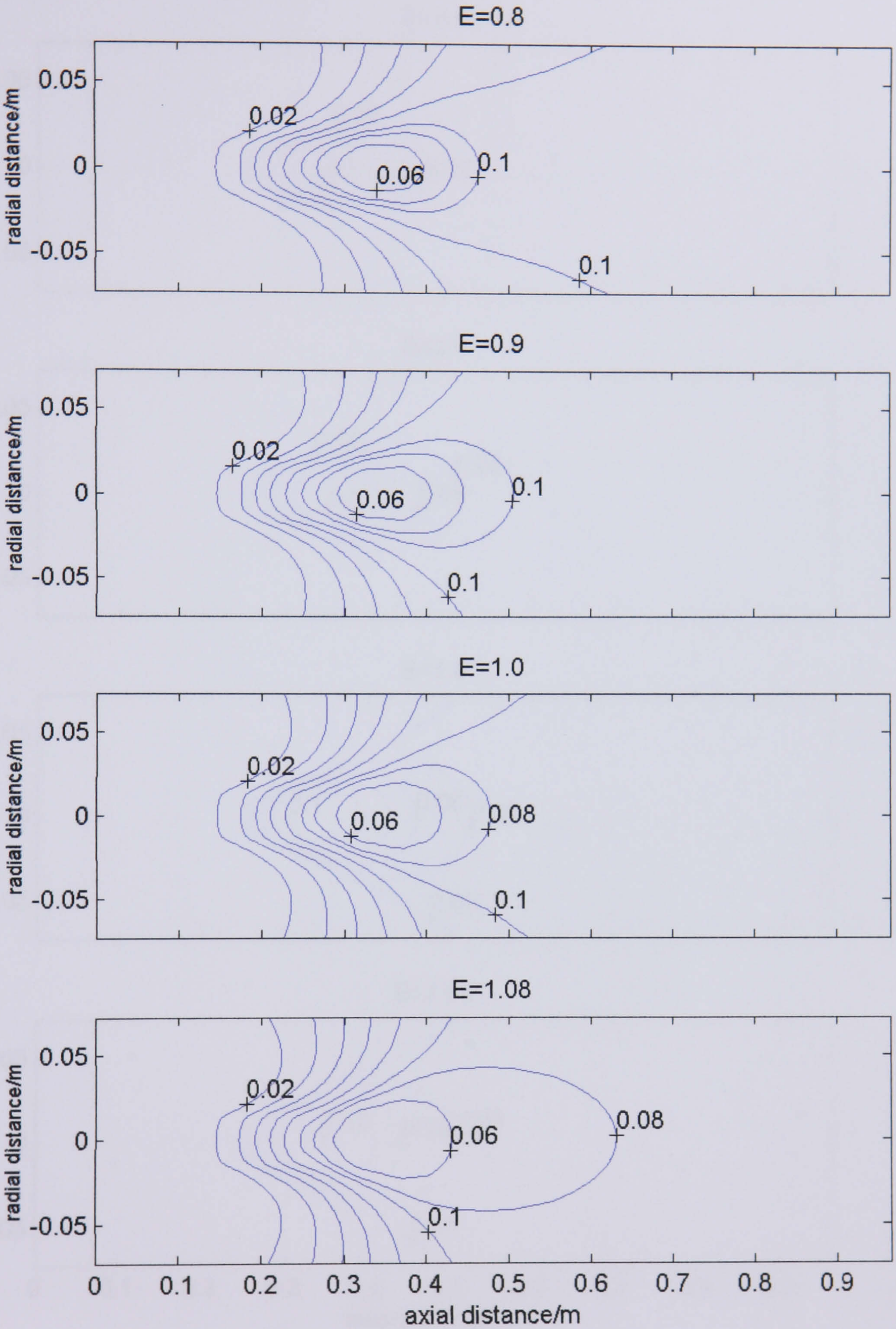

6. Effect of equivalence ratio on CO distribution

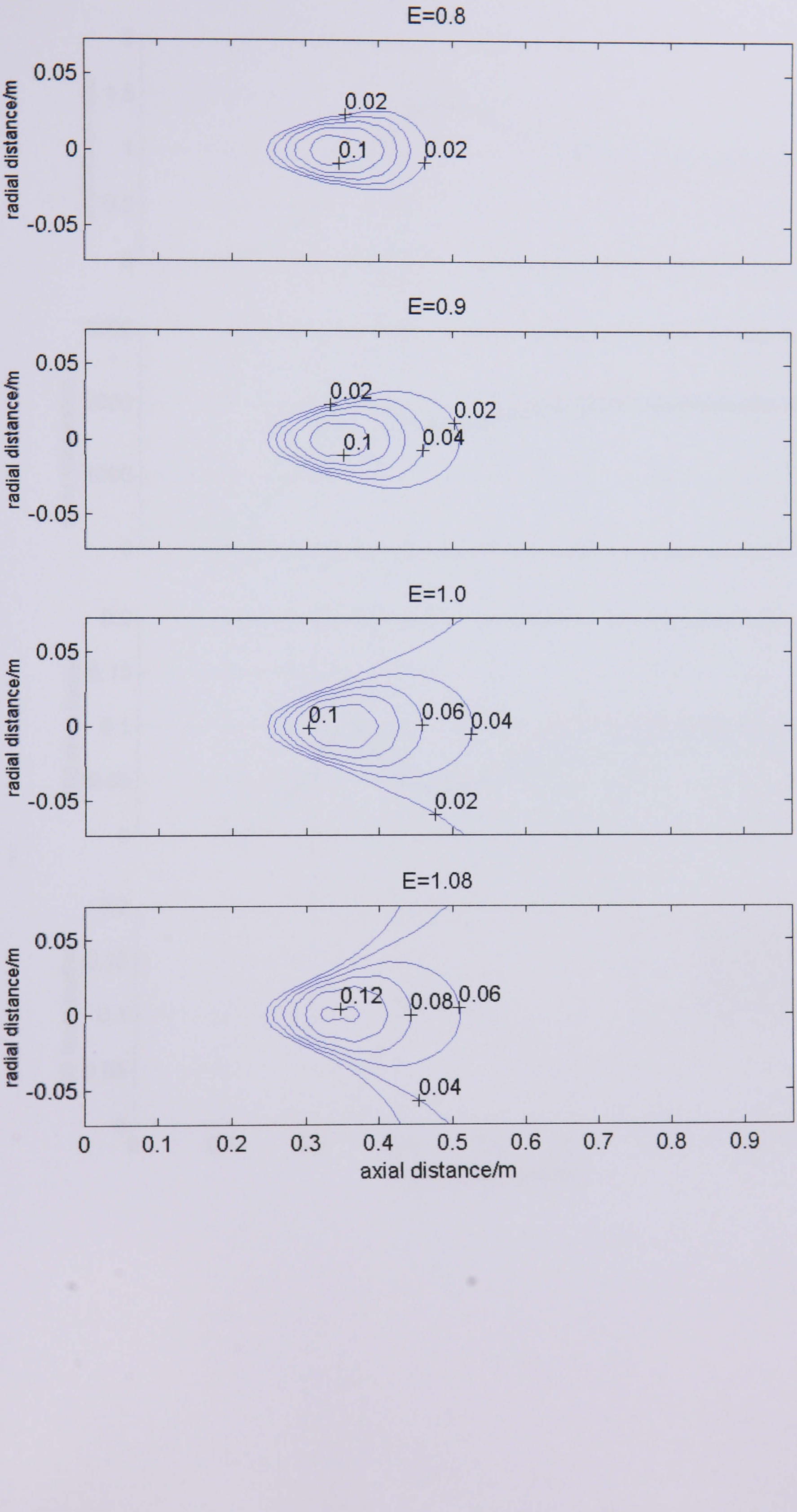

7. Axial variation of properties with change in equivalence ratio

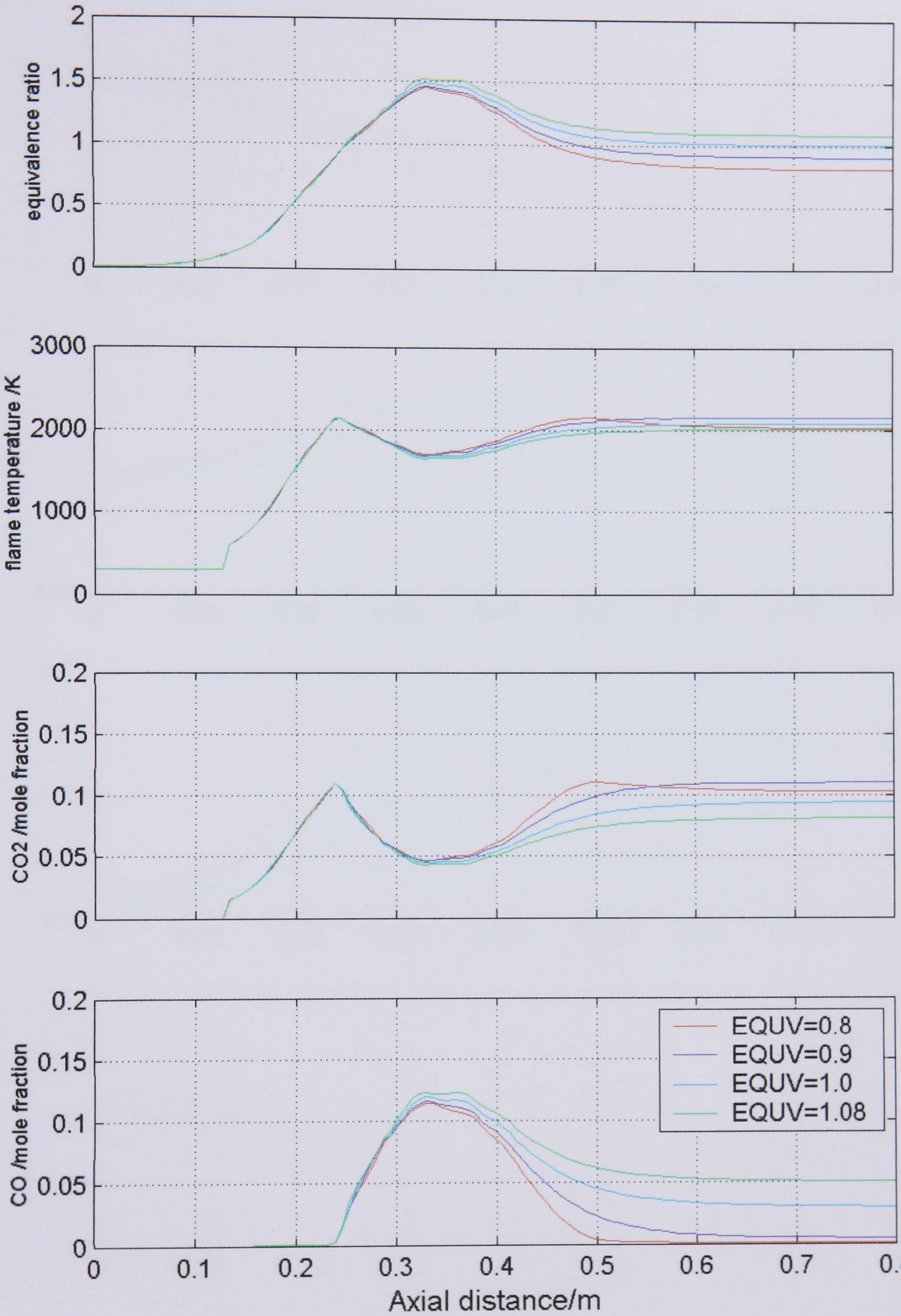

8. Radial variation of properties with change in equivalence ratio

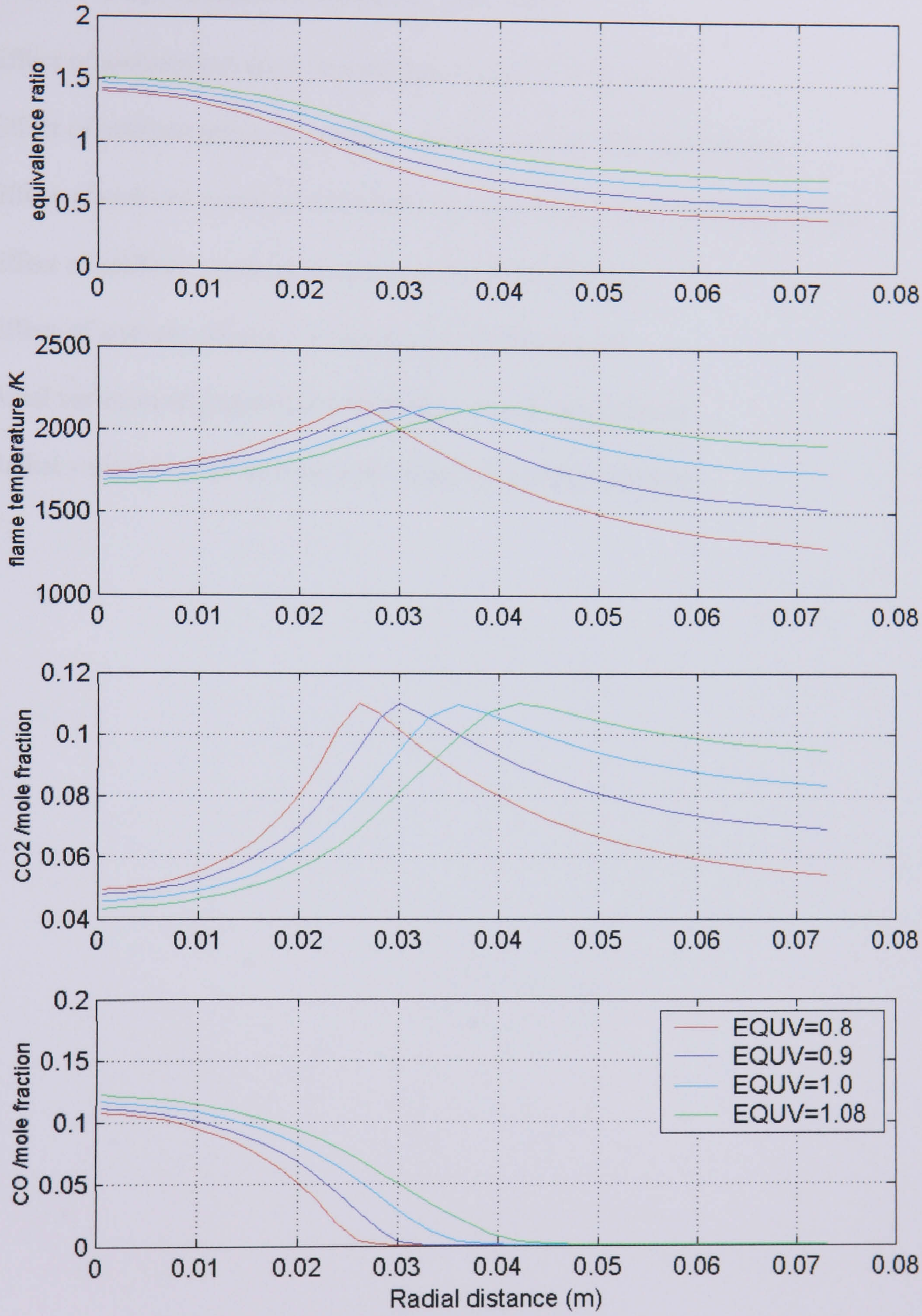

Appendix G

Parametric study: Effect of Ambient pressure

1. Effect of ambient pressure on gas phase velocity distribution
2. Effect of ambient pressure variation on equivalence ratio distribution
3. Effect of ambient pressure variation on combustion temperature distribution
4. Effect of ambient pressure variation on CO2 distribution
5. Effect of ambient pressure variation on CO distribution
6. Axial variation of properties with change in ambient pressure
7. Radial variation of properties with change in ambient pressure

1. Effect of ambient pressure on gas phase velocity distribution

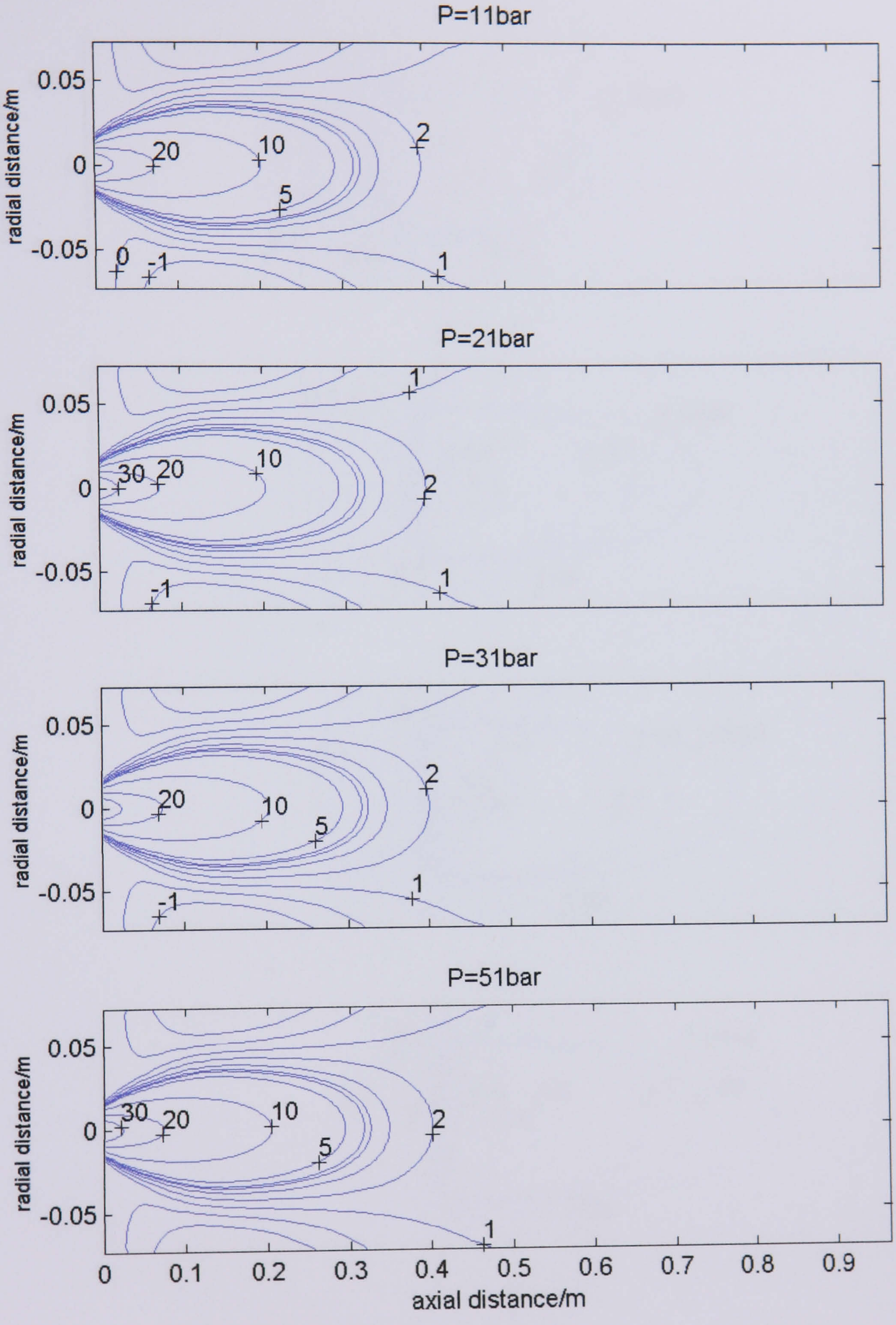

2. Effect of ambient pressure variation on equivalence ratio distribution

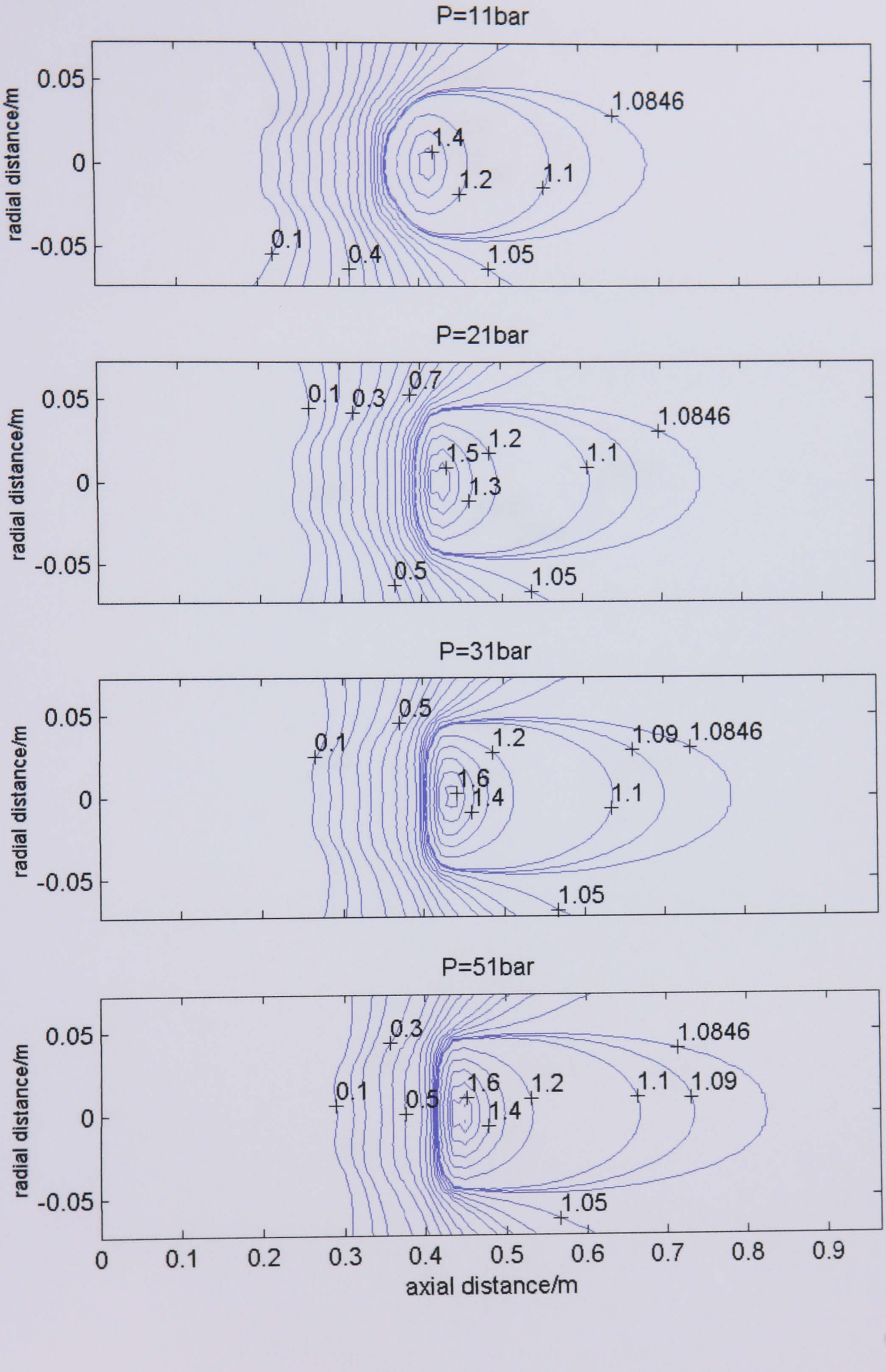

3. Effect of ambient pressure variation on combustion temperature distribution

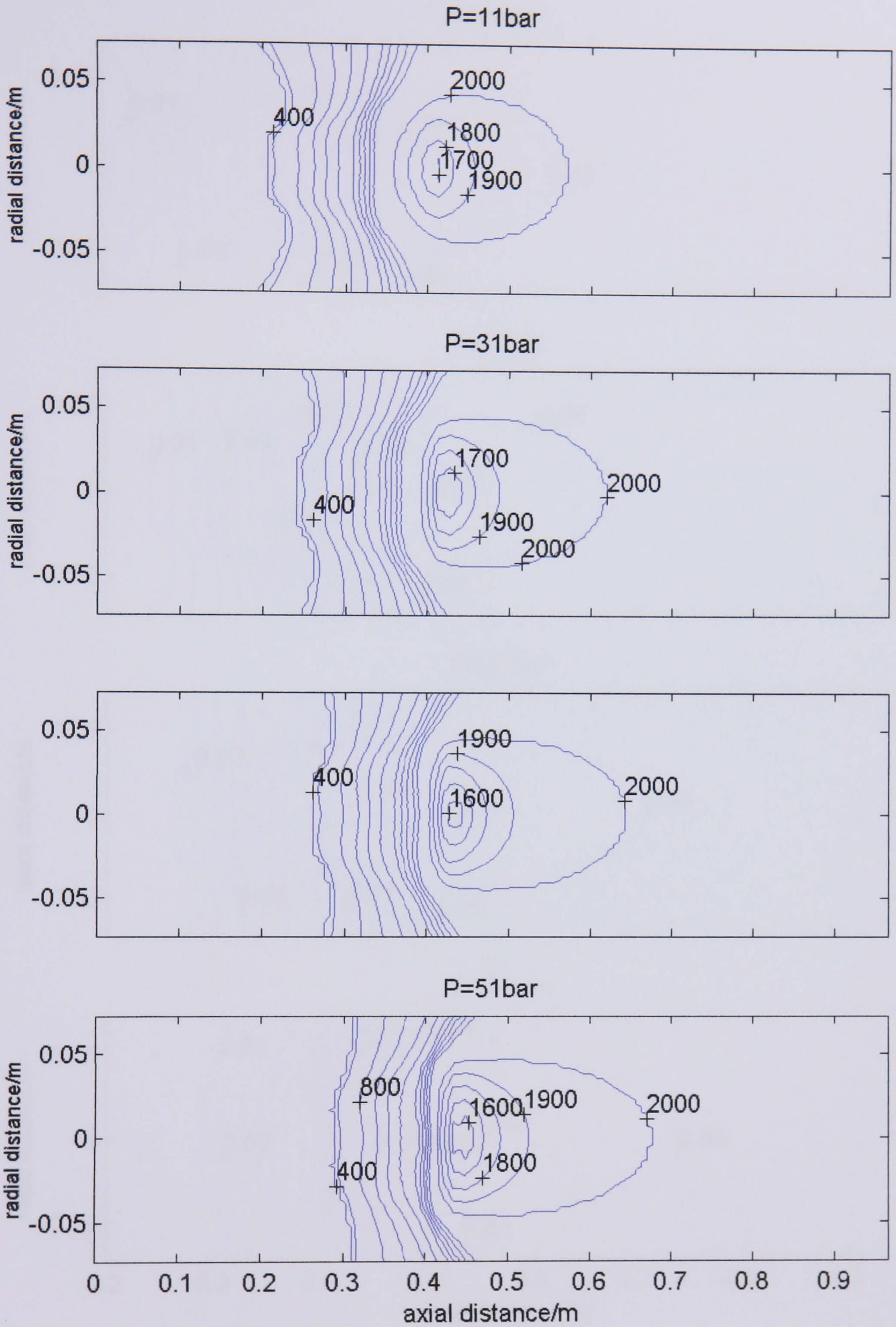

4. Effect of ambient pressure variation on CO2 distribution

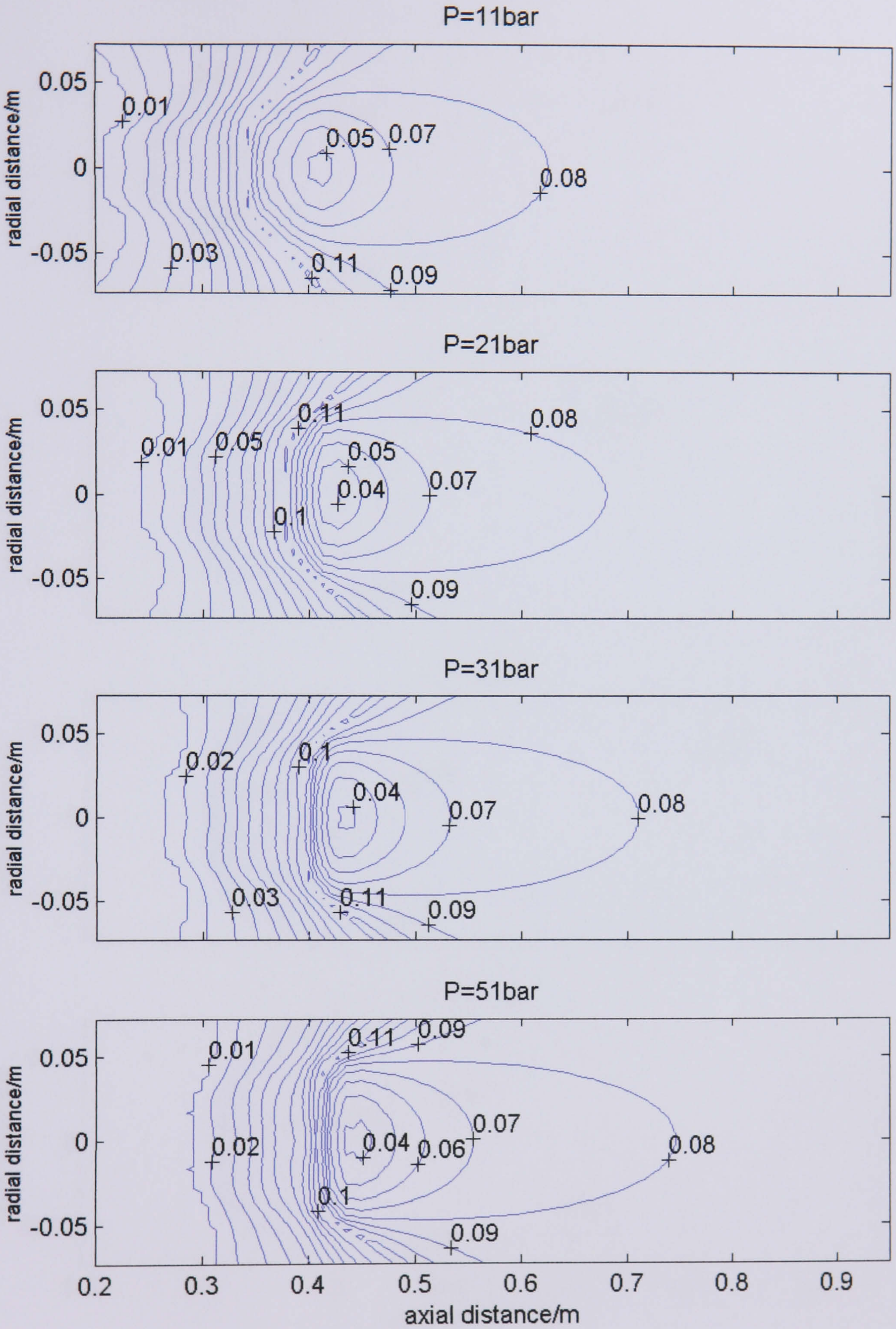

5. Effect of ambient pressure variation on CO distribution

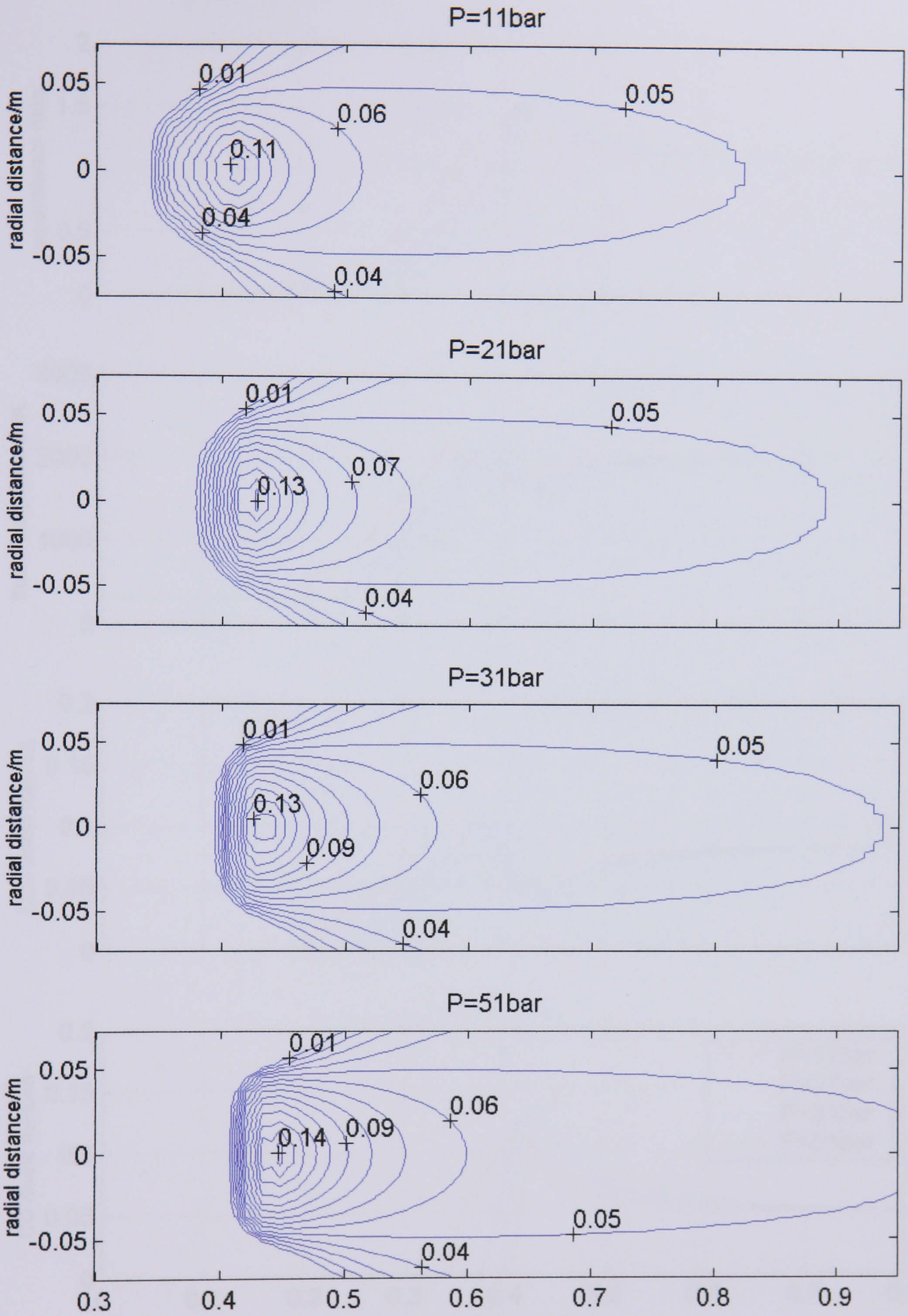

6. Axial variation of properties with change in ambient pressure

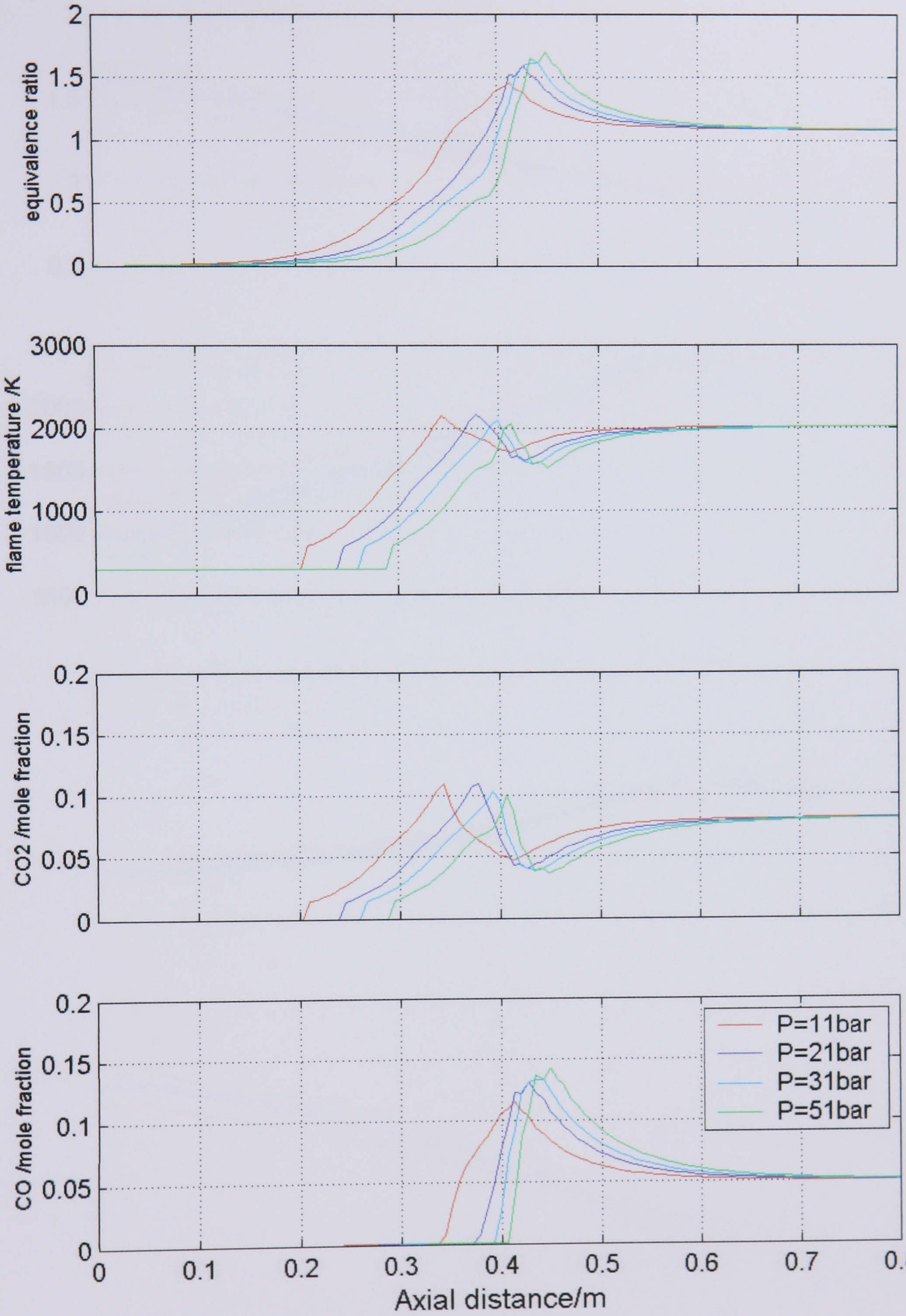

7. Radial variation of properties with change in ambient pressure

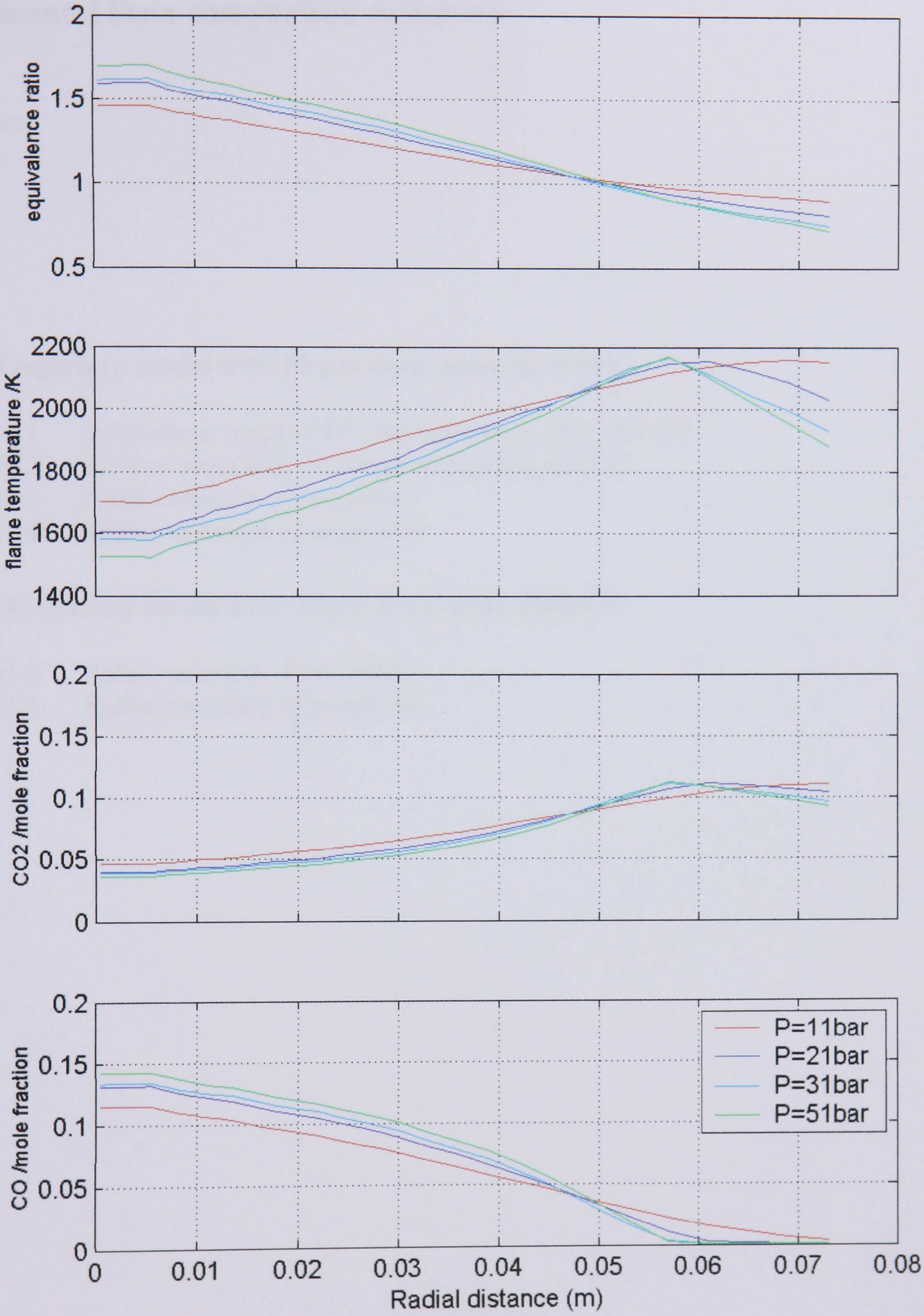

Appendix H

Experimental Data comparison Adiabatic

Parameters
P=6.5bar
E=1.08

- **Trajectory model with 20 μm drop mean diameter**

H-1 Iso-contour maps of E[1], Temeperature, CO_2 and CO
H-2 Surface plots of E, Temeperature, CO_2 and CO
H-3 Axial variation of properties
H-4 Radial variation of properties

- **Trajectory model with 30 μm drop mean diameter**

H-5 Axial variation of properties
H-6 Radial variation of properties

[1] Equivalence ratio

1. Iso-contour maps of E, Temeperature, CO_2 and CO

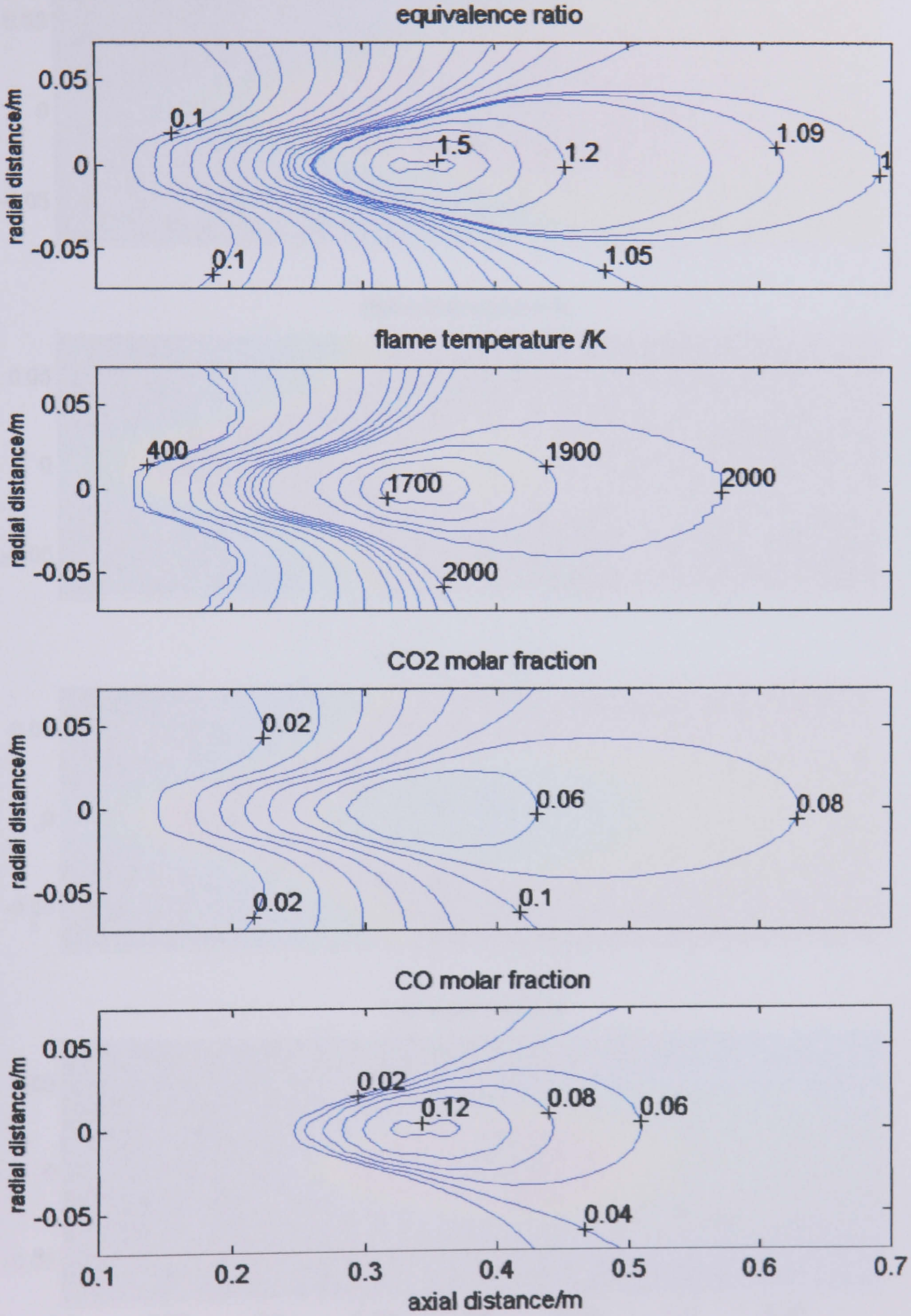

2 Surface plots of E, Temeperature, CO_2 and CO

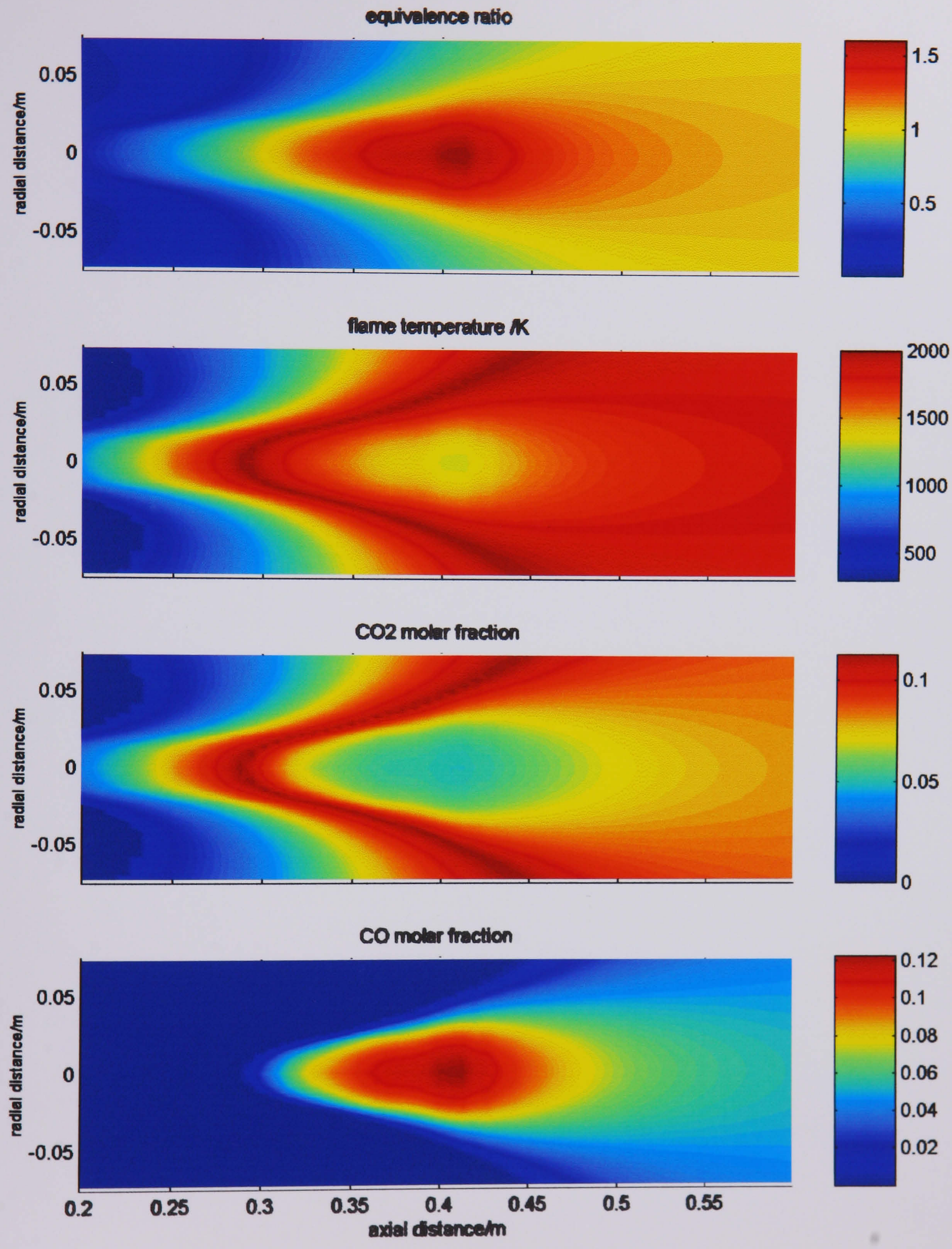

H2

3. Trajectory model with 20 μm drop mean diameter

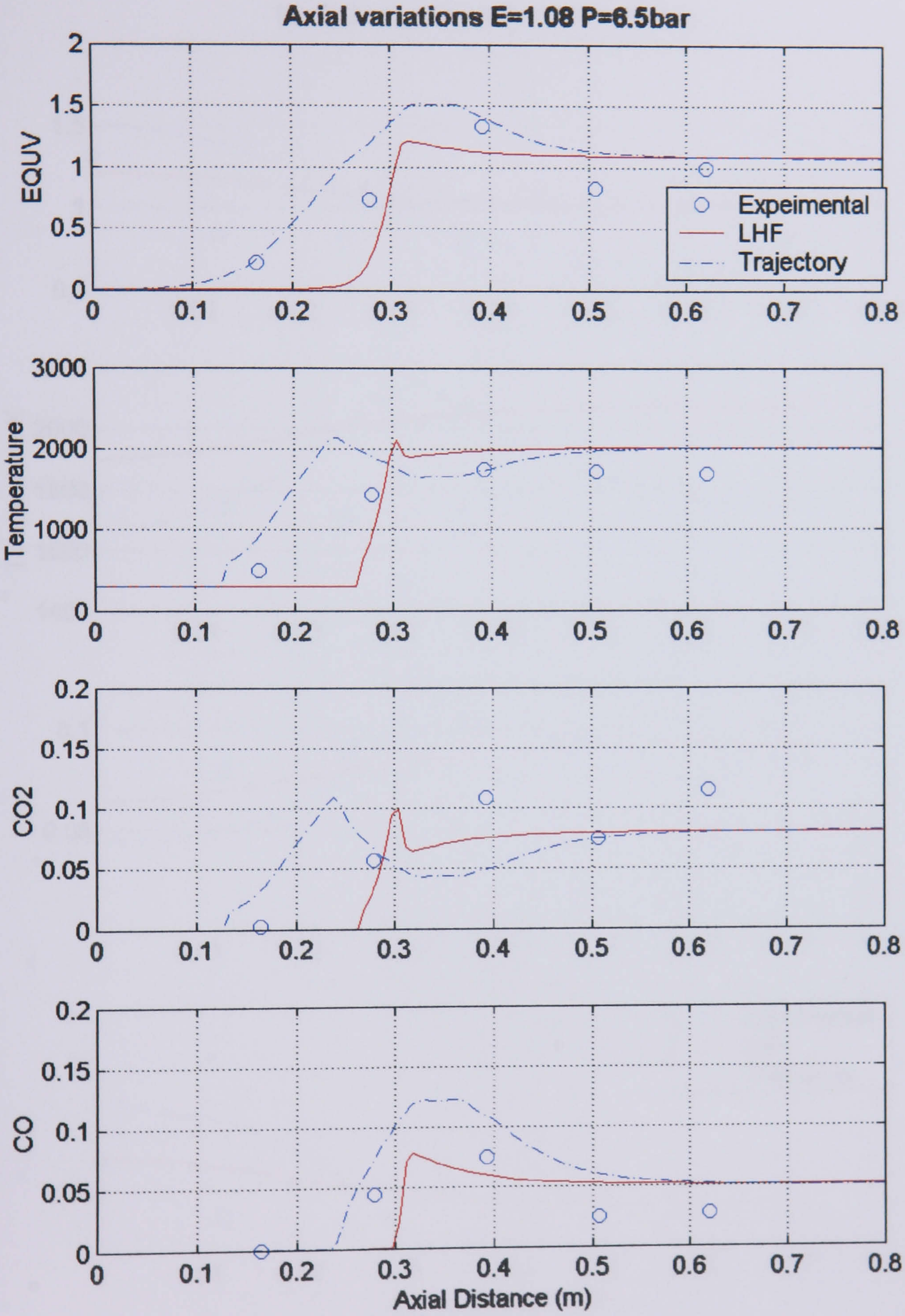

4. Trajectory model with 20 μm drop mean diameter

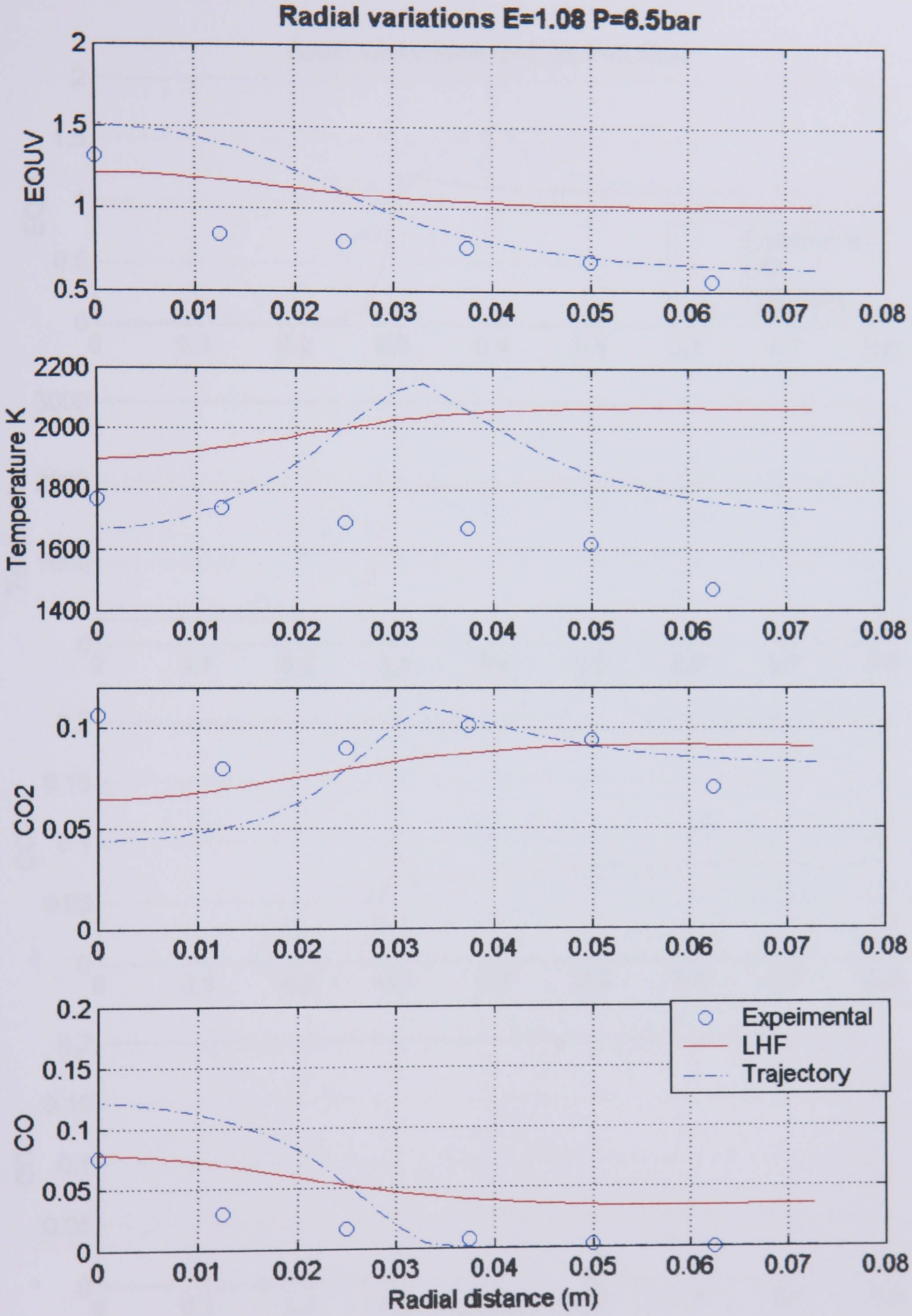

5. Trajectory model with 30 μm drop mean diameter

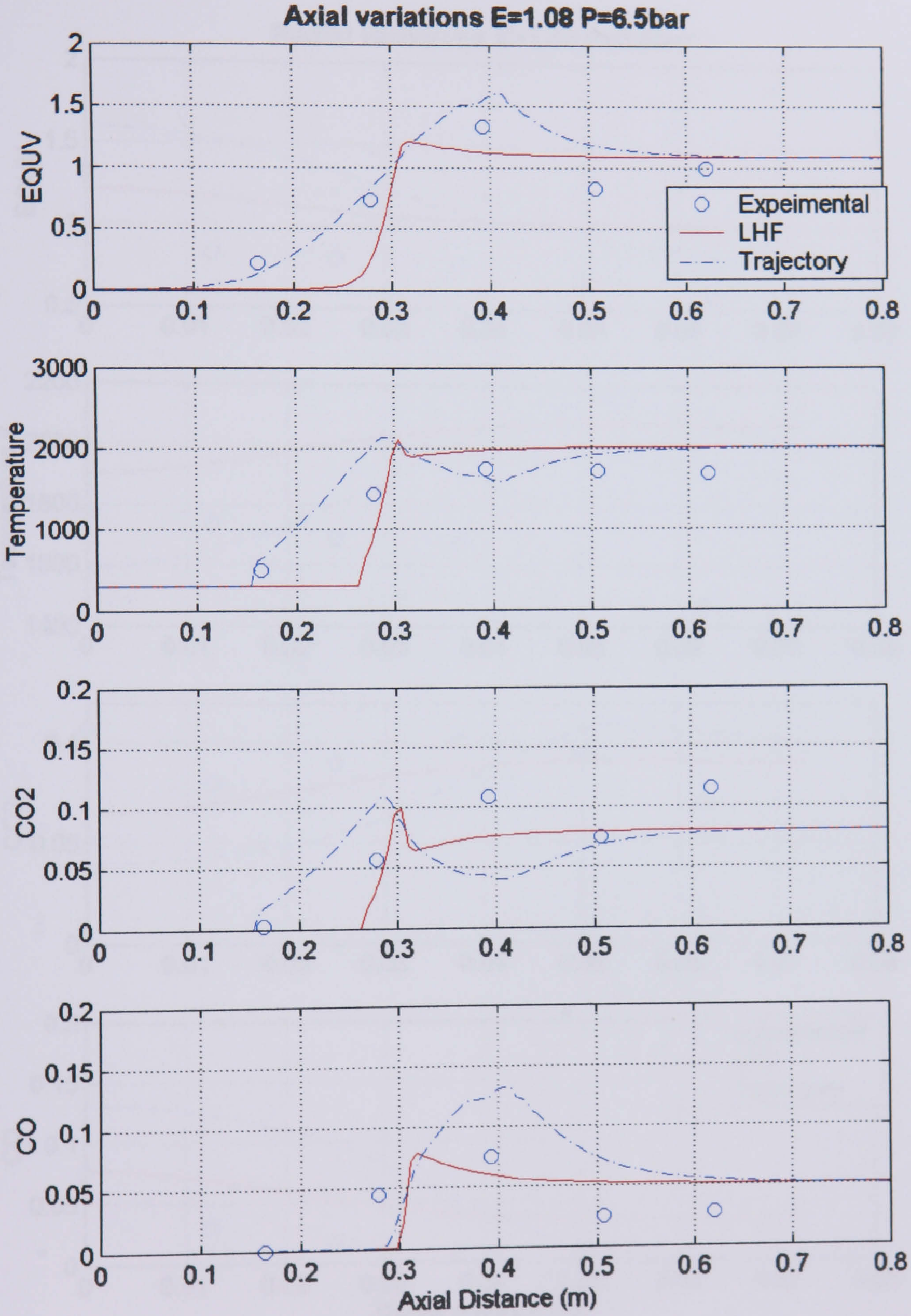

6. Trajectory model with 30 μm drop mean diameter

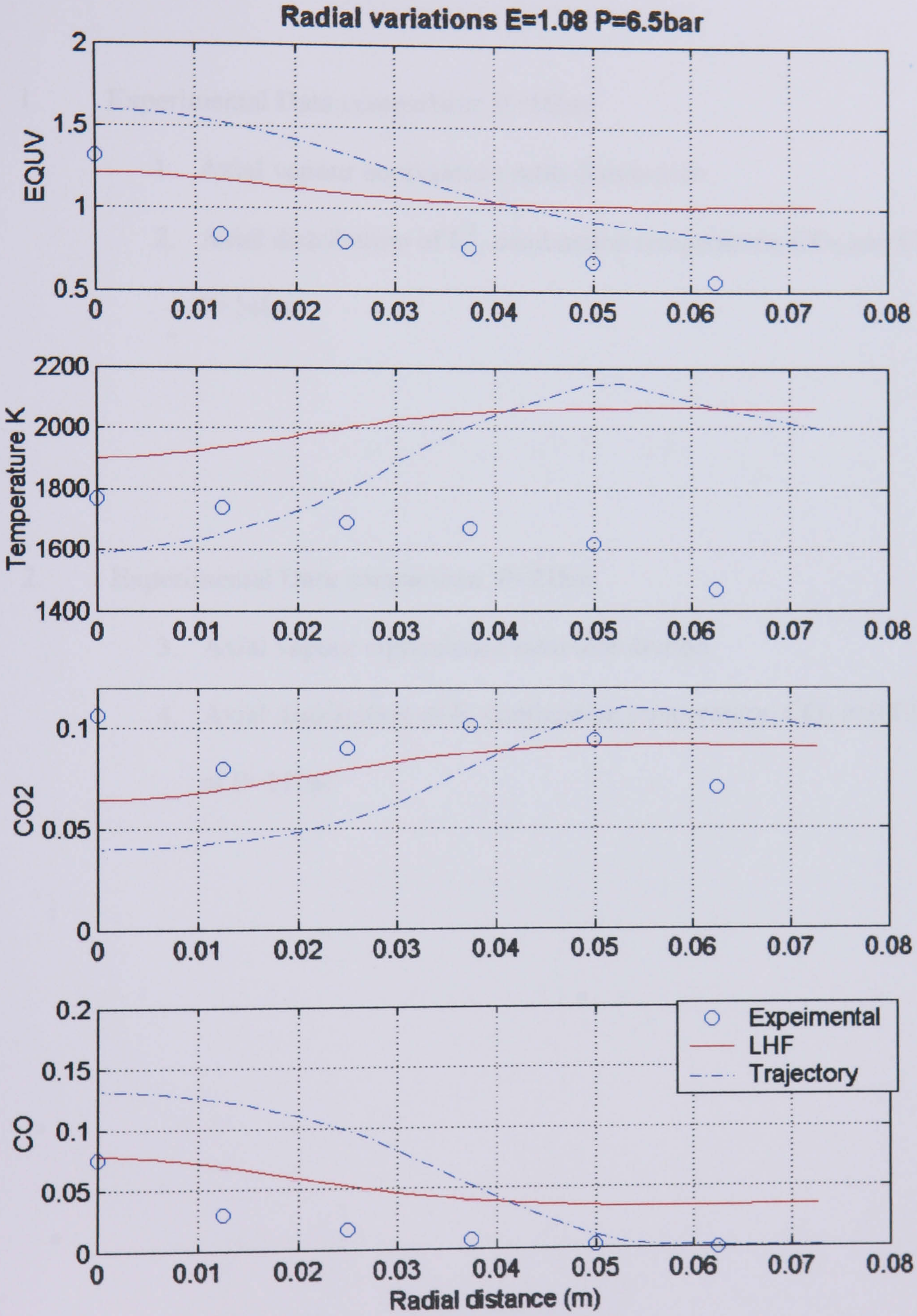

Appendix I

1. Experimental Data comparison: P=16bar

    1. Axial vapour equivalence ratio distribution

    2. Axial distribution of E^1, combustion temperature, CO_2 and CO at P=16bar

2. Experimental Data comparison: P=21bar

    3. Axial vapour equivalence ratio distribution

    4. Axial distribution of E, combustion temperature, CO_2 and CO at P=21bar

---

[1] Vapour Equivalence Ratio

Experimental Data comparison: P=16bar

1. Axial vapour equivalence ratio distribution

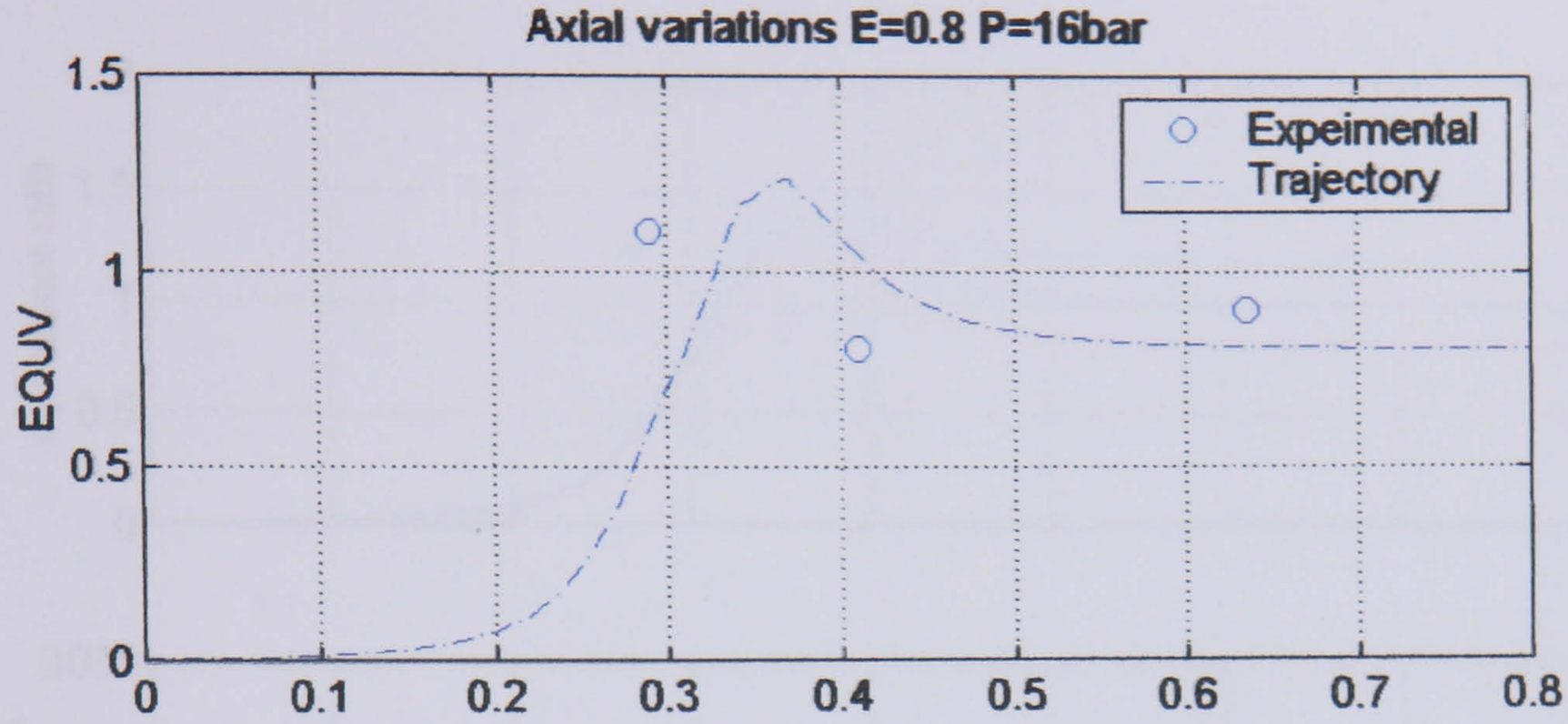

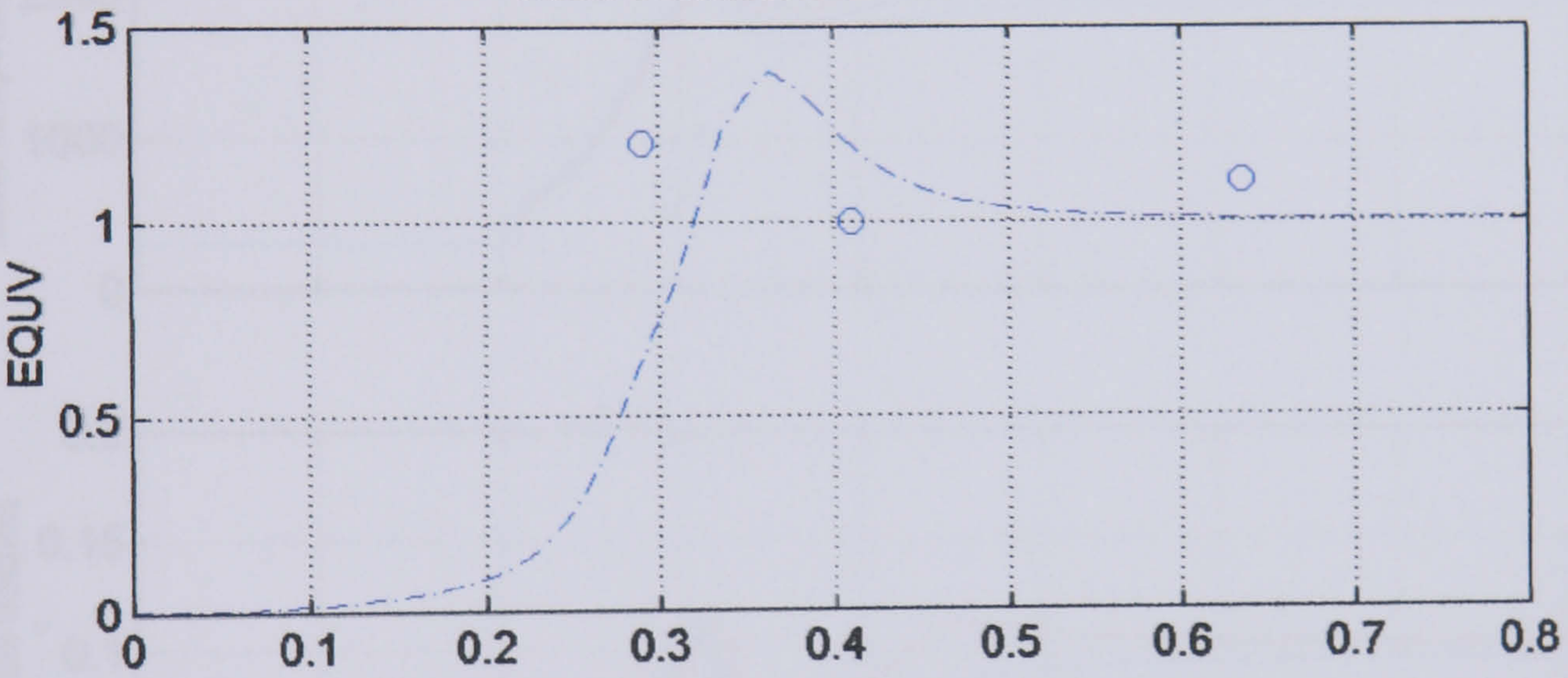

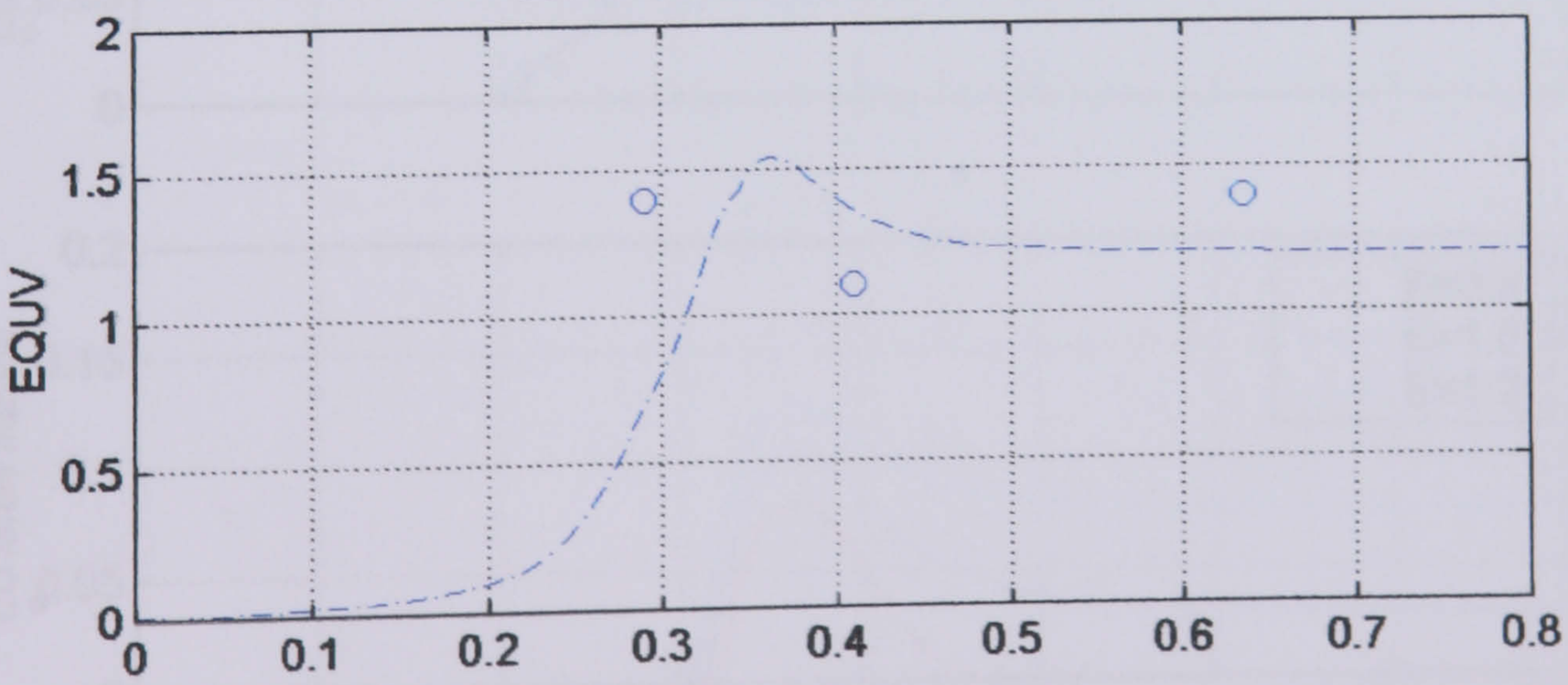

2. Axial distribution of E, combustion temperature, CO_2 and CO at P=16bar

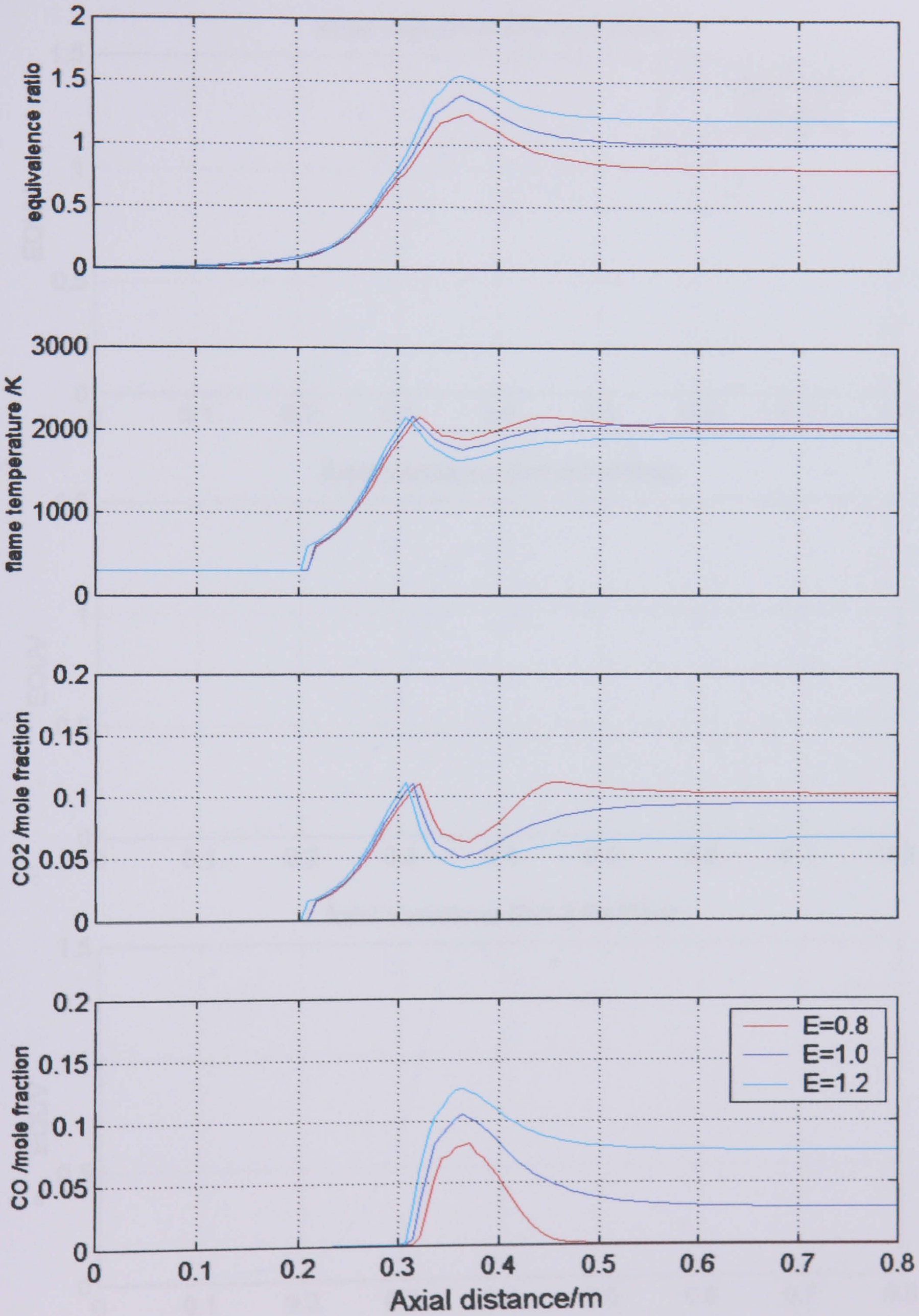

Experimental Data comparison: P=21bar

3. Axial vapour equivalence ratio distribution

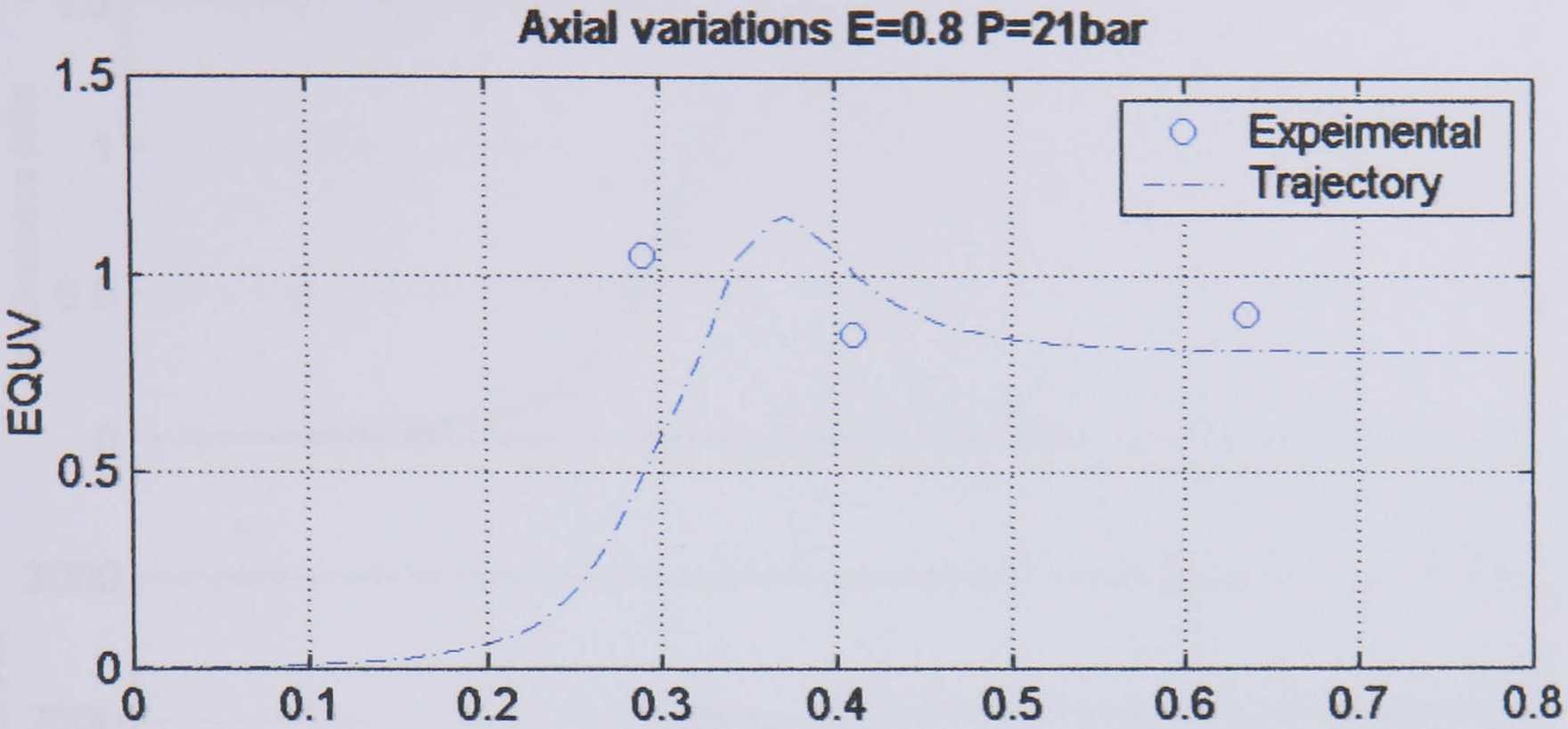

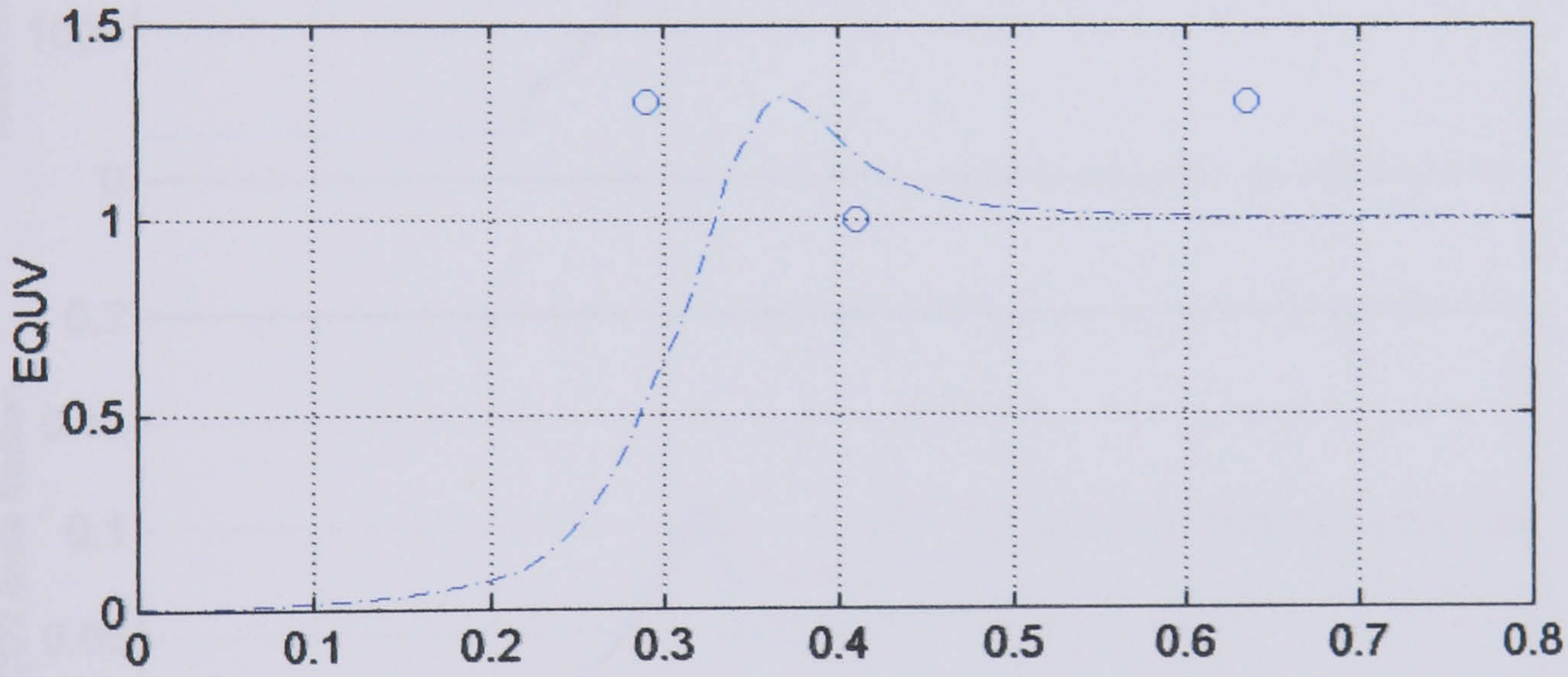

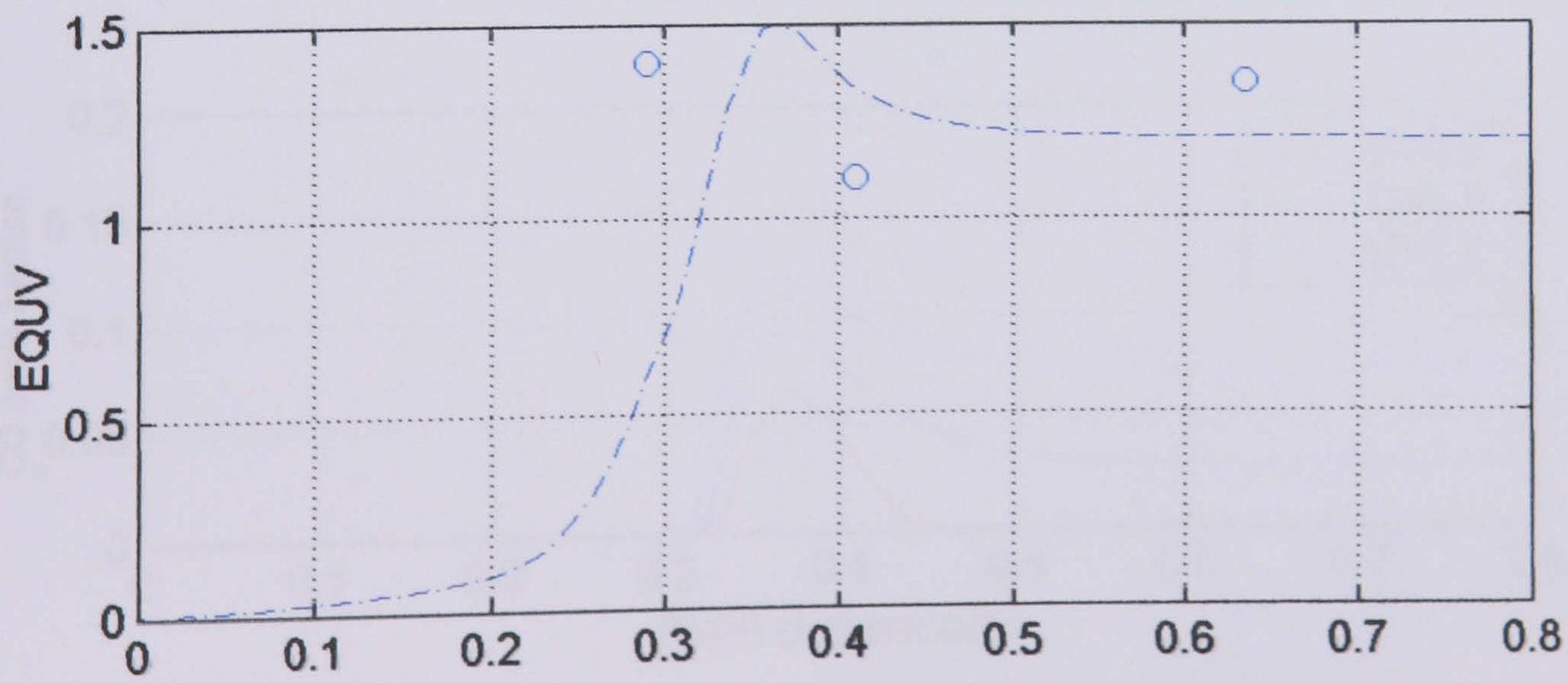

4 Axial distribution of E, combustion temperature, CO_2 and CO at P=21bar

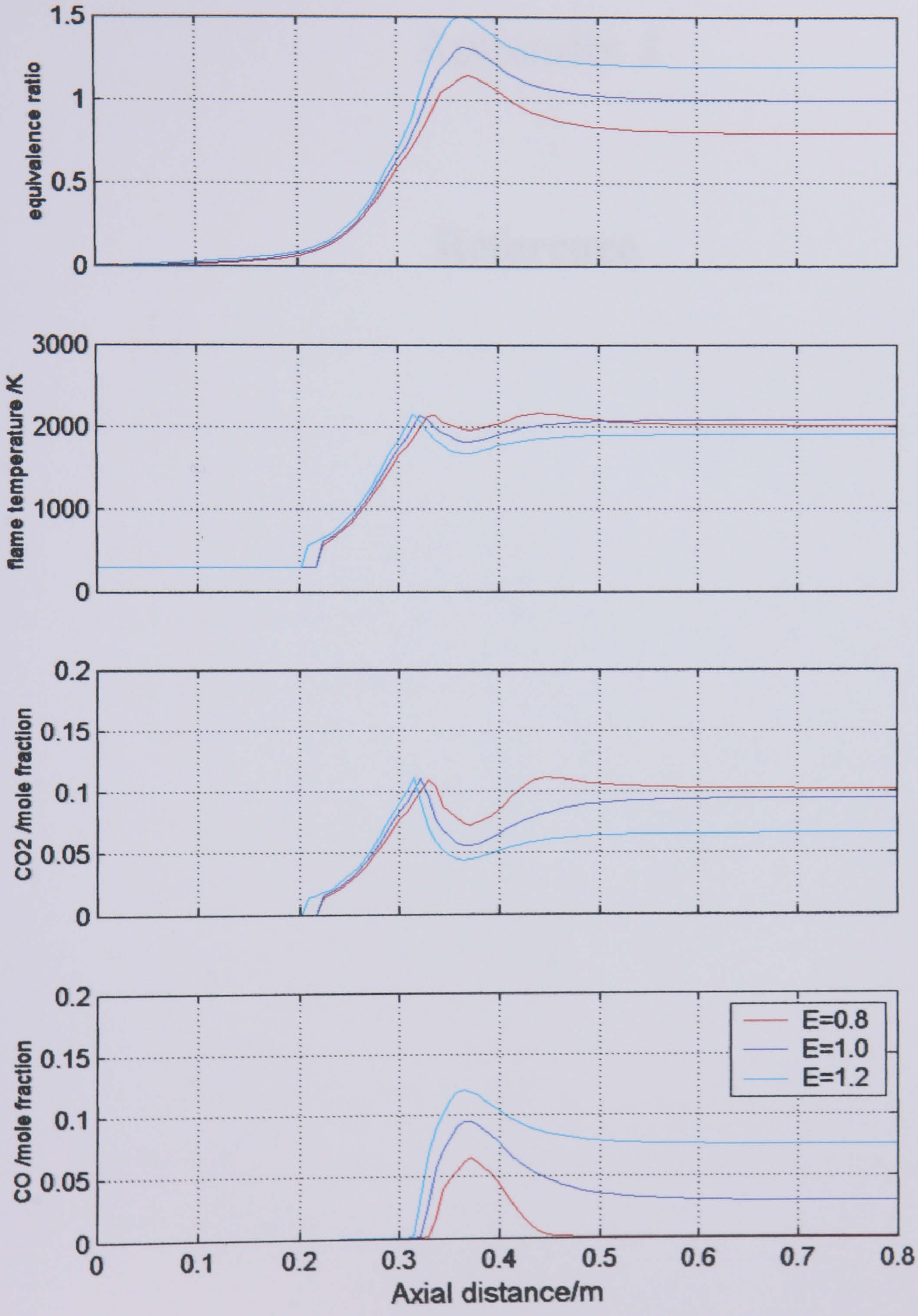

Appendix J

Reference

1. C. T. Crowe, Martin Sommerfield and Yutaka Tsuji,

"Multiphase flows with droplets and particles", CRC Press, Inc., USA, 1998

2. Zhou Lixing,

"Theory and Numerical Modelling of turbulent Gas-Particle Flows and Combustion", CRC Press, Inc., USA, 1993.

3. C.T. Crowe

"Modelling Turbulence in Multiphase Flows", Engineering Turbulence Modelling and Experiments 2 , pp. 899-913, Elsevier Science Publishers, 1993.

4. F. Durst, D. Milojevic and B. Schönung,

"Eulerian and Langrangian predictions of particulate two-phase flows, Appl..Math..Modelling", 1984, Vol. 8, April.

5. A. Berlemont, P. Desjonqueres and G. Gouesbet,

"Particle Tracking in Turbulent Flows", Gas-Solid Flows, ASME 1993, FED-Vol. 166, pp. 121-129, 1993.

6. C.T. Crowe, T.R. Troutt and J.N. Chung,

"Numerical Models for Two-Phase Turbulent Flows", Annual. Rev. Fluid. Mech. Pp. 11-43, 1996.

7. M.F. Lightstone and G.D. Raithby,

"A Stochastic Model of Particle Dispersion in a Turbulent Gaseous Environment", Combustion and Flame, Vol. 113, pp. 424-441, 1998.

8. H.K. Versteeg and W. Malalasekara,

"An Introduction to Computational Fluid Dynamics, The Finite Volume Method", Longman Group Ltd 1995, ISBN 0-582-21884-5.

9. Hobina Rajakaruna,

"A mathematical model for Liquid Fuel Spray Combustion", PhD theses, De Montfort University, Leicester, U.K., 1997

10. Maxey, M.R., Riley, J.J,

"Equation of a small rigid sphere in a non uniform flow", Physics of Fluids, 26,4, pp. 883-889, 1983

11. Riley J .J.,

PhD thesis, The Johns Hopkins University, Baltimore, Maryland, 1971

12. C.T. Crowe, M.P. Sharma and D.E. Stock,

"The Particle-Source-In-Cell (PSI-Cell) Model for Gas-Droplet Flows", Journal of fluids engineering, ASME, pp 325-332, April 1977. [***Insert Berlemont]

13. Elghobashi S.E.,

"On predicting particle laden turbulent flows", Applies Science Research, 52, pp. 309-329, 1994.

14. S. K. Aggarwal and S. Chitre,

"Computations of Turbulent Evaporating Sprays", Journal of Propulsion, Vol. 7, No. 2, March-April 1991.

15. Mawid, M. and Aggarwal, S. K.,

"Analysis of Transient Combustion of a Multi-component Liquid Fuel Droplet", Combustion and Flame, pp. 197-209, Vol. 84, 1991

16. G.M. Faeth,

"Current Status of Droplet and Liquid Combustion", Prog. Energy Combustion Science, Vol. 3. pp. 191-224, 1977.

17. N. Shaygan and S. Prakash,

"Droplet Ignition and Combustion Including Liquid-Phase Heating", Combustion and Flame, Vol. 102, pp. 1-10, 1995.

18. R. D. Reitz and R. Diwakar,

"Effect of Drop Break up on Fuel Sprays", SAE-860469, 1986.

19. S. L. Lee,

"Particle Drag in a Dilute Turbulent Two-Phase Suspension Flow", Int. J. Multiphase Flow, Vol. 10, No. 2, pp. 247-256, 1987.

20. W. A. Sirignano,

"Fluid Dynamics of Sprays1992, Freeman Scholar Lecture", Journal of Fluids Engineering, Vol. 115, pp. 345-378, 1993.

21. Park, T. W. Aggarwal, S. K. and Katta V. R.,

"Gravity Effects on the Dynamics of Evaporating Droplets in a Heated Jet ", Journal of Propulsion and Power, Vol. 11, No. 3, pp. 519-528, May-June 1995.

22. C.T. Crowe,

"Review- Numerical Models for Dilute Gas-Particle Flows", Journal of Fluid Engineering, Vol. 104, pp. 297-303, September 1982.

23. G.M. Faeth,

"Mixing, Transport and Combustion in Sprays", Prog. Energy Combustion Science, Vol.13, pp. 293-345, 1987.

24. Faeth, G. M., Hsiang, L. –P. and Wu, P. –K.,

"Structure and Breakup Properties of Sprays", Int. J. Multiphase flow, Vol. 21, pp. 99-127, 1995 [SM8]

25. G.M. Faeth,

"Evaporation and Combustion of Sprays", Prog. Energy Combustion Science, Vol. 9, pp. 1-76, 1983.

26. Bracco, F.V.,

"Modelling of engine sprays", Dept of Mechanical and Aerospace Engineering, Princeton University, Princeton, SAE paper 850394, pp. 113-136, 1985.

27. Chehroudi, B., Chen, S.H., Bracco, F.V., and Onuma, Y.,

"On the intact core of Full cone sprays", SAE paper 850126, 1985.

28. O' Rourke, P.J., and Bracco, F.V.,

"Modelling of Drop interactions in thick sprays and a comparison with experiments", Stratified charge Automotive Engine Conference, Inst. Of Mach. Engr. Pub ISBN 0852984693, 101, 1980.

29. David Lee Black, Mardson Queiroz McQuay, and Michel P. Bonin,

"Laser-based techniques for particle-size measurement: a review of sizing methods and their industrial applications", Prog. Energy Combust. Sci. Vol. 22. pp. 267-306. 1996.

30. Solomon, A.S.P., Shuen, J-S., Zhang, Q-F. and Faeth, G. M.

"Measurements and Predictions of the Structure of Evaporating Sprays", Journal of Heat Transfer, Vol. 107, pp. 679-686, August 1985.

31. Nukiyama, S., Tanasawa, Y.,

"Experiments on the atomization of liquids in an air stream", Report 3: on the droplet size distribution in an atomized jet. Society of Mech. Engrs. Japan. 5; pp. 62-67, 1939.

32. Rosin, P. and Rammler, E.,

"The laws governing the fineness of powdered coal", J. Inst. Of Fuel, Vol. 7, pp. 29-36, 1933.

33. Tate, R. W., and Marshall, Jr, W.R.,

"Atomization by centrifugal pressure nozzles", Chemical Engineering progress, Vol. 49, pp. 169-174, 1953.

34. Ayres, D., Caldas, M., Semião, V. and da Graca Carvalho, M.,

"Prediction of the droplet size and velocity joint distribution for sprays", Fuel, pp. 383-394, Vol. 80, 2001

35. E. Babinsky, P.E. Sojka,

"Modelling drop size distributions", progress in Energy and Combustion Science 28, pp. 303-329, 2002

36. Paloposki, T.,

"Drop size distributions in liquid sprays", Acta Polytech. Scandinavia, Mech Eng. Service, 1994.

37. Semiao, V., Andrade, P. and Carvalho, M.G.,

"Spray Characterization: numerical prediction of Sauter mean diameter and droplet size distribution", Fuel, Vol. 75, No. 15, pp. 1707-1714, 1996.

38. Marouan A. A. Nazha, Hobina Rajakaruna and Roy J. Crookes,

"An Effective Property, LHF-Type Model for Spray Combustion", Journal of Engineering for Gas Turbines and Power, ASME, Vol. 122, pp. 275-279, April 2000.

39. Mao, C.P., Wakamatsu, Y. and Faeth G. M.

"A simplified model for high pressure spray combustion", 18th symposium (International) on combustion. The combustion institute, pp. 337-347, 1981

40. Mao, C.P., Szekely, G. A. Jr. and Faeth G. M

"Evaluation of a Locally Homogeneous Flow model of Spray Combustion", NASA Contractor Report 3202. 1980.

41. Hobina Rajakaruna and Marouan A. A. Nazha,

" Variable Finite Liquid Diffusivity in Droplet Evaporation Modelling ", Vol. 377-1, Computational Technologies for Fluid/Thermal/Structural/Chemical Systems with Industrial Applications, Volume I, ASME 1998.

42. Lumley, J. E.,

"Whither Turbulence? Turbulence of the crossroads", Lecture notes in physics, Vol. 357, Springer-Verlag, New York, 1990.

43. Launder, B. E., and Spalding, D.B.

"Lectures in Mathematical models of turbulence" Academic press, New York, 1972.

44. Spalding, D.B.

"Concentration fluctuations in a round jet", J. of Chemical Engineering Science, Vol. 26, pp.95, 1971.

45. Spalding D.B.

"k-W model of turbulence", Imperial College Mechanical Engineering report TM/TN/A/16, 1972.

46. Harlow, F.H. and Nakayama, P.,

"Transport of turbulence energy decay rate", Los Alamos Science Lab., University of California Report LA-3854, 1968.

47. Shearer, A.J. and Feath, G.M.,

"Evaluation of locally homogeneous model for spray evaporation", NASA Contractor report 3198, 1979.

48. Mao, C.P., Wakamatsu, Y. and Faeth G. M.

"A simplified model for high pressure spray combustion", 18th symposium (International) on combustion. The combustion institute, pp. 337-347, 1981

49. Mao, C.P., Szekely, G. A. Jr. and Faeth G. M

"Evaluation of a Locally Homogeneous Flow model of Spray Combustion", NASA Contractor Report 3202. 1980

50. Kee Soo Han and Myung Kyoon Chung,

"Numerical Simulation of Two-Phase Gas-Particle Jet in a Cross-Flow", Aerosol Science and Technology, Vol. 16, pp. 126-139, 1992.

51. Huang, X. Q., Chen, L. H. and Zhou, L. X.,

"Numerical Modelling of 3-D Turbulent recirculating Gas-Particle Flows in a Combustor of Co-flow Jets with Large Velocity difference", Proc. 3rd Inter. Symp. of Gas-Solid Flows, La Jolla, CA, pp. 85-88, 1989.

52. Picart, A. Berlemont, A. and Gouesbet, G.,

"Modelling and Predicting Turbulence Fields and the Dispersion of Discrete Particles Transported by Turbulent Flows", Int. J. Multiphase Flow, pp. 237-261, Vol. 12, No. 2, 1986.

53. Guo, Y. C., Chan, C. K. and Lau, K. S.,

"A Pure Eulerian Model for Simulating Dilute Spray Combustion", Fuel, pp. 2131-2144, Vol. 81, 2002.

54. Xiaoqing Huang and Lixing Shou,

"Simulation of Three-Dimensional Turbulent Recirculating Gas-Particle Flows by an Energy Equation Model of Particle Turbulence", FED-vol. 121, Gas-Solid Flows, ASME 1991.

55. Hoffmann, N., Galea, E. R. and Markatos, N. C.,

"A Transient two-phase fire-sprinkler simulation", Proc. Of IASTED Int. Conf. Modelling, Simulation and Optimisation, Montreal, pp. 136-139, 22-24 May 1990.

56. Berlemont, A. Picart, A. and Gouesbet, G.

"The code DISCO-2 for predicting the behaviour of discrete particles in turbulent flows and its comparisons against the code DISCO-1 and experiments" Third Int. Conference on Numerical methods in Laminar and Turbulent Flow , Seattle, USA, pp. 963-973, 1983

57. Gouesbet, G. and Berlemont, A.

"Eulerian and Lagrangian approaches for predicting the behaviour of discrete particles in turbulent flows", Progress in Energy and Combustion Science, pp. 133-159, Vol. 25, 1999

58. Snyder W.H., Lumley J.L.,

"Some measurements of particle velocity autocorrelation function in turbulent flow", J. Fluid Mech. Vol. 48, pp. 41–71, 1971.

59. Wells M.R., Stock D.E.,

"The effect of crossing trajectories on the dispersion of particles in a turbulent flow", J. Fluid Mech. Vol. 136, pp. 31–62, 1983.

60. E. R. Perrell,

"Two-Phase CFD Calculations with Continuous Distribution of Particle sizes", AIAA-98-3459, 34th AIAA JPC, July 13-15, 1998.

61. John K. Dukowicz,

"A Particle-Fluid Numerical Model for Liquid Sprays", Journal of Computational Physics 35, pp. 229-253, 1980.

62. R. Borghi,

"Turbulent Combustion Modelling", Prog. Energy Combustion Sci. Vol.14, pp. 245-292, 1988.

63. C.T. Crowe,

"A numerical model for the gas-droplet flow field near an atomizer", proceedings of the 1st international conference on liquid atomisation and spray systems, The Fuel Society of Japan, Tokyo August 27-31, 1978.

64. Kenning, V. M. and Crowe, C. T.,

"Brief communication on the effect of particles on carrier phase turbulence in gas-particle flows", Int. J. Multiphase Flow, Vol. 23, No. 2, pp. 403-408, 1997

65. Richard V. Calabrese and Stanley Middleman,

"The Dispersion of Discrete Particles in a Turbulent Fluid Field", AIChE Journal, Vol. 25, No. 6, pp.1025-1035, November, 1979.

66. Shirolkar, J. S. and McQuay, M. Q.,

"Parametric evaluation of a particle dispersion sub model used in a two-dimensional, pulverized- coal combustion code", Energy and Fuels, pp. 919-927, Vol. 7, Issue 6, 1993

67. Smoot, L.D., Smith, P.J., Brewster, B.S. and Baxter, L.L.,

"Revised users manual: Pulverized Coal Gasification or Combustion -2 Dimensional", Brigham Young University, Utah, 1988.

68. Jurewicz, J.T., and Stock, D.E.,

"A numerical model for turbulent diffusion in gas particle flows", ASME paper 76-WA-FE-33, 1976.

69. Ron J. Litchford and San-Mou Jeng,

"Efficient Statistical Transport Model for Turbulent Particle Dispersion in Sprays", AIAA Journal, Vol. 29, No. 9 , September 1991.

70. M. Mizukami, R.N. Parthasarathy and G.M. Faeth,
"Particle-Generated Turbulence in Homogeneous Dilute Flows", International Journal of Multiphase Flow Vol. 18, No. 3, pp. 397-412, 1992.

71. Rafal J. Sornek, Ritsu Dobashi and Toshisuke Hirano,
" Effect of Turbulence on Vaporization, Mixing and Combustion of Liquid-Fuel sprays", Combustion and Flame 120: 479-491, 2000.

72. Coimbra, C. F. M., Shirolkar, J. S. and McQuay, M. Q.,
"Modelling particle dispersion in a turbulent, multiphase mixing layer", Journal of Wind Engineering and Ind. Aerodynamics, pp. 79-97, Vol. 73, 1998

73. Gosman, A.D. and Ioannides, E.,
"Aspects of computer simulation of liquid-fueled combustion", AIAA Paper No. 81-0323, 1981.

74. Shuen J.S., Chen L.D., Faeth G.M.,
"Evaluation of a stochastic model of particle dispersion in a turbulent round jet", AIChE J. 29, pp. 167–170, 1983.

75. Chang, E.J., Kailasanath, K. and Aggarwal S.K.,
"Two-way coupled Gas-Particle systems in an Axisymmetric Ramjet

Combustor", Technical Notes (95-2561), AIAA Journal, Vol. 37, No. 3, pp. 396-398, 1998

76. Kee Soo Han and Chung M. K.,
"Numerical simulation of Two-phase Gas-Particle jet in a Crossflow", Aerosol Science and Technology, Vol. 16, pp. 126-139, 1992.

77. Crowe, C.T., and Pratt, D.T.,
"Two-Dimensional Gas-Particle flow", Proceedings of 1972 Heat Transfer and Fluid Mechanics Institute, Stanford University press, pp. 386-398, 1972.

78. Chen P.P., Crowe C.T.,
"On the Monte-Carlo modelling particle dispersion in turbulence", in: Proc. Int. Symp. on Gas–Solid Flows, ASME FED, Vol. 10, pp. 37-41, 1984.

79. Ormancey, A., and Martinon, A.,
"Prediction of particle dispersion in turbulent flows" Physico-Chem. Hydrodynamics, Vol. 5, pp. 229-240, 1984.

80. A. Berlemont, P. Desjonqueres and G. Gouesbet,
"Particle Lagrangian Simulation in Turbulent Flows", Int. J. Multiphase Flows, Vol. 16 No. 1, pp. 19-34, 1990.

81. Burry D., and Bergeles G.,

"Dispersion of particles in anisotropic turbulent flows", Int. J. Multiphase Flow , Vol.19 (4), pp. 651–664, 1993.

82. Chen, X.-Q. and Pereira, J. C. F.,

"Efficient computation of particle dispersion in turbulent flows with a stochastic-probabilistic model", lnt. J. Heat Mass Transfer. Vol. 40, No. 8. pp. 1727- 1741, 1997

83. Shirolkar, J. S. and McQuay, M. Q.,

"A PDF propagation approach to model turbulent dispersion in swirling flows", Eur. J. Mech. B - Fluids 20, pp. 699–726, 2001.

84. Demoulin, F.X., and Borghi, R.,

"Modelling of Turbulent Spray Combustion with Application to Diesel Like Experiment", Combustion And Flame Vol. 129, pp. 281–293, 2002.

85. Shirolkar, J. S. and McQuay, M. Q.,

"Probability Density Function propagation model for turbulent particle dispersion", Int. J. Multiphase Flow, Vol. 24 (4), pp. 663-678, 1998.

86. Lu, Q. Q., Frontaine, J. R. and Aubertin, G.,

"Particle Motion in Two-Dimensional Confined Turbulent Flows", Aerosol Science and Technology, Vol. 17, pp. 169-185, 1992

87. Lu, Q.Q.,

"An approach to modelling particle motion in turbulent flows-I. Homogeneous, isotropic turbulence", Atmospheric Environment Vol. 29, No. 3. pp. 423-436. 1995.

88. Chen, X.-Q. and Pereira, J. C. F.,

"Computation of particle dispersion in turbulent liquid flows using an efficient Lagrangian trajectory model", International Journal For Numerical Methods In Fluids, VOL. 26, 345–364 1998.

89. Farzad Mashayek,

"Stochastic simulations of particle-laden isotropic turbulent flow", International Journal of Multiphase Flow, Vol. 25, pp.1575-1599, 1999.

90. Mostafa, A. A., Mongia, H. C., McDonnell, V. G. and Samuelsen, G. S.,

"Evolution of particle-laden jet flows: a theoretical and experimental study", AIAA Journal, 1989, 27, 167-183.

91. Marie-Sophie Grancher, Gĕrard Gouesbet, Alain Berlemont,

"Lagrangian Simulation of Heat and Mass Transfer in Dispersed Two-Phase Flows", Engineering Turbulence Modelling and Experiments, pp. 867-875, Elsevier Science Publishers, 1990.

92. Xu, Z. G., Walklate, P. J., Rigby, S. G. and Richardson, G. M.,
"Stochastic modelling of turbulent spray dispersion in the near-field of orchard sprayers", J. of Wind Engineering and Industrial Aerodynamics, pp. 295-304. Vol. 74-76, 1998

93. Berlemont, A., Grancher, M. S. and Gouesbet, G.,
"Heat and mass transfer coupling between vaporising droplets and turbulence using a Lagrangian approach", Int. J. Heat Mass Transfer, pp. 3023-3034, Vol. 38, No. 16, 1995

94. Desjonqueres, P., Berlemont, A. and Gouesbet, G.,
"Lagrangian Simulation of a Two Phase Turbulent Round Jet", Sixth Symp. on Turbulent Shear Fows, France, pp. 2131- 2135, Sept. 7-9, 1987

95. Shao, Y.-P.,
"A Lagrangian Stochastic Model for Nonpassive Particle Diffusion in Turbulent Flows", Mathl. Comput. Modelling Vol. 21, No. 9, pp. 31-37, 1995.

96. Chang, K.-C. and Wu, W.-J.,
"Sensitivity study on Monte-Carlo solution procedure of two-phase turbulent flows", Numerical Heat Transfer, Part B, Vol. 25, pp. 223-244, 1994

97. Chen, X.-Q. and Pereira, J. C. F.,
"Computation of turbulent evaporating sprays with well-specified

measurements: a sensitivity study on droplet properties", International Journal of Heat and Mass Transfe*r,* 1996, 34, 441-454.

98. Karl, J.-J., Schaeffer, T., Huilier, D., and Burnage, H., "Dispersion Of A Polydisperse Spray In A Constant Shear Turbulent Flow.", Mechanics Research Communications, Vol. 22, No. 3, pp. 305-312, 1995.

99. Glaze, D.J., and Frankel, S.H., "Effect of dispersion characteristics on particle temperature in an idealized non-premixed reacting jet", International Journal of Multiphase Flow 26, pp. 609-633, 2000.

100. MacInnes, J. M. and Bracco, F. V., "Stochastic particle dispersion and the tracer particle limit", Phys. Fluids A, Vol. 4, 1992

101. Shirolkar, J. S., Coimbra, C.F.M., and McQuay, M. Q., "Fundamental aspects of modelling turbulent particle dispersion in dilute flows", Prog. Energy Combustion Sci., Vol. 22, pp. 363-399, 1996.

102. Friedlander, S. K., "Behavior of Suspended Particles in a Turbulent Fluid", A. I. Ch. E. Journal, pp. 381-385, Vol. 3, No. 3, Sept. 1957.

103. Carvalho Jr., J. A., McquaY, M. Q. and Gotac, P. R.,
"The interaction of liquid reacting droplets with the pulsating flow in a Rijke-tube combustor", Combustion and Flame, pp. 87-103, Vol. 108, 1997

104. Dombrovsky, L. A., Sazhin, S. S., Sazhina, E. M., Feng, G., Heikal, M. R., Bardsley, M. E. A. and Mikhalovsky, S. V.,
"Heating and evaporation of semi-transparent diesel fuel droplets in the presence of thermal radiation", Fuel, pp. 1535-1544, Vol. 80, 2001.

105. T.X. Li, D.L. Zhu and C.K. Law,
"Droplet Combustion, Micro-explosion and Sooting Characteristics of Several Energetic Liquid Propellants", Journal of Propulsion and Power, Vol. 14, No. 1, January-February 1998.

106. Chung, T.J.,
"Numerical modelling in combustion", Taylor and Francis, 1993.

107. Forman A. Williams,
"Combustion theory", Second edition, The Benjamin/ Cummings Publishing Company, 1985.

108. Stephen R. Turns,
"An introduction to combustion, Concepts and applications", McGraw-Hill, Inc., 1996.

109. Nazha, M.A.A,

"Burning Sprays of water-diesel fuel emulsions", PhD thesis Queen Mary College, University of London, 1983.

110. Gung Chen and Alessandro Gomez,

"Dilute Laminar Spray Diffusion Flames near the Transition from Group combustion to Individual Droplet Burning", Combustion and Flame 110: 392-404, 1997.

111. W. A. Sirignano,

"Fuel Droplet Vaporization and Spray Combustion Theory", Prog. Energy Combust. Sci. , pp. 291-322, 1983.

112. Beer, J.M., Chomiak, J. and Smoot, L.D.,

"Developing coal combustion technologies", Progress in Energy and Combustion Science, Vol. 10 (2), pp. 87-144, 1984.

113. Spalding, D.B.,

"Combustion as applied to engineering", J. of Inst. of Fuel, 196, Apriel 1971.

114. Spalding, D.B.,

"Combustion and mass transfer", A text book with multiple-choice exercise for engineering students, Imperial college of science and technology, London, England, 1979.

115. Lockwood, F.C.,

"The modelling of turbulent premixed and diffusion combustion in the computation of engineering flows", Combustion and Flame, Vol. 29, pp. 111-122, 1977.

116. Spalding, D.B.,

"Mixing and chemical reaction in steady confined turbulent flames", Thirteenth symposium (international) on combustion, Combustion Institute, Pittsburgh, pp. 649-657, 1971.

117. Lockwood, F. C. and Naguib, A.S.,

"The prediction of the fluctuations in the properties of free, round-jet, turbulent, diffusion flames", Combustion and Flame, Vol. 24, pp. 109–124, 1975.

118. Jones, W.P. and Priddin, C.H.,

"Predictions of the flow field and local gas composition in gas combustors", Seventeenth symposium (International) on combustion, The combustion Institute, pp. 399-407, 1978.

119. Richardson, J.M., Harward, Jr. H.C. and Smith Jr. R.W.,

"The relation between sampling-Tub measurements and concentration fluctuations in a turbulent gas jet", Fourth symposium (International) on Combustion, The combustion Institute, pp.182-189, 1953.

120. Jones, W. P. and J. H. Whitelaw,

"Calculation methods for reacting turbulent flows: a review", Combustion and Flame Vol. 48, pp. 1–26, 1982.

121. Owen, K.,

"Measurements and observations in turbulent recirculating jet flows", AIAA Journal, Vol. 14, pp. 1556-1562, 1976.

122. Pope, S.B.,

"The probability approach to the modelling of the turbulent reacting flows", Combustion and flame, Vol. 27, pp. 299-312, 1976.

123. Pope, S.B.,

"Implication of probability equations for turbulent combustion models", Combustion and flame, Vol. 29, pp. 235-246, 1977.

124. Pope, S.B.,

"A Monte Carlo method for the PDF equations of turbulent reactive flows", Combustion science and technology, Vol. 25, pp. 159-174, 1981.

125. Pope, S.B.,

"PDF methods for turbulent reactive flows", Progress in Energy and Combustion Science, Vol. 11, pp. 119–192, 1985.

126. Pope, S.B.,

"Computations of turbulent combustion: progress and challenges", Twenty-Third Symposium (International) on Combustion, The Combustion Institute, pp. 591–612, 1990.

127. Crowe, C. T.,

"On models for turbulence modulation in fluid-particle flows", Int. Journal of Multiphase Flow, pp. 719-727, Vol. 26, 2000

128. Crowe, C. T.,

"Modelling Fluid-Particle Flows: current status and future directions", AIAA Paper No. 99-3690, 1999

129. Chang, K-C,

"Turbulent Flow Computations in Combustors" , Proc. Natl. Sci. Counc. ROC(A), pp. 413-421, Vol. 24, No. 6, 2000

130. Crookes, R.J., Sivalingam, G., Nazha, M.A.A. and Rajakaruna, H.,

"Analysis of soot particulate formation in a high pressure confined spray flame", SAE technical paper, 1999-01-3488, 1999.

131. Crookes, R.J., Sivalingam, G., Nazha, M.A.A. and Rajakaruna, H.,

"Prediction and measurement of soot particulate formation in a confined diesel

fuel spray-flame at 2.1 MPa", Int. J. of Thermal science, Vol. 42, pp.639-646, 2003.

132. Nazha, M.A.A. and Rajakaruna, H. and Malalasekera, W.,
"Effects of radiation on predicted flame temperature and combustion product of a burning liquid fuel spray", Sixth International conference on "Technologies and combustion for a clean environment", Vol. II, pp639-643, 2001.

133. Jurewicz, J. T. Stock, D. E. and Crowe, C. T.,
"The Effect of Turbulent Diffusion on Gas Particle Flow in an Electric Field", Proceedings Symposium on Turbulent Shear Flows, University Park, PA, pp. 12/27 - 12/33, April 1977

134. Migdal, D. and Agosta, V.D.,
"A source flow model for continuous gas-particle flow", J. Applied Mechanics, Vol. 35, pp. 860-865, 1967.

135. Patankar, S.V. and Spalding D.B.,
"A computer model for three-dimensional flow in furnaces", Fourteenth symposium (Int.) on combustion, Combustion Institute, pp. 605-614, 1973.

136. Patankar, S. V.,
"Numerical Heat Transfer and Fluid Flow", Taylor and Francis, 1980.

137. Harlow, F.H. and Welch, J.E.,

"Numerical calculation of time-dependent viscous incompressible flow of fluid with free surface", Phys. Of Fluids, Vol. 8, pp. 2182-2189, 1965.

138. Patankar, S.V. and Spalding D.B.,

"A calculation procedure for Heat, Mass and Momentum transfer in three-dimensional parabolic flows" , Int. J. of Heat and Mass Transfer, Vol. 15, pp. 1787, 1972.

139. Gosman, A.D. and Pun, W.M.,

"The TEACH program", HTS course notes, Mech. Eng. Dept. Imperial College, 1974.

140. Sussman, M. A.,

"Source term evaluation for combustion modelling", AIAA Paper No. 93-0239, 1993.

141. Robert C. Reid, John M. Prausnitz and Bruce E. Poling,

"The Properties of Gases & Liquids", Forth Edition, McGraw-Hill Book Company, 1987.

142. Faeth, G.M.,

"Spray Combustion Phenomena", Thirty-sixth Sym. (International) on Combustion, The combustion institute, pp. 1593-1612, 1996.

143. W. H. Press, S.A. Teukolsky, W.T. Vetterling and B.P. Flannery, "Numerical Recipes in Fortran, The art of Scientific Computing", second edition, Cambridge University Press, 1992.

144. Daniel D. McCracken and William I. Salmon, "Computing for Engineers and Scientists with Fortran 77 (second edition)", ISBN 0-471-62552-3, John Wiley & Sons, Inc., 1988.